PB82-214099

BuMines OFR 76-82

A minerals research contract report
October 1981

THE EFFECT OF IN SITU RETORTING ON OIL SHALE PILLARS

Bureau of Mines Open File Report 76-82

Contract H0262031
Excavation Engineering and
Earth Mechanics Institute
Colorado School of Mines

BUREAU OF MINES ★ UNITED STATES DEPARTMENT OF THE INTERIOR
Minerals Environmental Technology

The views and conclusions contained in this document are those of the author and should not be interpreted as necessarily representing the official policies or recommendations of the Interior Department's Bureau of Mines or of the U. S. Government.

FOREWORD

This report was prepared by the Excavation Engineering and Earth Mechanics Institute, Colorado School of Mines, Golden, Colorado under U.S.B.M. Contract Number H0262031. The contract was initiated under the Minerals Environmental Technology Program. It was administered under the technical direction of Twin Cities Mining Research Center, with Mr. Sam Demou acting as Technical Project Officer. Mr. Kent Charles was the Contract Administrator for the Bureau of Mines.

This final report is a summary of the work accomplished as part of this contract during the period June 28, 1976 to May 31, 1981. The report was submitted by the authors in October 1981.

ABSTRACT

This report is submitted as a Final Report covering the work accomplished under U.S. Bureau of Mines Contract H0262031, entitled "The Effect of In-Situ Retorting on Oil Shale Pillars". The primary objective of this investigation was to determine the mechanical properties of oil shale at elevated temperatures and confining pressures, the thermal properties at elevated temperatures, and to provide mathematical models that can be utilized for effective mine and pillar design for an in-situ oil shale retorting operation.

As part of the Phase I investigation, a review of current activity in the area of the in-situ retorting was undertaken and the findings are included as an appendix to this report. Also provided is a comprehensive list of references for literature related to in-situ retorting.

Laboratory mechanical property tests were performed with oil shale samples taken parallel to the bedding, as well as samples taken perpendicular to the bedding. Tests were conducted under varying conditions of temperature, confining pressure and grade. The temperature range tested was from 20°C to 500°C, confining pressures up to 1,500 psi were applied, and kerogen content varied from 10 to 30 gallons per ton. The program was subsequently expanded to include samples of higher grades up to 40 gallons per ton, and to perform an in-situ heater test for model verification.

Laboratory tests were performed to determine the following properties: uniaxial and triaxial compressive strength, Young's modulus and Poisson's ratio, Brazilian tensile strength, density, thermal conductivity and thermal diffusivity, thermal expansion, electrical and acoustical properties.

Laboratory were undertaken on oil shale core samples taken perpendicular and parallel to bedding planes. The vertical cores (those taken perpendicular to bedding) were tested so that the direction of load was perpendicular to bedding. Whereas the horizontal cores (those taken parallel to bedding) had a loading direction parallel to bedding planes.

Tests conducted under nitrogen-flushed and oxygen available atmosphere did not show any discernable effect of heating atmosphere on oil shale strength. Heating time was also found to have little or no effect on oil shale strength after the time required for thermal equilibrium to occur in the sample.

Compressive strength was highly sensitive to temperature with a major loss of strength occurring in heating only to 140^{o}C. Also observed was a strength regain in heating from 380^{o}C to 500^{o}C, particularly for vertical cores (loading perpendicular to bedding planes) at all grades tested. Increasing grade resulted in lower compressive strength with the vertical cores showing more sensitivity to grade than the horizontal cores. The rate of reduction in compressive strength was greater at lower grades. Confining pressure was found to be very effective in increasing sample strength for all temperature and grade levels tested. Overall, the horizontal cores yielded higher compressive

strengths than vertical cores.

As expected, the measured elastic properties, the Young's modulus and the Poisson's ratio showed a large degree of variation.

The Brazilian tensile strengths showed a similar sensitivity to temperature as did the compressive strength with major loss of strength occurring in heating only to 140°C. For vertical cores, high temperatures (beyond 380°C) resulted in virtually a complete loss of tensile strength.

Laboratory measurements for each property determined were analyzed through multiple regression techniques to develop equations to represent oil shale properties in terms of grade, temperature and physical properties. Except for elastic properties, the developed equations had reasonably good correlation coefficients.

Thermal properties were also found to be temperature dependent but not as sensitive as the physical and elastic properties. Thermal, electrical and accoustical properties all showed anamolous behavior when the sample was heated through the retorting temperatures.

Preliminary tests showed creep to be a major factor in determining overall deformation in heated oil shale.

The measured thermal and physical properties were utilized to develop several mathematical models to: determine resultant temperature profiles surrounding an in-situ retort; estimate kerogen recovery from the walls; and predict stress distribution in pillars during an in-situ retorting operation.

As was expected, oil shale was determined to be an excellent insulator and retorting isotherms were found to have minimal penetration into the pillars.

Finite-element structural analysis indicated that during retorting a very high compressive strength in the vertical direction will be generated at the edge of the pillar. It was determined that at 120 hours of retort heating, about three percent of the pillar support area would be lost. The corresponding loss of pillar support area for 800 hours of heating was estimated to be approximately 10 percent.

Due to occurence of creep even with mildly heated oil shale, it was determined that quantitative predictions of subsidence over an in-situ retort will have to take into account the long term creep effects.

The results of finite-element model simulating the in-situ heater tests showed good correlation with those measured in the field. The temperature profiles measured in the in-situ heater test experiment further confirmed the conclusion that the oil shale is an excellent insulator.

CONTENTS

LIST OF TABLES

LIST OF FIGURES

1.0 INTRODUCTION

1.1 Background

The oil shale deposits of the United States represent nearly 170 trillion barrels of potential shale oil in beds containing 5 to 100 gallons of oil per ton of raw shale. These domestic deposits are the most extensive to be found anywhere in the world. If this substantial resource were developed, the recovered shale oil would satisfy the nation's liquid-fuel requirements for many thousands of years. Unfortunately nearly all domestic oil shale beds that are not too lean are too thin, and/or too deeply buried to permit economical development. The oil shale of the Green River formation is an outstanding exception to this rule.

The Green River formation is a geological entity which underlies portions of northwestern Colorado, northeastern Utah, and southwestern Wyoming. The formation is divided into several discrete basins. The Green River, Great Divide, Washakie, and Sand Wash basins underlie some 14,000 square miles of Wyoming, Utah, and Colorado; and the Piceance and Uinta basins underlie approximately 20,000 square miles of Colorado and Utah. In the distant past, these basins were the sites of two large and durable fresh-water lakes. Silt and algal remains, the raw materials for oil shale, were deposited on the beds of these lakes over a 20-million-year interval which ended approximately 35 million years ago. The lakes disappeared as a result of climatic changes and upheavals in the surrounding terrain, but the rich oil shale beds remained (1).

Green River oil shale beds are continuous over intervals of up to several thousand feet, and the total potential shale oil resource is estimated to be well over eight trillion barrels. A conservative resource evaluation estimates a net recoverable oil reserve of nearly 80 billion barrels, a liquid-fuel reserve equivalent of 20 years of production from domestic petroleum and natural-gas wells at present production rates. In addition, substantial quanities of fuel gas, sodium compounds, and aluminum minerals could be produced as co-products of shale oil extraction.

Although the potential energy and mineral yields of Green River shales are fantastic, many problems must be resolved before any substantial portion of the resource can be utilized. Many of the problems are legal and political, since much of the shale resource is on public property. Many of the problems are economical, since extraction of shale-based fuels is expensive and shale oil must compete with more easily obtained conventional fuels in the market place. Many of the problems are environmental and social, since the shale deposits are located in sparsely populated regions. And many of the problems are technical, since oil shale processing has not yet been demonstrated on a sustained large-scale basis. Government and industry are cooperating in addressing these problems through an extensive program of research, development, and demonstration. Principal government agencies are the Department of the Interior (through its leasing program and through its in-house and contract research projects) and the Department of Energy (through

in-house projects at the national laboratories and research centers, and through numerous projects with universities and private firms). Smaller programs are also being sponsored by the Environmental Protection Agency and the National Science Foundation. In addition, several private firms are conducting oil shale research and development programs, some with financial participation by the government.

Nearly all of the present work on shale oil extraction is concerned with retorting or thermal conversion of the solid hydrocarbon constituent of oil shale into gaseous and liquid fuels. Although other processing techniques are available, retorting is the most highly developed and is the most likely candidate for near-term commercialization. Retorting may be conducted above ground in fabricated vessels, or it may be conducted underground (in-situ) within the oil shale formation. Above ground processing requires mining the raw shale, transporting it to the retorting vessels, and finally transporting the retorted shale for disposal either in a surface disposal area or back into the exhausted regions of the mine. Requirements for capital investment, for labor, and for process water are relatively high although probably not prohibitive, and substantial pollution problems may be associated with retorted shale disposal. In-situ retorting requires significantly less mining, and most of the retorted shale is left in its native environment. Estimated capital, labor, and water requirements are significantly lower than those for aboveground retorting. Pollution of surface drainage is only a very remote possibility,

but contamination of aquifers in the retorting zones may be a problem and must be avoided.

Thus, in-situ retorting is a promising method for developing Green River oil shale and particularly for extracting fuel values from the less attractive deposits which could not economically be developed by mining and aboveground retorting. The in-situ technique appears technically feasible, environmentally acceptable, and economically competitive. However, many technical questions remain to be answered before in-situ processing can be applied on any substantial scale. One of the most important questions involves the effect of heat generated during in-situ retorting on the oil shale pillars which comprise the walls of the in-situ retort. These pillars must be strong and competent to protect personnel during retort preparation and firing, and they must have sufficient strength during and after retorting to prevent subsidence, ground motion, surface damage, and, inter-retort leakage. Oil shale, containing volatile organics, is by nature a thermally unstable rock, and the copious heat generated during retorting is bound to degrade the oil shale in pillars and barrier walls. The fundamental information required to predict severity of pillar degradation is lacking from the technical literature. In particular, data on the thermal and mechanical properties of oil shale at elevated temperatures and under severe confining pressures are unavailable to those who wish to study pillar degradation. The research program covered by Bureau of Mines Contract No. H0262031 was designed to provide this essential information.

The work described in this report was performed under Contract No. H0262031 by personnel from the following organizations:

Excavation Engineering and Earth Mechanics Intitute, Colorado School of Mines

Mathematics Department, Colorado School of Mines

Electrical Engineering and Civil Engineering Departments, Colorado State University

Energy Resources Division, Colorado School of Mines Research Institute

1.2 Objectives

The principal objectives of the program were the identification and measurement of properties which significantly affect oil shale pillars and barrier walls during in-situ retorting. The program was designed to provide information on the effects of heat on pillar strength and integrity, use of rubble for pillar support, fuel recovery from pillars, and extent of subsidence and ground motion.

1.3 Approach

Following is a discussion of each of the major research efforts, i.e., phase I review and program development, sample characterization, physical testing, thermal and acoustic properties, electrical properties, and mathematical modeling and in-situ heater test.

1.3.1 Phase I status review

Phase I of the program called for a study of availabale literature and review of ongoing contracts to assess present and projected requirements of the shale oil industry. The review of ongoing projects and the comprehensive reference list have been included in this report as appendices. (pages 264-282)

1.3.2 Sample characterization and preparation

Oil shale is a heterogeneous mineral containing substantial concentrations of organic matter. It is not a true shale, but it does have a laminar structure and it does exhibit preferential cleavage. It does not contain oil, but its organic fraction can be converted to oil by heating. Oil shale is commonly classified according to the quantity of oil which is obtained from a crushed sample when the sample is heated to 500°C in a Fischer retort. In the United States, oil yield is generally expressed in gallons of oil per ton of raw material.

The heterogeneity of oil shale complicates study of shale's thermal and physical properties. Although the composition of the organic matter in Green River oil shale does not vary significantly from point to point in the formation, composition of the mineral fraction may vary substantially, particularly in the direction perpendicular to the bedding planes and especially in the saline-mineral zones which are primary candidates for in-situ development. Oil yield also varies substantially in a direction perpendicular to the bedding planes but varies relatively little along the bedding planes.

Principal mineral species in typical Green River shale are calcite (calcium carbonate) and dolomite (calcium magnesium carbonate). Together, these species constitute about 55% of the total mineral constituent. [2,3] Other common minerals include clays, quartz, pyrite, and 28 distinct sodium minerals, 7 of which are unique to Green River oil shale. [4] Of particular economic interest are nahcolite (sodium bicarbonate) which is a potential source of soda ash, dawsonite (dihydroxy sodium aluminum carbonate) and nordstrandite (aluminum hydroxide) which are potential sources of aluminum, and halite (sodium chloride). Nahcolite and halite often occur as highly visible inclusions in the shale beds, but they also occur as individual crystals disseminated through the mineral matrix. Dawsonite is generally not visible since it occurs as small disseminated crystals.

These minerals present problems to a thermal study for three reasons. First, identification and quantification of mineral phases is difficult, costly, and time consuming. Second, even if two shale samples have the same total concentration of mineral matter, their physical and thermal properties will be different if the mineral species in the respective samples are significantly different. Finally, many of the oil shale minerals are thermally unstable and decompose endothermically at elevated temperatures. Confusing measurements and erroneous interpretations can result if the heats of decomposition and the subsequent alterations in shale properties are not considered.

The original contract stated that the program was to be confined to shale from beds which did not contain significant quantities of nahcolite and dawsonite. A further restriction on the experimental program was that the testing temperature was not to exceed 500°C. These restrictions simplified the program considerably. The imposed temperature limit was below the normal decomposition temperature of calcite and dolomite - - the major mineral species in typical Green River shale. Nahcolite and dawsonite decompose at less than 500°C, but they were specifically excluded from the program. Sample characterization then was a matter of determining oil yield, identifying principal mineral species and their concentrations, and assuring that nahcolite and dawsonite are not present in significant quantities. Oil yield determination is not by itself sufficient for sample characterization. This is illustrated by the work of Smith and Young [5] who analyzed a large number of Green River shales for oil yield and for concentrations of nahcolite and dawsonite. They found that shales with essentially identical oil yields could have widely varying mineral compositions. For example, one sample with an oil yield of 16.7 gallons per ton had a dawsonite concentration of 4.63% and a nahcolite concentration of 35.8%. A sample with a nearly identical oil yield contained 13.34% dawsonite and 0.44% nahcolite. Thus variations in nahcolite concentration of two orders of magnitude were measured for samples with very similar oil yields, and dawsonite concentrations in the same two samples varied by a factor of three.

It is possible to estimate nahcolite and dawsonite concentrations from results of Fischer assay. [6] The method is generally satisfactory for Green River shales, but it does not provide information on any other minerals which might be present. Furthermore, the analyst is restricted to use of the modified Fischer assay method for determining oil yield. This method is highly developed and is the normal assay procedure, but it is destructive and cannot be utilized unless at least 100 grams of shale are available. It was concluded that some specific mineralogical characterization was essential to reliability of the program results. X-ray diffraction was considered the most convenient and economical method.

1.3.3 Mechanical properties research program

It was the purpose of the mechanical properties tests to determine those properties essential to the structural design of an in-situ retorting system. By the very nature of the system, this required that the physical behavior of oil shale be determined for the full range of temperatures and kerogen contents likely to be encountered in the area of the retort. The mechanical properties determined were: the uniaxial and triaxial compressive strength, the tensile strength, the modulus of elasticity, Poisson's ratio, and the density.

The factors considered likely to affect the compressive strength and elastic constants of the oil shale are: temperature, kerogen content, time at a temperature, orientation (loading with respect to bedding planes) and confining pressure.

Temperature is known to dramatically affect the strength of

oil shale [7], and initial tests in the current program were designed to examine this effect in the temperature range of ambient to 500°C for different oil contents. The U.S. Bureau of Mines' tests on Green River oil shale at elevated temperatures identified distinct "yield temperatures" at which the strength of oil shale became very low. [7,8] Although the determination of thermal properties of thermally weakened oil shale is necessary for determining temperature profiles in a pillar, it is unlikely that the weakened shale will have any significant supporting capability. Also, it is doubtful that meaningful physical properties can be measured for very high temperatures due to disintegration and exfoliation of the sample. Therefore, the yield temperature determined by the Bureau can be used as an upper bound temperature for a more extensive evaluation of oil shale physical properties.

Another important factor in determining the physical behavior of oil shale at elevated temperatures is the time a sample is kept at a specific temperature. Prolonged heating of oil shale at temperatures well below 500°C will tend to drive off the kerogen at some rate. Earlier tests analyzing the rate of retorting of large blocks of oil shale suggested a total-time-at-temperature of 32 hours will be sufficient to ensure kerogen transfer stabilization in the test samples. [9] A lower bound of 2 hours at temperature based on heat flow analysis, should ensure equilibrium and allow reasonable times between tests. The range of kerogen contents is recommended as 10 to 30 gallons per ton. Confining pressure effects should be kept below 1,500 psi since

it is unlikely rubblized shale will provide any support to the pillar at greater pressures.

1.3.4 Thermal property measurements

Hydrocarbons may be recovered from oil shale by several exotic methods (solvent extraction, biological degradation, direct hydrogenation) but the only practical method at present is pyrolysis -- chemical reaction induced by heat. The other methods have been tested only on a small laboratory scale, and all technologies which are currently being considered for commercial recovery of fuels of oil shale involve some form of pyrolysis or retorting.

A retort is a "vessel" in which heat is applied to broken oil shale and from which carbonaceous fuels are recovered in the form of oil or gas. In aboveground retorts, heat is applied by contacting a heat-carrying gas, liquid, or solid with small pieces of shale which are generally less than three inches in the largest dimension. In in-situ retorts, heat is applied by contacting a heat-carrying gas or liquid with shale particles which are much larger and which cover a wide range of particle sizes. Particles to be retorted in an in-situ retort may range from a fraction of an inch to many feet.

The economy of both aboveground and in-situ retorting operations is strongly affected by the rate at which the shale can be heated to retorting temperatures (ie. 900^{o}F). In aboveground retorts, rapid heating rates are assured by the small particle sizes of the broken shale. Rapid heating rates are much more difficult to obtain in in-situ retorts. Except for discrete

leached zones, shale beds in the Green River formation are nearly impermeable to fluid flow. The beds must be fractured artificially in order to obtain reasonable flow rates of heat-carrier fluid. Creating any extensive fracture pattern in buried shale formation is difficult, and creating an in-situ retort with a uniform distribution of small shale particles is nearly impossible without mining and controlled blasting. In-situ retorts will therefore contain very large particles. Such large particles can be completely retorted, as indicated by simulated in-situ experiments in the NTU retort at Laramie [9,10], but much time is required since heat transmission from the ambient heat carrier to the interior of such large particles is conduction limited. Oil shale has a thermal conductivity about equal to that of insulating firebrick so heat conduction and subsequent fuel recovery are very slow processes.

Quantification of heat transfer rates is critical to technical and economic evaluation of candidate retorting schemes. In addition, heat transfer into pillars or barrier walls which confine the rubbled shale in an in-situ retort could have serious repercussions on the surface environment and on the safety of mining personnel. As was discussed in detail previously, retorted oil shale has little compressive strength. Rich oil shale which has been fully decarbonized loses its competent structure and disintegrates into a fine powder [11]. The outer regions of support pillars will be retorted along with the adjacent rubbled shale, and the retorted portion of the pillars will contribute little to support of the retort roof. If

the retorted zone penetrates too far into the pillars, total compressive strength may be insufficient, and the pillars may collapse with consequent surface subsidence and with destructive ground motion.

Penetration of the retorted zone into the interior of support pillars will depend in part upon the temperature history of the retort and in part upon the thermal properties of the pillar material. Thermal studies to evaluate such penetration and to design for subsidence prevention require knowledge of the thermal properties of oil shale. Several prior investigators have defined some of oil shale's thermal properties [8,12-17] These workers studied thermal-property variation over a wide temperature range and for a significant range in oil yield. To our knowledge, however, no adequate work has been conducted on oil shale which is confined under pressures approaching the static load on a deeply buried pillar. The current program did, however, investigate the effect of confining pressure on thermal properties.

The underlying heat-flow mechanisms which determine retorting rates in oil shale have been investigated. Studies are quite complicated since oil shale is a complicated material. It is heterogeneous, anisotropic, and often discontinuous. It is essentially a mineral, but the composition of its mineral fraction may vary widely from point to point. Organic matter may constitute a few weight percent of lean oil shale or many weight percent of very rich shale. Thermal properties of oil shale are functions of organic content, of mineral composition, of

pressure, of temperature, of temperature history, and of the direction of heat flow. A large body of data needs to be accumulated before a coherent understanding of oil shale's thermal properties can be obtained.

Because of this heterogenity and variability, any thermal property measurement method which uses data obtained from different samples at different times is highly suspect. The complex problem of experimental measurement is simplified somewhat by the lateral continuity of the varves, or sedimentary stratification layers within a given oil shale bed. Because of the nature of its deposition, oil shale's varve structure may be traced for great distance in a horizontal direction. Thus, a single slab of oil shale may yield several samples which are consistent in composition and thermal behavior. Samples taken from the same slab will provide a much more consistent model of the variation in properties than will multiple samples obtained from widely separated locations in the formation. Previously published studies of the thermal properties of oil shale used the "transient line probe" method [12,15]. The method is not well suited to oil shale. For a low-conductivity solid material such as oil shale, the small probe-size required in this method, coupled with problems of probe-to-sample contact resistance, relative location of sample boundaries and temperature sensor, and the need to drill long uniform holes in the sample for probe insertion, severely limit the accuracy of the results. As mentioned by Tihen, et.al.[12], "only the first portion of the heat curve could be used... perfect contact between the shale and

the heating source is unattainable". Of equal importance is the requirement of line-probe theory that the time-temperature relationship be approximated by an exponential integral. This approximation implies a simple diffusional heat flow mechanism [25]. Oil shale undergoes a number of chemical and physical transformations during heating, and heat flow is definitely not a simple diffusional mechanism. Data obtained indicate that significant changes occur in the thermal conductivity and electrical impedance in the vicinity of transformation temperatures. At high temperatures, for example, the effective thermal conductivity increases, probably due to increasing electronic transport mechanisms.

These complications limited previous investigators to data acquisition at only a few temperature points [12,15]. Techniques which are limited to a few data points or which must rely on a thermal history technique of heating the sample and then measuring the thermal properties while reheating are not well suited to oil shale. We have found that temperature cycling and rate of heating can significantly affect the behavior and the properties of oil shale.

Finally, the absolute measurements required by the line-probe method depend upon the applicability of a particular heat-flow model and upon the transient response and accuracy of the measurement devices which are employed. The chemical, structural, and orientational dependence of oil shale properties do not lend themselves well to measurements of this type.

We used the "comparative method" of thermal property measurement for the current program, since this method has particular advantages for oil shale studies. It requires only relative temperature measurements and relies less on absolute measurements than do other techniques such as the transient line-probe method. Two known references are used to eliminate the directional dependence of heat flow. Large samples are used, which are more representative of in-situ shale formations. Contact areas are large and are easily maintained as heating progresses. After the initial preparation stages of coring, sawing, and grinding; samples need not be disturbed by drilling of thermocouple wells.

The comparative technique is applicable over wide ranges of temperature, pressure, and thermal conductivity. Of particular importance , the technique is readily amenable to measurement of several parameters during a single run. For example, thermal conductivity can be measured at arbitrary points over the entire temperature interval of interest in a single run on one sample. Several other thermal properties, such as thermal expansion coefficient, can be measured simultaneously with the conductivity measurement.

Properties to be measured during this task were thermal conductivity, thermal diffusivity, thermal expansion coefficient, electrical resistivity, electrical impedence, and dynamic elastic properties. These properties were measured for shale samples with oil yield varying from 10 gallons per ton to 60 gallons per ton. Temperature was varied from 100 to 1000^{o}F, and pressure was

varied from 0 to a pressure equivalent to overburden pressure on a deeply buried oil shale pillar. Properties were measured for heat flow both parallel with and perpendicular to the bedding planes of the shale samples.

Electrical resistivity provides valuable supplementary information on thermal property behavior. For example, experiments at CSU have revealed that both thermal conductivity and electrical resistivity increase at high temperatures, pointing to a possible electronic heat-flow mechanism. There are also possible field applications of electrical resistivity measurements to thermal condutivity measurements in-situ. For example, a borehole probe which reads electrical resistivity can be used to determine thermal conductivity of deeply buried oil shale formations. An even stronger correlation may be obtained between thermal impedance and electrical impedance.

Electrical resistivity and electrical impedance are readily obtained experimentally and have been included along with the thermal properties.

As a cross check with the moduli determined from compression testing, and as an identifier of transition stages in heated oil shale, dynamic wave velocities were determined concurrently with the other thermal tests. This could provide valuable information relative to future remote monitoring of in-situ retorting processes and thermal effects.

1.3.5 Modeling and structural calculations

The mechanical and thermal test data are organized, and analyzed and correlated to form a material property model. This

material model is be used to perform two types of structural calculations. One conventional calculation is based on simple mechanics, and the other calculation involves mathematical or computer simulation using finite difference or finite element techniques. The effect of temperature on strength of pillars, extent of weakening of support pillars, rubble as pillar support to prevent subsidence, kerogen recovery from pillars and extent of surface and subsurface damage or disruption are evaluated with the methods developed.

A mathematical model of a physical or chemical process is a very useful research tool. In general, only a limited amount of experimental work is required to develop and verify the model, and once development and verification are complete, proposed alterations to the process may be examined and evaluated without additional experimentation. Subtle aspects of the process can often be examined in greater detail in the model than is possible under normal experimental conditions. The expense involved in developing a model can easily be justified by the savings in experimental equipment and manpower and by the greater understanding of the process which results from careful application of the model.

In some cases, mathematical modeling may be the only accurate route by which a very large scale process can be evaluated without actually constructing and operating a full-size physical model of the system. In-situ retorting of oil shale is a good example. Proposed in-situ retorts are enormous by comparison with the small surface units which have been used to

simulate in-situ retorting. Predictions based on data from such surface units must be made with great care since flow characteristics, local heating rates, and overall conversion rates are often sensitive to the physical size of the unit.

Our research program uses mathematical simulation for three purposes. First, a conductive heat-transport model was modified to utilize the temperature and pressure variant thermal properties which were derived in the experimental program. Data on reaction kinetics and transport mechanisms is obtained from the literature [19-24]. The transport model is used to predict temperature distributions in in-situ pillars corresponding to imposed temperature histories at the pillar surface. Surface temperature variation is selected to correspond to that anticipated for actual in-situ retorting on a large scale. This model yields data on the depth of penetration of the retorting isotherm into the pillar and permits calculation of oil yield (kerogen conversion) in the pillar itself.

Temperature-distribution predictions are used in a structural analysis program to evaluate thermal stresses within the pillar. Thermal expansion coefficients derived in the experimental program are incorporated into the model as well as exfoliation and loss of strength in the outer portion of the pillar due to penetration of the retorting isotherm. The effect of confining pressures from adjacent oil shale rubble is also evaluated.

Stress/strength predictions are coupled with results of physical testing to predict pillar strength and possible pillar failure.

1.3.6 In-situ heater tests

As discussed previously, part of the study was the development of a mathematical model of an oil shale pillar using the thermal and physical properties determined. Several aspects of the model had to be qualitatively determined, such as retort wall condition, effective heat transfer at the wall, temperature history of the retort, and condition of the oil shale surrounding the retort (i.e., presence of blast damage or thermally induced fractures). Since these parameters can significantly affect the conditions predicted by the model, reasonable estimates of these parameters are required.

The only realistic way to obtain estimates of these conditions is through observation of conditions in the field surrounding an in-situ retort, and most importantly, to measure temperature profiles in the retort wall as the flame front progresses through the retort.

The proprietary nature of current in-situ retorting experiments has made it impossible to be able to directly monitor an actual retort. It is possible, however, to simulate retort conditions in the field with a reduced scale heated borehole test. Temperatures, burn rates, and thermal distributions of an in-situ retort can be simulated using proportionally controlled segmented electric heaters. Carefully placed and monitored thermocouples can be used to provide both vertical and radial temperature distributions in the oil shale surrounding the simulated borehole.

A simulated in-situ retorting system, as described above, was created consisting of a heated borehole with a matrix of thermocouples surrounding it to determine temperature profiles before, during and after retorting, and the results applied for verification of the developed model.

Since the surface of oil shale surrounding the borehole is vertically loaded, and changes in the load monitored during testing, estimates of thermal expansion and relaxation (due to creep) can be assessed from the data.

Such a program provides the essential information required to complete the development of mine design criteria, and allow the determination of environmental consequences related to potential surface subsidence associated with in-situ oil shale retorting.

1.3.7 Testing of higher grades

The intent of the U.S. Bureau of Mines sponsored research on "The Effects of In-Situ Retorting on Oil Shale Pillars" was to provide the necessary information for effective modeling and design of an in-situ retorting operation. The original concept was that in-situ methods would be principally applied to areas of relatively lower grade in the range of 10 to 30 gallons per ton. However, it had become apparent that initial commercial in-situ retorts will contain significant zones having grades higher than 30 gpt. Zones of approximately 40 gpt occur in thickness of 10 to 50 feet in several current and planned retorts. At higher temperatures, these zones may have controlling importance in the design of an in-situ retorting operation. It thus became

apparent that to establish a complete criteria for pillar design and subsidence prediction, oil shale grades up to 40 gpt should be included in the testing program.

Since the personnel, equipment, and expertise required were available as part of the U.S. Bureau of Mines' effort, the most efficient approach was to accomplish the required tests concurrently with the Bureau's program. It was therefore decided to expand the testing program to include oil shale samples with grades 35 to 40 gpt, following the procedures outlined for the U.S. Bureau of Mines program for oil shale grades of 10 to 30 gpt.

2.0 PROCEDURES

2.1 Status Review

As part of the Phase I assessment of the current and projected needs of the oil shale industry, organizations active in the design or development of in-situ retorting techniques were contacted. Their input was solicited as to the pertinent variables that should be investigated and the respective levels of those variables. Also reviewed were various retort configurations and system layouts to include size of chambers, chamber separation, pillars, depth, burn rate, duration of temperature, and time during which extraction continues. The discussions confirmed the need for the work planned for this investigation and were very helpful in the model selection and evaluation portions.

Often a company, for proprietary reasons, could not provide

us with much information, but in all cases considerable interest was shown in the potential results of the investigation. A brief summary of the information gained from the more communicative organizations, along with a comprehensive reference list, is included in the appendices.

2.2 Sample Selection and Characterization

2.2.1 Sample acquisition

On October 5, 1976, project personnel visited the oil shale operations at Anvil Points near Rifle, Colorado, and at Logan Wash near De Beque, Colorado. Eight large blocks of oil shale were obtained from Logan Wash - - site of Occidental Petroleum's in-situ operations - - and 5 sample blocks were obtained from Anvil Points -- site of the Paraho operation. Samples were selected in the field by measuring the approximate specific gravity of pieces broken from the sample and by estimating the potential oil yield from the oil-yield/specific gravity tables of Hendrickson [25]. More precise oil yields were subsequently determined by modified Fischer assay at Colorado School of Mines Research Institute.

2.2.2 Selection and preparation

It is possible to estimate nahcolite and dawsonite concentrations from the results of Fischer assay [26]. The method is generally satisfactory for Green River shales, but it does not provide information on any other minerals which might be present. Furthermore, the analyst is restricted to use of the modified Fischer assay method for determining oil yield. This method is highly developed and is the normal assay procedure, but

it is destructive and cannot be utilized unless at least 100 grams of shale are available. We concluded that specific mineralogical characterization is essential to reliability of the program results, and we chose x-ray diffraction as the most convenient and economical method.

Test specimens were prepared by cutting and coring the large blocks obtained from Anvil Points and Logan wash sites. Coring was done perpendicular and parallel to bedding. In this report, cores taken perpendicular to bedding are referred to as the vertical cores whereas those parallel to bedding are the horizontal cores. The pieces which remained after the samples were recovered were assayed for oil yield and analyzed for mineral content. Oil-yield determination was done by modified Fischer assay, if at least 100 grams of material were available, or by a non-destructive technique such as nuclear magnetic resonance if the analysis sample was insufficient for Fischer assay. Mineral composition was estimated by x-ray diffraction (27,28). Individual samples were inspected for presence of visible inclusions of saline minerals such as nahcolite and halite. Samples containing such inclusions were not run. Cored or cut samples were prepared for testing by parallel-grinding the radial faces. After preparation, the samples were inspected for surface cracks by spraying with alcohol to highlight any fractures which might be present. Cracked samples were not run. Coring, cutting, and grinding of samples were conducted at the Colorado School of Mines. Fischer assay and x-ray diffraction were conducted at the Colorado School of Mines

Research Institute.

2.2.3 X-ray diffraction

Following oil-yield determinations, 8 samples with oil yields in the range of interest were selected for additional testing. Each sample was submitted to qualitative x-ray diffraction analysis on CSMRI's diffractometer to determine gross mineralogy and to check for presence of nahcolite and dawsonite.

Two complete diffractometer runs were made for each sample. The first run was on Fischer assay feed which had been subjected to fairly vigorous grinding in a Bleuler mill. A second diffractometer scan was run on screened fines from a single pass through a jaw crusher. The two tests were run to detect any effect of grinding on carbonate composition.

One additional run was made on a single piece of shale which contained a visible inclusion of material suspected to be nahcolite. X-ray analysis showed the inclusion to be analcime.

2.2.4 Wet-chemical analysis

The x-ray results indicated negligible dawsonite concentration but no corresponding evidence was found for nahcolite. Consequently, it was decided to analyze the samples for nahcolite according to the rigorous chemical procedure derived by Smith and Young [29]. The procedure involves dissolution of nahcolite from the oil shale in cold water. Sodium is determined in the leachate by atomic absorption and provides a direct measurement of nahcolite concentration in the sample. Aluminum and non-water-soluble sodium are dissolved from the water-leached residue in hydrochloric acid. Acid-soluble

sodium can be used as a direct indication of dawsonite content if interfering minerals such as analcime are not present. Acid-soluble aluminum can be used as a second check on dawsonite concentration in the absence of interfering minerals. In these tests, analcime was known to be present, but acid solution and atomic absorption analyses were still performed to provide a check on x-ray results for analcime.

2.3 Physical Properties Tests

It is the purpose of the physical properties tests to determine those properties essential to the structural design of an in-situ retorting system. By the very nature of the system, this requires that the physical behavior of the oil shale be determined for the full range of temperatures and kerogen contents likely to be encountered in the area of the retort. Earlier studies (30-33) have helped to identify those factors which affect the behavior of oil shale in an underground retorting system. Those considered as most significant are: temperature, kerogen content, time at temperature, mineral content, orientation to the bedding planes, and confining pressure. Within this range of variables, the design engineer is interested in the compressive and tensile strengths, elastic moduli, and thermal properties at all levels of conditions likely to be encountered in the field.

An upper bound temperature of 500°C was selected as it approximated the likely retorting temperature of an in-situ retort. To provide a sufficient number of points to determine a temperature change relationship, the range of temperature from

20°C to 500°C was divided into 5 temperature stages; 20°, 140°, 260°, 380° and 500°C.

Since the application of in-situ retorting is envisaged for the lower grade beds less suitable for underground or open pit mining, the range of kerogen content was initially set at from 10 to 30 gallons per ton and later extended to 40gpt. Mineral content was not to be a controlled variable. However, samples were characterized with respect to mineral content. Again, for statistical purposes, kerogen content was divided into seven levels: 10, 15, 20, 25, 30, 35 and 40 gallons per ton.

Since at any given temperature some kerogen may be driven off, it becomes important to consider the time the sample was at that temperature. A series of preliminary tests were undertaken to define the time-at-temperature affect.

Three confining pressures were used: 3.4, 6.9 and 10.3 MPa (500, 1000, 1500 psi). An upper bound of 10.3 MPa (1500 psi) was selected as it is unlikely higher confining pressures would be generated in currently envisioned retorting systems.

The full series of tests was performed for orientations perpendicular and parallel to the bedding. (Vertical and horizontal cores, respectively). Figure 2.1 illustrates the loading direction with respect to bedding for the vertical and the horizontal cores.

The triaxial compression tests were accomplished in a specially designed high-temperature pressure cell. Included in the cell are devices for measuring load, axial deformation, and radial deformation of the sample. Also, temperature and pressure

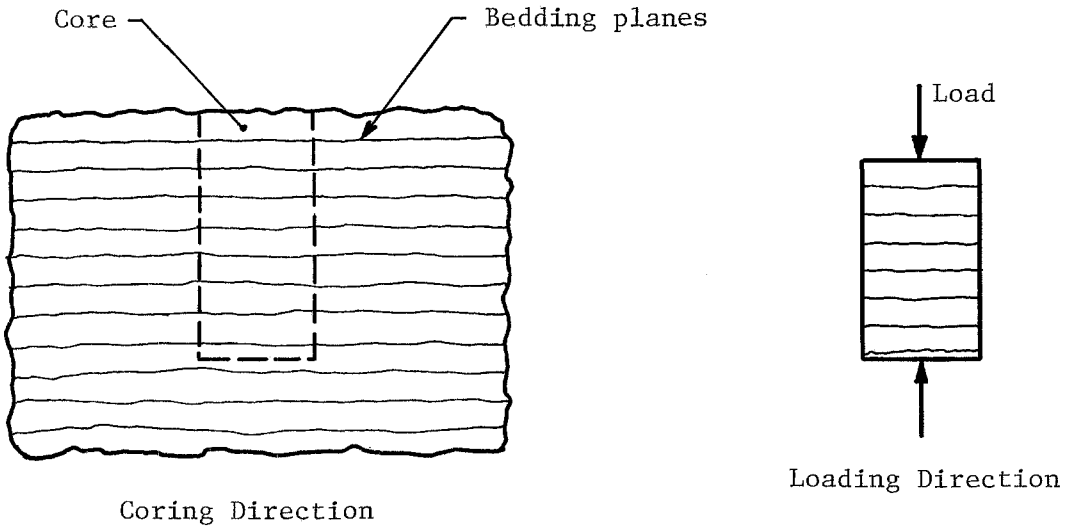

a. VERTICAL CORES

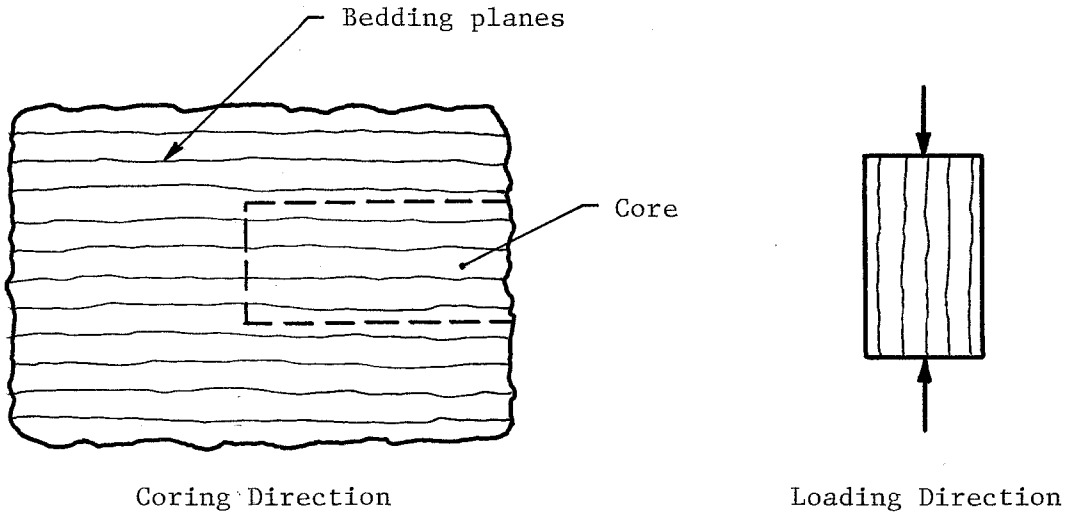

b. HORIZONTAL CORES

Figure 2.1 Coring and loading directions for the vertical and the horizontal cores used in mechanical property tests for oil shale.

are continuously monitored and controlled. Due to the high temperature involved, nitrogen gas is used as the confining media. The sample is heated by means of a jacket surrounding the sample which consists of a three-zone heater controlled so as to maintain a uniform temperature over the length of the sample. The 2-inch diameter by 4-inch long oil shale specimen is placed in a special aluminum-cylinder-and-platen-system and mechanically sealed with a taper ring arrangement. The sample is then vented to the outside of the cell by means of a stainless steel tube. This is to allow escape of off gases during heating and testing, and to maintain atmospheric pressure on the inside of the aluminum-cylinder-and-platen system. The samples, already in their sealing containers, are preheated at the desired test temperature for at least 12 hours. Immediately prior to testing, the sample is transfered to the high-temperature pressure cell. After closing the cell and placing it in the testing machine, the internal heater jacket is turned on and the desired confining pressure applied. Due to the thermal mass of the system, it takes about 5 minutes for the system to come to equilibrium at the required temperature. After reaching thermal stability, the loading of the sample is begun. All conditions within the cell are continuously monitored. The load, along with axial and radial deformations are recorded on an x-y-y recorder over the duration of the test. This information is also sent to a PDP-11 computer for analysis and presentation. Following failure of the sample, the heater jacket is turned off, the pressure reduced, and the sample removed for visual inspection. The process can

then be repeated.

The Brazialian indirect tensile strength tests were fairly easy to accomplish. Samples were prepared 2 inches in diameter by 1-inch long and, as for the triaxial samples, preheated for 12 hours at the desired temperature prior to testing. The samples are then taken one by one from the oven and placed on edge in the compression testing machine. Thin pieces of cardboard are placed along the upper and lower edges to slightly distribute the load. The sample is then loaded to failure and the corresponding maximum load recorded.

2.4 Thermal, Electrical and Acoustic Properties

As a member of the program team, Colorado State University (CSU) carried out laboratory experiments to derive the key thermal properties required in the analyses and evaluations being carried out at the Colorado School of Mines. The CSU program was initially formulated to provide basic data on the thermal transport properties of oil shale of various grades, the thermal expansion of the shale and the electrical properties of shales during retorting which might be useful in the design and application of in-situ instrumentation to monitor retorting effects. As a result of recent improvements in high-temperature ultrasonic-measurement techniques, the CSU program was expanded (February 1977) to include the measurement and analysis of ultrasonic-wave propagation in oil shale samples during retorting. Such ultrasonic data provides further insight into the physical mechanisms controlling thermal expansion, plastic deformation and sample creep during retorting and provides direct

data on modifications in the effective elastic moduli during retorting. In subsequent sections, the experimental method developed and employed at CSU, the data obtained on oil shale samples of a broad range of grade, and the analysis of this data in terms of in-situ oil shale pillar response are discussed.

2.4.1 Thermal transport properties

The thermal transport properties of an isotropic material are completely defined by any two of the three parameters: conductivity (K), diffusivity (k), and heat capacity (C_p). As these three properties are related by the equation:

$$K = p\ C_p k$$

where p is the density, knowledge of any two can be utilized to calculate the third. The experimentally most straight forward method for determining thermal conductivities involves measurement of steady-state heat flow in a one-dimensional geometry. The experimental arrangement illustrated in Figure 2.1 has been used at CSU as well as by several other investigators to determine thermal conductivities in numerous materials. Nominally one-dimensional heat flow is realized in the stack arrangement illustrated in Figure 2.2 by surrounding the cylindrical sample and reference materials with a guard heater maintained at the same temperature as that measured at the interior of the sample. A thermal gradient maintained across the stack and sample by the upper and lower stack heaters, provides the one-dimensional thermal transport. Under steady-state conditions the same heat flux is transported across any horizontal plane in the stack and a knowledge of the thermal

Figure 2.2 Thermal Conductivity Test Stack

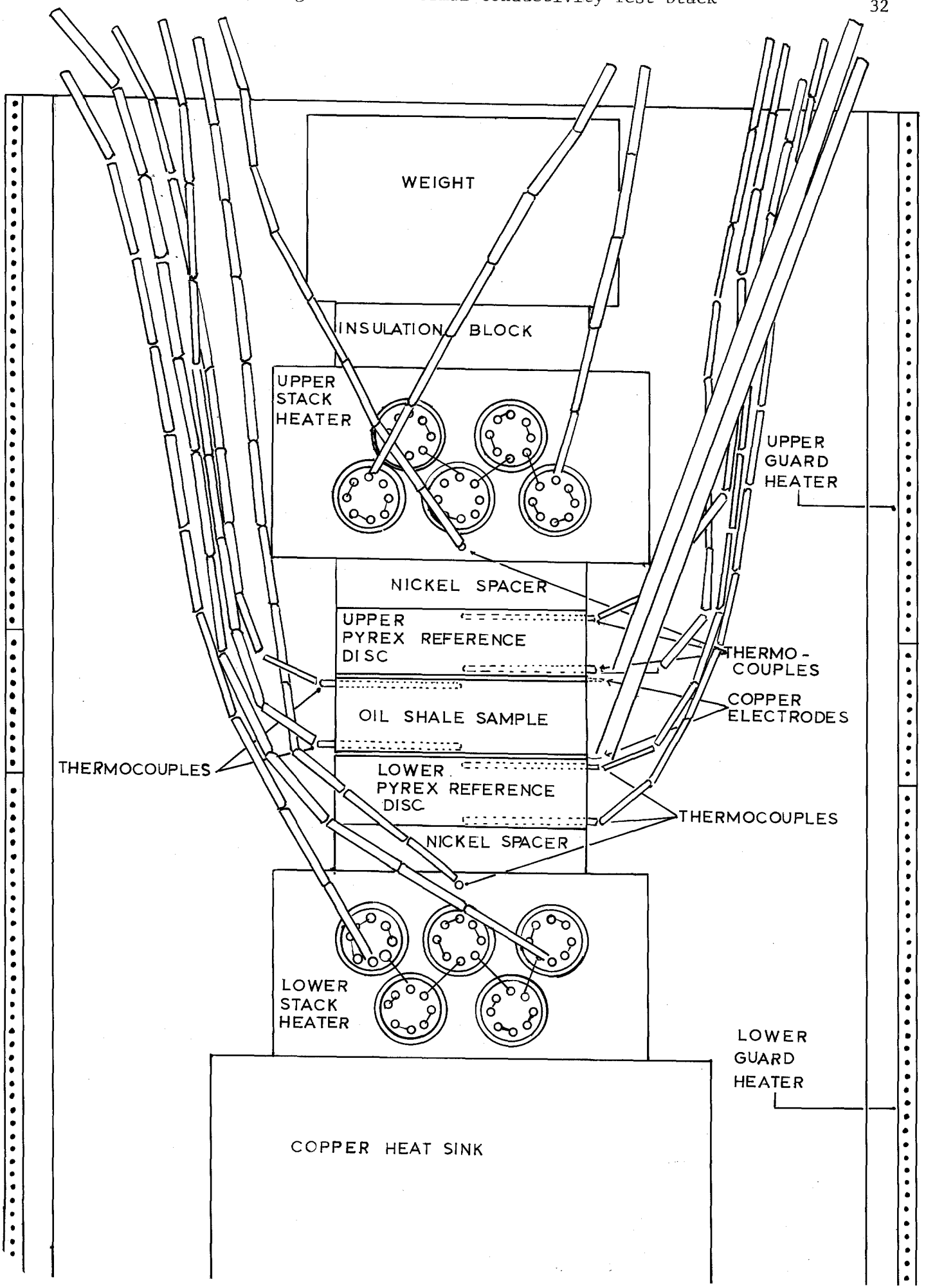

properties and temperature gradient across the reference disks (pyrex) allows this heat flux to be precisely determined. This heat flux, when coupled with the measured thermal gradient across the sample, provides a unique and precise measurement of the sample's thermal conductivity. In the CSU program, steady-state conditions were obtained at numerous temperature levels during the heating (and occasionally during the cooling and reheating) of oil shale samples. The validity of the steady-state assumption was evaluated by comparing the heat flux across the two pyrex reference disks and thus the energy balance of the sample.

The biggest limitation of the steady-state method to the determination of thermal conductivities in oil shale relates to the predominatly endothermic chemical reactions which began to occur in this rock at elevated temperatures. These reactions make it extremely difficult and time consuming to obtain good thermal conductivity data and do not allow for the determination of effective thermal conductivities or heat capacities as the reactions are taking place. As will be discussed in more detail in later paragraphs, a transient-thermal-analysis method has been developed at CSU in an effort to obtain thermal transport data on chemically reactive samples.

Using the steady-state thermal-conductivity method, data has been obtained on a broad range of oil shale grades for material obtained from both the Logan Wash Mine of Occidental Petroleum Corporation and the Anvil Points Mine of the Department of Energy located near Rifle, Colorado. Thermal conductivities have been

obtained for heat flow both perpendicular and parallel to the varve structure of the shale.

True steady-state thermal-conductivity data is difficult to obtain once significant kerogen decomposition begins to occur, due to the endothermic* nature of the reaction. Consequently, data on thermal conductivities and/or heat capacities over 350° should be obtained with a method capable of yielding effective conductivities and heat capacities which would include directly the effects of kerogen decomposition. As long as the endothermic reactions, which would appear as perturbations to heat capacity, are not strongly time dependent, the effective thermal conductivities and heat capacities obtained with a transient analysis method over short laboratory time would be reasonably applicable to analysis of field situations with much longer characteristic times.

Due to the need for data on the effective thermal conductivities and heat capacities during kerogen decomposition, a transient-thermal-analysis method has been developed at CSU for determining these properties in oil shale samples, even when they are undergoing significant chemical transformation. The transient-thermal-analysis method employs an experimental configuration very similar to that used in the steady-state thermal measurements and also in the ultrasonic-velocity measurements discussed in a later section. The important features of the stack geometry utilized for the transient measurements is illustrated schematically in Figure 2.2. As for

*For experiments conducted in an inert (nitrogen) atmosphere where oxidation of the kerogen is precluded

the steady-state measurements, pyrex reference disks are utilized on both sides of the sample to provide known thermal boundary conditions for the oil shale sample. As for the steady-state measurements, one-dimensional heat flow is assumed and an appropriately-regulated guard heater is utilized to minimize lateral heat transport into or out of the sample. In contrast to the steady-state measurement method, the transient method does not require that a temperature gradient be carried across the sample stack. Rather than utilize thermocouples embedded in the oil shale samples and the pyrex reference disks as in the steady-state measurements (see Figure 2.2) highly conductive thin disks of aluminum are utilized to equilibrate temperatures in lateral directions and provide a reference plane for making temperature measurem ultrasonic-velocity measurements discussed in a later section. The important features of the stack geometry utilized for the transient measurements is illustrated schematically in Figure 2.3. As for the steady-state measurements, pyrex reference disks are utilized on both sides of the sample to provide known thermal boundary conditions for the oil shale sample. As for the steady-state measurements, one-dimensional heat flow is assumed and an appropriately-regulated guard heater is utilized to minimize lateral heat transport into or out of the sample. In contrast to the steady-state measurement method, the transient method does not require that a temperature gradient be carried across the sample stack. Rather than utilize thermocouples embedded in the oil shale samples and the pyrex

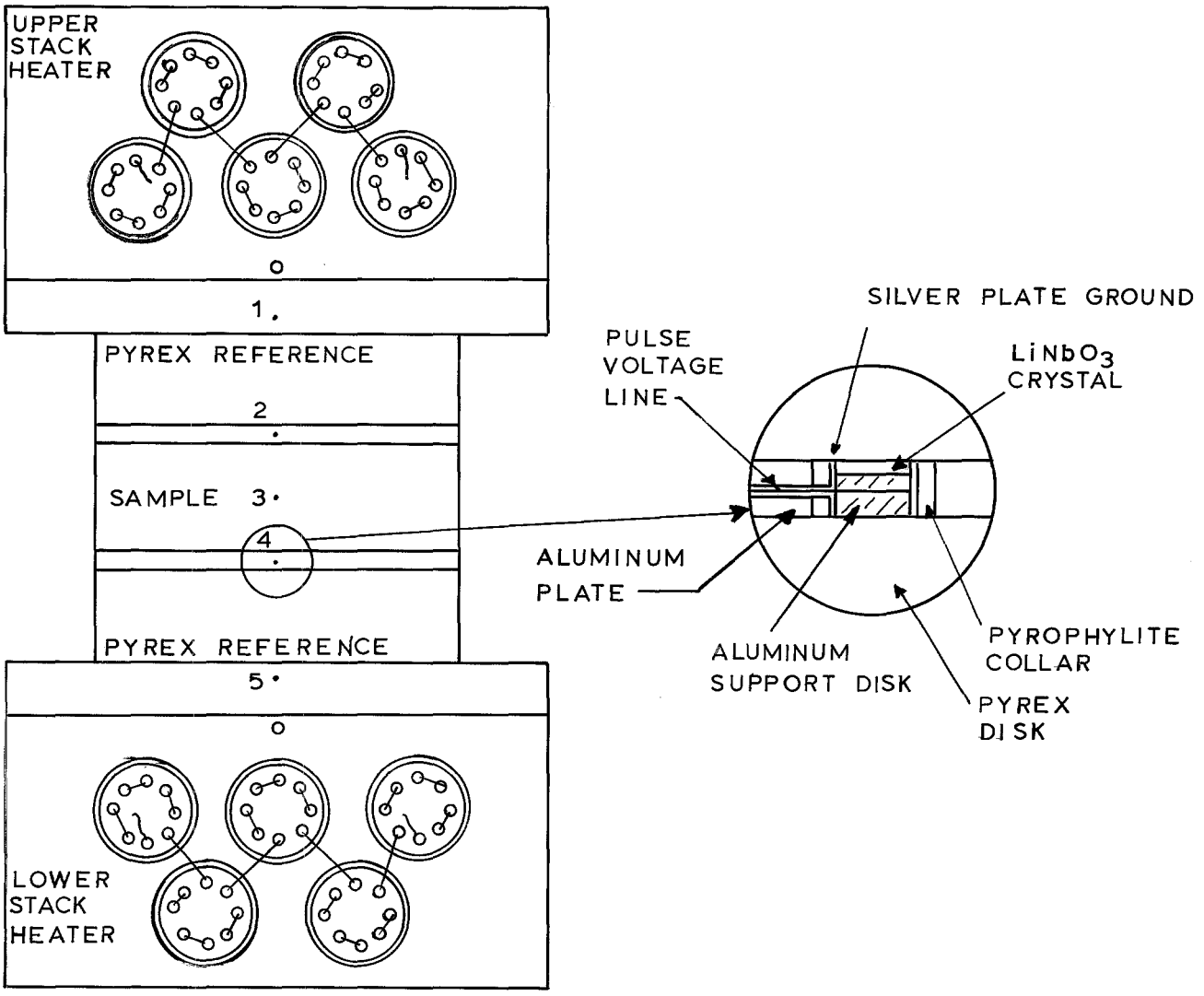

Figure 2.3--Stack arrangement for determining thermal properties by a transient analysis (Inset shows geometry of $LiNbO_3$ Transducers used in ultrasonic measurements.)

reference disks as in the steady-state measurements (see Figure 2.2), highly conductive thin disks of aluminum are utilized to equilibrate temperatures in lateral directions and provide a reference plane for making temperature measurements. Use of these disks, as illustrated in Figure 2.3 reduces significantly the sample preparation time required for thermocouple emplacement. Only one thermocouple, at the center of the oil shale sample, need be installed for any experimental run.

The method of data analysis in the transient method basically involved two independent operations, one for determining the heat capacity of the sample and the other for determining thermal diffusivity of the sample. Because the thermal state of the pyrex reference disks are well known, it is possible, with measurement of temperature versus time on each side of the pyrex disks, to calculate the temperature profile in each disk. From these profiles the rate of heat transport into the oil shale sample can then be calculated. The temperature derivative of this heat transport provides directly the effective thermal capacity of the sample. If endothermic or exothermic chemical reactions are occuring within the sample they will appear as perturbations in the heat capacity with the apparent heat capacity obtained from the analysis being a good representation of the physical processes which should be accounted for in any detailed modeling efforts. Measurements of the thermal lag of the sample, as indicated by comparing the central thermocouple to the temperatures of the two aluminum disks bounding the sample, coupled with the time derivatives of

the temperature changes on the two sample boundaries enables the one-dimensional diffusivity equation to be solved so that the effective thermal diffusivity of the sample as a function of temperature is obtained. This diffusivity may then be combined with the independently determined heat capacity to arrive at an effective thermal conductivity for the oil shale sample. Details on the basic theory for the transient method of analysis and the supporting numerical data-treatment methods are discussed in Appendix 6.4.

As the transient-thermal-analysis method requires that a minimum of five temperatures be continuously monitored and that significantly complicated mathematical operations be performed on these temperatures in order to derive thermal diffusivity, heat capacity and conductivity, it is necessary that the raw temperature data be digitally recorded. As illustrated in Figure 2.4, a Hewlett-Packard 9825 microcomputer is utilized both to control the data recording and to perform the data analysis. The ultrasonic measurements discussed in the following section are also controlled and monitored by the HP-9825, and the interfacing of these measurements is also shown in Figure 2.4. Temperatures are read by means of a Hewlett-Packard 3495A programmable scanner interfaced to the basic thermocouple monitoring unit which includes electronic cold junctions. As the transient method requires relatively uniform and rapid heating rates it would have been advantageous to have had temperature programmers available to control the stack and guard heaters. Due to the limited number of experiments performed, however, it was considered more

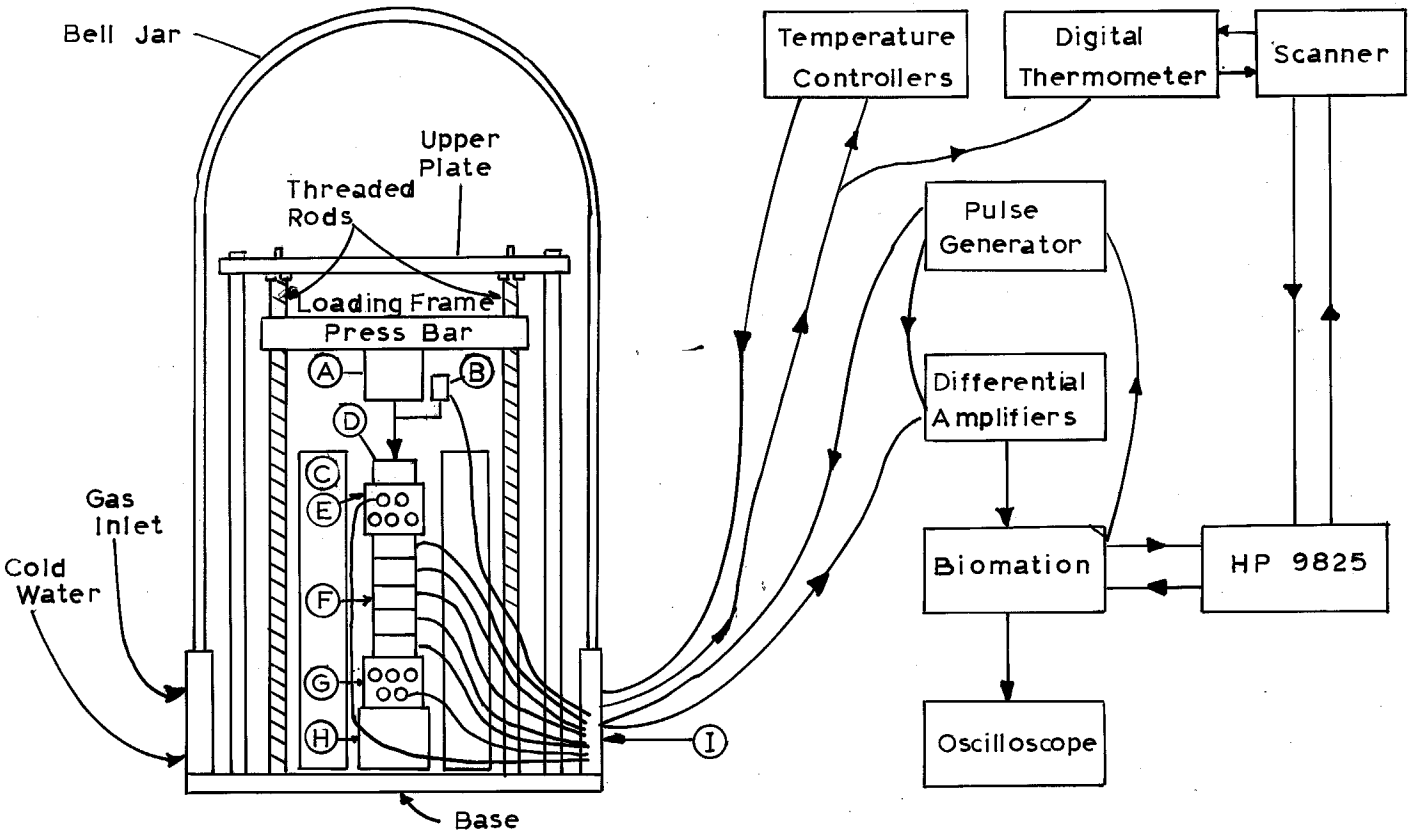

A - Pneumatic Cylinder
B - LVDT
C - Guard Heaters
D - Upper Cooling Block
E - Upper Stack Heater
F - Oil Shale Sample
G - Lower Stack Heater
H - Lower Cooling Block
I - Base Ring or Electrical Lead Throughs

Figure 2.4 Schematic Arrangement of Digital Data Acquisition Systems for Thermal and Accoustic Measurements

cost effective to manually program the temperature controlling units so that adequately uniform heating rates were achieved. Experiments were performed with heating rates of 2 to 4°C per minute. The faster heating rate was found to give more reliable data due to the fact that lateral and other unknown to the controlled one-dimensional heat flow into the sample.

2.4.2 Ultrasonice measurements

The various ultrasonice measurement techniques provide a well developed and accepted means for rapidly determining the elastic properties of most materials. Ultrasonic methods have been successfully used at room temperature for measuring the anisotropic elastic properties of oil shale (34). The ultrasonic methods are only limited when the elastic response is extremely non-linear and the very small strains characteristic of ultrasonic measurements are not representative of the strains experienced in a particular application. Because ultrasonic measurements could be used to rapidly determine the modification and possible degradation of elastic properties during heating of oil shale, the CSM program was expanded in February of 1977 to include ultrasonic measurements.

There are two basically different techniques which have been used to measure the velocity of both longitudinal and shear waves in rocks and other materials (35) (36). The simpler of these techniques is based upon the precise measurement of pulse transmission times of characteristic waves across a sample of known dimensions (36). This technique requires that two

ultrasonic transducers (a sender and a receiver) be in contact with the sample, but has the advantage that "first arrivals" are measured and reflections and reverberations in the sample and any supporting apparatus do not perturb the measurement. The second, and more sophisticated technique, involves the determination of the ultrasonic frequencies at which continuous (or tone-burst) sinusoidal waves propagate repetitively across the sample with constructive interference (37). This technique includes variations referred to as "pulse-echo-overlap" (38) ultrasonic interferometry (39) and resonance frequency methods. Because the frequency at which constructive interference occurs can be determined with much higher accuracy than can the delay times in the pulse transmission techniques, wave velocities and elastic constants can be determined to a much higher precision. The relative precision of the two techniques are typically 1 in 100 for pulse transmission and 1 in 10,000 for the interferometric techniques. The interferometric technique has the advantage that only one transducer can be used (as both sender and receiver) and the disadvantage that sample geometry and transducer bonding are critical.

The traditional piezoelectric crystals used for ultrasonic measurements (quartz, barium titanate, and PZT) are restricted in that they have low piezoelectric Currie points (250^{o}C) and cannot be used directly for high temperature measurements. These materials can only be used directly for high temperature studies if appropriate buffer rods are incorporated into the sample assembly (39). More recently the capabilities of lithium

($LiNbo_3$) as a high-temperature piezoelectric transducer have been demonstrated (40). If measurements at both high temperature and high pressure (.1 to 1 Gpa) (14,500 to 145,000 psi) are desired, it is necessary to incorporate the lithium niobate transducers in a pressure resistant probe such that the transducers see a lower pressure (40). For measurements on oil shale, however, the maximum uniaxial and confining stresses are low enough (less than 10 MPa)(1450 psi) that such encapsultation will not be necessary. The high-temperature capabilities of lithium niobate, on the other hand, make it attractive for making active measurements during the actual retorting of oil shale samples.

Preliminary measurements with the pulse-transmission technique at elevated temperatures revealed that very high attenuation of elastic wave energy coupled with increasing electrical noise (probably caused by the products of kerogen decomposition) gave extremely poor signal to noise ratios at temperatures over 350°C. Examination on an oscilloscope of multiple, successive transmitted-pulse traces indicated that the electrical noise was relatively random while the basic signal associated with P and S-wave arrivals remained quite stable. It was concluded that a signal averaging technique could be used to significantly enhance the signal to noise ratio. Consequently, a Biomation (Model 805) transient digital recorder was utilized to record the transmitted pulse signals in digital form, and by interfacing the Biomation to a Hewlett-Packard 9825 microcomputer, multiple traces could be recorded and transmitted in digital form to the 9825 for signal averaging. The

interfacing of the ultrasonic measurements to the HP-9825 is shown schematically in Figure 2.4. Experience to date has shown that the average of 10 signals is nearly always adequate to provide good signal-to-noise ratios. As the averaged signal traces displayed such consistant qualities it was decided to develop algorithms which would enable the 9825 to pick automatically the P and S-wave arrival times, thus eliminating the need for a visual inspection and arrival time determination of the many averaged traces obtained during the course of an experiment. The procedure developed employs essentially identical algorithms for determining independently the P and S-wave arrival time. Initiation of the procedure, at the beginning of an experiment requires that the times of pulse initiation by the pulse generator, the P-wave arrival and, finally, the S-wave arrival, be visually determined and keyed into the 9825. As the oil shale sample is heated, often with transient-thermal and/or thermal-expansion measurements being made simultaneously, averaged pulse transmission records are obtained at approximately each five degrees of temperature change. Beginning with the operator determined arrival times and the concordant averaged transmitted record each subsequent averaged record is cross correlated with the preceding record to reconfirm pulse initiation time and to approximately locate the slightly changed P and S-wave arrival times. Once a small, ten word or two microsecond, time window has been established for the P and S-wave arrival times separately, then an absolute signal amplitude algorithm is used to select the word (time) most closely

corresponding to P and S-wave arrivals. These new arrival times and the new averaged trace are then saved for a similar analysis of the next averaged trace. Details of the instrumentation setup, the digital data acquisition system, the signal averaging technique and the algorithms for determining P and S-wave arrivals are given in Appendix 6.5.

2.4.3 Thermal expansion

The design of the heaters and test stack used for making thermal transport and ultrasonic velocity measurements was such that thermal expansion tests could be readily incorporated into and run concurrently with the other types of tests. Details on the modified stack arrangement follows.

In order to obtain thermal expansion data it was necessary to make several minor modifications to the stack heating apparatus which has been used for the ultrasonic velocity and thermal conductivity measurements. These modifications involved 1) replacement of the load cell used in the original stiff loading frame with a pneumatic cylinder allowing constant load to be applied to the stack, (see Figure 2.4) the installation of a linear variable differential transformer (LVDT) in parallel with the stack and 3) the installation of an analog to digital converter and a BCD interface so that displacements measured by the LVDT could be read directly by the Hewlett-Packard 9825 micro-computer controlling the experiment. The thermal expansion tested for each combination of grade and temperature. As characteristics of the stack alone were calibrated by performing several experiments utilizing either no sample or a pyrex

reference disk as a sample. Due to the high thermal expansion coefficients of oil shale, elongation due to shale expansion is roughly equivalent to that due to the thermal expansion of all other components in the stack. Thus, the thermal expansion data has been obtained with a relatively good signal to noise ratio. The thermal expansion modifications were made so that any other type of experiment, such as ultrasonic velocity and/or thermal conductivity, could be performed simulatneously.

2.5 Mathematical Modeling

An important activity under the research program is the mathematical analysis of the behavior of oil-shale pillars and barrier walls during in-situ retorting operations. This objective was approached through two basic types of mathematical analysis.

1) A conductive heat-transport model was developed to utilize the temperature and pressure variant thermal properties that were obtained in the experimental program. Data on reaction kinetics and transport mechanisms was adopted from the literature (19-24). The transport model was used to predict temperature distributions in in-situ pillars corresponding to imposed temperature histories at the pillar surface. Surface temperature variation was selected to correspond to that anticipated for large-scale in-situ retorting. This model yielded information on the depth of penetration of the retorting isotherm into the pillar and permitted calculation of oil and gas production as a result of kerogen decomposition in the pillar itself.

2) A finite element structural analysis was performed to evaluate the effect of thermal stress on a pillar. The model used the temperature dependent thermal and mechanical properties developed from the laboratory testing program. The analysis considered the effect of side loading of the pillar by the rubblized shale. Analysis included the case with no thermal effects and with thermal effects at 120 and 800 hours of heating of the entire side of the pillar. Contour plots of the horizontal, vertical and shear stresses and the displacement of the pillar are presented along with comparison plots of the vertical stress and the temperature dependent compressive strength along the pillar center line to illustrate the probable zone of failure in the pillar.

2.5.1 Preliminary thermal model

A critical aspect of any modeling effort is verification of the model predictions so that the model can be applied with confidence. In some cases, verification can be accomplished by comparing model predictions with experimental measurements. This approach is not feasible in the present project because no data is available for in-situ oil-shale retorting and obtaining such data through field work is well beyond the limitations of the contract. It was therefore decided to develop a simplified primary model using the mathematics of finite differences, to verify the predictions of the finite-difference model with analytical solutions from the literature, and to use the finite-difference predictions to check the results of the finite-element model.

The finite-difference model was developed and verified by Dr. Tom Sladek, with the cooperation and assistance of Dr. Fausett. Following is a description of the modeling procedure.

In-situ retorting is an unsteady-state operation, i.e., thermal conditions within the retort change with time. consequently, the gas temperatures and flow rates to which a pillar is exposed also change with time. A pillar model must be capable of simulating these changes, and the model equations must therefore include time as a variable.

The thermal properties (density, specific heat, and thermal conductivity) of oil shale change with temperature and are functions of organic content and of direction of heat flow. The model equations must include these properties as variables, and functional relationships for their behavior must be included in the formulation.

Heat will be conducted in three directions within an in-situ retort pillar. Temperature gradients will exist between the surface and the axial center of the pillar due to transient conditions at the surface. Temperature gradients will also exist in the vertical direction, corresponding to the locations of preheat, retorting, combustion, and cool-down thermal waves within the retort rubble. And temperature gradients will exist in the lateral direction as a result of varying degrees of physical contact between the pillar surface and the outer edges of the rubble. All three gradients will be aggravated if the pillar geometry and surface are irregular and if by-passing and/or non-flow regions exist in the rubbled bed.

An exact mathematical model should be three-dimensional to account for these gradients. Sophisticated programming techniques to satisfy this requirement may be very desirable for the finite-element program, but they were considered less important for the verification program. Consequently, it was decided to simulate an in-situ pillar as a uniform right-circular cylinder, exposed to a uniform ambient along its entire length. Thus, the only temperature gradient was in the radial direction, between the central axis and the surface of the cylinder. Axial and angular gradients were ignored.

As oil shale heats, it passes through a complex series of chemical and physical changes involving dehydration, kerogen conversion, product vaporization and mineral decomposition. Thermal effects are associated with each change, and each change alters the thermal properties of the shale matrix. An exact model should account for these changes. Finite-difference codes can be developed which have this capability, but it was decided that the extensive programming effort was not justified at this stage of the project. Consequently, only thermal convection and conduction were modeled and other thermal effects were ignored.
In summary, the pillar system which was modeled consisted of a right-circular cylinder of uniform cross section. Thermal properties were allowed to vary, but other physical and chemical changes were ignored, along with their associated thermal effects. It was assumed that the surface of the cylinder was exposed to a uniform ambient. This latter assumption permitted the cylinder to be reduced to a disk-shaped body of unit

height. Results and conclusions from this preliminary analysis are presented in later sections.

2.5.2 Fenix and Scisson retort model

The retort system selected for modeling was the Room and Pillar Method determined by Fenix and Scisson. (45) This configuration is depicted in Figure 2.5. As shown, the retorts are square in cross section, and the rubbled shale surrounds a central support pillar. Adjacent retorts are separated by a barrier wall of solid shale. Modeling was focused on a single retort module. The contained rubble bed was 220 feet square, and the center pillar was 100 feet square. The barrier wall was 50 feet thick. Retort height was variable. Heat transfer into the center pillar and the barrier wall was modeled. Temperature in the rubble bed was treated as a defined boundary condition, and it was assumed that heat was transferred to the surrounding solid shale by convection. Only conductive heat transfer was modeled in the solid shale. Mass transport and chemical reaction were neglected.

The heat-balance equations were initially derived for transient thermal conduction into a right circular cylinder of solid shale (preliminary thermal model). This system of equations was solved analytically, and the predicted temperature profiles were expressed in terms of Bessel functions. A one-dimensional numerical model was then developed for the same equations and was implemented under the same boundary conditions. Temperature profiles predicted by the model agreed very well with the analytical solution. The computer code was

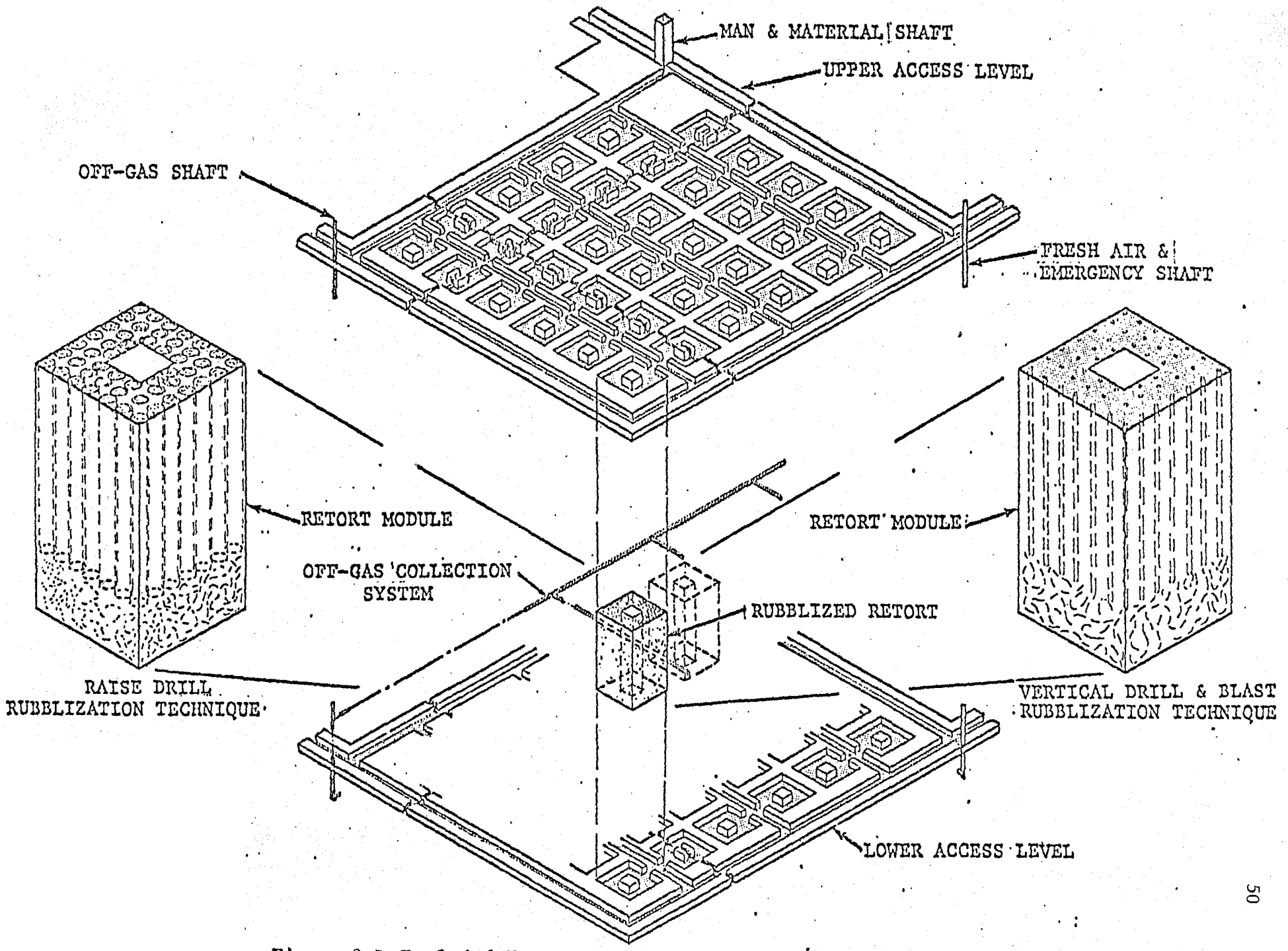

Figure 2.5 Exploded Isometric View - Room & Pillar mining System

then used as a basis for development of a more general two-dimensional model which was verified with the predictions of the one-dimensional model.

In the absence of actual field data, the model predictions must be regarded as somewhat speculative, but it is hoped that their accuracy will be sufficient for preliminary analysis of pillar behavior.

2.6 In-Situ Temperature Profile Measurement

As discussed earlier, the only effective way to confirm the validity of any developed models is to directly monitor conditions in the field surrounding an in-situ retort. However, the proprietary nature of current in-situ retorting experiments makes it impossible to be able to directly monitor an actual retort. It is possible, however, to simulate retort conditions in the field with a reduced-scale heated borehole test.

A field testing program was initiated with the objective of creating a simulated retort by drilling a borehole into the floor of an existing oil shale mine, inserting a heater, and instrumenting the oil shale surrounding the borehole for temperature and vertical expansion. The site selected for carrying out this experiment was a section of the Colony oil shale mine. The site was approximately 300 feet from the mine portal. The mine floor in the area used for experiments was relatively smooth and did not show any visible blast damage.

A schematic representation of the testing setup is shown in Figure 2.6. A 6-inch diameter borehole was drilled in the mine floor and the core recovered for determining oil shale grade and for performing some basic laboratory tests. The hole was drilled to a depth of five feet.

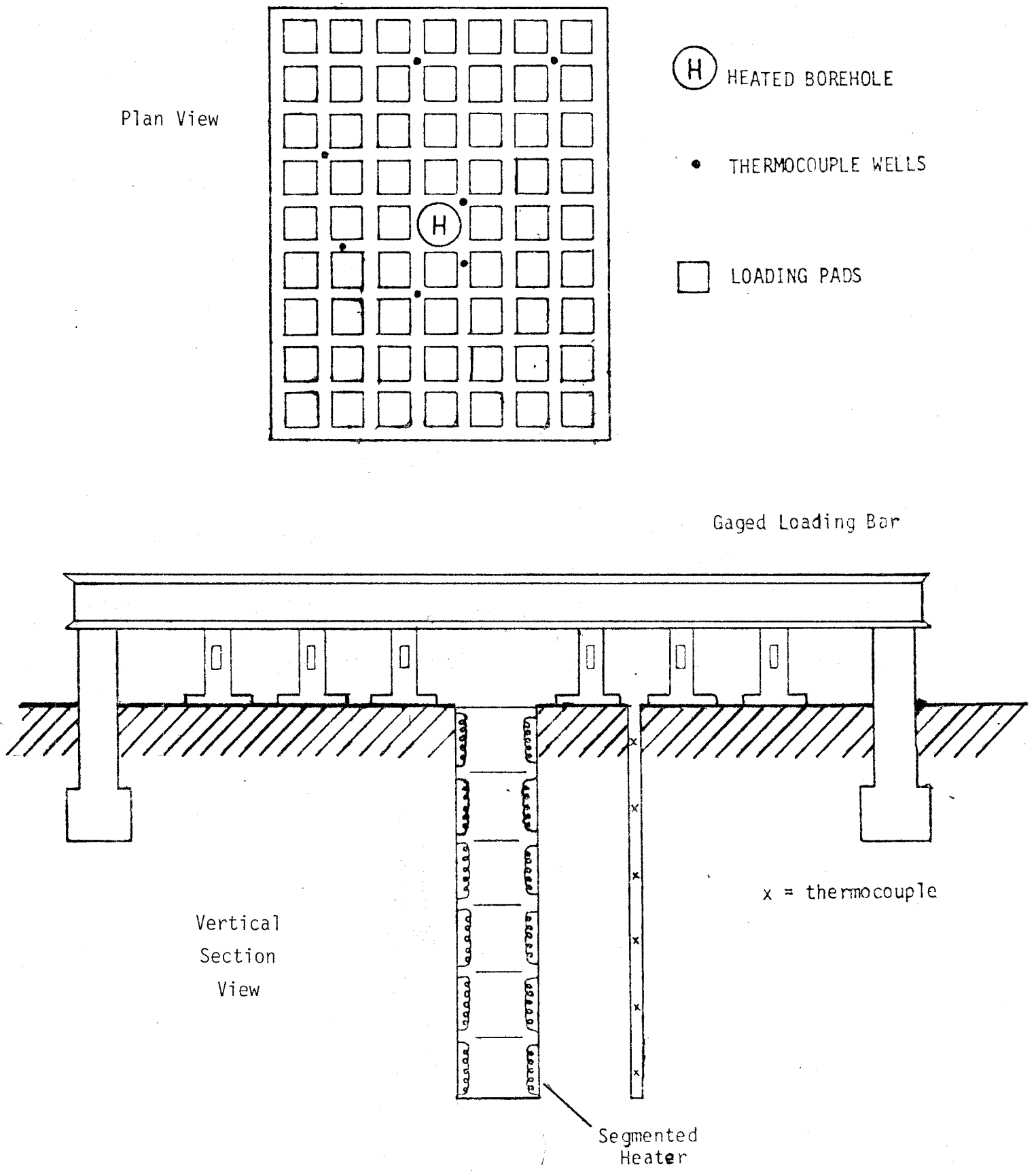

Figure 2.6
In-Situ Heater Test

A heater stack was assembled consisting of 10 circular heater units, 6 inches in height and $5\frac{1}{2}$ inches in diameter (Figures 2.7 and 2.8). A thermocouple was placed at the center point of each heater coil and the lead wires together with those for heater coils were brought up through porcelain tubing to the top of the stack. Individual heater halves were joined together with wire. Heat resistant tape was used to stack heater units upon one another.

Temperature monitoring in oil shale surrounding the heater hole was done by means of thermocouples placed in small diameter holes which were drilled in a pattern as shown in Figure 2.6. A total of 8 holes at incrementally farther distance away from the heater hole was used for thermocouple installation. The thermocouple holes were in a spiral pattern and at distances of 6", 12", 18", 24", 30", 36", 42" and 48" from the wall of the heater hole. Each hole contained a set of 12 thermocouples with each thermocouple aligned with the center of each heater unit in the horizontal direction. The thermocouples were housed within PVC tubing of a slightly less diameter than the drill hole. (Figure 2.9). The thermocouples used were type K and their temperatures were monitored by a digital temperature indicator.

The thermal expansive strain in the vertical direction surrounding the borehole was monitored by 24 load cells placed between the floor and the test frame (Figure 2.10). The frame was composed of six, I-beams tied together with an end beam on each side which were in turn anchored to the mine floor at each corner. A total (Figures 2.11 and 2.12) of four load cells were placed on each I-beam at 12 inch centers. The load cells were

FIGURE 2.7

Heater stack showing the thermocouples and heater wires

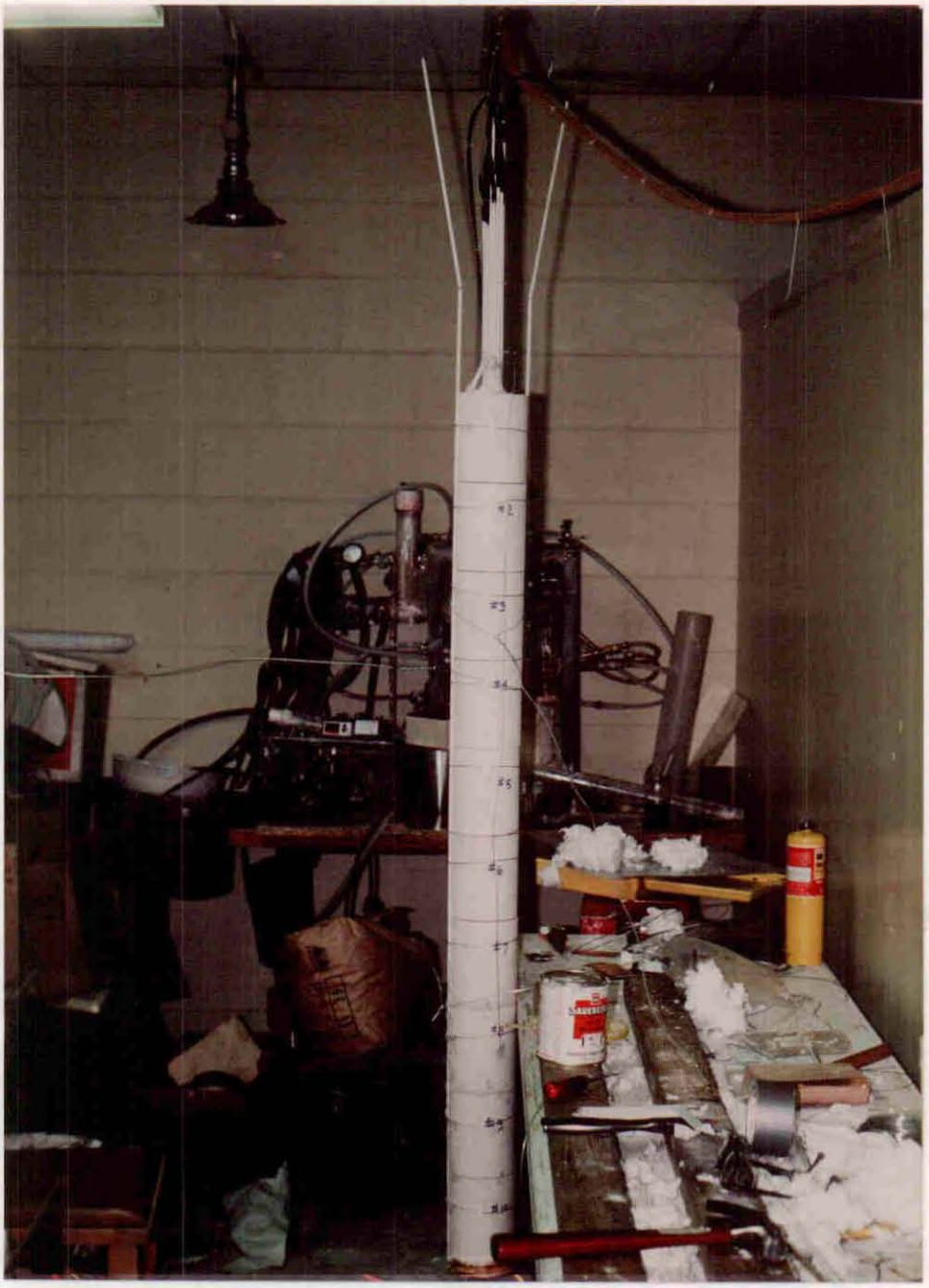

FIGURE 2.8

View of the assembled heater stack

FIGURE 2.9

View of a thermocouple column in the field

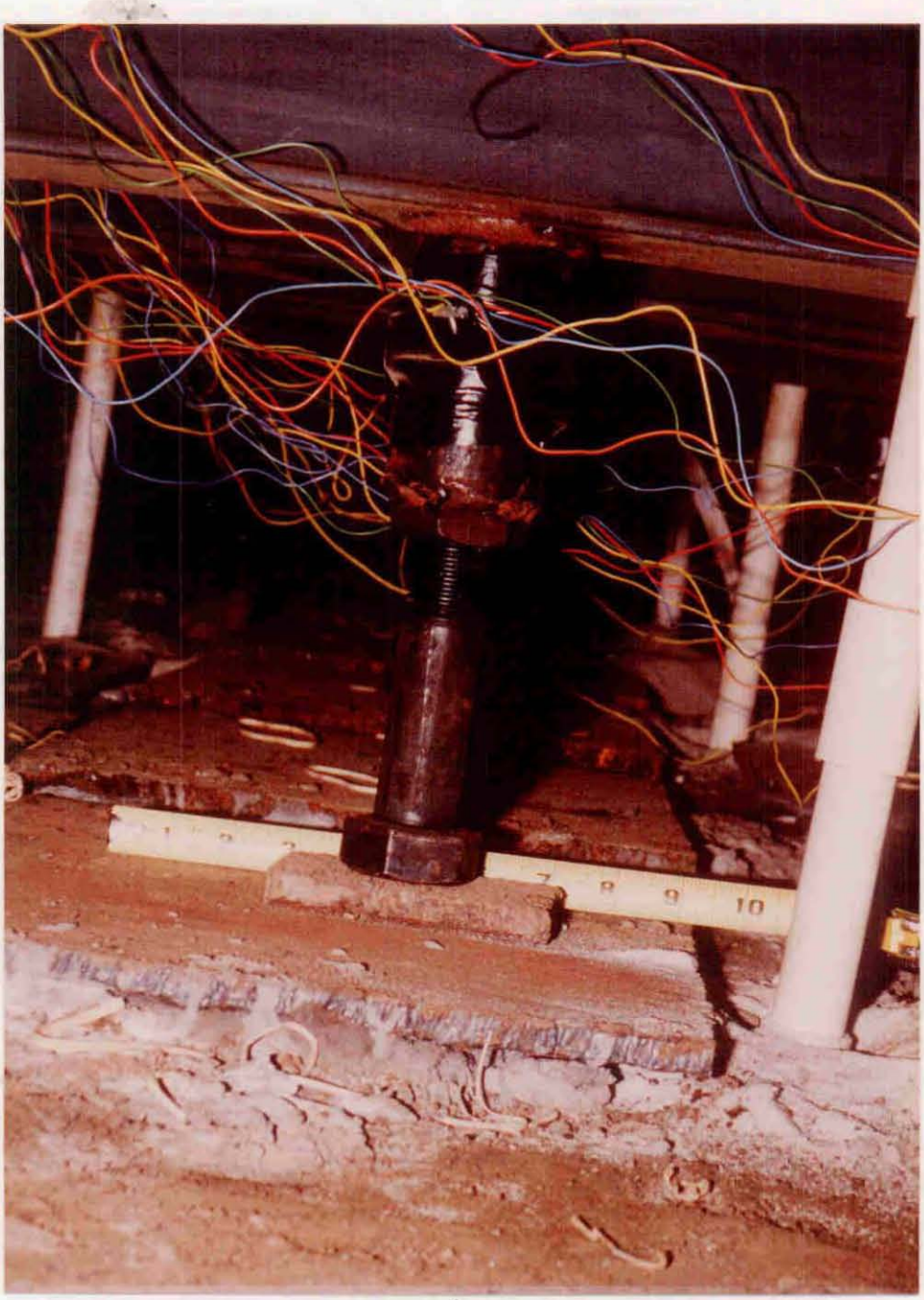

FIGURE 2.10

Load cells used for displacement measurement in the field

FIGURE 2.11

Overall view of the in-situ heater test detup

FIGURE 2.12

View of the control panel for in-situ heater test

right circular cylinders with four, 120 ohm, SR-4 strain gages connected into a full bridge circuit. Strain readings were accomplished with a multi-channel strain indicator.

The purpose of using segmented heaters for the heater borehole was to simulate the flame front progression of an in-situ retort by sequencing the desired temperature distribution incrementally down the hole. After a careful evaluation of various alternatives, it was decided to have three heaters on at a given heating sequence. With three heaters operating, the top heater was set at 100°C, the middle at 500°C, and the bottom heater running at 100°C. Every 12 hours then, the heating sequence was moved one heater segment downward. Three separate temperature controllers were used to control individual heater unit temperatures.

Although the test startup was delayed because of several unanticipated problems, all the problems encountered were corrected and the test was brought to a successful completion. A major problem occurred with repeated shorting and subsequent burn out of heater units (Figure 2.13) This was caused by fusing of silica sand used to fill the heater hole with the heater coils. This problem was later corrected by going to a new heater design in which the heater coils were completely encased in high temperature cement. Instead of silica sand, the inside of the heater stack was filled with insulating material and the top and bottom of the heater stack was then sealed off with high temperature cement. By doing so, it was assured that no silica sand came into contact with the heater coils during testing. (Figure 2.14)

FIGURE 2.13

A picture of a burnt out heater segment

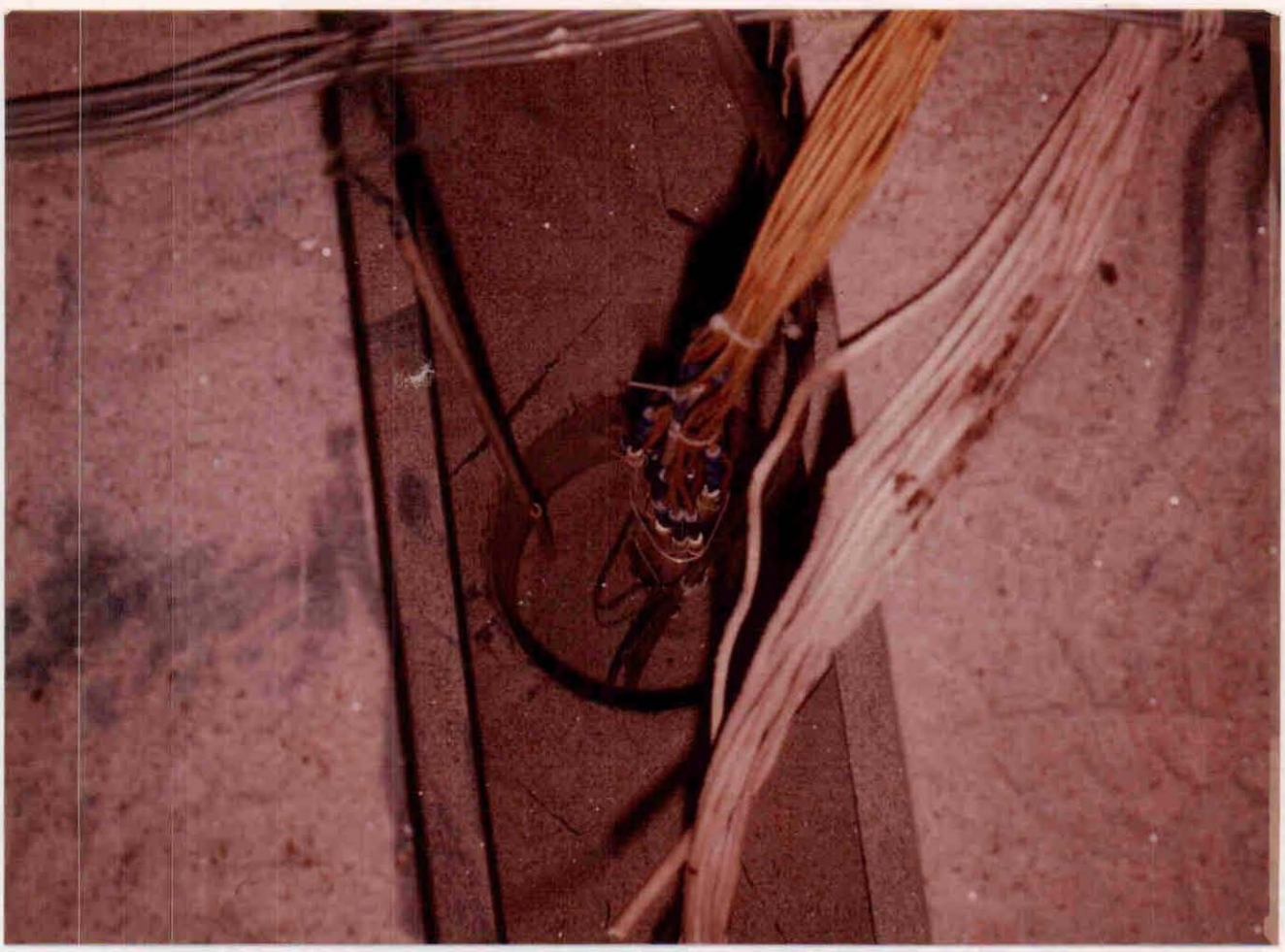

FIGURE 2.14

View of the heater hole for in-situ heater test

The testing involved a total of 8 heating sequences with each sequence comprising 12 hours of heating with three heaters running. The thermocouple outputs were recorded at three hour intervals while the strain readings were made every 12 hours just before a new heating sequence was started.

As stated earlier, the objective of the in-situ heater test was to provide actual data to confirm the validity of the finite element structural analysis model developed for in-situ pillar stresses and temperature profiles. The results of the test and the comparison with those obtained from the model are given in Section 3.4.4.

3.0 RESULTS

3.1 Sample Selection and Characterization

As discussed earlier, two sites were visited, and samples collected from each for characterization. Fischer assay, x-ray diffraction and wet chemical analyses were performed on representative samples. A summary of the results of that analysis follows.

3.1.1 Sample acquisition

Oil yields determined by Fischer assay are presented in Table 3.1. Included for comparison is a tabulation of oil yields estimated in the field from specific gravity measurements. As shown, field estimates were not very accurate. Inaccuracies are probably related to the crude field procedure which was employed and to the problem of obtaining Fischer samples equivalent to the pieces examined in the field.

We attempted to obtain samples covering the 10-30 gallon per ton range from each location. Sampling at Anvil Points yielded shale in the high, medium, and low ranges. Sampling at Logan Wash provided high-yield and low-yield shale, but did not provide shale in the medium-yield range. Although sampling was not completely satisfactory, it was adequate as an initial effort.

3.1.2 X-ray diffraction

Samples 6 and 8 from the Occidental group and samples 1, 12, and 13 from the Anvil Points group were selected for mineralogical analyses. These samples provided oil yields of 9.5 and 33.1 gallons per ton for Occidental and 12.9, 18.2, and 27.3 gallons per ton for Anvil Points. A portion of the Fischer assay feed material for each sample was submitted to CSMRI's mineralogy

Table 3.1 Fischer Assay Analysis of Initial Oil Shale Samples

Sample	Source	Oil Yield, Field estimate gal/ton	Oil Yield, Fischer assay gal/ton
1	Anvil Points	---	27.3
2	Occidental	---	8.9
3	Occidental	---	51.2
4	Anvil Points	10	4.8
5	Occidental	---	37.7
6	Occidental	low	9.5
7	Occidental	15	8.9
8	Occidental	21	33.1
9	Occidental	10	6.9
10	Anvil Points	42	36.8
11	Occidental	high	33.4
12	Anvil Points	14	12.9
13	Anvil Points	28	18.2

group for bulk x-ray diffraction scans. Results are tabulated in Table 3.2 and typical diffractometer output is depicted in Figure 3.1.

As shown in Table 3.2, all samples contained major quantities of dolomite and quartz. With the exception of Sample 13, calcite was also a major phase. Analcime was a major phase in samples 1 and 13, and orthoclase was a major phase in Sample 8.

Major-phase composition is typical of Green River oil shale in which dolomite, calcite, quartz, clays, and zeolites comprise over 97% of the mineral matter. Analcime and orthoclase were somewhat higher than normal. Usually, these two minerals comprise a total of only 11% of the mineral matter.

No evidence of either dawsonite or nahcolite was found in any of the diffraction patterns. This is encouraging but inconclusive, since it is possible that both species were partially destroyed during Fischer assay sample preparation. Because these determinations were highly critical to the program, further work was conducted on fresh portions of each of the five samples. A second run was made on fine material screened from the product of a single pass through a jaw crusher. This shale was subjected to a much lower level of attrition heating than was the material which had been prepared for Fischer assay. Consequently, any nahcolite present in the raw material should not have been altered during preparation.

Diffractometer scans for the second set of samples were essentially identical to those obtained for the first set. Constituent phases were essentially unchanged and nahcolite and

Table 3.2 Results of X-Ray Diffraction Analysis of Selected Samples

Sample	Source	Fischer Oil Yield, gal/ton	Major Phases	Minor Phases	Trace Phases
6	Occidental	9.5	Quartz, dolomite calcite	Alstonite, orthoclase	Analcime, halloysite, montmorillonite
8	Occidental	33.1	Quartz, dolomite, calcite, orthoclase	Analcime, alstonite	Montmorillonite, halloysite
12	Anvil Points	12.9	Quartz, dolomite calcite	Orthoclase, analcime	Alstonite, montmorillonite
13	Anvil Points	18.2	Quartz, dolomite, analcime	Orthoclase, alstonite	Calcite, montmorillonite, halloysite
1	Anvil Points	27.3	Quartz, dolomite calcite, analcime	Orthoclase, alstonite	Montmorillonite, halloysite

Composition Key

Name	Chemical Formula
Quartz	SiO_2
Dolomite	$CaMg(CO_3)_2$
Calcite	$CaCO_3$
Orthoclase	$KAlSi_3O_8$
Analcime	$NaAlSi_2O_6 \cdot 2H_2O$
Alstonite	$BaCa(CO_3)_2$
Halloysite	$Al_2Si_2O_5(OH)_4$
Montmorillonite	$(Na, Ca)_{0.33}(Al, Mg)_2 Si_4O_{10} \cdot nH_2O$

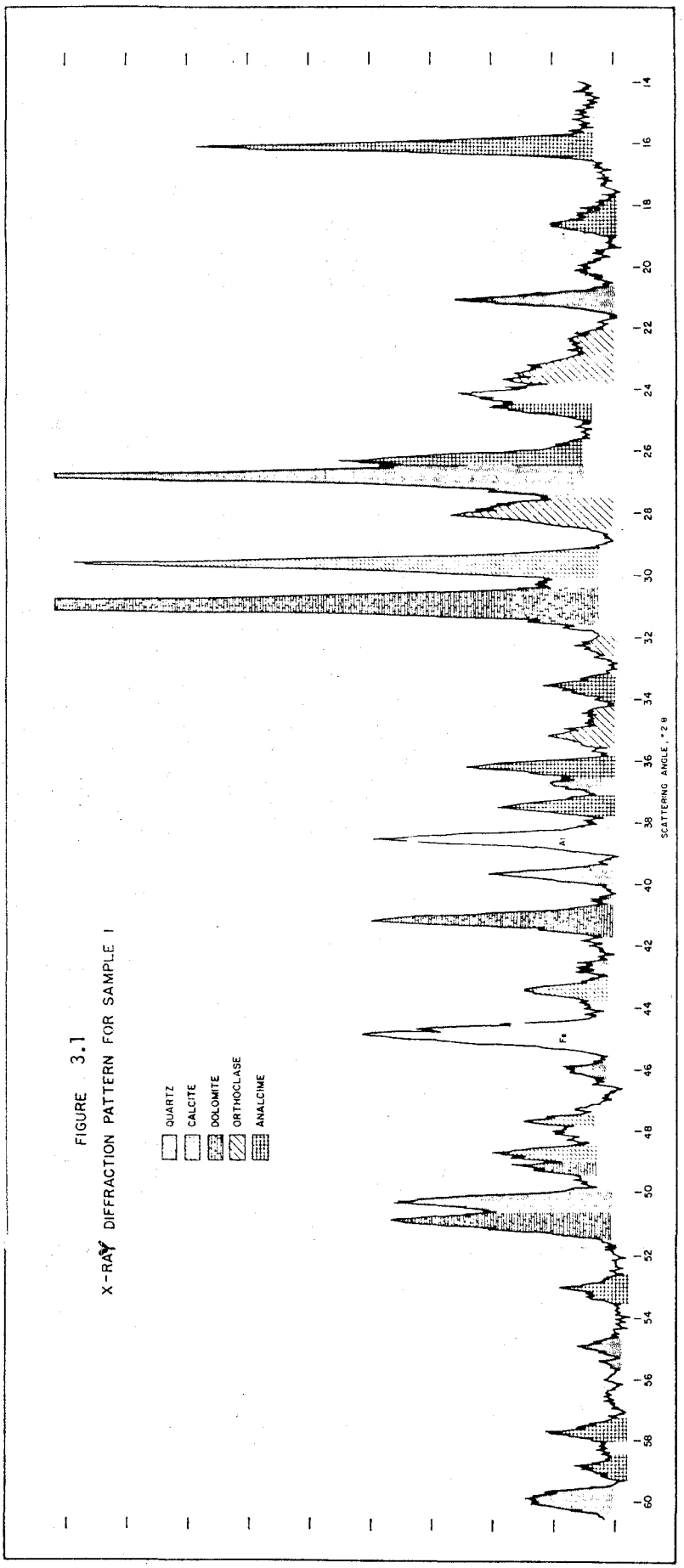

FIGURE 3.1

X-RAY DIFFRACTION PATTERN FOR SAMPLE I

dawsonite were not detected in any of the samples. Presence of analcime in each of the samples ruled out the possible presence of dawsonite, but x-ray results were inconclusive for nahcolite.

3.1.3 Wet-chemical analyses

Chemical analysis results for the 5 samples are tabulated in Table 3.3. As shown, water-soluble sodium was present in very small concentrations. Maximum calculated nahcolite concentration was less than 0.6% by weight. Acid-solution aluminum from analcime dissolution ranged from 0.41 to 1.56% by weight. These measurements were qualitatively consistent with x-ray estimates of analcime concentration.

3.2 Physical Property Tests

As noted previously in Section 2.3, an extensive laboratory testing program was undertaken to determine oil shale mechanical and thermal properties for the full range of conditions likely to be encountered in the area of the retort. The variables included in the laboratory testing were: temperature, grade, confining pressure, orientation of bedding planes, time at temperature and mineral content. The oil shale properties measured were: compressive and tensile strengths, elastic modules, Poisson's ratio and thermal properties.

As described in Section 2.3, triaxial compression tests were performed on a stiff testing machine using a specially designed high-temperature pressure cell (Figures 3.2, 3.3, 3.4 and 3.5). A standard compression testing machine was used for the Brazilian indirect tensile strength tests.

Before the laboratory physical property tests on oil shale could be commenced, two factors which were known to affect oil

Table 3.3

Wet Chemical Analysis

Sample	Source	Water-soluble sodium, wt. %	Nahcolite wt. %	Acid-soluble Aluminum wt. %	Analcime Concentration by X-ray
6	Occidental	.042	0.15	0.41	Trace
8	Occidental	.160	0.58	0.84	Minor
1	Anvil Points	.082	0.30	1.06	Major
12	Anvil Points	.062	0.23	1.37	Minor
13	Anvil Points	.155	0.57	1.56	Major

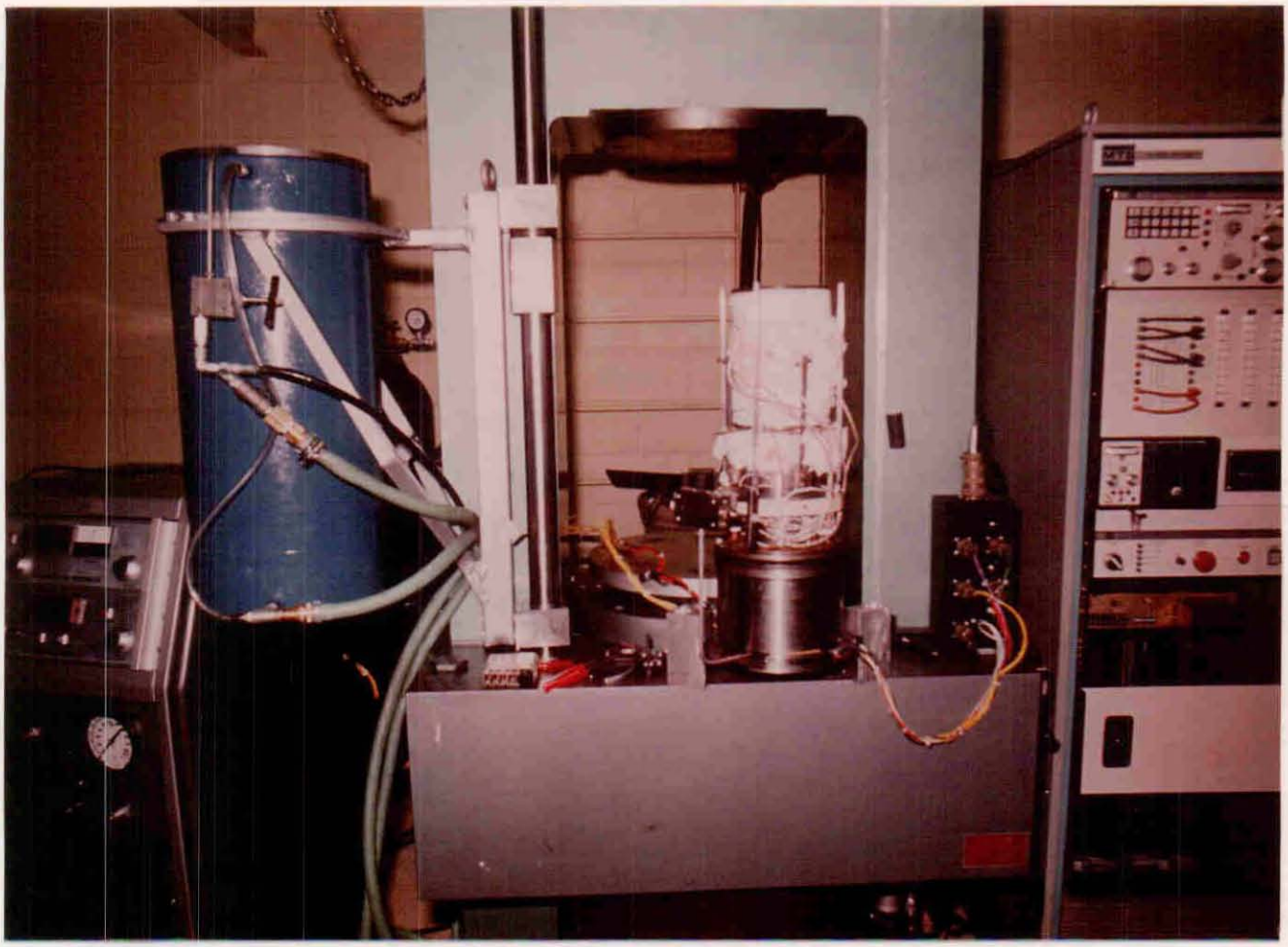

FIGURE 3.2

The stiff testing machine used for laboratory tests

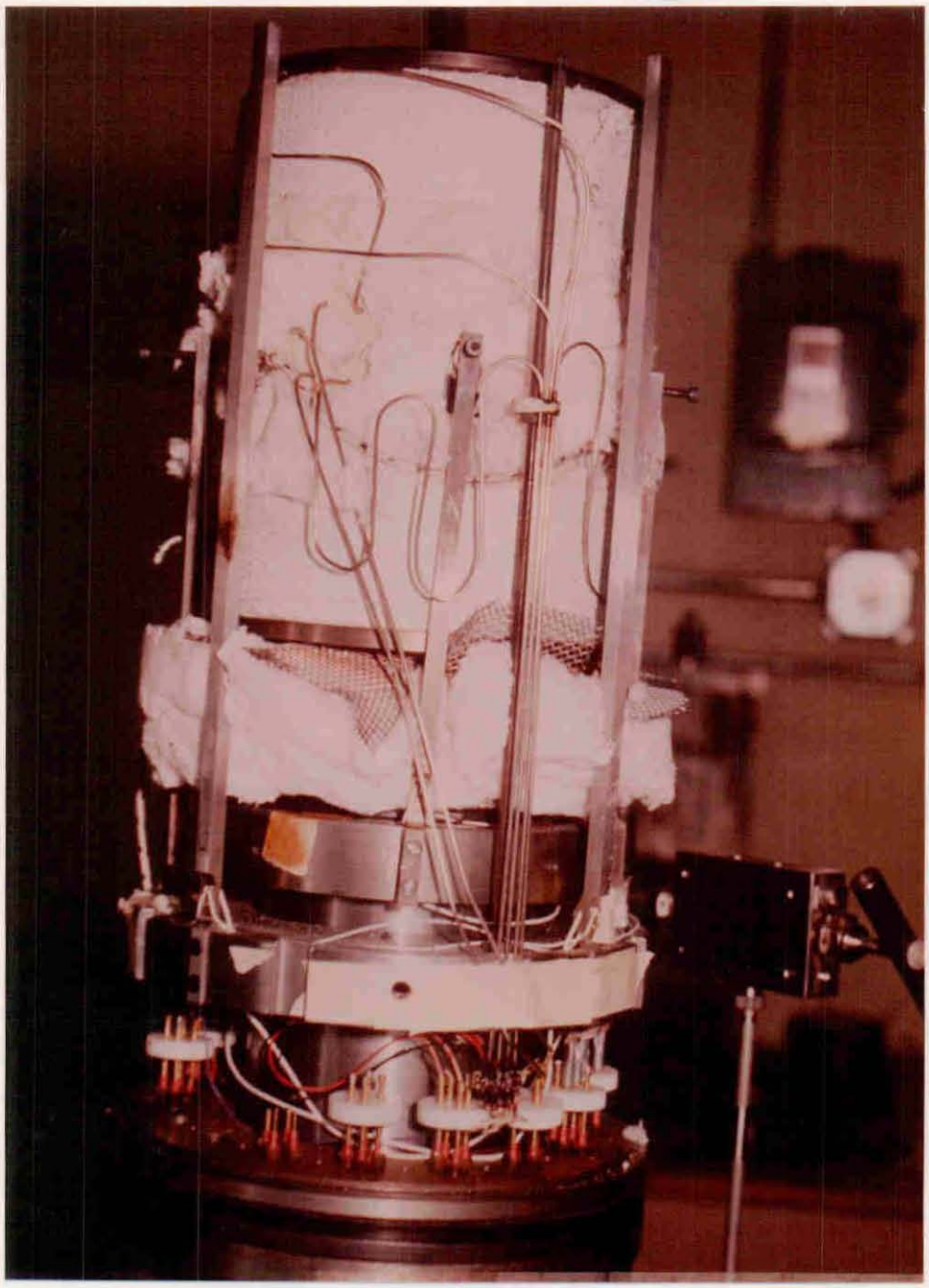

FIGURE 3.3

A view of the high pressure-high temperature cell

FIGURE 3.4

Oil Shale sample with retainer cap

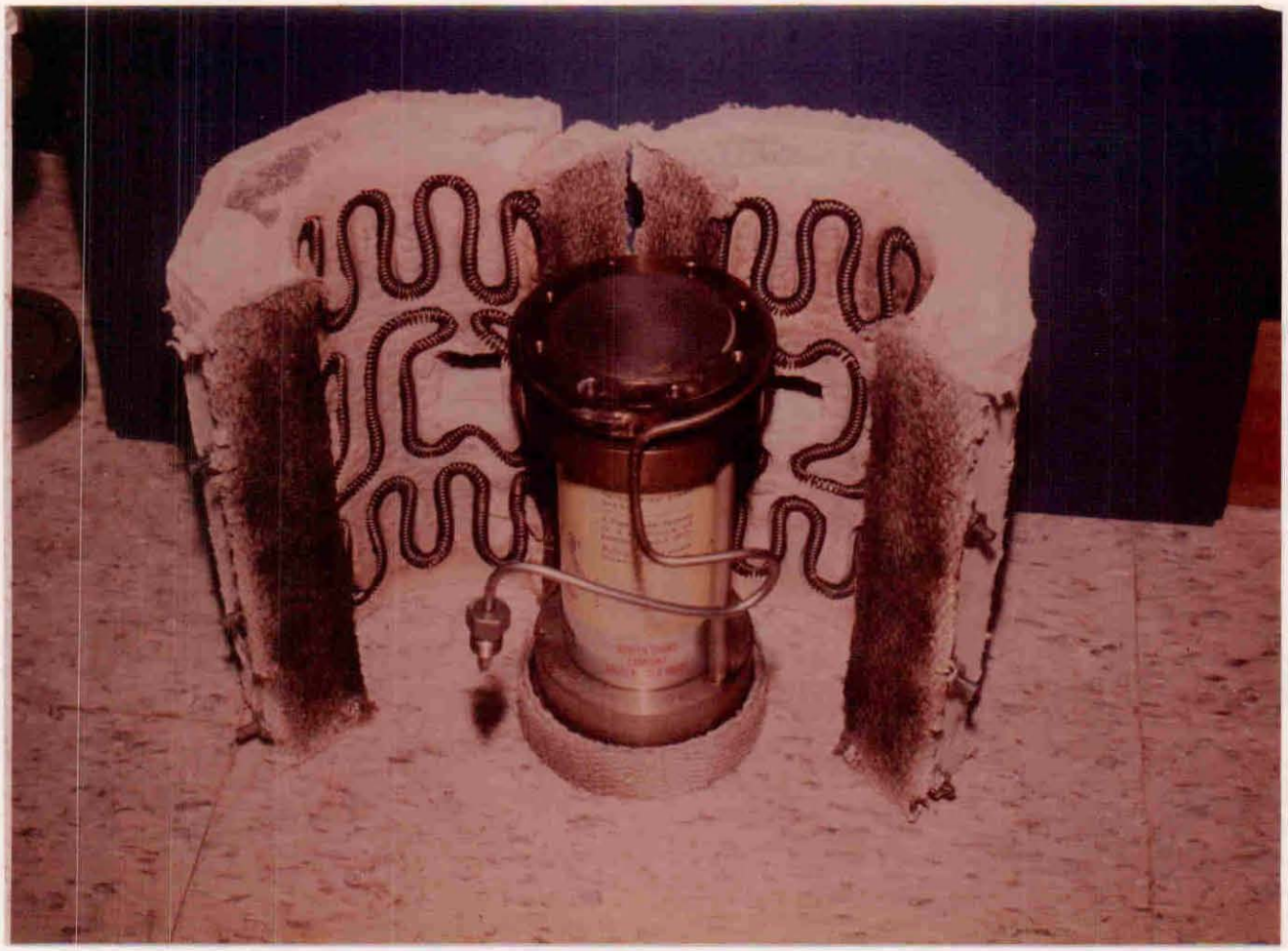

FIGURE 3.5

Oil shale sample encased in aluminum containers with heater in background

shale behavior had to be investigated and their effect evaluated. These factors were the heating atmosphere effects and the heating time effects on oil shale strength. It was imperative to quantitivily evaluate these effects so that they can be standardized for the traixial and the Brazilian strength tests.

3.2.1. Heating atmosphere effects on oil shale strength

It is a known fact that the presence of even small amounts of oxygen during heating process can significantly affect the thermal behavior of oil shale. Its effect on final strength, however, has not been determined. To evaluate this effect, a large number of Brazilian tensile strength and uniaxial compressive strength tests were performed under both nitrogen-flushed and oxygen-available atmospheres. These tests showed absolutely no effect of heating atmosphere on indirect tensile strength for the full range of kerogen contents and temperatures investigated. For the compressive strength, initially an approximately 25% increase was observed for the samples heated in air over those heated in nitrogen. However, in further tests where all samples were encased in a vented aluminum case and restrained so as to prevent axial exfoliation, strengths were not significantly different. On the basis of these findings, it was thus concluded that the heating atmosphere did not have a significant bearing on the strength of oil shale.

3.2.2 Heating-time effects

Heating-time refers to the time duration during which oil shale is maintained at a constant temperature. Because the majority of physical property tests were to be accomplished under elevated

temperatures, it was crucial that the heating-time effects be evaluated in detail.

From the estimated thermal properties, the time required for thermal equilibrium to occur in oil shale test samples was determined to be approximately 2 hours. A large number of Brazilian test samples were then tested at heating times ranging from 2 to 88 hours. No consistent effect of heating time was evident in the results. As a result of these preliminary tests and to assure that future tests would represent an equilibrium situation, all samples were then heated for at least 16 hours prior to testing.

3.2.3 Compressive Strength

As previously described, the testing program for the laboratory physical property measurements for oil shale was designed to cover the full range of variables likely to be encountered in the area of the retort. For oil shale grade, the initial test plan called for testing of grades from 10 to 30 gpt at 5 gpt increments. This selection was based on the original concept that the in-situ retorting would be applied principally to oil shale zones of lower grade. However, later in the program it became apparent that the some of the planned commercial in situ retorts will also contain richer oil shale zones having grades up to 40 gpt. Since these richer zones coupled with high retort temperatures could have a significant controlling effect on the stability of pillars and openings, it was decided to include these higher grades in the overall testing program. As noted earlier, an upper limit of $500^{0}C$ was selected for the temperature. This was divided into five equally-spaced levels

starting from 20°C. Finally, for the confining pressure on the sample, four levels consisting of 50, 500, 1000, 1500 psi were chosen..Tests were conducted both for vertical and horizontal cores as depicted in Figure 2.1.

It becomes obvious that a testing program devised according to the above levels of variables constituted several hundred tests. Moreover, due to inter-sample variations in mineralogy and varve structure, it was required to undertake several replications of each test in order to provide consistent results.

The entire triaxial compression data for both vertical and horizontal cores are given in Appendix 6.6. Tables 3.4 and 3.5 present the grouped data for the vertical and the horizontal cores, respectively. The data grouping is done according to the grade for different temperature and confining pressure values. Included in these tables are the compressive strength, Young's modulus and Poisson's ratio measurements for each combination of grade, temperature and confining pressure. Those data points which represent the average of two or more replications are marked with an asterisk.

Although a major effort was placed on completing all the laboratory testing as called for in the test plan, this objective could not be achieved. As seen in tables summarizing the triaxial test results for lower grades some data are missing, corresponding to those tests which could not be performed. This gap in data is considerably magnified for higher grade testing. The reason for not being able to perform these tests was the lack of sample availability at those particular grades. To fill the gaps, two trips were made to the site of Colony Oil Shale Mine to

TABLE 3.4
THE RESULTS OF TRIAXIAL COMPRESSION TESTS FOR OIL SHALE
(Vertical Cores compression perpendicular to bedding)

Gallons per ton (GPT)	Temperature T(^{o}C)	Confining Pressure P(psi)	Compressive Strength σc(ksi)	Young's Modulus E(ksi)	Poisson's Ratio v
15	20	0	14.6	1.65	0.09
15	20	50	3.0*	24.73	0.17
15	20	500	21.46*	7.31*	0.73*
15	20	1000	20.76*	2.02*	0.31*
15	20	1500	25.16	11.382	1.472
15	140	0	8.7	0.80	0.13
15	140	50	13.8	1.59	0.18
15	140	500	16.92*	5.02*	0.84*
15	140	1000	13.68*	3.21*	0.59*
15	260	50	10.54	2.83	0.15
15	260	500	10.72*	2.01*	
15	260	1000	15.74*	2.72*	0.439*
15	260	1500	20.66*	5.20*	0.904*
15	380	50	7.0*	1.056*	0.152*
15	380	500	5.03*	0.751*	0.563*
15	380	1000	10.58*	3.43*	1.079*
15	380	1500	12.22	1.466	0.269

15	500	50	13.7*	2.16	0.30
15	500	500	11.25*	3.29*	0.575*
15	500	1000	16.46*	1.42*	0.311*
15	500	1500	20.02	3.10	0.823
20	20	0	11.70*	0.875*	0.250*
20	20	50	13.49*	10.064*	0.180*
20	20	500	15.09*	2.916*	0.385*
20	20	1000	17.36*	2.801*	0.258*
20	140	0	4.9	0.25	0.59
20	140	50	8.26*	1.239*	0.298*
20	140	500	10.55*	2.675*	1.50*
20	140	1000	10.72*	0.985*	0.405*
20	140	1500	13.26*	3.592*	0.690*
20	260	50	9.11*	1.04*	0.527
20	260	500	12.78*	1.334*	0.244*
20	260	1000	12.12*	1.592*	0.242*
20	260	1500	17.95	5.286	0.288

20	380	0	14.20	0.04	0.270
20	380	50	2.1	0.19	0.25
20	380	500	6.4	1.08	0.80
20	380	1000	9.3	0.70	0.88
20	380	1500	10.12	0.955	0.234
20	500	50	4.51*	0.406*	0.201*
20	500	500	8.19*	0.629*	0.458*
20	500	1000	9.61*	0.691*	0.384*
25	20	0	16.9	0.96	0.14
25	20	50	11.9*	5.95*	0.293*
25	20	500	13.15*	0.845*	0.25*
25	20	1000	13.45*	0.755*	0.45*
25	20	1500	16.17	2.350	0.592
25	140	0	3.90*	0.25*	0.595*
25	140	50	5.53	0.647*	0.470*
25	140	500	5.65*	0.735*	0.736*
25	140	1000	7.43*	2.056	0.322

25	260	50	4.60*	0.542*	0.322
25	260	500	4.98*	0.605*	
25	260	1000	8.54*	0.523*	0.259
25	260	1500	9.38	0.927	0.514
25	380	0	17.0	0.05	0.22
25	380	50	0.865*	0.045*	0.21*
25	380	500	2.18*	0.197*	0.442*
25	380	1000	4.41*	0.179*	0.182*
25	500	50	2.44*	1.656*	0.406*
25	500	500	6.53*	0.570*	0.392*
25	500	1000	8.45*	0.35*	0.150*
25	500	1500	8.09	0.609	0.224
30	20	0	11.9	0.63	0.16
30	20	500	13.5	0.67	0.36
30	20	1000	13.7	0.74	0.18
30	140	50	9.4	0.45	0.10
30	140	1000	6.5	0.21	0.86
30	380	0	9.8	0.02	0.19

30	500	0	1.1	0.06	0
30	500	500	4.1	0.19	0.15
40	20	500	12.90	2.028	0.469
45	140	50	3.43	0.258	0.528
45	260	1000	10.54	0.432	0.535
45	500	1500	6.26	0.324	0.278
55	20	1500	12.18	1.466	0.309
55	140	1000	7.52	0.330	0.229
55	260	50	2.87	0.968	
55	500	500	3.52	0.132	0.477

*Data points representing an average of two or more replications.

TABLE 3.5
THE RESULTS OF TRIAXIAL COMPRESSION TESTS FOR OIL SHALE
(Horizontal Cores, compression parallel to bedding)

Gallons per ton (GPT)	Temperature T(°C)	Confining Pressure P(psi)	Compressive Strengths σc(ksi)	Young's Modulus E (ksi)	Poisson's Ratio V
15	20	50	18.46*	16.03*	0.465*
15	20	500	21.9*	34.06*	1.760*
15	20	1000	21.42*	13.27*	1.196*
15	20	1500	23.41*	11.99*	0.802*
15	140	50	11.80*	4.76*	0.239*
15	140	500	18.46	12.37	0.918
15	140	1000	11.94	7.24	0.408
15	140	1500	19.05*	11.55*	2.003*
15	260	50	10.06*	5.28*	0.870*
15	260	500	13.71*	6.01	0.492*
15	260	1000	21.59*	5.13*	0.501*
15	260	1500	16.73*	6.13*	1.133*
15	380	50	6.87*	2.87*	0.447*
15	380	500	15.11*	6.14*	0.540*
15	380	1000	13.76*	4.31*	0.878*
15	380	1500	14.26*	4.59*	0.684*

15	500	50	11.70*	4.91*	0.445*
15	500	500	9.25*	3.13*	0.732*
15	500	1000	18.86*	3.15*	0.396*
15	500	1500	19.99*	4.47*	0.907*
20	20	500	22.70	8.222	0.839
20	20	1000	24.32	24.643	1.845
20	140	50	5.62	4.714	0.626
20	140	500	13.84	8.705	0.356
20	140	1000	12.35	4.626	0.465
20	260	500	16.03*	7.047*	0.940*
20	260	1000	13.88	2.996	0.296
20	260	1500	17.03	5.693	1.589
20	380	50	5.23	1.977	1.238
20	380	1000	10.56	8.222	1.119
20	500	50	0.70	0.428	1.445
20	500	1000	11.33*	2.252*	0.497*

25	20	1000	16.46	8.705	0.948
25	140	500	8.94	1.409	0.384
25	140	1000	8.24	3.084	0.630
25	260	1000	9.12	1.725	0.511
25	380	1000	5.22	0.959	0.411
25	500	1000	6.16	1.520	0.683
30	20	50	9.43	4.112	0.252
30	260	50	4.00	0.911	1.098
35	20	50	9.67*	3.233*	0.602*
35	20	500	14.00	4.17	0.536
35	20	1000	13.37	2.96	0.654
35	20	1500	15.04*	5.256*	0.790*
35	140	50	3.78*	0.952*	0.545*
35	140	500	8.28	0.579	1.925
35	140	1000	9.55	0.694	0.677
35	140	1500	10.19*	0.931*	0.630*

35	260	50	4.23*	0.684*	0.419*
35	260	500	7.40*	0.801*	0.644*
35	260	1000	10.40*	1.291*	0.355*
35	260	1500	10.78*	0.993*	0.670*
35	380	50	1.61*	0.081*	0.548*
35	380	1000	4.15*	0.313*	0.311*
35	380	1500	7.06*	2.366*	0.532*
35	500	50	1.77*	1.541*	0.558*
35	500	500	1.82	0.845	0.873
35	500	1000	14.96	1.875	0.536
35	500	1500	5.58	0.658	0.372
40	20	50	14.32	5.94	0.069
40	20	500	14.23*	4.30*	0.874*
40	20	1000	18.46	3.82	0.780
40	20	1500	17.51	5.03	1.027

40	140	50	5.41	1.286	0.630
40	140	500	6.63*	1.243*	0.482*
40	140	1000	9.27*	1.812*	0.664*
40	140	1500	11.78	0.796	0.384
40	260	50	5.09	0.930	0.512
40	260	500	5.84*	1.086*	0.593*
40	260	1000	7.64	1.191	0.373
40	260	1500	10.82	1.343	0.621
40	380	500	3.06	0.514	0.551
40	380	1000	7.00	0.350	0.233
40	380	1500	4.41*	0.482*	0.923*
40	500	50	4.32	0.986	0.172
40	500	500	4.73*	0.988*	0.679*
40	500	1000	5.52	0.314	0.074
40	500	1500	9.55	0.498	0.594

*Data points representing an average of two or more replications.

collect rock samples having the desired grades. Field sample selection was accomplished by measuring the approximate specific gravity of small pieces broken from the sample. The oil yield was then estimated by using the oil yield/specific gravity tables supplied by Hendrickson (25). More precise oil yields for laboratory classification was then determined by modified Fisher Assay analysis after the samples were brought into the laboratory. The field trips to Colony Mine were successful in providing oil shale samples for some of the missing grades. However, despite intensive effort, samples with higher oil yields still could not be found. As the project was nearing its completion and the funds remaining were not sufficient to cover further sample collection expenses, it was decided to terminate the testing program for higher grades.

Although the testing for higher grades could not be completed as planned, an extensive amount of testing was conducted for lower grades which was the main goal of the initial project plan. For those grades where sample availability was not a problem, several repetitions of individual tests were undertaken. Because of a large variability of oil shale physical properties, such replications were very useful for providing more confidence in the results.

The evaluation of laboratory physical property test results for determining the effects of grade, temperature and confining pressure on oil shale properties was pursued through two seperate analyses. First, the actual test results were analyzed and the basic trends in oil shale behavior with changing levels of the variables involved were established. Secondly, an intensive

computer analysis of all available data was undertaken to formulate regression equations to mathematically represent the oil shale properties. The trends derived from the former analysis was used as a guide and input for the regression analysis.

As will be discussed later, it is not recommended that the actual test results be utilized by design engineers as a sole means of determining oil shale properties at a given level of grade, temperature and confining pressure. As noted earlier, due to inter sample variations in minerology and varve structure, oil shale properties exhibit highly variable behavior. Even for those tests where several replications were performed, large standard deviations were observed. Furthermore, because of missing data points particulary for higher grades, it is difficult to quantify the effects of some variables on oil shale behavior from the laboratory test results. The regression analysis, on the other hand, is more meaningful and accurate as it furnishes relationships based on evaluation of all available data.

To evaluate the effect of grade, temperature and confining pressure on oil shale compressive strength, the test results summarized in tables 3.4 and 3.5 were plotted for each variable versus the compressive strength. These plots are given in Appendix 6.7 for both the vertical and the horizontal cores. For discussion purposes, the graphs which included the most data points are presented in this section.

The effect of temperature on compressive strength for 15 gpt oil shale is displayed in Figures 3.6 and 3.7 for vertical and

horizontal cores, respectively. In these graphs, the compressive strength is depicted for various levels of confining pressure on the samples. These plots indicate a very dramatic effect of temperature on compressive strength with a significant loss of compressive strength occurring as the sample is heated to higher temperatures. It is also seen that the greatest portion of the strength is lost in heating only to 140°C. Of major importance is the trend observed in strength in heating beyond 380°C. For 15 gpt oil shale in particular for vertical cores, some portion of the strength lost due to heating to 380°C is regained when sample is heated to 500°C. For vertical cores, this observed behavior of strength above 380°C appears to hold true for all grades tested. The horizontal cores show this characteristic for 15 gpt grade, but the data is not conclusive to confirm the occurence of strength regain for higher grades. Thus it can be concluded that an apparent increase in strength beyond 380°C is more of a characteristic of vertical cores than the horizontal cores.

The regain of strength beyond 380°C for vertical cores is believed due to a significant loss of kerogen occurring in heating to this temperature. As the major portion of kerogen is driven off at this temperature, the remaining material would behave more like a solid mass, a phenomena which could result in strength increase. The magnitude of this strength regain is not as dramatic for higher grades because higher grades probably have more kerogen remaining in the sample beyond 380°C. Unfortunatly no data is available for temperatures beyond 500°C to determine whether the strength increase is a continual process.

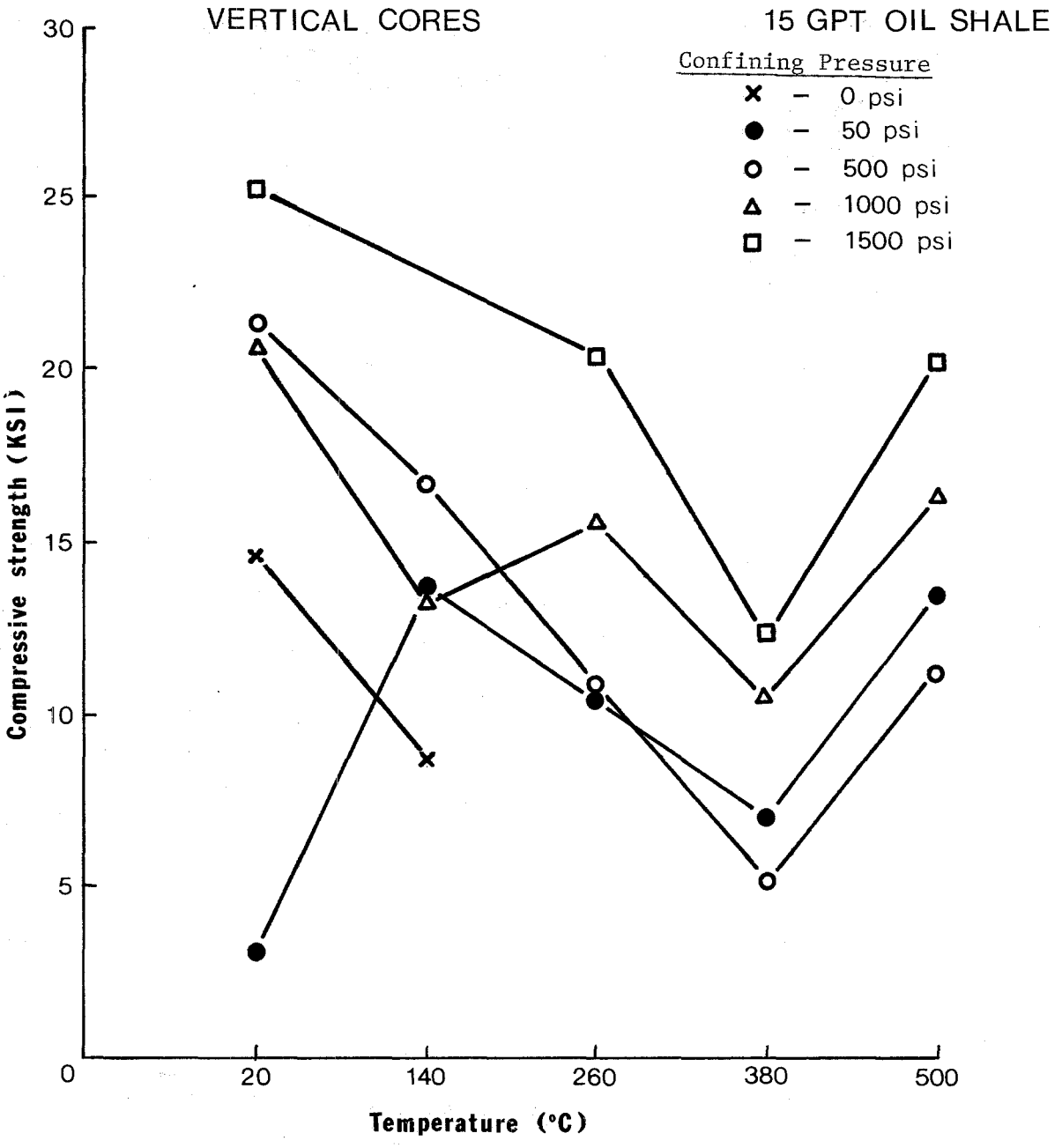

EFFECT OF TEMPERATURE ON COMPRESSIVE STRENGTH FOR 15 GPT OIL SHALE AT VARIOUS CONFINING PRESSURES
(Vertical cores, compression perpendicular to bedding)

FIGURE 3.6

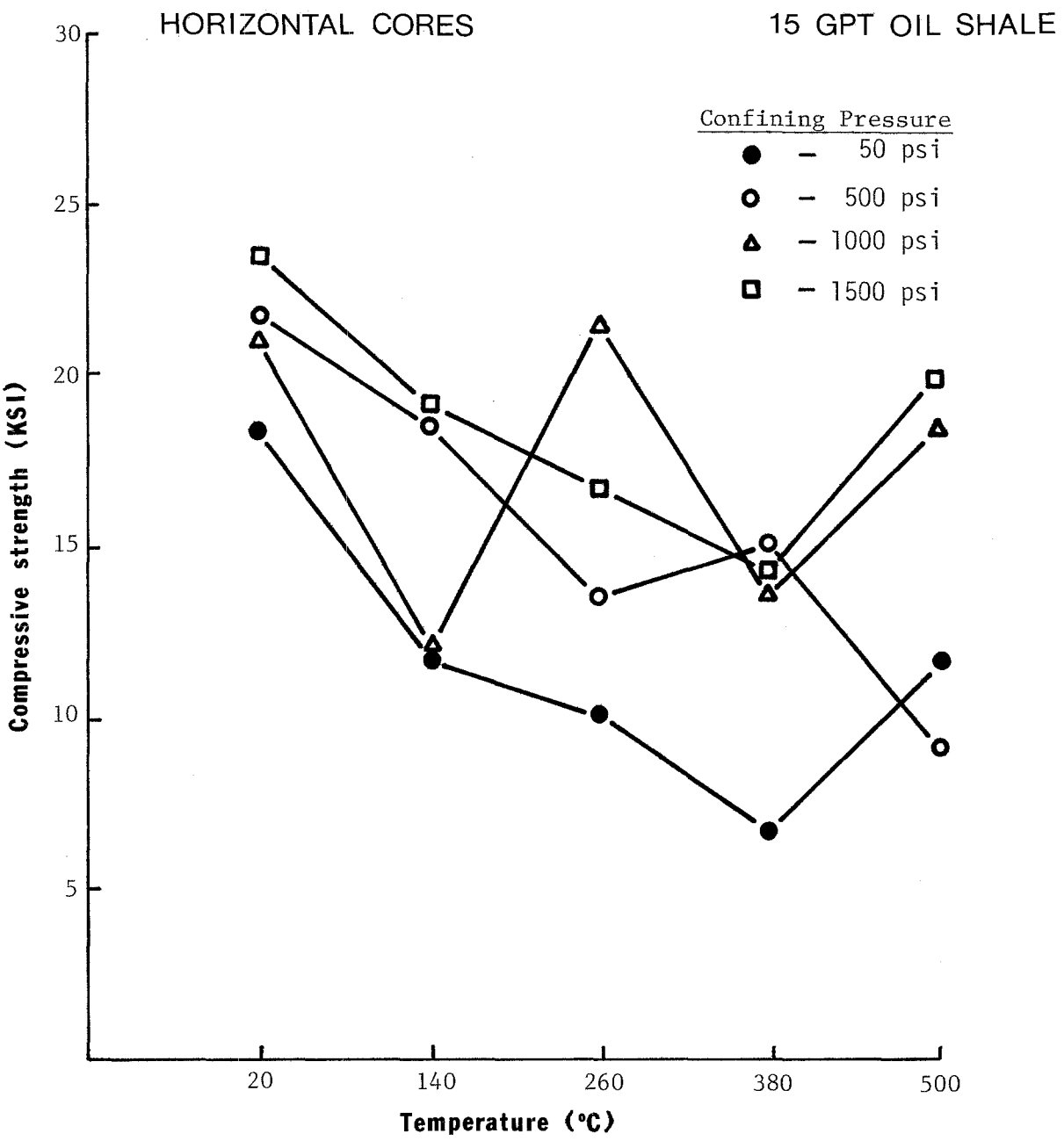

EFFECT OF TEMPERATURE ON COMPRESSIVE STRENGTH FOR 15 GPT OIL SHALE AT VARIOUS CONFINING PRESSURES
(Horizontal cores, compression parallel to bedding)

FIGURE 3.7

Regarding the compressive strength-confining pressure relationship, the results indicate the confining pressure to be very effective in increasing sample strength. Moreover, as the compressive strength becomes very low at higher temperatures, a greater proportionate effect of confining pressure is observed.

As expected, increased grade results in a consistent reduction of strength as shown in two representative plots in Figures 3.8 and 3.9 The rate of reduction in strength is greater at lower grades and appears to level off with higher grades. The strength of vertical cores seem to be more sensitive to grade than that for horizontal cores.

The comparison of the compressive strengths for vertical and horizontal cores are shown in graphical form in Figures 3.10, 3.11 and 3.12 for various confining pressures. The strength values for the horizontal cores are generally higher than those for vertical cores. This finding was contrary to expectations since ores containing bedding planes perpendicular to the direction of loading would be expected to withstand higher loads before failure. What might have caused this reverse trend is not clearly understood, however, it is strongly believed to be a result of variation in varve structure. A vertical core containing a rich band of kerogen would be more succeptible to premature failure than a horizontal core having a similar rich band. As can be seen in Figure 3.13, one or more kerogen rich bands present in a vertical core can contribute to excessive sample deformation and subsequent premature sample failure.

As previously stated, the second method of data analysis and evaluation involved the development of regression equations to

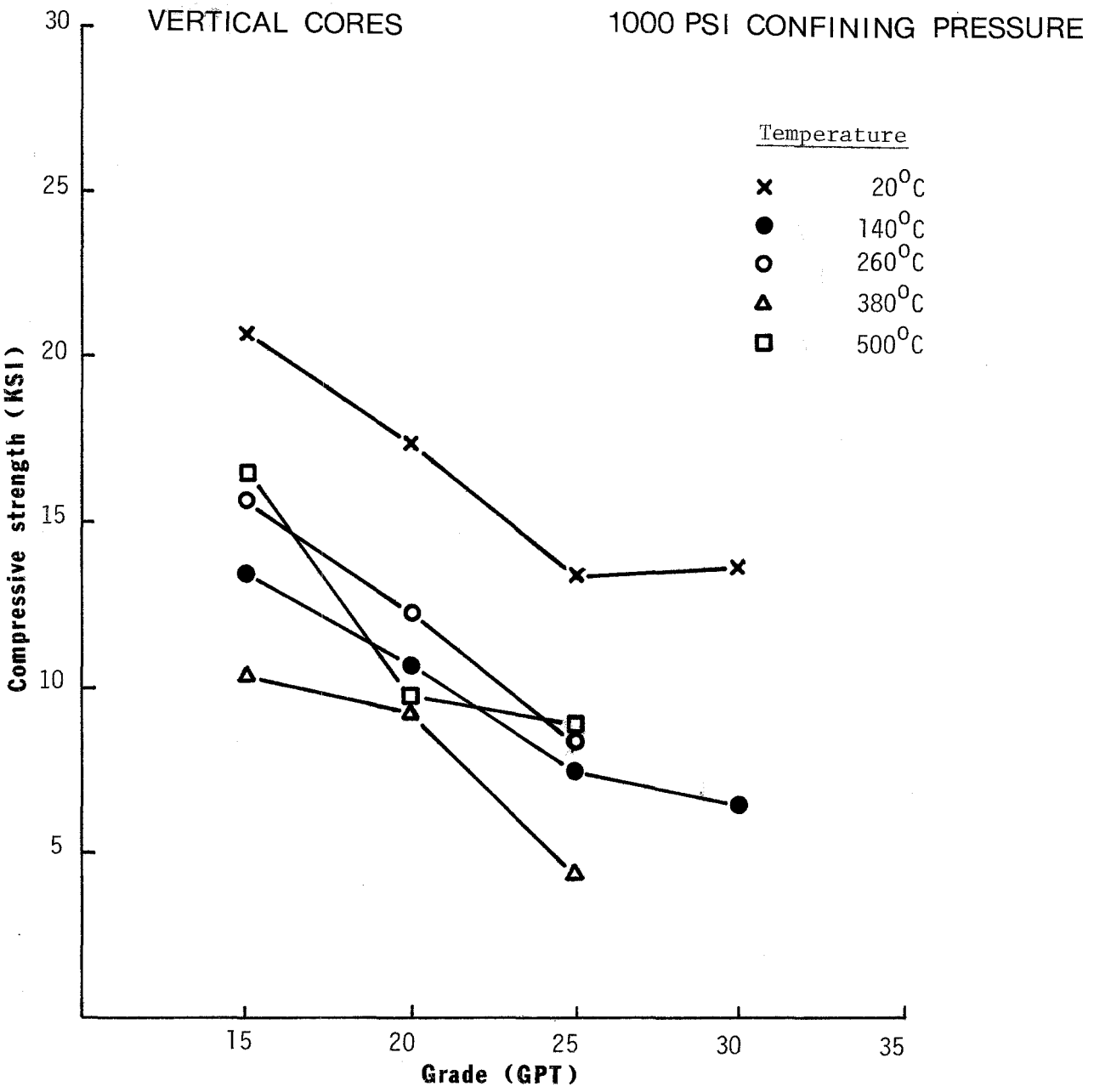

EFFECT OF GRADE ON COMPRESSIVE STRENGTH OF OIL SHALE

FOR VARIOUS TEMPERATURES AT 1000 psi CONFINING PRESSURE
(Vertical cores, compression perpendicular to bedding)

FIGURE 3.8

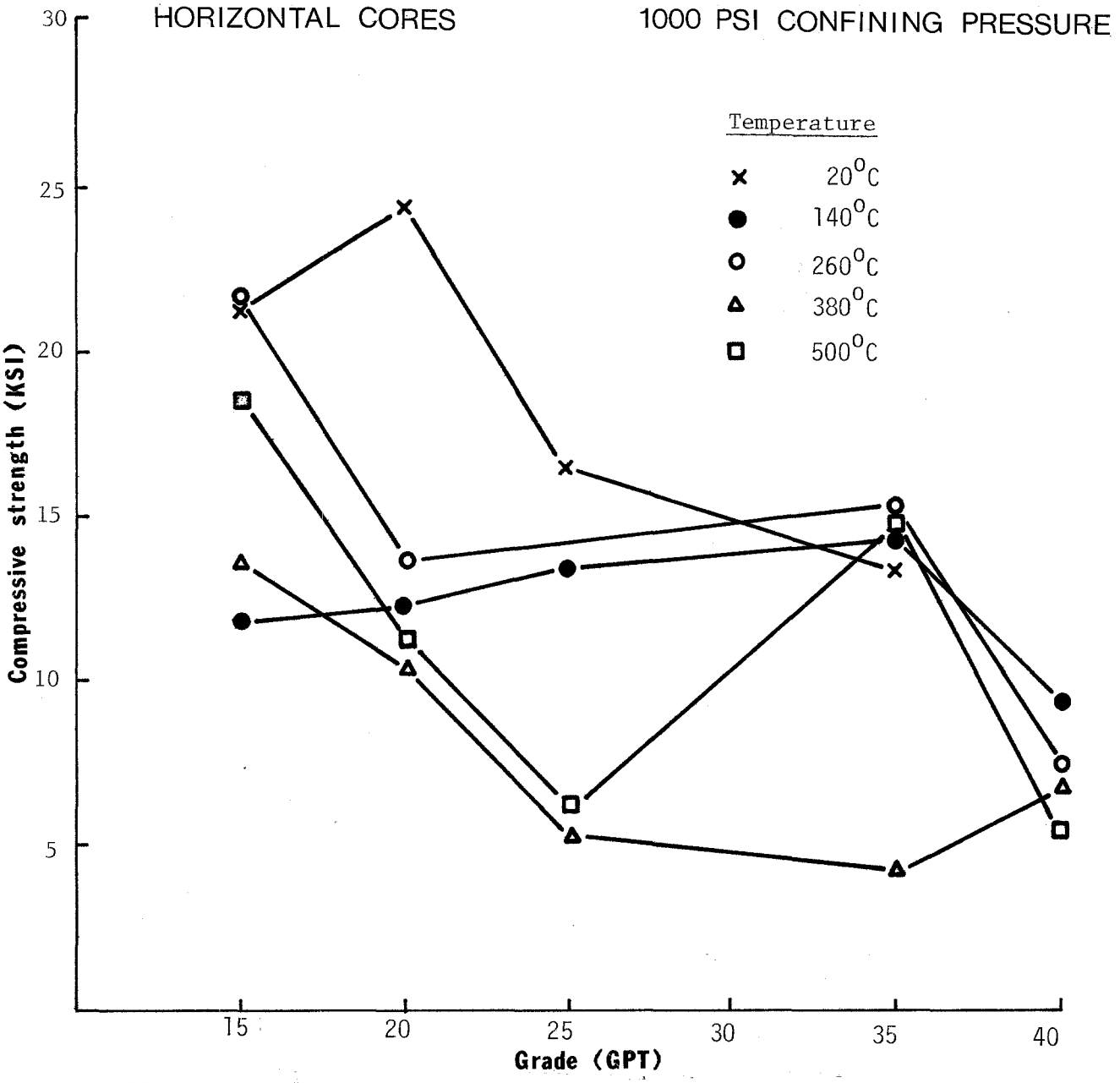

EFFECT OF GRADE ON COMPRESSIVE STRENGTH OF OIL SHALE FOR VARIOUS TEMPERATURES AT 1000 PSI CONFINING PRESSURE.
(Horizontal cores, compression parallel to bedding)

FIGURE 3.9

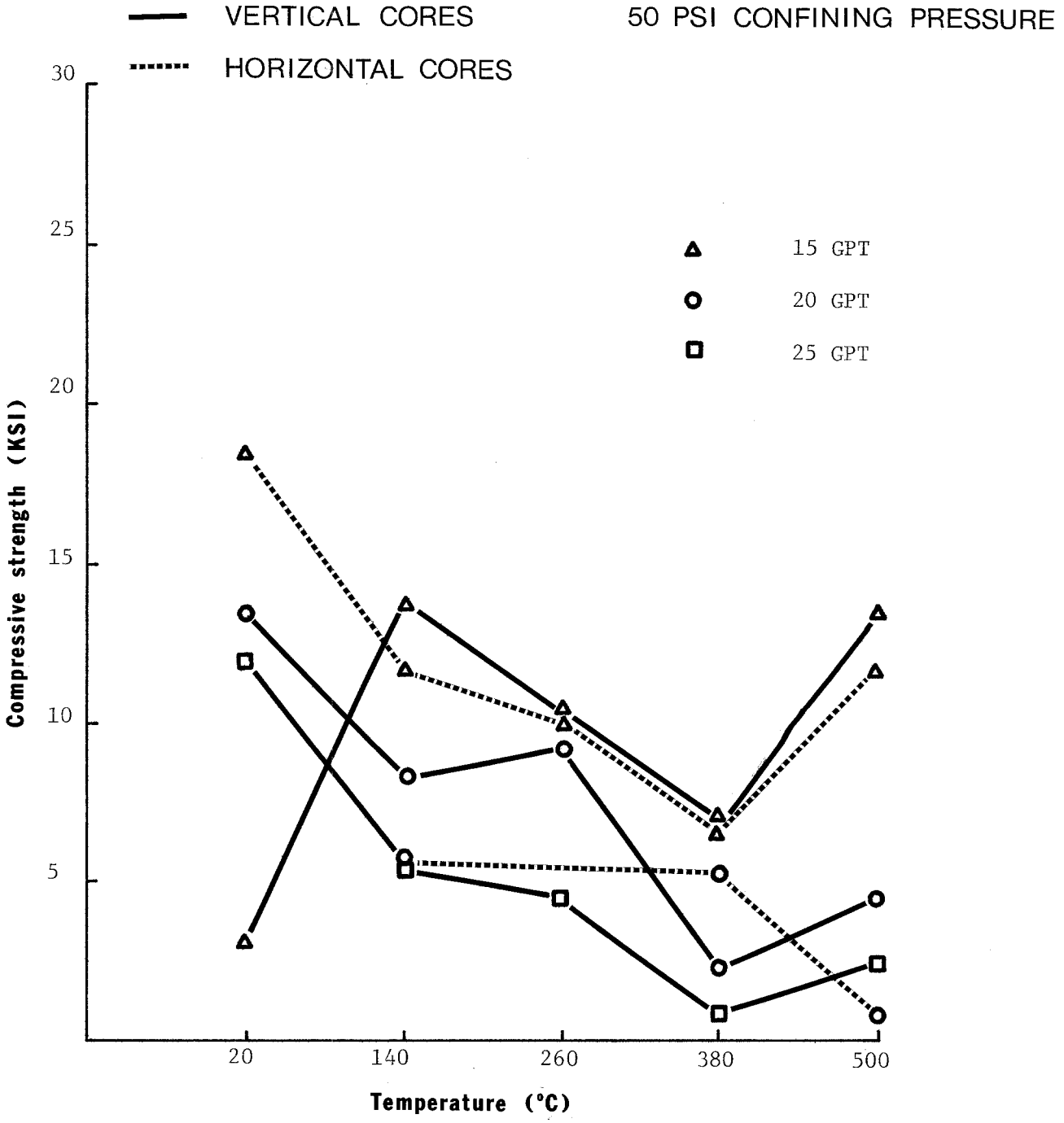

EFFECT OF BEDDING ORIENTATION ON THE COMPRESSIVE STRENGTH OF OIL SHALE AT VARIOUS TEMPERATURES AND GRADES FOR A 50 PSI CONFINING PRESSURE.

FIGURE 3.10

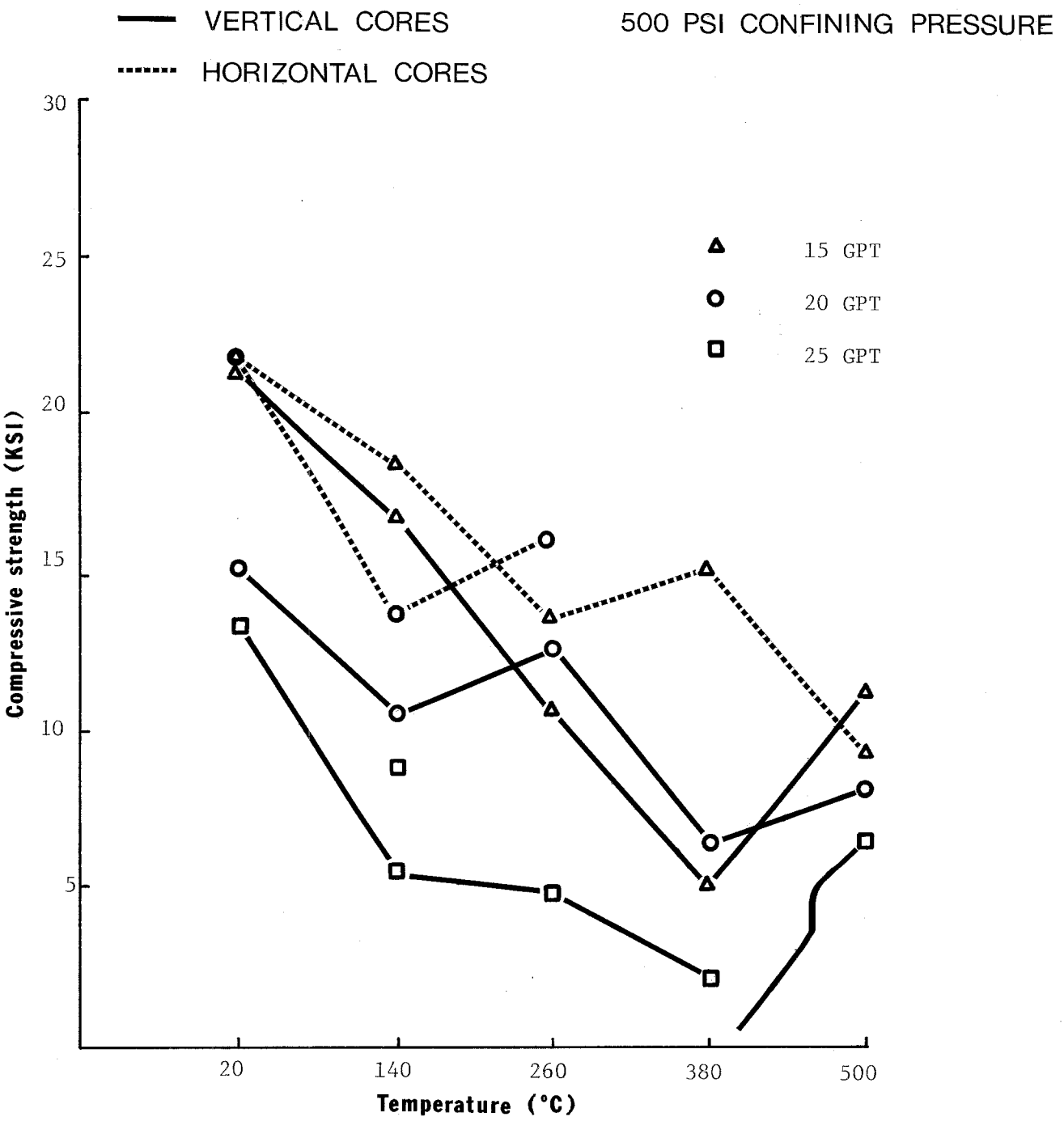

EFFECT OF BEDDING ORIENTATION ON THE COMPRESSIVE STRENGTH OF OIL SHALE AT VARIOUS TEMPERATURES AND GRADES FOR A 500 psi CONFINING PRESSURE

FIGURE 3.11

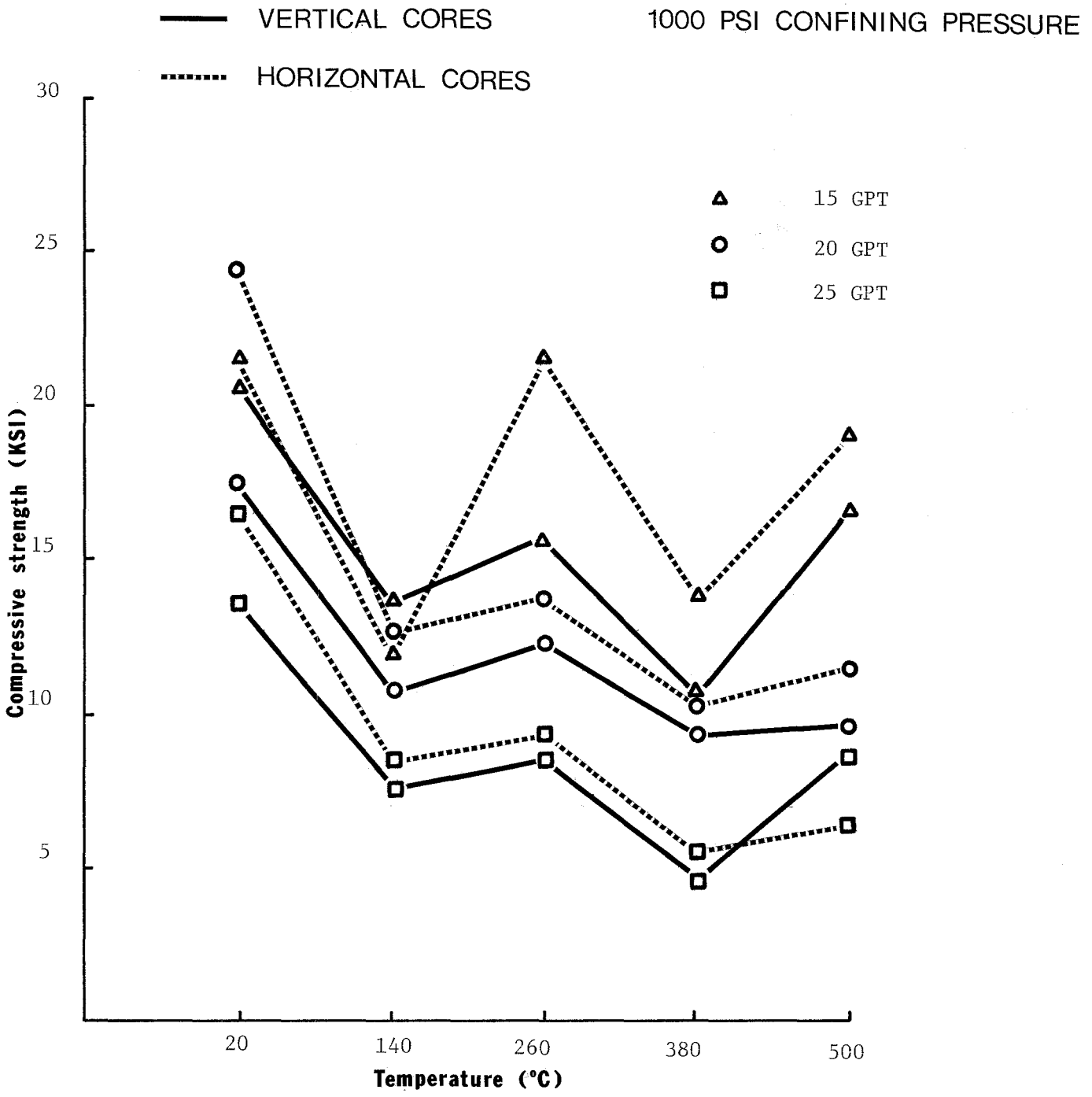

EFFECT OF BEDDING ORIENTATION ON THE COMPRESSIVE STRENGTH STRENGTH OF OIL SHALE AT VARIOUS TEMPERATURES AND GRADES FOR A 1000 psi CONFINING PRESSURE.

FIGURE 3.12

FIGURE 3.13

Two oil shale samples after high temperature-high pressure testing

mathematically represent the oil shale physical properties in terms of grade, temperature and confining pressure. The objective of the regression analysis was to derive a functional relationship between the variables and the oil shale properties that can adequately describe the behavior of oil shale under elevated temperatures and pressures for a range of grades.

The data fitting procedure employed was a stepwise regression approach. The process involved starting with simple single variable fits and then progressing by adding more complicated components until the increase in the quality of the fit did not compensate for the increase in the complexity of the equation.

At the outset of the data fitting procedure using the stepwise regression technique, exponential, logarithmic, reciprocal and low order polynomial fits were attempted. These elementary functions were selected for their high level of versatility, simplicity and because of their familiarity. After developing regression equations based on the preliminary functions, more complex functions were introduced into the analysis. These primarily included the combined terms of two or more variables in their various respective functions.

The evaluation of the quality of the individual equations derived to fit the data was based on three considerations. First evaluation involved the multiple correlation coefficient (R). Secondly, F statistics were calculated and compared for different equations developed. As a third method to assess the quality of the fit, the residual sums of errors were determined and compared. Of these three evaluation techniques, the one

involving the residuals was given the most consideration and the highest priority as a decision aid in the selection of "best fit" equation.

Once the "best fit" equation was developed through stepwise regression techniques, the functions included in the equation were then input into a computer program for running multiple linear regression analysis. Tables 3.6 and 3.7 summarize the results of this analysis regarding the compressive strength. The final forms of the equations formulated are as follows:

For Vertical Cores:

$$\sigma c = 10.75 + 186.6/G - 2.40 \ln T + .0040 P$$

For Horizontal Cores:

$$\sigma c = 12.9 + 212.6/G - 2.85 \ln T + .0045 P$$

Where:

σc = Compressive strength (psi)

G = Oil shale grade (gpt)

T = Temperature (^{o}C)

P = Confining pressure (psi)

Table 3.6
The Results of Multiple Linear Regression Performed on
Oil Shale Compressive Strength
(VERTICAL CORES)

Sample Size 137

Dependent Variable: S

Independent Variables: INVG LNT P

Coefficient of Determination 0.58282

Multiple Correlation Coeff. 0.76342

Estimated Constant Term 10.754525

Standard Error of Estimate 3.6208964

Analysis of Variance

for the Regression

Source of Variation	Degrees of Freedom	Sums of Squares	Mean Square	F-Probability
Regression	3	2436.07	812.023	61.93
Residuals	133	1743.75	13.1109	
Totals	136	4179.82		

Variable	Regression Coefficient	Standard Error of Regression Coefficient	F-Value DF (1, 133)	Probability	Correlation Coefficient With S
INVG	186.6076	22.82	66.85	0.0000	0.4410
LNT	-2.401117	.2622	83.8	0.0000	-0.4650
P	0.3997062E-02	.6353E-03	39.59	0.0000	0.3931

Table 3.7
The Results of Multiple Linear Regression Performed on Oil Shale Compressive Strength
(HORIZONTAL CORES)

Sample Size 128

Dependent Variable: S

Independent Variables: INVG LNT P

Coefficient of Determination 0.75568

Multiple Correlation Coeff. 0.86930

Estimated Constant Term 12.898222

Standard Error of Estimate 3.2297560

Analysis of Variance

For the Regression

Source of Variation	Degrees of Freedom	Sums of Squares	Mean Square	F	Probability
Regression	3	4000.79	1333.60	127.8	0.0000
Residuals	124	1293.48	10.4313		
Total	127	5294.27			

Variable	Regression Coefficient	Standard Error of Regression Coefficient	F-Value DF (1,124)	Probability	Correlation Coefficient With S
Invg	212.6147	14.83	205.5	0.0000	0.6115
LNT	-2.850600	.2509	129.1	0.0000	-0.4748
P	0.4483545E-02	.5300E-03	71.56	0.0000	0.3363

As shown in Tables 3.6 and 3.7 the multiple correlation coefficients (R) for the above equations are .76 and.869 for the vertical an horizontal cores, respectively. Even though the data fitting for the horizontal cores was based on a smaller sample size, the equation developed shows a higher correlation coefficient than that for vertical cores. This was due to larger variability of the laboratory measured physical property data for the vertical cores. As mentioned earlier, visual inspection of core samples after testing indicated that the varve structure influenced the load response behavior of vertical cores to a larger extent.

Another valuable piece of information that can be gained from the regression analysis is the relative importance of each variable in terms of their effect on the compressive strength. The degree of these effects are determined by comparing the F-statistic values given in Tables 3.6 and 3.7. The higher the F-value for a particular variable, the larger its effect on the response (i.e. the compressive strength in this case). The F-value calculations show that both for vertical and horizontal cores, the confining pressure had the least effect of all three variables on the strength. For the vertical cores, the temperature contributed the largest effect, followed by grade. This sequence was reversed for the horizontal cores, the results showing the grade to be the most significant variable affecting strength. As stated previously, similar conclusions were also evident from the analysis of laboratory physical property data.

A significant observation from the developed regression equations is that they both contain the same functions of the

variables involved with only differences being in the coefficients. This leads to the conclusion that the basic strength behavior of oil shale under elevated temperatures and pressures and for a wide range of grade is the same whether the load direction is parallel or perpendicular to bedding planes.

Following the derivation of regression equations, the predicted behavior of strength versus each variable was plotted using computer plotting techniques. Figures 3.14 through 3.18 display some representative graphs both for vertical and horizontal cores. The remaining plots for various grades, temperatures and confining pressures are given in Appendix 6.8.

Figures 3.14 and 3.15 show the strength versus temperature relationship for vertical and horizontal cores at different confining pressures. As the sample is heated from the ambient temperature, a significant loss of strength occurs. The rate of reduction in strength becomes smaller with further increases in temperature as the curves are seen to level off. A major loss of strength in heating to lower temperatures was also observed in analyzing the results of laboratory tests. As would be remembered, the laboratory data showed significant loss of strength occurring in heating only to 140^{o}C.

The strength-temperature relationships plotted according to the developed regression equations show the same general trend as that observed from the analysis of actual laboratory data. There appears to be disagreement between the two, however, for temperatures beyond 380^{o}C. As previously discussed, the laboratory data indicated a regain of strength, particularly for vertical cores, when the samples were heated from 380^{o}C to

FIGURE 3.14

PREDICTED BEHAVIOR OF COMPRESSIVE STRENGTH VS. TEMPERATURE

FOR 20 gpt OIL SHALE AT VARIOUS CONFINING PRESSURES

(Vertical Cores, compression perpendicular to bedding)

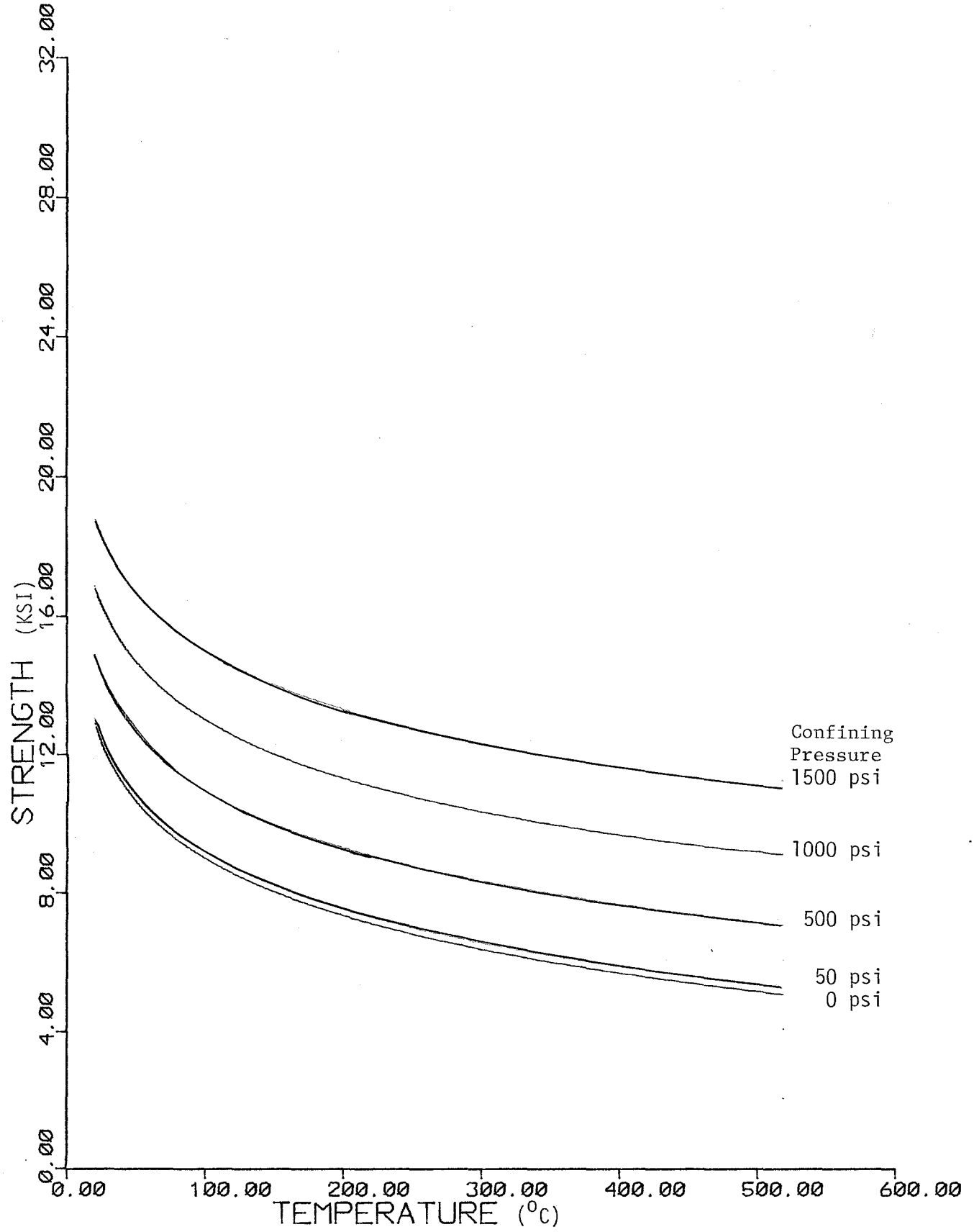

FIGURE 3.15

PREDICTED BEHAVIOR OF COMPRESSIVE STRENGTH VS. TEMPERATURE
FOR 20 gpt SHALE AT VARIOUS CONFINING PRESSURES
(Horizontal cores, compression parallel to bedding)

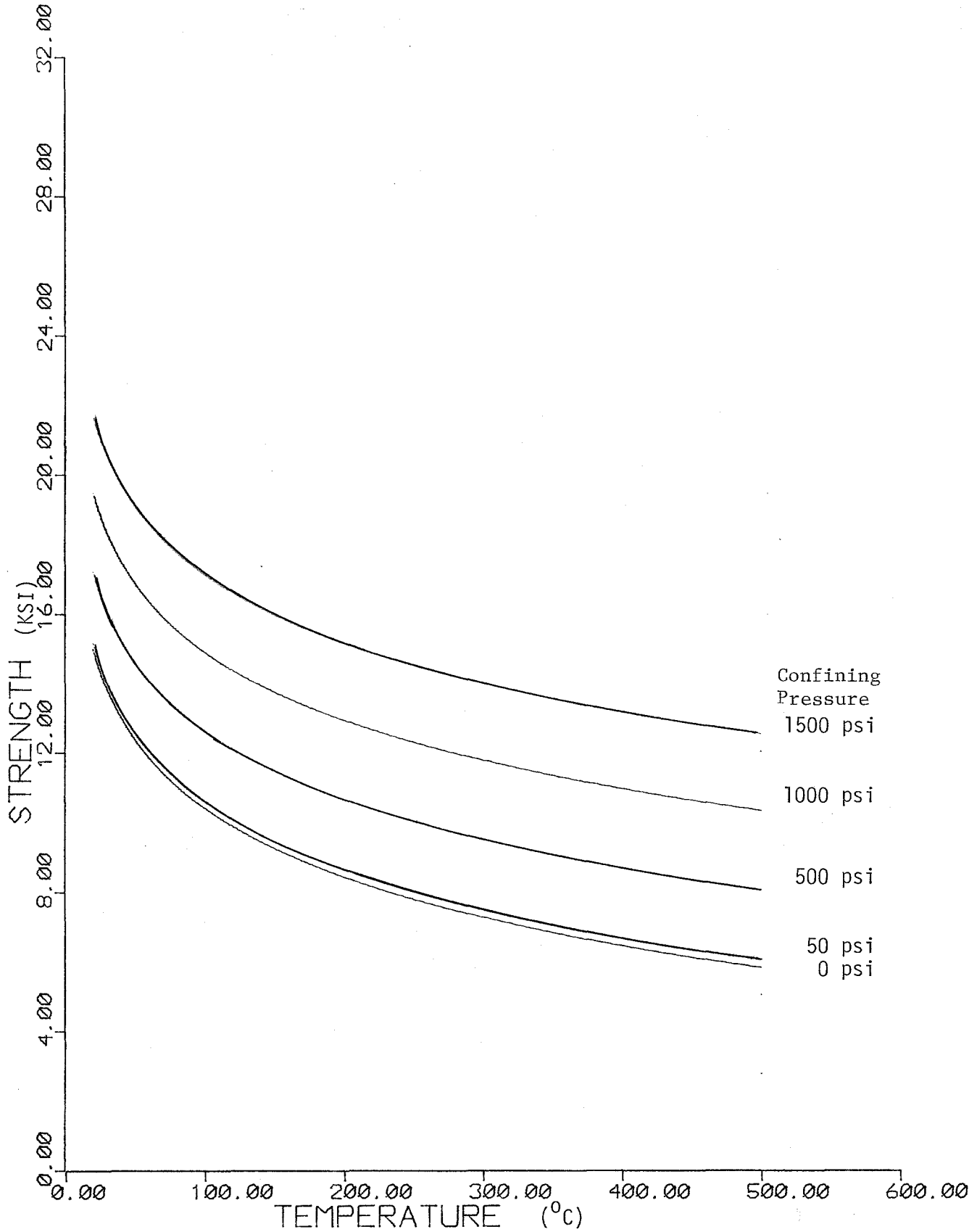

FIGURE 3.16

PREDICTED BEHAVIOR OF COMPRESSIVE STRENGTH VS. GRADE
FOR OIL SHALE AT 500 psi CONFINING PRESSURE
(Vertical cores, compression perpendicular to bedding)

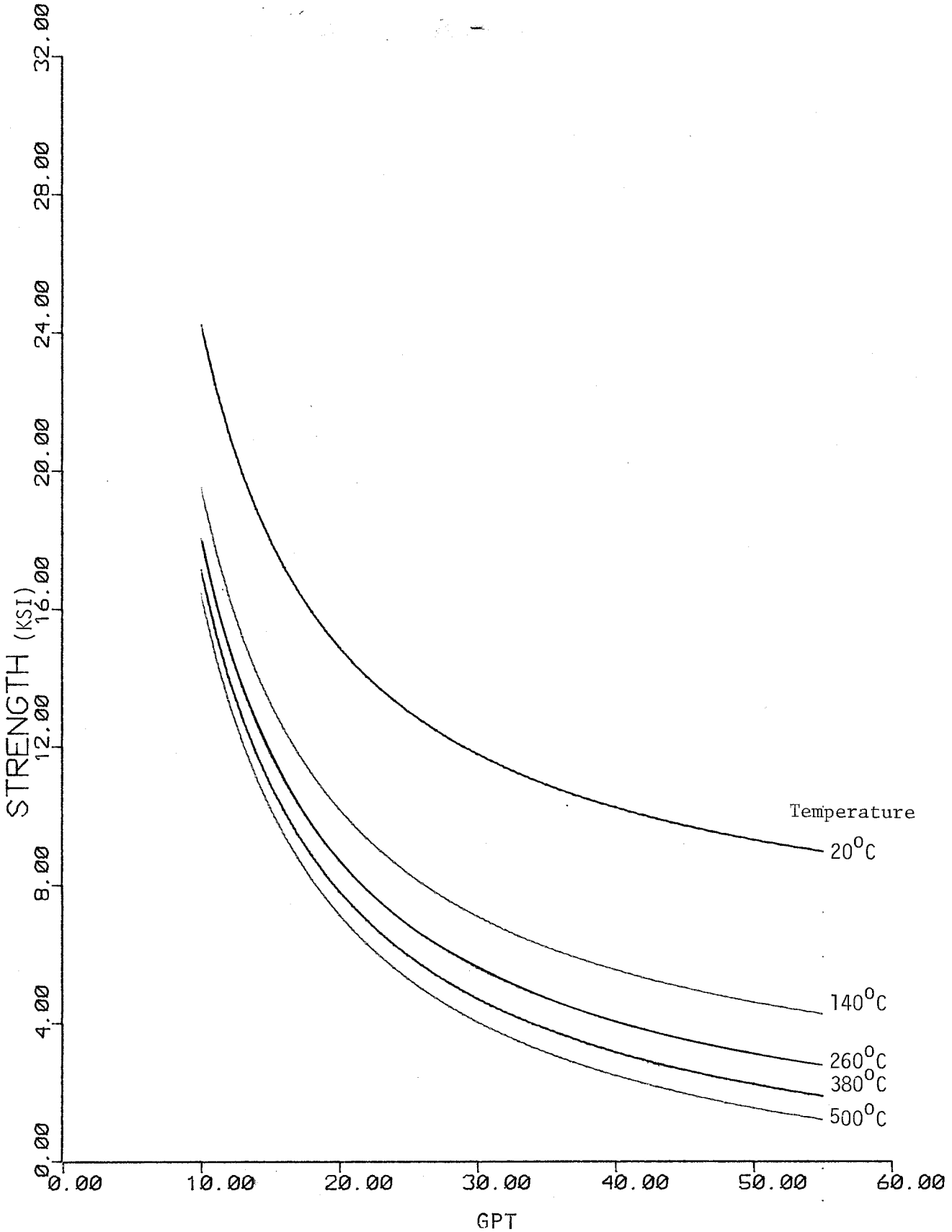

FIGURE 3.17

PREDICTED BEHAVIOR OF COMPRESSIVE STRENGTH VS. GRADE
FOR OIL SHALE AT 500 psi CONFINING PRESSURE
(Horizontal cores, compression parallel to bedding)

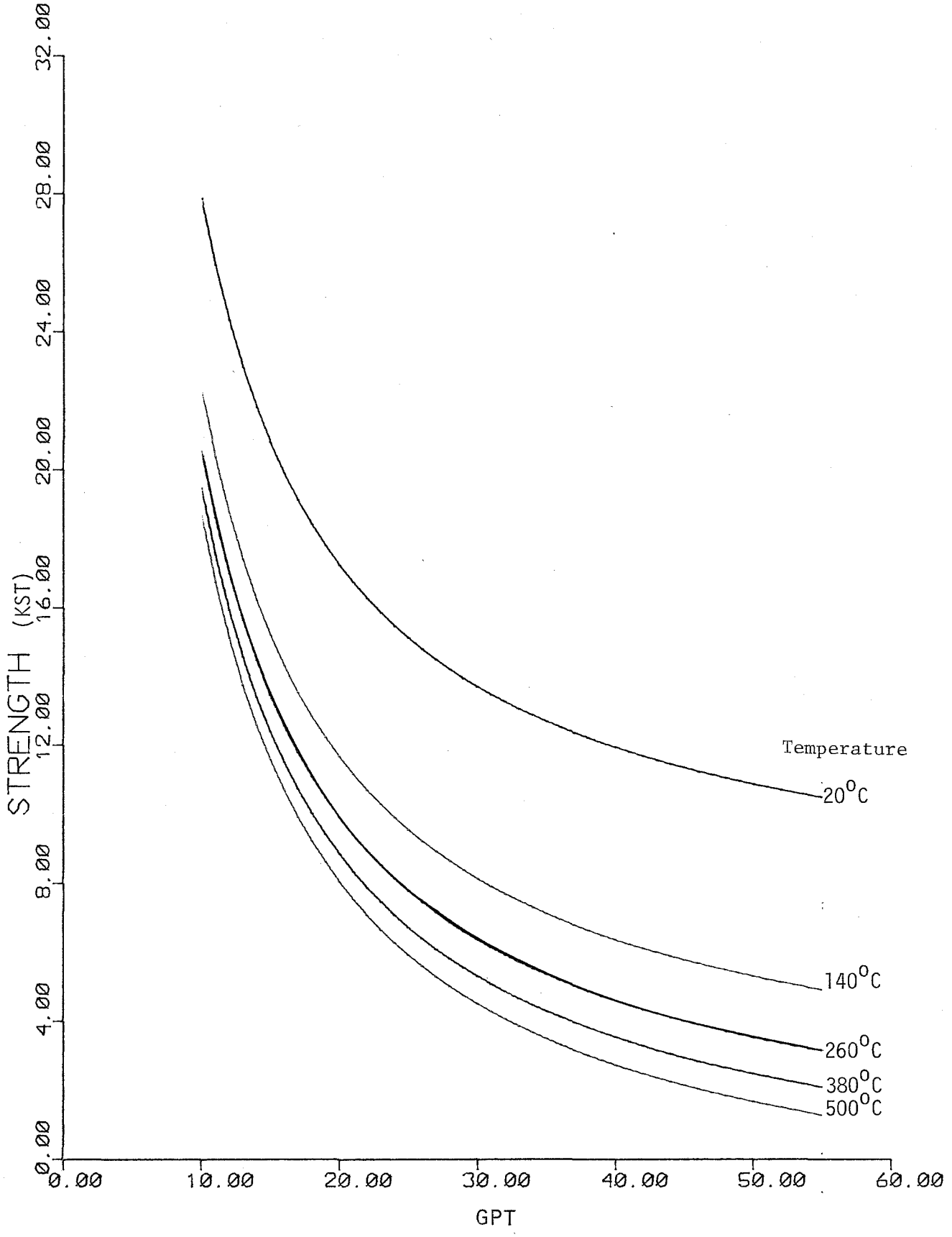

FIGURE 3.18

PREDICTED BEHAVIOR OF COMPRESSIVE STRENGTH VS. CONFINING PRESSURE
FOR 20 gpt OIL SHALE AT VARIOUS TEMPERATURES
(Horizontal cores, compression parallel to bedding)

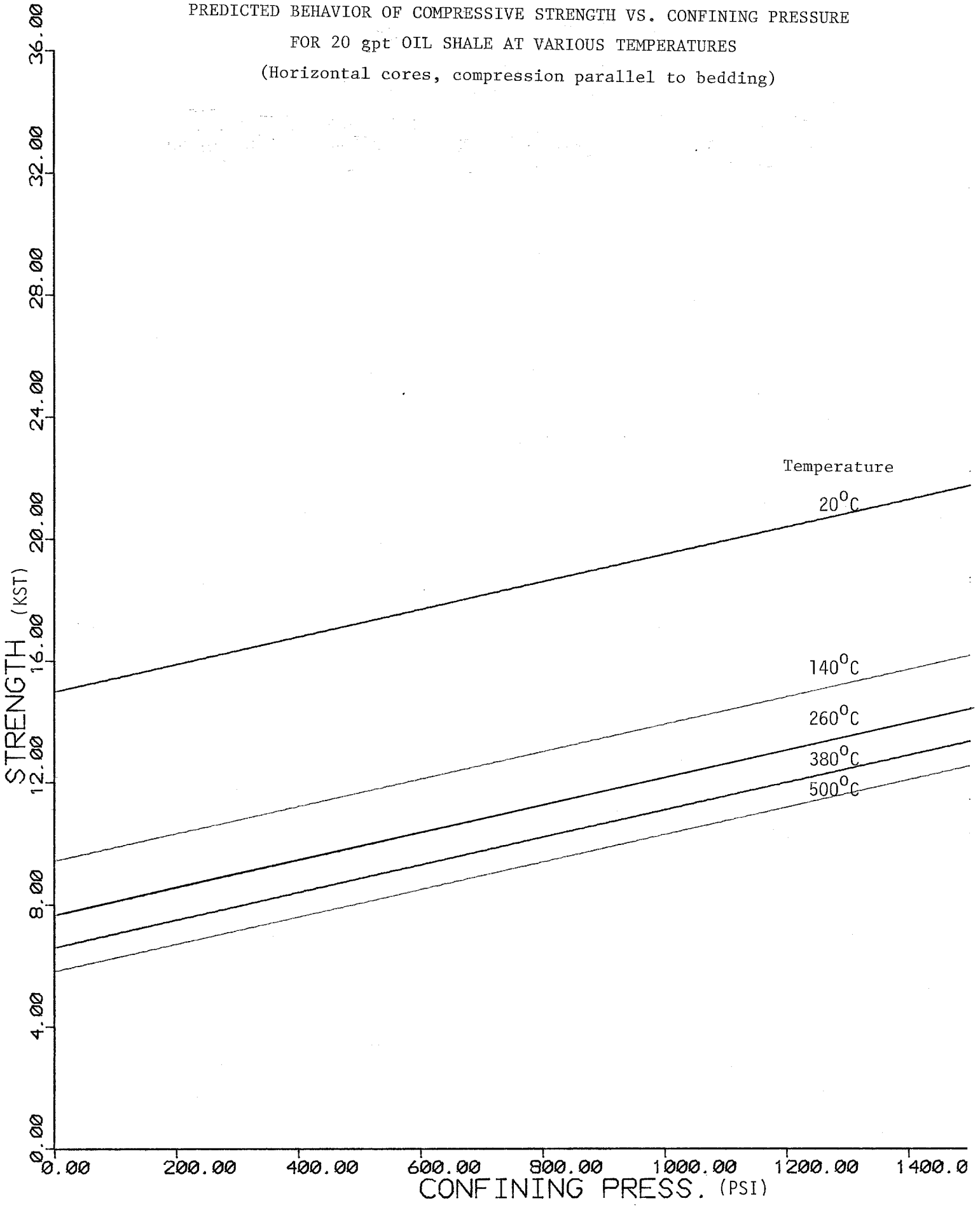

500°C. Such a trend is not present in the curves drawn from the developed equations. The cause of this discrepancy is due to a combined effect of two factors. First, the graphs displaying the results of laboratory physical property measurements regarding the effect of temperature on strength were evaluated on a grade by grade basis. In this analysis, the general trend of increased strength with increasing temperature from 380°C to 500°C was observed. In the computer analysis for equation development, however, all of the data are used, including the replications of all tests, if they were available. Thus, the computer analysis was based on a large source of data from which the equations representing the oil shale behavior at elevated temperatures and pressures and for various grades were derived. The second factor was due to the requirement of formulating simple equations without introducing complex functions. If certain high degree polynomials were included in the equations, the apparent strength increase beyond 380°C could be observed in the predicted strength behavior. Formulation of long, complicated equations was not desired since it was the intent of regression analysis to provide the design engineer with simple, easy to use equations which represent the actual data as accurately as possible. Thus, with the developed equations, it is reasonable to assume that at a temperature of 500°C, the equations would provide a lower strength value than actually possible. Thus, the strength values calculated by the equations would be on the conservative side for these high temperatures. Since no strength data was available at higher temperatures, it is not known how temperature affects strength at values above 500°C.

Figures 3.16 and 3.17 show the relationship between grade and strength as determined from the developed regression equations. The grade appears to have a consistent effect on strength, causing an appreciable reduction of strength for increases within the lower grade ranges. At higher grades the strength loss due to increasing grade is seen to be much lower than for lower grades.

A representative plot of confining pressure strength relationship based on developed regression equations is shown in Figure 3.18 As expected, the relationship is linear with confining pressure being indicated as an effective means of increasing oil shale strength for all levels of temperatures and grades included in the testing program.

3.2.4 Brazilian (indirect) Tensile Strength

The Brazilian tensile strength tests were performed using a standard compression testing machine. The samples used were 2 inches in diameter and 1 inch thick. Tests were undertaken both with vertical and horizontal cores (Figure 2.1). For the vertical core testing, samples were oriented so that the direction of loading was perpendicular to the bedding planes. The load direction for the horizontal cores was parallel to the bedding planes.

The results of tensile strength tests are shown in Tables 3.8 and 3.9 for the vertical and the horizontal cores, respectively. Included in the tables are the average strength values, the standard deviations and the number of samples tested for each combination of grade and temperature. As expected, even

TABLE 3.8

BRAZILIAN TENSILE STRENGTHS

(Vertical cores, loading perpendicular to bedding)
All strengths in PSI

Grade (gpt)		Temperature °C 20	140	260	380	500
10	Mean	1646				
	Std.Dev.	±407				
	# Samples	(4)				
15	Mean	1745	1021	794	296	284
	Std.Dev.	±891	±415	±569	±313	±181
	# Samples	(5)	(7)	(10)	(5)	(8)
20	Mean	1200	576	575	47	14
	Std.Dev.	±416	±231	±298	±74	±14
	# Samples	(5)	(5)	(5)	(5)	(4)
25	Mean	1601	543	284	211	99
	Std.Dev.	±675	±177	±94	±334	±160
	# Samples	(6)	(7)	(7)	(8)	(7)
30	Mean	1309	477	131	133	15.2
	Std.Dev.	±935	±315	±49	±10	--
	# Samples	(4)	(5)	(5)	(5)	(1)
35	Mean	1541	500	195	0	0
	Std.Dev.	±182	±126	±136		
	# Samples	(5)	(5)	(5)		
40	Mean	1122	399	262	0	0
	Std.Dev.	±518	±87	±93		
	# Samples	(5)	(5)	(5)		

TABLE 3.9

BRAZILIAN TENSILE STRENGTHS

(Horizontal cores, loading parallel to bedding)
All strengths in PSI

Grade (gpt)		Temperature (°C) 20°	140°	260°	380°	500°
15	Mean	584	606	360	199	352
	Std.Dev.	±557	±401	±154	±105	±142
	# Samples	(5)	(5)	(5)	(5)	(5)
20	Mean	1049	586	357	460	462
	Std.Dev.	±265	±247	±165	±19	±306
	# Samples	(5)	(5)	(5)	(5)	(5)
25	Mean	812	913	609	326	456
	Std.Dev.	±175	±166	±297	±197	±215
	# Samples	(5)	(5)	(5)	(5)	(5)
30	Mean	1099	616	645	407	333
	Std.Dev.	±266	±197	±84	±217	±128
	# Samples	(5)	(5)	(5)	(5)	(5)
35	Mean	1279	711	177	293	138
	Std.Dev.	±161	±73	±75	±142	±35
	# Samples	(5)	(5)	(5)	(5)	(5)
40	Mean	949	482	324	195	96
	Std.Dev.	±460	±67	±215	±74	±25
	# Samples	(5)	(5)	(4)	(5)	(5)

with high replication rates (up to 10 tests per condition), standard deviations were quite large.

Figures 3.19 and 3.20 show the effect of temperature on tensile strength for vertical and horizontal cores, respectively. Temperature is seen to have a dramatic effect on strength with a significant loss of strength occurring over a temperature increase from 20 to 140°C. This sensitivity of tensile strength to temperature is quite similar to that observed for the compressive strength in which a major strength loss was found to occur in heating only to 140°C. The graphical results also indicate that heating from 380°C to 500°C results in a minor or no loss in tensile strength. As previously discussed, for the compressive strength a general increase in strength was observed within this temperature range. Thus, the explanation given earlier to support this finding can also be applied to tensile strength in that as the major portion of kerogen is driven off the oil shale samples, strength reduction due to higher temperatures is minimal or non-existent.

The behavior of tensile strength with varying grade is shown in Figure 3.21 for vertical cores and in Figure 3.22 for horizontal cores. As can be observed in these plots, due to large variation in data, no consistent effect of grade on strength is present. However, for vertical cores, a gradual reduction of strength appears to occur with increasing grade.

Figure 3.23 is drawn to delineate the comparison of tensile strengths for vertical and horizontal cores. Plotted in this figure are the tensile strengths averaged over grade. At a

FIGURE 3.19

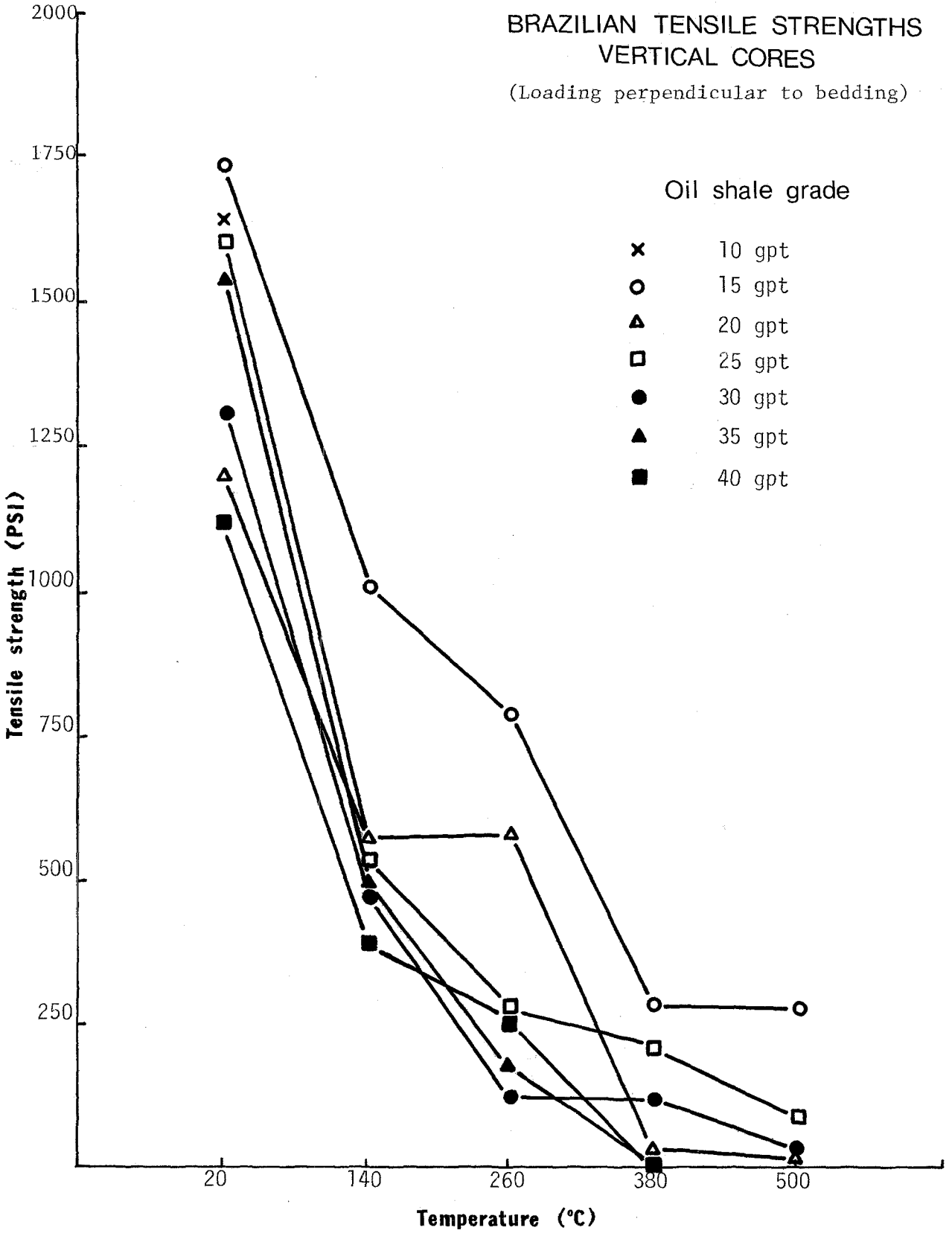
BRAZILIAN TENSILE STRENGTHS
VERTICAL CORES
(Loading perpendicular to bedding)
Oil shale grade
10 gpt
15 gpt
20 gpt
25 gpt
30 gpt
35 gpt
40 gpt
Tensile strength (PSI)
2000
1750
1500
1250
1000
750
500
250
20
140
260
380
500
Temperature (°C)

FIGURE 3.20

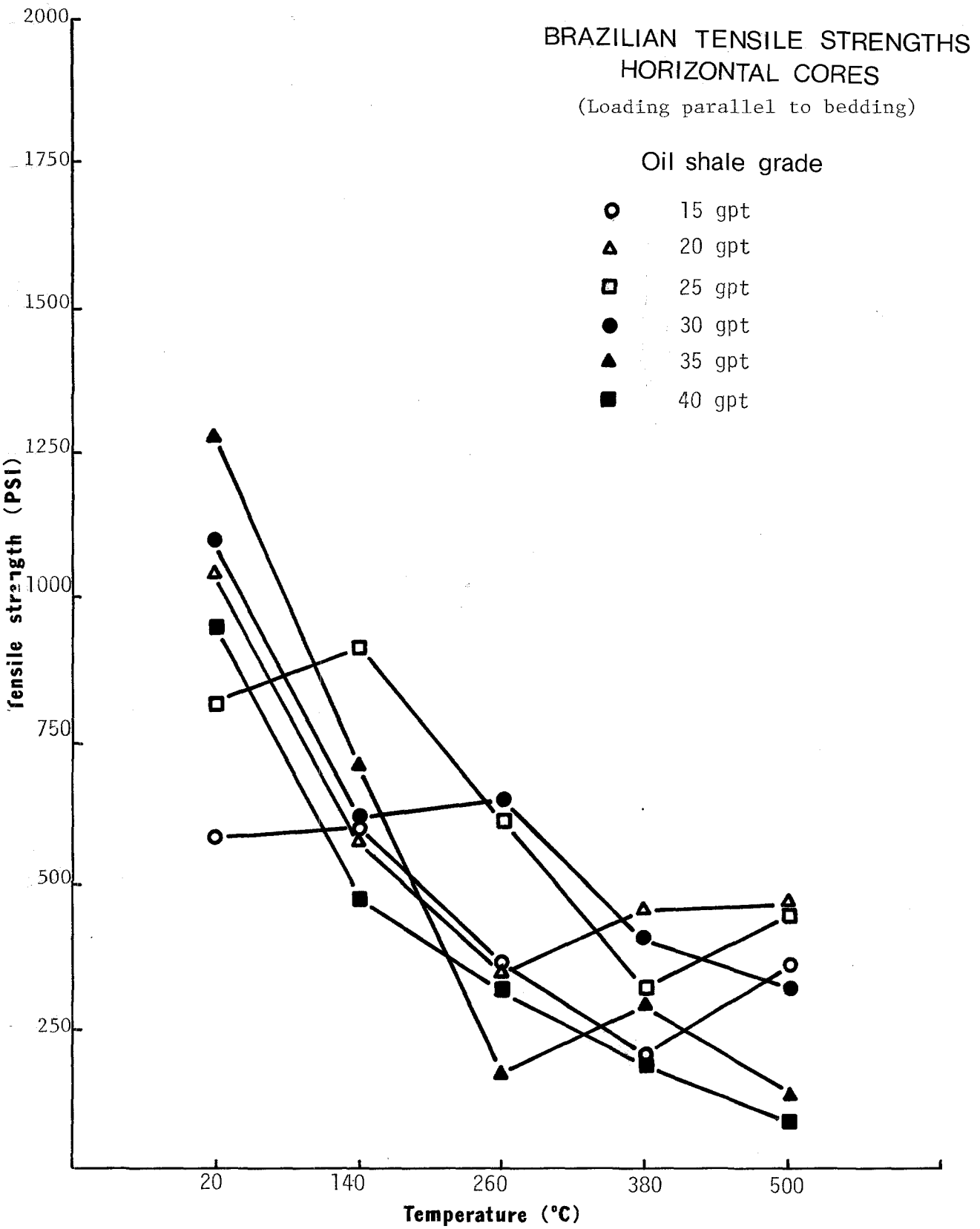
BRAZILIAN TENSILE STRENGTHS
HORIZONTAL CORES
(Loading parallel to bedding)
Oil shale grade
15 gpt
20 gpt
25 gpt
30 gpt
35 gpt
40 gpt
Tensile strength (PSI)
2000
1750
1500
1250
1000
750
500
250
20
140
260
380
500
Temperature (°C)

FIGURE 3.21

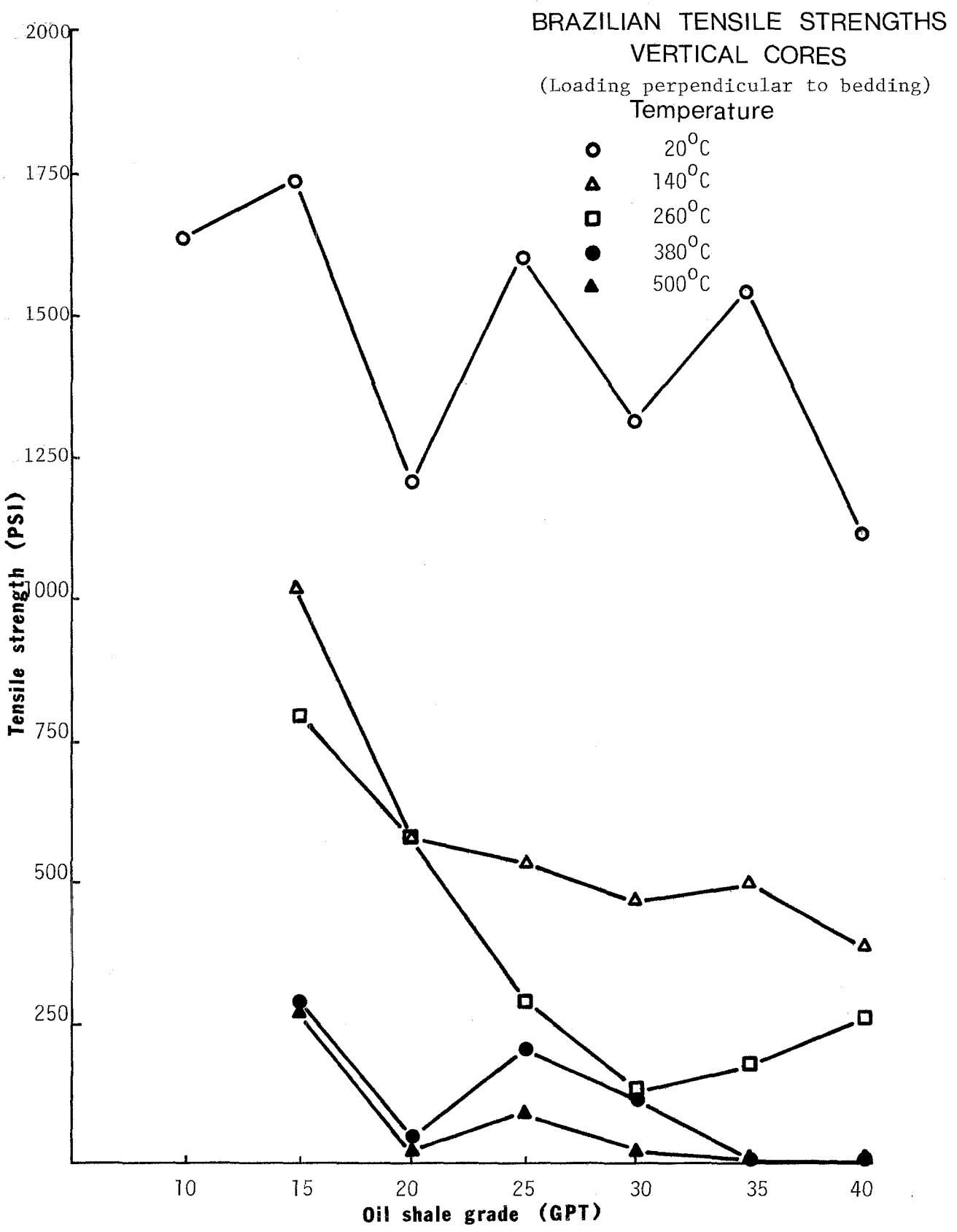
BRAZILIAN TENSILE STRENGTHS
VERTICAL CORES
(Loading perpendicular to bedding)
Temperature
20°C
140°C
260°C
380°C
500°C
Tensile strength (PSI)
2000
1750
1500
1250
1000
750
500
250
10
15
20
25
30
35
40
Oil shale grade (GPT)

FIGURE 3.22

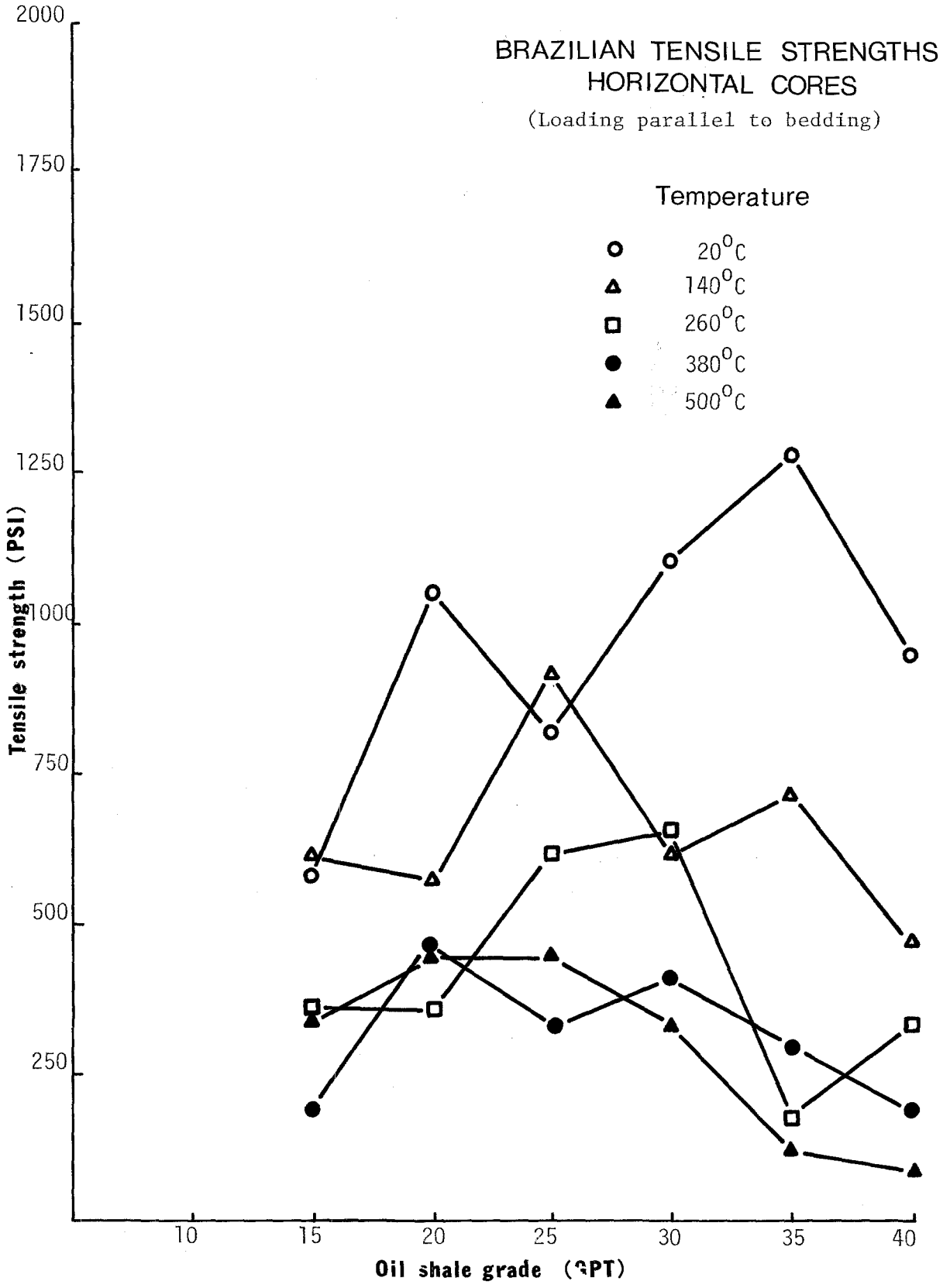
BRAZILIAN TENSILE STRENGTHS
HORIZONTAL CORES
(Loading parallel to bedding)
Temperature
20°C
140°C
260°C
380°C
500°C
Tensile strength (PSI)
2000
1750
1500
1250
1000
750
500
250
10
15
20
25
30
35
40
Oil shale grade (GPT)

FIGURE 3.23

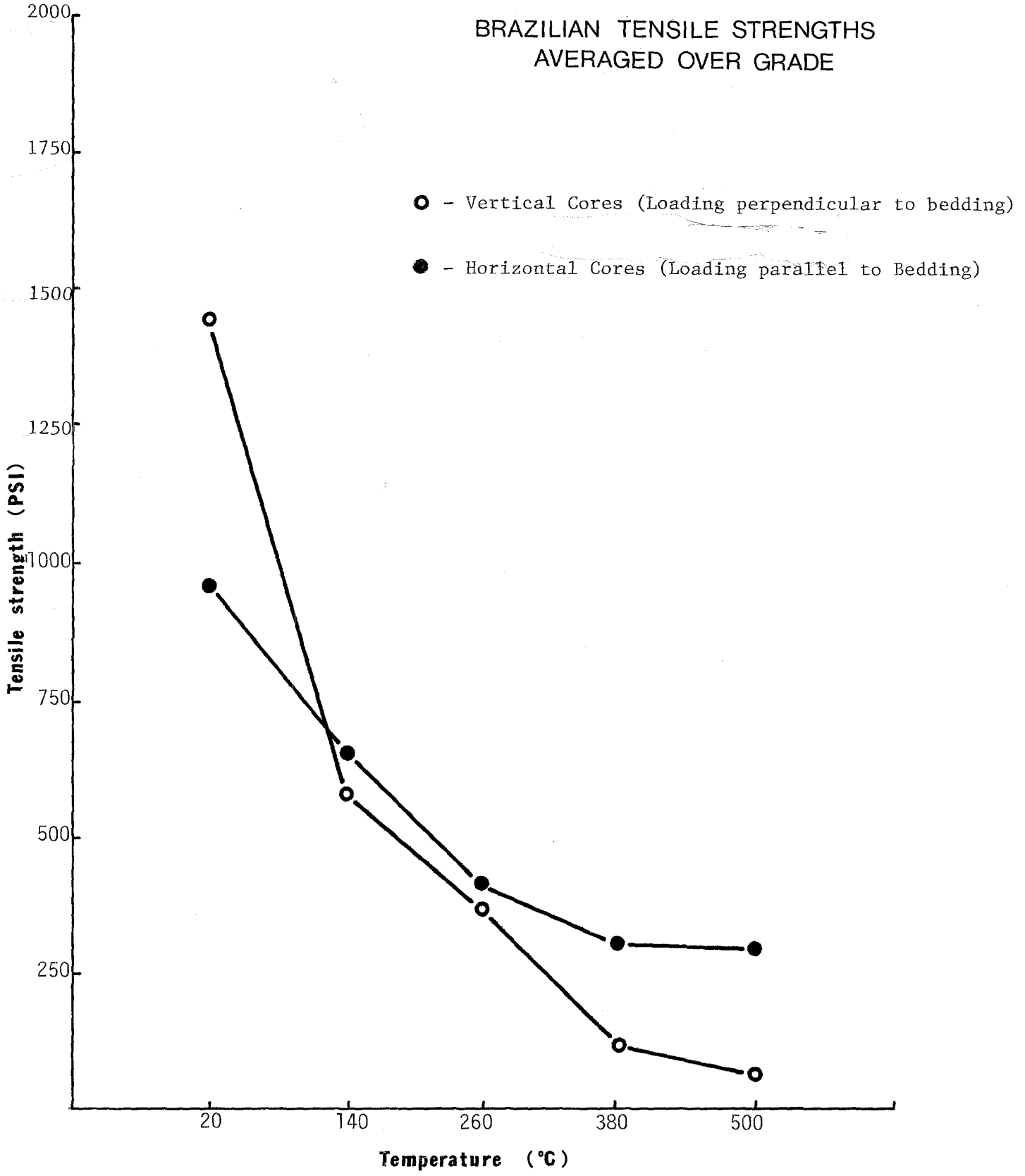
BRAZILIAN TENSILE STRENGTHS
AVERAGED OVER GRADE
O - Vertical Cores (Loading perpendicular to bedding)
● - Horizontal Cores (Loading parallel to Bedding)
Tensile strength (PSI)
2000
1750
1500
1250
1000
750
500
250
20
140
260
380
500
Temperature (°C)

temperature of 20°C, the tensile strength of vertical cores is more than 50% higher than that for horizontal cores. However, the vertical cores suffer a considerable loss of strength in heating to 140°C, resulting in consistently lower tensile strength than the horizontal cores for temperatures above 140°C. Furthermore, at high temperatures (above 380°C), the vertical cores virtually lose all of their tensile strength.

Following the evaluation of laboratory tensile strength data, the entire data were input into a computer program with the objective of developing regression equations to represent the tensile strength in a mathematical form as functions of temperature and grade. The procedure employed for this analysis was the same as that used for the compressive strength, involving a stepwise regression technique.

From the computer analysis, the following regression equations were developed (Tables 3.10 and 3.11)

For vertical cores,

$$T_o = 3105-425.71n\ T - 14.84\ G$$

For horizontal cores,

$$T_o = 1666-214\ 1n\ T - 1.416\ G$$

Where T_o= Tensile Strength (psi)

T= Temperature (°C)

G= Grade (gpt)

Table 3.10

The Results of Multiple Linear Regression Performed on Indirect (Brazilian) Tensile Strength of Oil Shale (Vertical Cores)

Sample Size 30

Dependent Variable: S

Independent Variables: LNT G

Coefficient of Determination 0.93177

Multiple Corr. Coeff. 0.96528

Estimated Constant Term 3104.8906

Standard Error of Estimate 144.21772

Analysis of Variance

For the Regression

Source of Variation	Degrees of Freedom	Sums of Squares	Mean Square	F	Probability
Regression	2	0.766910E+07	.383455E+07	184.4	0.0000
Residuals	27	561566	20798.8		
Total	29	0.823067E+07			

Variable	Regression of Regression Coefficient	Standard Error DF Coefficient	F-Value Coefficient (1,27)	Probability	Correlation With S
LNT	-425.7409	22.90	345.6	0.0000	-0.9345
G	-14.84090	3.084	23.16	0.0001	-0.2419

Table 3.11

The Results of Multiple Linear Regression Performed on Indirect (Brazilian) Tensile Strength of Oil Shale (Horizontal Cores)

Sample Size 30

Dependent Variable: S

Independent Variables: LNT G

Coefficient of Determination 0.69528

Multiple Corr Coeff. 0.83383

Estimated Constant Term 1665.9597

Standard Error of Estimate 171.88285

Analysis of Variance

For the Regression

Source of Variation	Degrees of Freedom	Sums of Squares	Mean Square	F	Probability
Regression	2	0.182004E+07	910019.	30.80	0.0000
Residuals	27	797680.	29543.7		
Total	29	0.261772E+07			

Variable	Regression Coefficient	Standard Error of Regression Coefficient	F-Value DF (1,27)	Coefficient Probability	Correlation With S
LNT	-213.9828	27.30	61.46	0.0000	-0.8328
G	-1.415994	3.675	.1485	0.7030	-0.0409

The multiple correlation coefficients for the regression equations were .96 and .83 for the vertical and horizontal cores, respectively.

The F-values calculated for the regression variables (Tables 3.10 and 3.11) indicate that between the two variables, the temperature by far has the largest effect on the tensile strength. The F-value for the temperature is several orders of magnitude larger than that for grade. With its very low F-value, it thus can be concluded that grade has very little effect on tensile strength.

3.2.5. Elastic Properties

The measured elastic properties, the Young's modulus and the Poisson's ratio were presented earlier in Tables 3.4 and 3.5. A quick glance at the data listed in these tables shows a large variation in the elastic properties determined from triaxial tests. The magnitude of the spread in results is more evident in measured Poisson's ratio values which are seen to vary from .06 to over 1.0.

Before proceeding with the discussion of results concerning the elastic properties, it is appropriate to explain the cause of large variation in these properties. As mentioned previously on several occasions, the grade assigned to a particular sample of oil shale is actually an average grade over many intra-sample layers of often widely varying kerogen content. At room temperature, it is quite feasible to obtain a reasonably valid stiffness. However, when heating begins, the layers of various

kerogen contents react differently depending on their richness. The load response characteristic of the sample will thus be influenced by the range and relative distribution of grades within the sample. This means a lean sample with relatively uniform distribution of kerogen would respond to load differently than the one with a band of rich material. The latter could display excessive deformation due to the collapse of the more temperature sensitive rich zone. Moreover, for those samples containing one or more kerogen rich layers, the radial deformation will be dependent on the probe placement with respect to the location of rich zones. If the probes are placed against a particular rich zone, the excessive deformation of this zone would result in high radial deformation readings. Visible rings of highly deformed material were evident in many failed samples. (Figure 3.13)

The effect of temperature on Young's Modulus are graphically displayed in two representative graphs in Figures 3.24 and 3.25. The rest of the graphs for other grade ranges are included in Appendix 6.7. For all grades tested, a major reduction of Young's modulus occurs in heating only to 140^{o}C. For 15 gpt oil shale, the reduction of Young's Modulus appears to continue for temperature increases beyond 140^{o}C, but at a much lower rate. Such continous reduction for higher temperature ranges is not evident at higher grades for which the Young's Modulus is seen to undergo minimal reduction.

The grade appears to have a consistent effect on Young's Modulus as shown in Figures 3.26 and 3.27 for two temperature

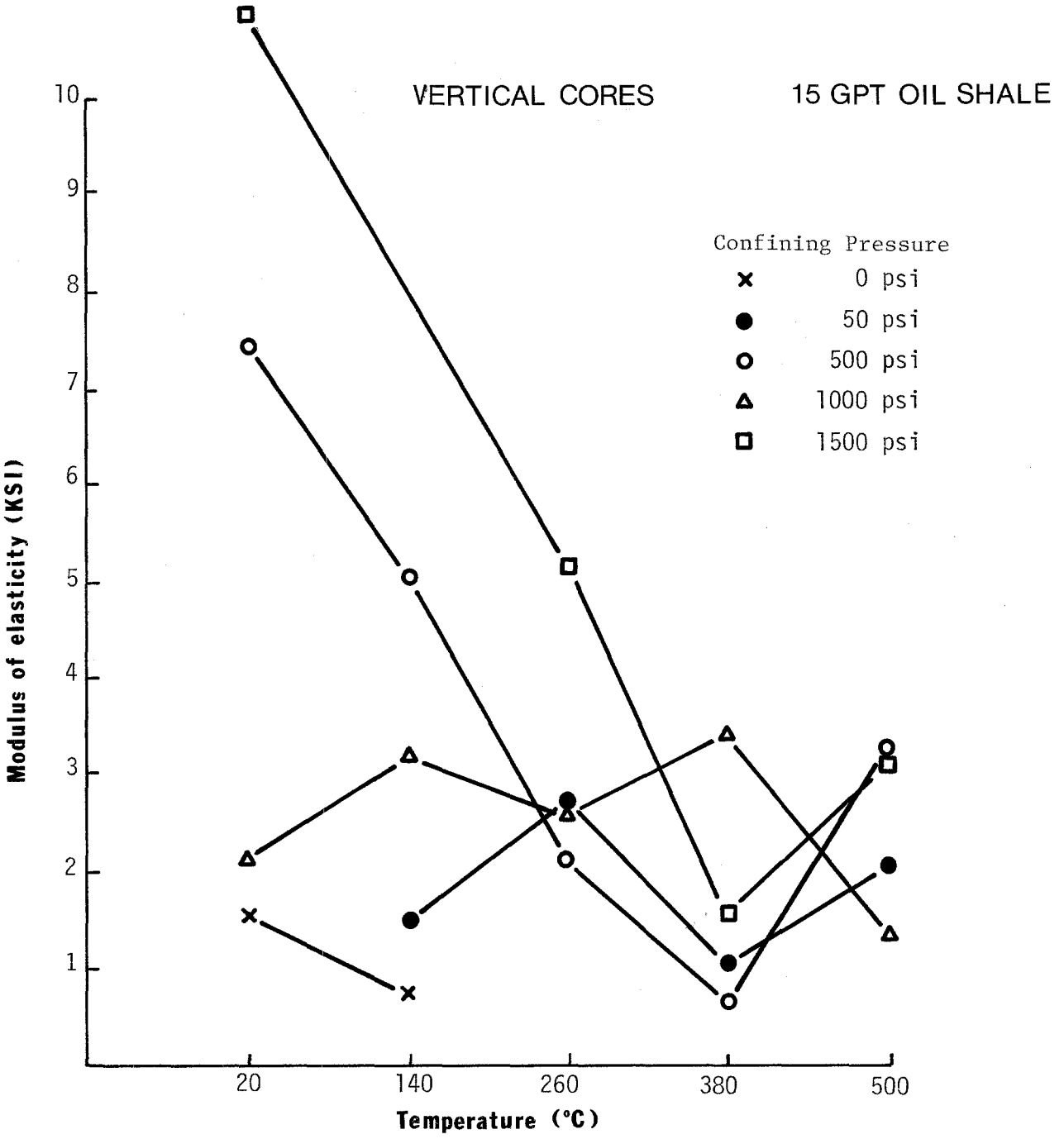

EFFECT OF TEMPERATURE ON MODULUS OF ELASTICITY FOR 15 gpt OIL SHALE AT VARIOUS CONFINING PRESSURES

(Vertical Cores, compression perpendicular to bedding)

FIGURE 3.24

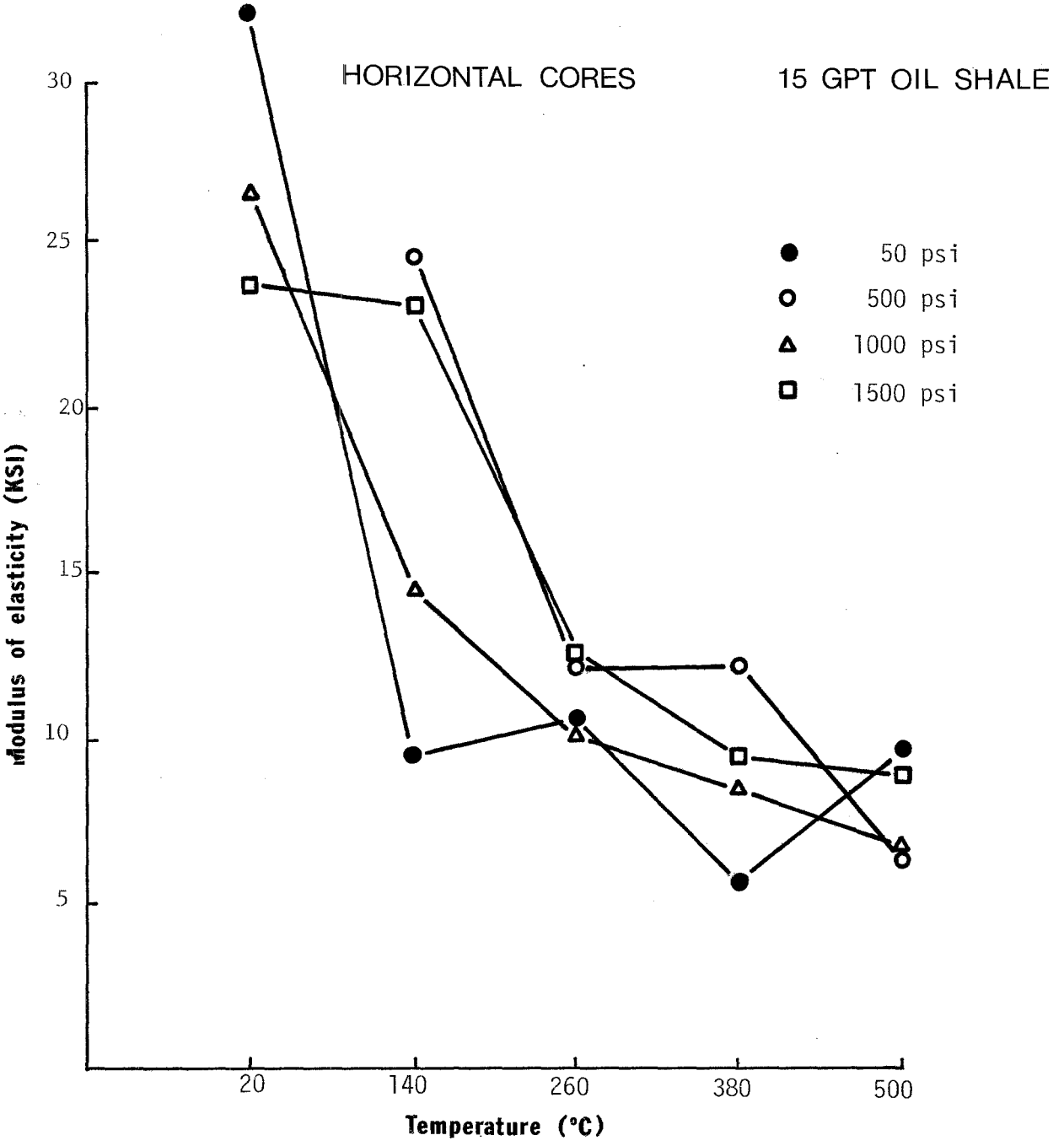

EFFECT OF TEMPERATURE ON MODULUS OF ELASTICITY FOR 15 gpt OIL SHALE AT VARIOUS CONFINING PRESSURES

(Horizontal cores, compression parallel to beddings)

FIGURE 3.25

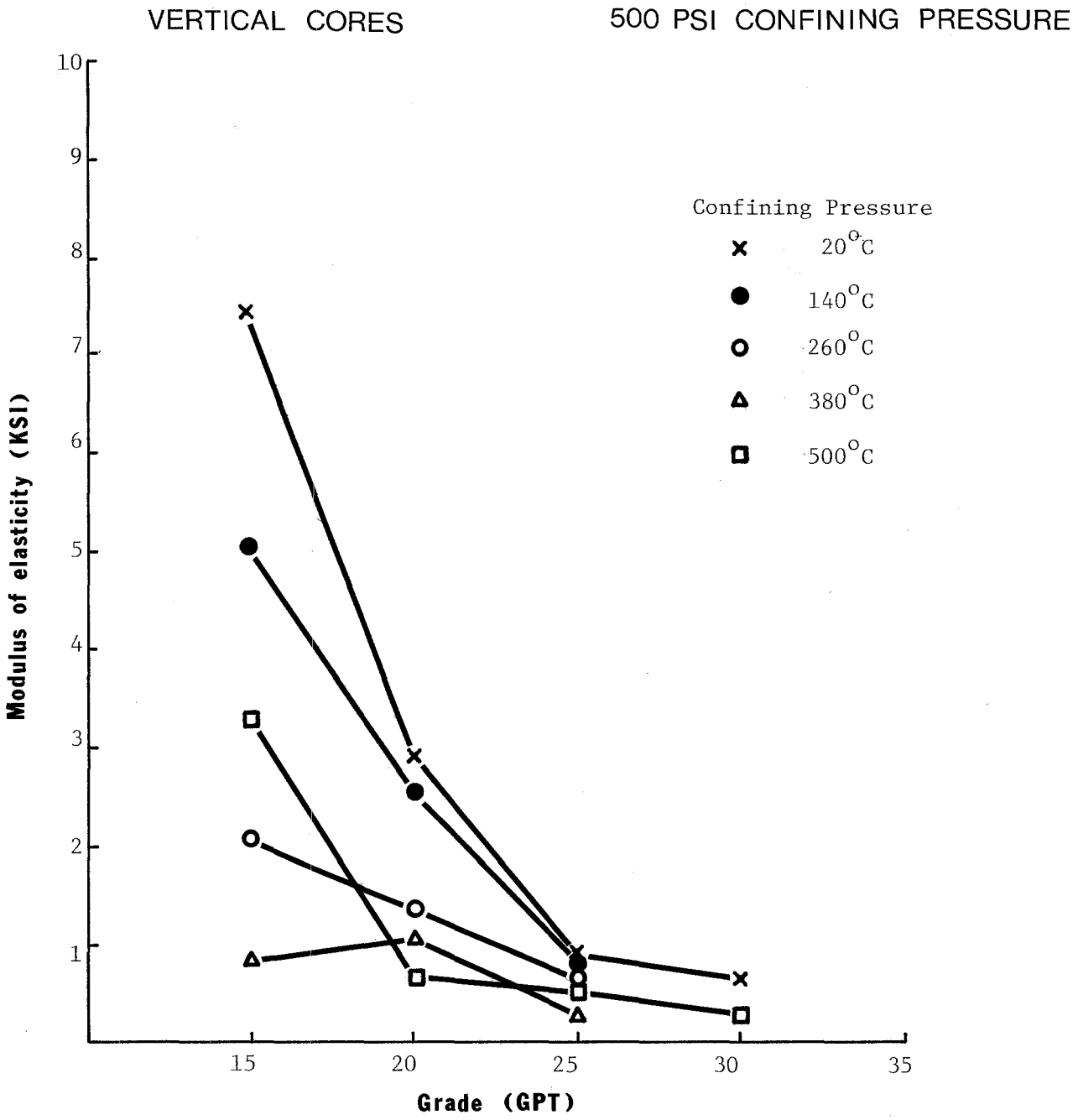

EFFECT OF GRADE ON MODULUS OF ELASTICITY AT 500 psi CONFINING PRESSURE FOR VARIOUS TEMPERATURES

(Vertical cores, compression perpendicular to bedding)

FIGURE 3.26

HORIZONTAL CORES 500 PSI CONFINING PRESSURE

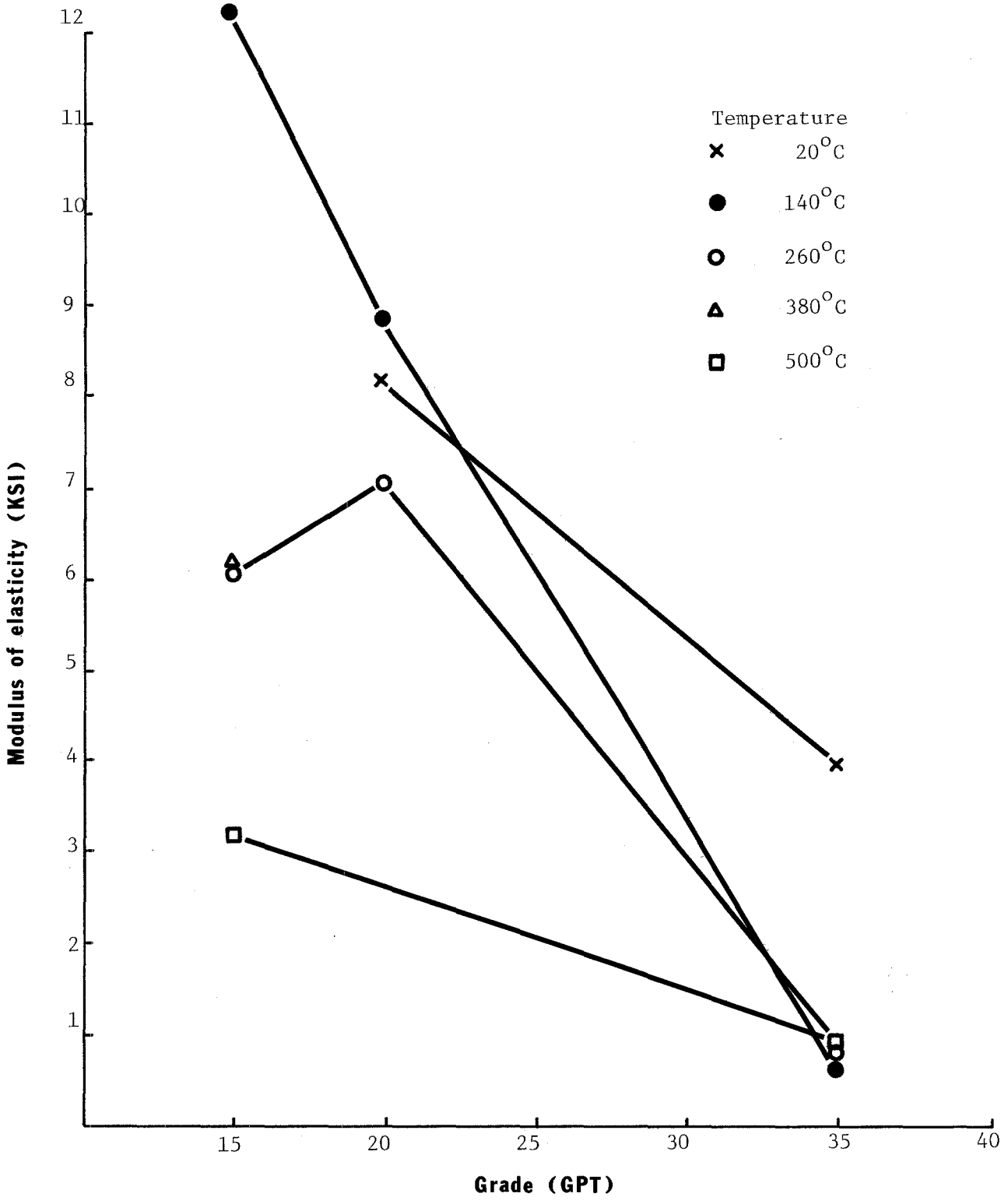

EFFECT OF GRADE ON MODULUS OF ELASTICITY AT 500 psi CONFINING PRESSURE FOR VARIOUS TEMPERATURE

FIGURE 3.27

values. A continuous reduction of modulus is seen to occur with increasing grade.

Tables 3.12 and 3.13 summarize the results of the regression analysis performed on data for Young's Modulus. The procedure used to develop the regression equation was the same as that used for the compressive strength, as described in section 3.2.3. The following equations were derived from the regression analysis:

For Vertical Cores:

$$E=2.61 + 86.7/G-\ln T$$

For Horizontal Cores:

$$E=9.01 + 134.3/G-2.2 \ln T$$

Where

E = Young's modulus (psi)

G = Grade (gpt)

T = Temperature (^{o}C)

The calculated correlation coefficients are .514 and .79 for the vertical and horizontal cores, respectively. As evidenced by relatively low correlation coefficients, the resulting equations do not provide as good a data fit as the compressive and tensile strength. This is, of course, due to the higher sensitivity of the elastic properties to the variations in intra-sample layer structure of oil shale samples.

As can be seen, the regression equations do not include a term for confining pressure. During the stepwise regression

Table 3.12
The Results of Multiple Linear Regression Performed on
Young's Modulus of Oil Shale
(Vertical Cores)

Sample Size 132

Dependent Variable: E

Independent Variables: INVG LNT

Coefficient of Determination 0.26373

Multiple Corr Coeff. 0.51355

Estimated Constant Term 2.6138840

Standard Error of Estimate 2.7102638

Analysis of Variance

For the Regression

Source of Variation	Degrees of Freedom	Sums of Squares	Mean Square	F	Probability
Regression	2	339.418	169.709	23.10	0.0000
Residuals	129	947.573	7.34553		
Total	131	1286.99			

Variable	Regression Coefficient	Standard Error of Regression Coefficient	F-Value DF (1,129)	Probability	Correlation Coefficient With E
INVG	86.73330	17.56	24.39	0.0000	0.3440
LNT	-0.9956383	.1973	25.47	0.0000	-0.3529

Table 3.13
The Results of Multiple Linear Regression Performed on
Young's Modulus of Oil Shale
(Horizontal Cores)

Sample size 128

Dependent Variable: E

Independent Variables: INVG LNT

Coefficient of Determination 0.63022

Multiple Corr. Coeff. 0.79386

Estimated Constant Term 8.9985070

Standard Error of Estimate 2.7114940

Analysis of Variance

for the Regression

Source of Variation	Degrees of Freedom	Sums of Squares	Mean Square	F	Probability
Regression	2	1566.29	783.145	106.5	0.0000
Residuals	125	919.025	7.35220		
Total	127	2485.32			

Variable	Regression Coefficient	Standard Error of Regression Coefficient	F-Value DF (1, 125)	Probability	Correlation Coefficient With E
IVG	134.3296	12.44	116.5	0.0000	0.5733
LNT	-2.124895	.2105	101.9	0.0000	-0.5343

process, several functions of confining pressure was tried, but none was found to contribute any increase to the correlation coefficient. This led to the conclusion that the confining pressure had no significant effect on Young's Modulus for oil shale.

The computed F-values for the regression variables (temperature and grade) are of close magnitude, meaning that the temperature and pressure are equally significant variables affecting Young's Modulus.

A major effort was also directed toward developing regression equations to mathematically express the Poissons ratio in terms of the three variables involved in the testing program. Despite repeated trials with numerous functions of all three variables, equation with resonable correlation coefficients could not be derived. Due to extremely low correlation coefficients brought about by large variation in data, it was concluded that the present data does not allow the development of any meaningful regression equations for Poisson's ratio.

In summarizing the discussion of physical property results for oil shale, it becomes evident that a significant loss of strength occurs for oil shale even at temperatures well below the retorting temperature. The elastic properties are also greatly affected by temperature. Increasing kerogen content (grade) also causes a proportionate reduction in strength. The Poisson's ratio on the other hand, shows a rapid increase with temperature. It thus becomes important that the temperature affects be given utmost consideration in the design of pillars around an in-situ retort.

3.2.6 Time-dependent deformation

Time-dependent deformation, or creep, was not intended for investigation under the original program. Its occurrence and effects were unavoidable, however, and had to be considered. Particularly at elevated temperatures, creep rates were so high that the determined modulus was seriously affected by the loading rate. To illustrate the degree and rate of this creep, Figure 3.28 shows a special test run at 140°C on a 25 gpt sample. At several increments, loading was stopped and maintained constant for one minute, then resumed. The horizontal displacement at constant load represents the amount of creep occurring in one minute at that load. Note the rapid increase in creep rate for each incremental increase in load. From these very preliminary analyses, it is apparent that creep can significantly affect pillar behavior and, consequently, surface subsidence over an in-situ retorting operation.

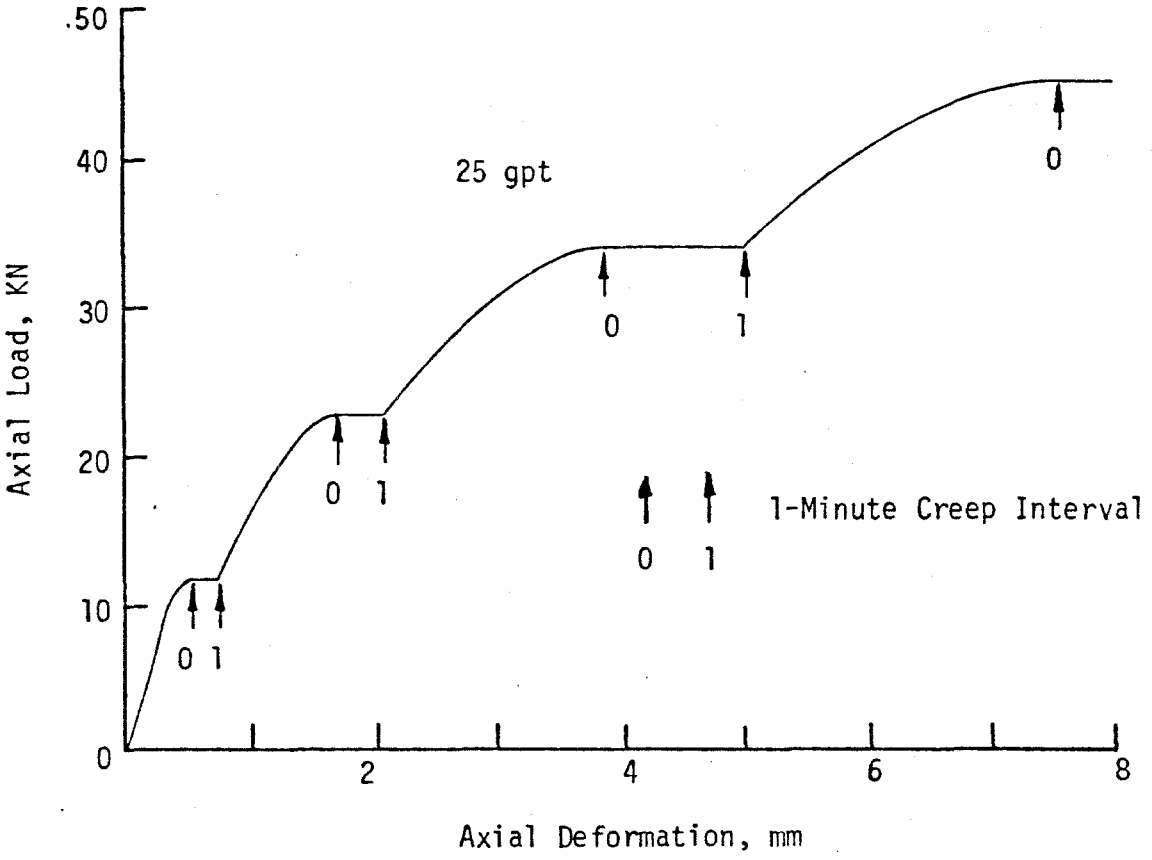

CREEP BEHAVIOR FOR A 25 gpt SAMPLE HEATED AT 140°C AND HELD AT VARIOUS LOADS FOR 1-MINUTE

FIGURE 3.28

3.3 Thermal, Electrical and Acoustic Properties

3.3.1 Steady-state thermal properties

The thermal conductivities for samples with oil shale grade ranging from 17.4 to 50.9 gallons per ton for heat flow perpendicular to the varves or bedding are given in Figure 3.29. The solid lines drawn through the data points represent second-order polynomials with the least squares fit to the data. Data for a comparable set of samples from Logan Wash, but oriented so that heat flow was parallel to or along the varves, is given in Figure 3.30. Comparison of Figure 3.29 with Figure 3.30 illustrates that for heat flow parallel to the varves thermal conductivities are significantly higher than for heat flow perpendicular to the varves in samples of comparable grade. As illustrated in Figure 3.31, this anisotropy in thermal conductivities is more marked for leaner samples than for richer samples. For samples of 50 gallons per ton or more, the anisotropic behavior of the thermal conductivity has essentially disappeared.

The thermal conductivities for heat flow both perpendicular and parallel to the varves for Logan Wash samples are well behaved at temperatures up to 350°C, after which significant decomposition of kerogen begins to occur. This well behaved nature of the thermal conductivity data indicates that thermal conductivity should not show unusually large variations in field test data. The consistency of the data on Logan Wash samples is illustrated in Figure 3.32 where selected curves are compared to similar data on material from the Anvil Points Mine near Rifle

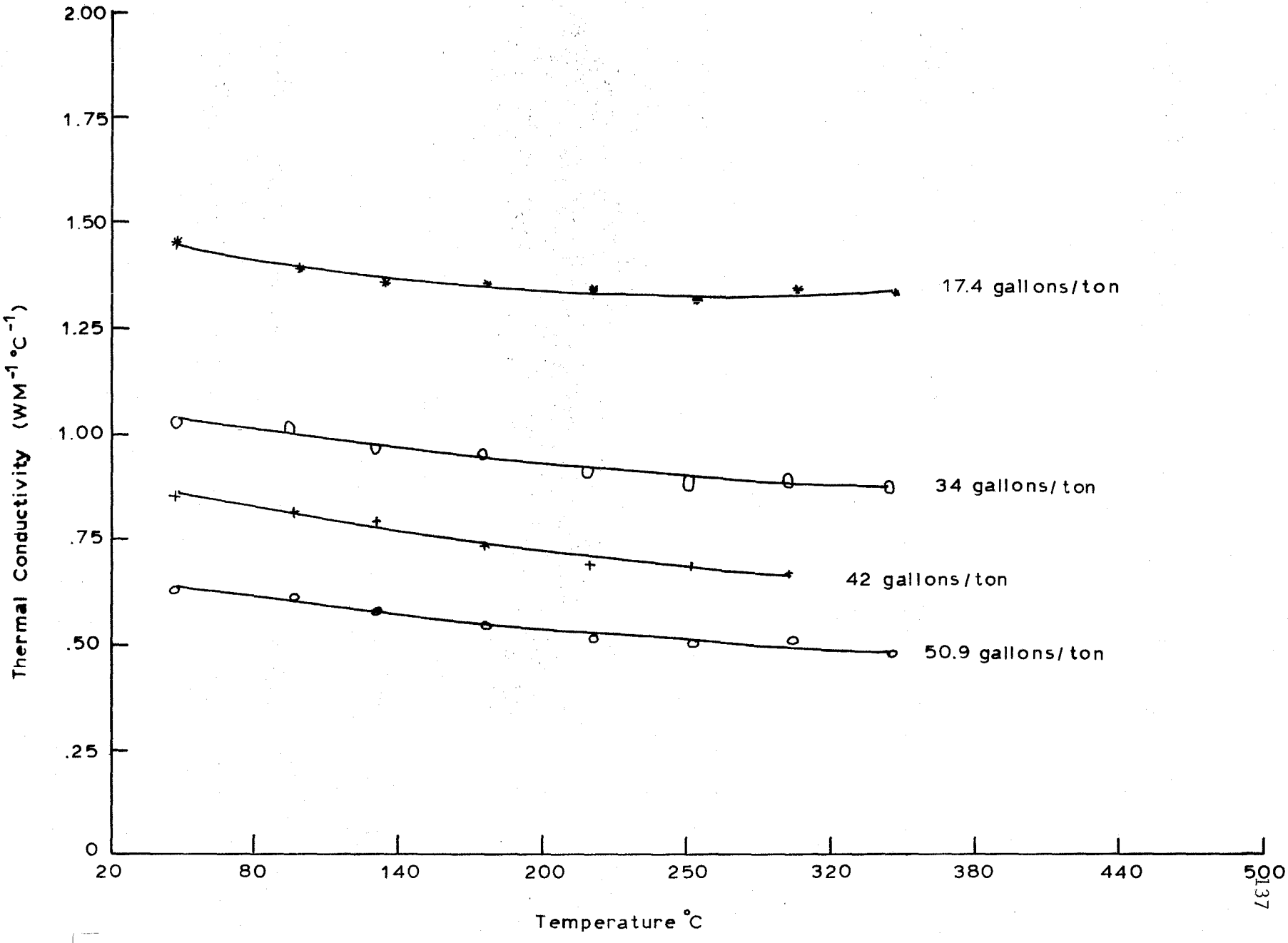

Figure 3.29 Thermal Conductivity versus Temperature for heat flow perpendicular to the bedding plane in Logan Wash samples.

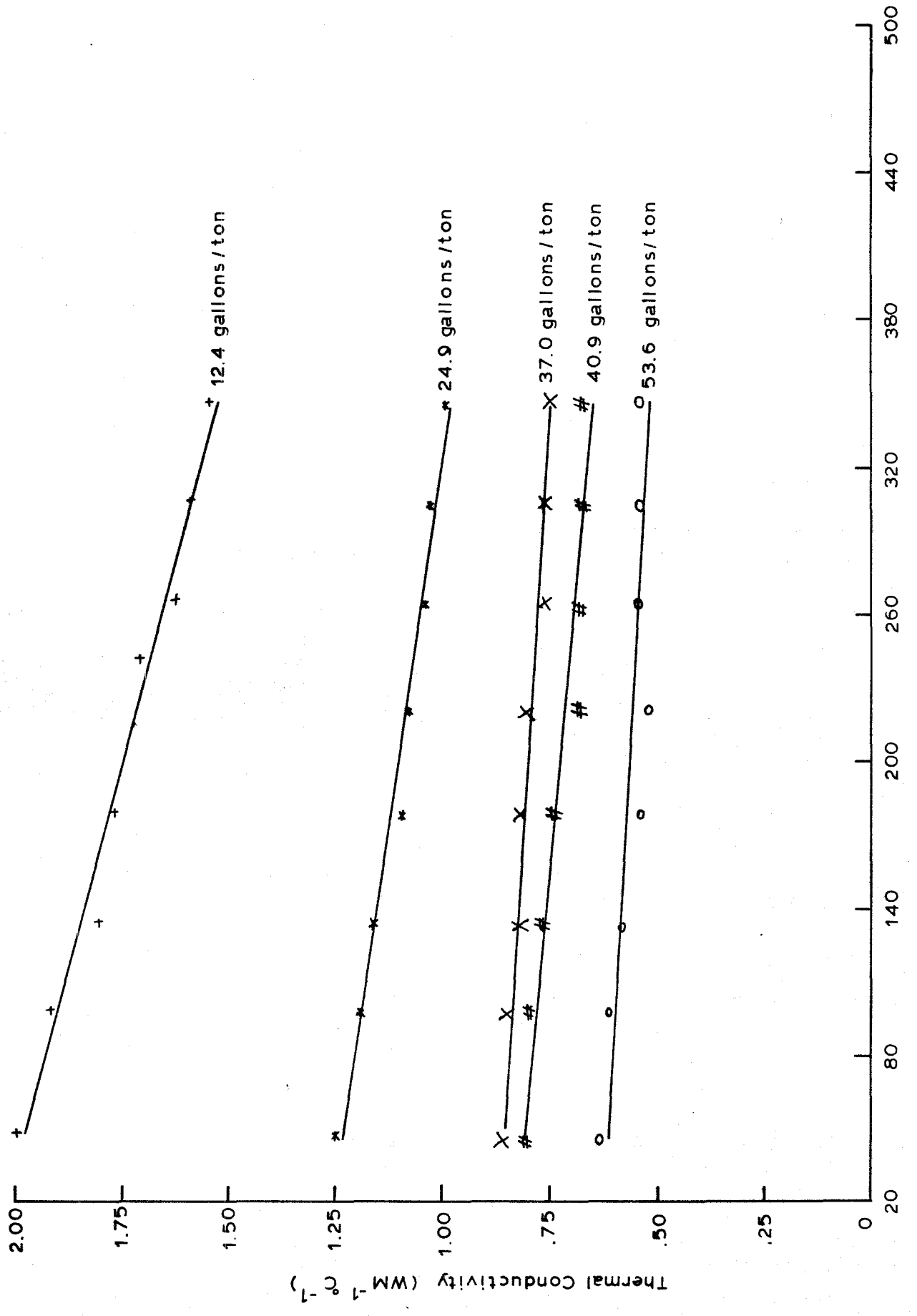

Figure 3.30 Thermal Conductivity versus Temperature for heat flow parallel to the bedding plane in Logan Wash samples.

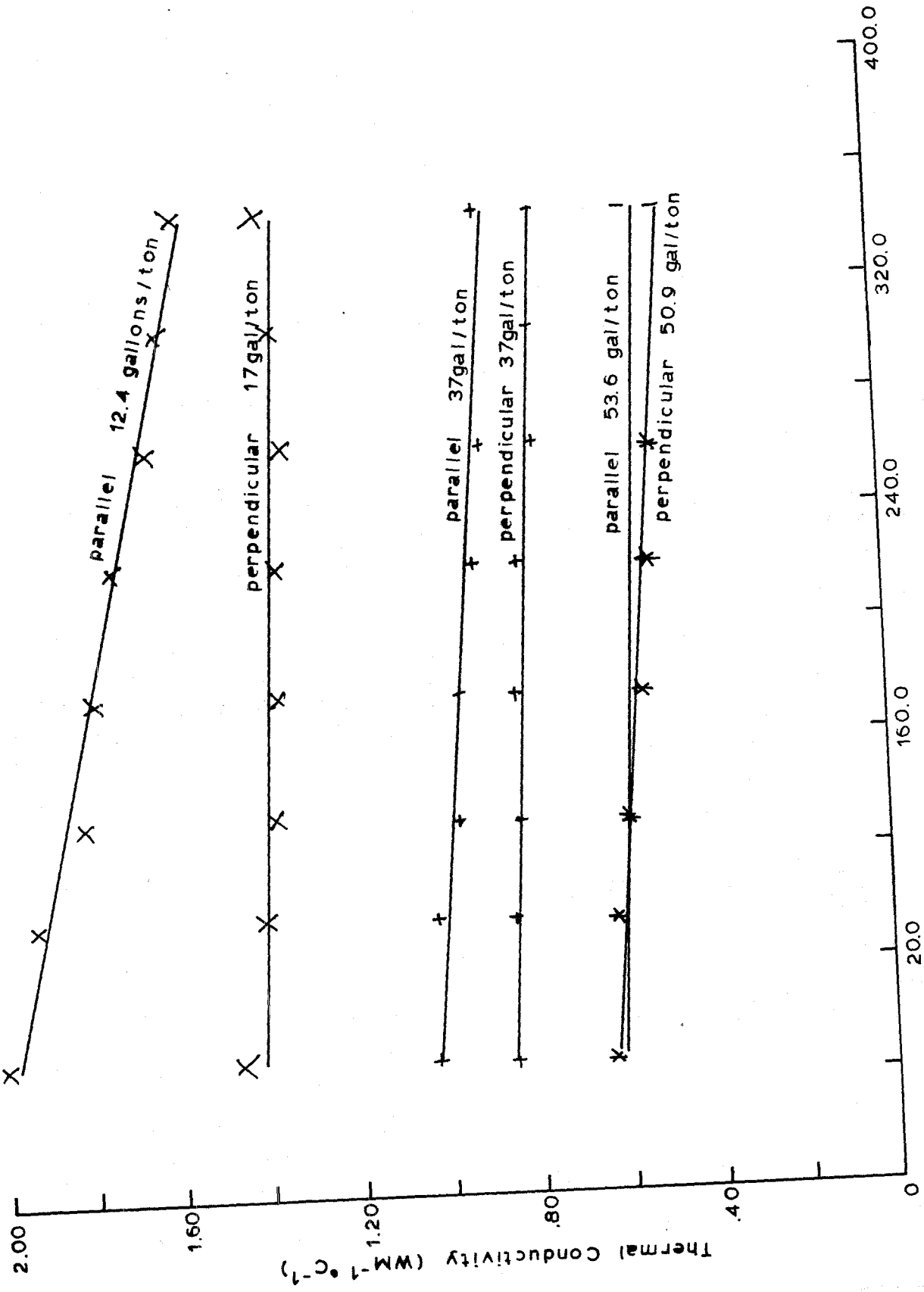

Figure 3.31 Comparison of Thermal Conductivity behavior for perpendicular and parallel samples at similar grades.

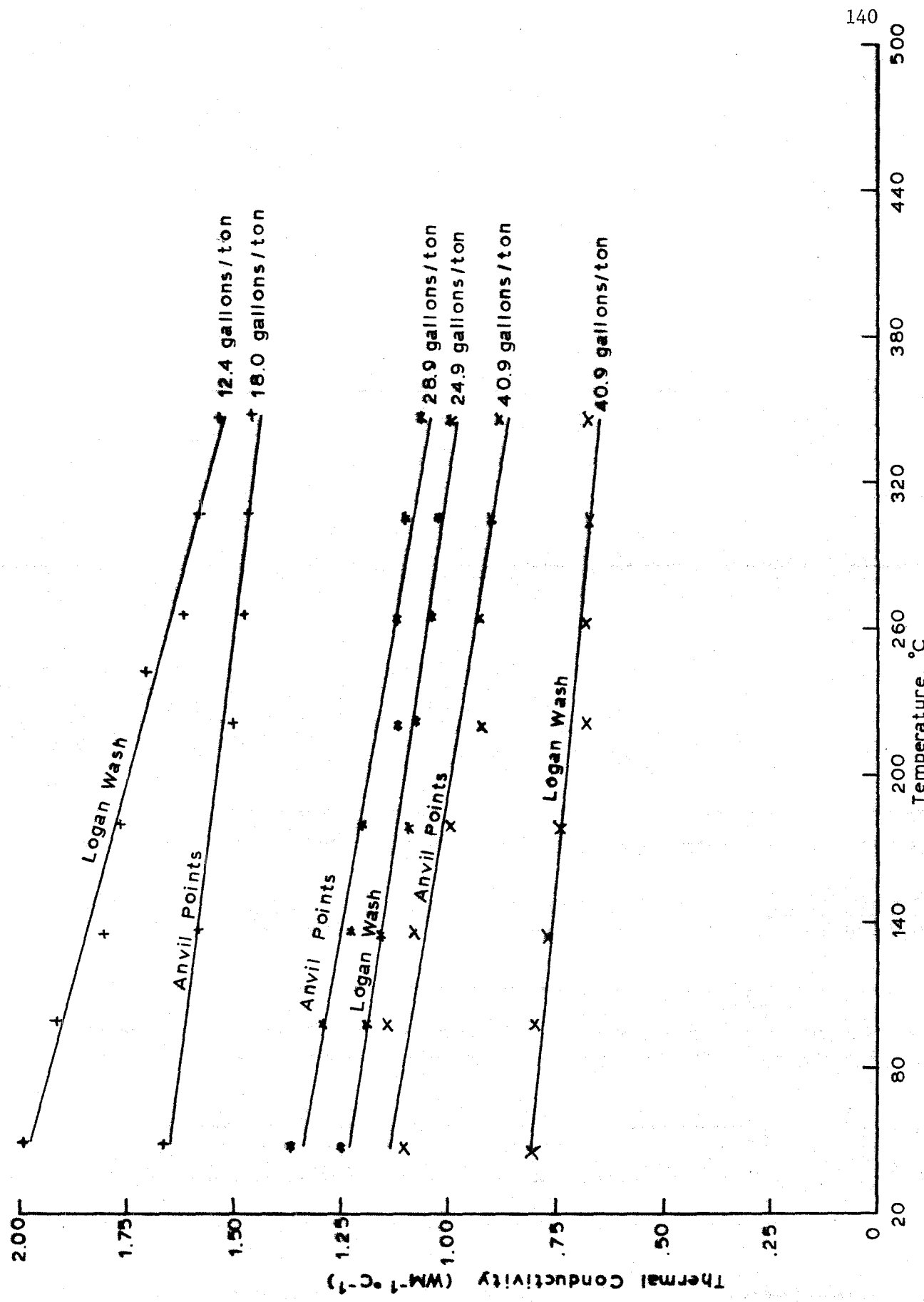

Figure 3.32A comparison of thermal conductivity as a function of temperature for Anvil Points and Logan Wash samples of similar grades

Colorado. It is clear from Figure 3.32 that both Logan Wash and Anvil Points data show very similar and well behaved trends with consistent and monotonic decreases in thermal conductivity with both increasing temperature and increasing grade. The small differences between the Anvil Points and Logan Wash data can probably be attributed to subtle mineralogical variations, but these variations are so slight that they can be considered a second order effect and ignored for most purposes of analysis and modeling.

3.3.2 Transient method thermal properties

The thermal diffusivity, heat capacity and consequent thermal conductivity, as calculated directly by the Hewlett-Packard 9825, are illustrated in Figure 3.33. It is noteworthy that the decrease in thermal diffusivity occurring between 200 and 250°C is largely attributable to a transient increase in heat capacity over this temperature range and is not significantly observed in the thermal conductivity. As will be discussed in more detail later, this increase in heat capacity between 200 an 250°C was observed in essentially all of the experimental runs made with the transient method and is believed to be due to an endothermic reaction associated with the dehydration of hydrous minerals in the oil shale. That this perturbation in effective heat capacity is observed equally in rich and lean oil shale samples indicates that it is not due to any initial endothermic decomposition of kerogen.

Thermal conductivities for three grades of Logan Wash oil shale samples for heat flow perpendiular to the bedding are

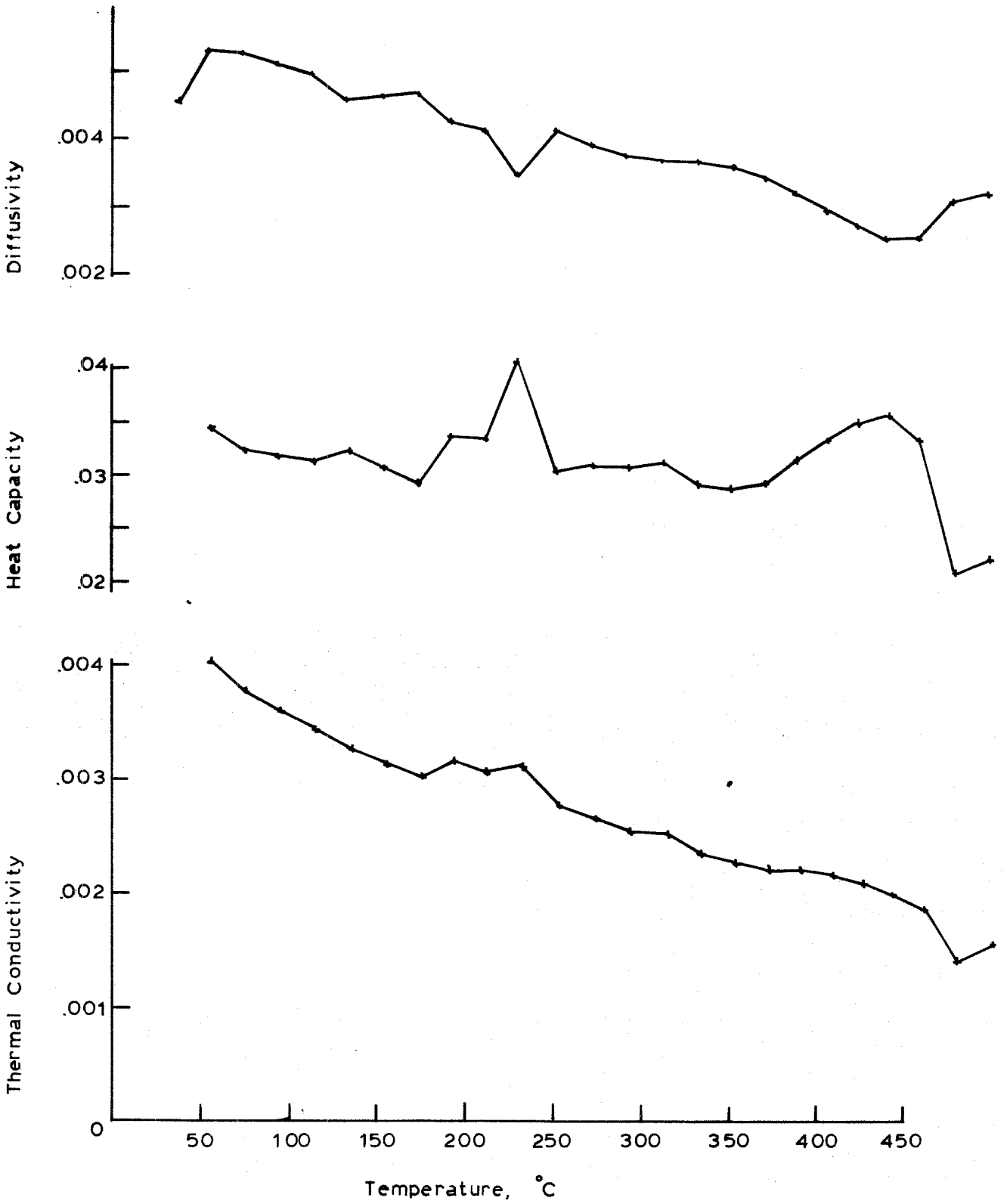

Figure 3.33 Graphical output of thermal diffusivity, heat capacity and thermal conductivity as obtained by transient thermal analysis.

illustrated in Figure 3.34, along with the thermal conductivities on nearly identical samples obtained by the steady-state method. For the leaner samples, the thermal conductivities obtained by the transient method show a greater temperature dependence than is observed for the steady-state conductivities.

Values for heat capacity, C_p, as obtained from the transient-thermal analyses are given in Figure 3.35. All of the raw data on heat capacity, such as illustrated in Figure 3.35 show a marked increase in C_p in the temperature range 200 to 250°C. Because this narrow peak in C_p is believed to be due to endothermic chemical reactions and because it could not be adequately accounted for in a second-order polynomial representation of the data, the high C_p data points were excluded from the curve fitting calculations yielding the solid curves in Figure 3.35. When the anomalous C_p data is excluded, the remaining data can be quite adequately represented by second-order polynomials as shown in Figure 3.35. Although heat capacity is a scalar quantity, not dependent upon direction of heat flow, the sample orientation is given for reference in Figure 3.35. If a functional description of heat capacity is required in numerical models, then it would be best to use a linear or perhaps a second-order representation of data excluding the 200 - 250°C anomalies. The higher heat capacities in the range of 200 - 250°C could then be included by a triangular or box-car function over the narrow temperature range of the anomalous data.

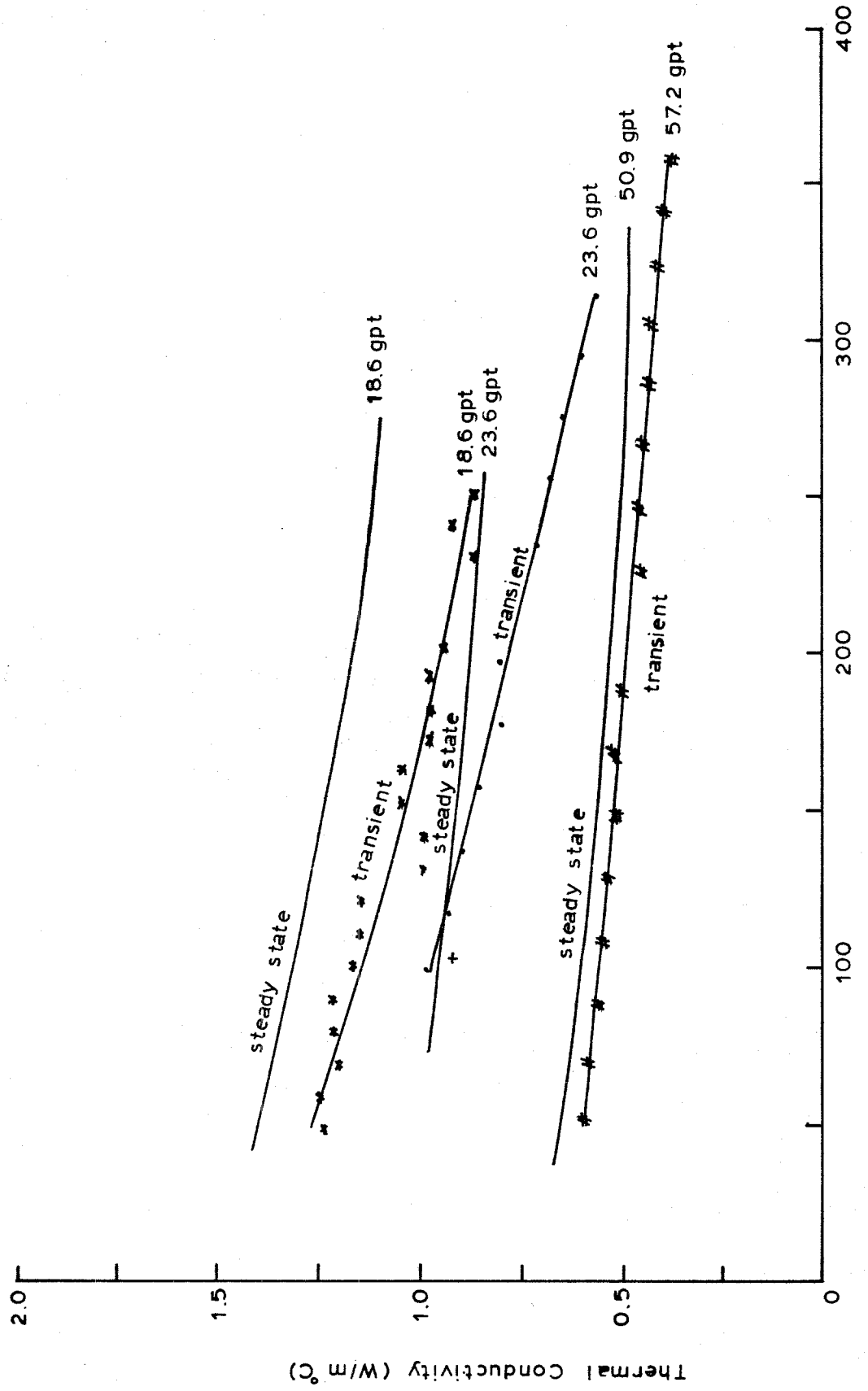

Figure 3.34 Comparison of thermal conductivities obtained by the steady state method and the transient method.

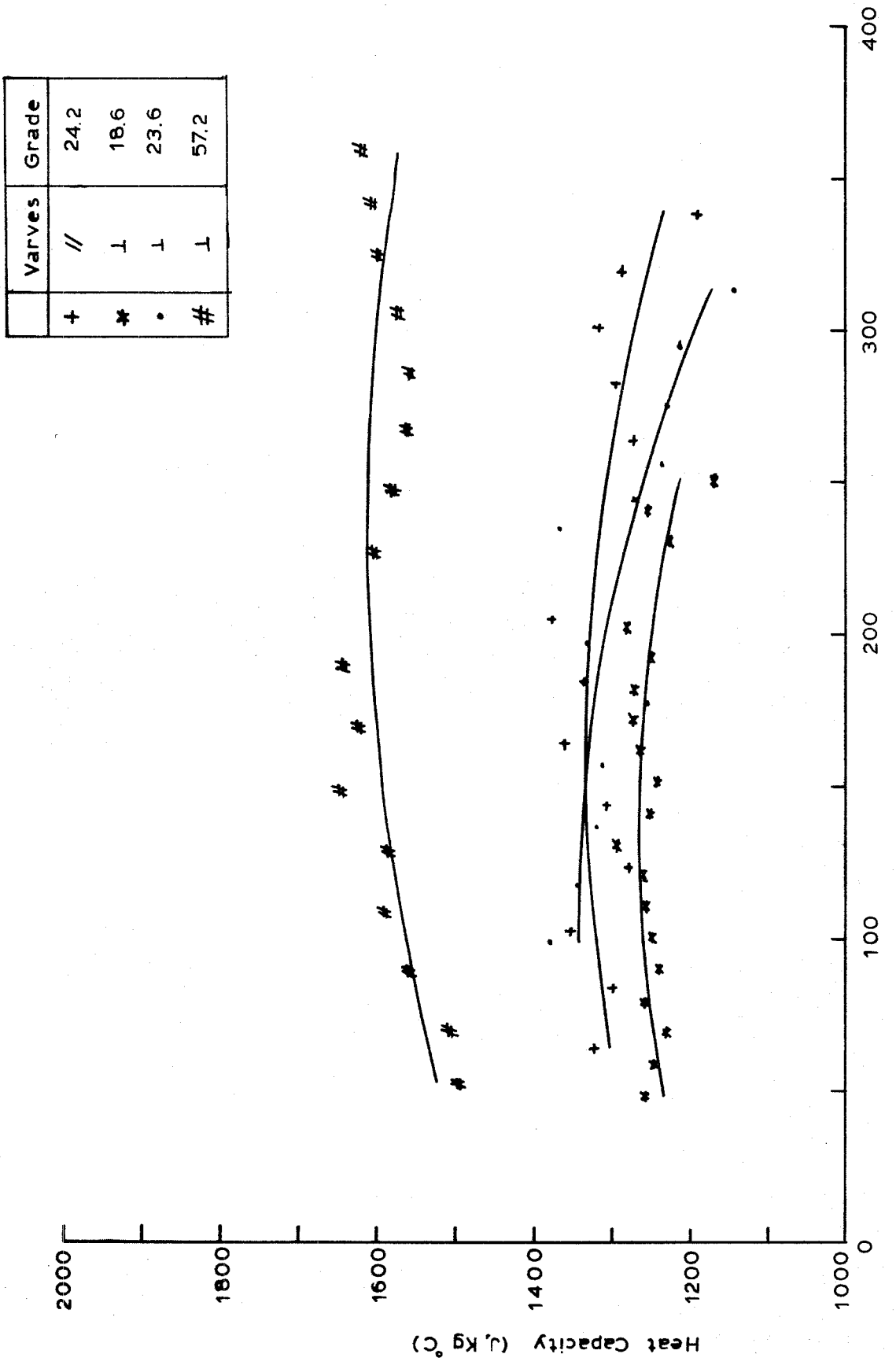

Figure 3.35 Heat Capacity vs. Temperature for Oil Shale Samples of Different Grades Cored Perpendicular (⊥) and Parallel (//) to the Bedding Planes

3.3.3 Ultrasonic Properties

Averaged transmitted pulse records obtained at five different temperatures during the heating of an oil shale sample are illustrated in Figure 3.36. The data shown in this figure, obtained on a nominal 17 gpt oil shale, illustrate the very marked variation in P- and S-wave transit times and the corresponding elastic moduli found to be so characteristic of heated oil shale materials.

All grades of oil shale tested have shown significant changes in P an S-wave travel times and the concordant elastic moduli. For samples with nominal oil yields of over 20 gpt, the changes in travel times are quite large and the concordant degradation of elastic moduli is rather severe. To the extent that the small-strain moduli determined by the ultrasonic-pulse transmission method are representative of the large-strain moduli, the observed variations in moduli could have very important consequences on the design and response of in-situ oil shale pillars during retorting. Although they were obtained simultaneously, the P and S-wave arrival times as a function of temperature for various grades of oil shale are illustrated separately in Figures 3.37 & 3.38, respectively. As seen in Figures 3.37 & 3.38 both the P and S-wave travel times show their maximum increase at around 400°C with a significant reduction in travel time and concordant increase in elastic modulus occuring between 400 and 500°C. As the elastic moduli vary as the square of the changes in travel time or velocities, the maximum increase in P-wave travel time by a factor of 3.8 corresponds to a degradation of the constrained modulus for loading perpendicular

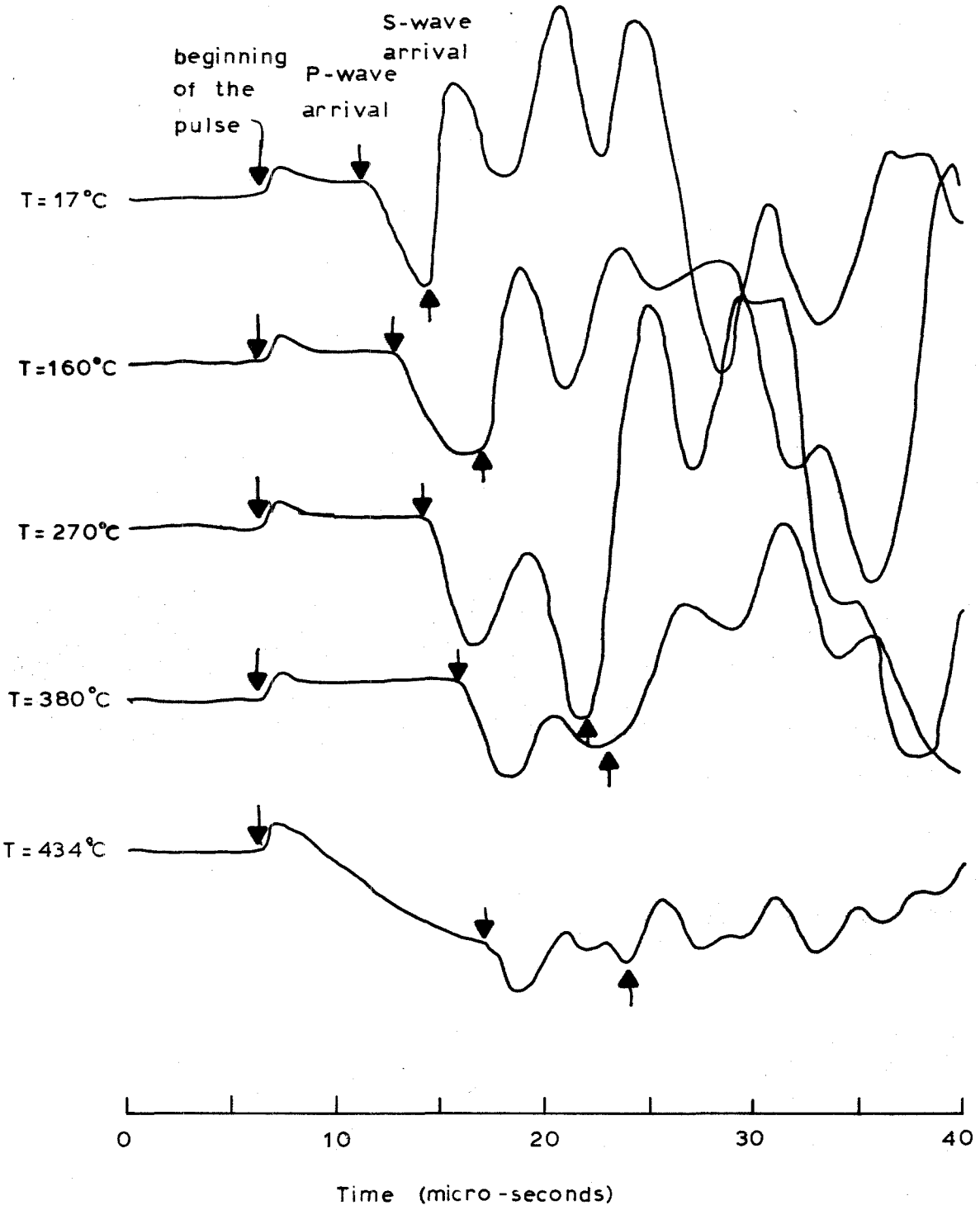

Figure 3.36 Transmitted signals (average of ω) at different temperatures

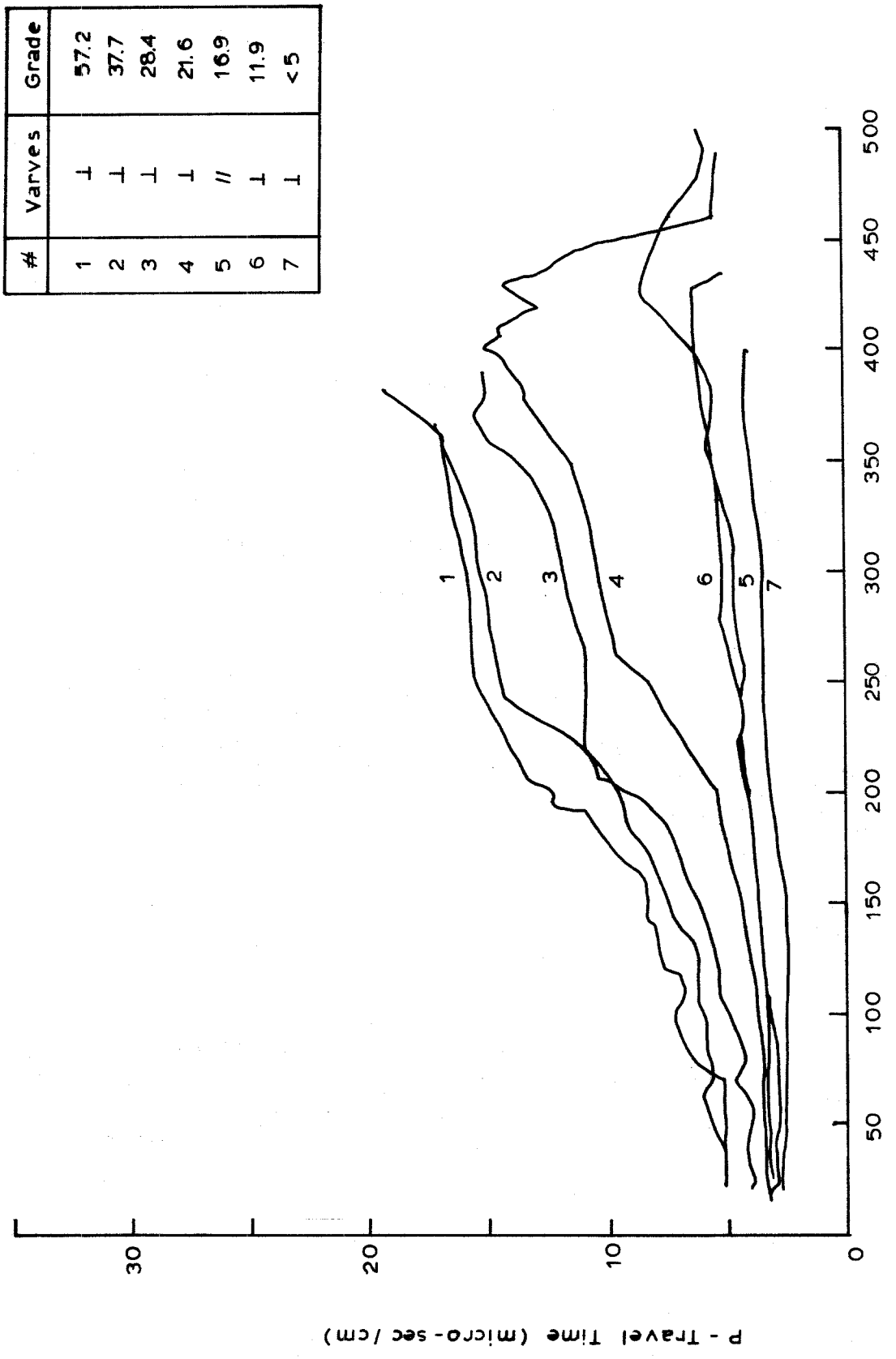

#	Varves	Grade
1	⊥	57.2
2	⊥	37.7
3	⊥	28.4
4	⊥	21.6
5	//	16.9
6	⊥	11.9
7	⊥	<5

Figure 3.37 P-wave Travel Time vs Temperature for Oil Shale Samples Different Grades

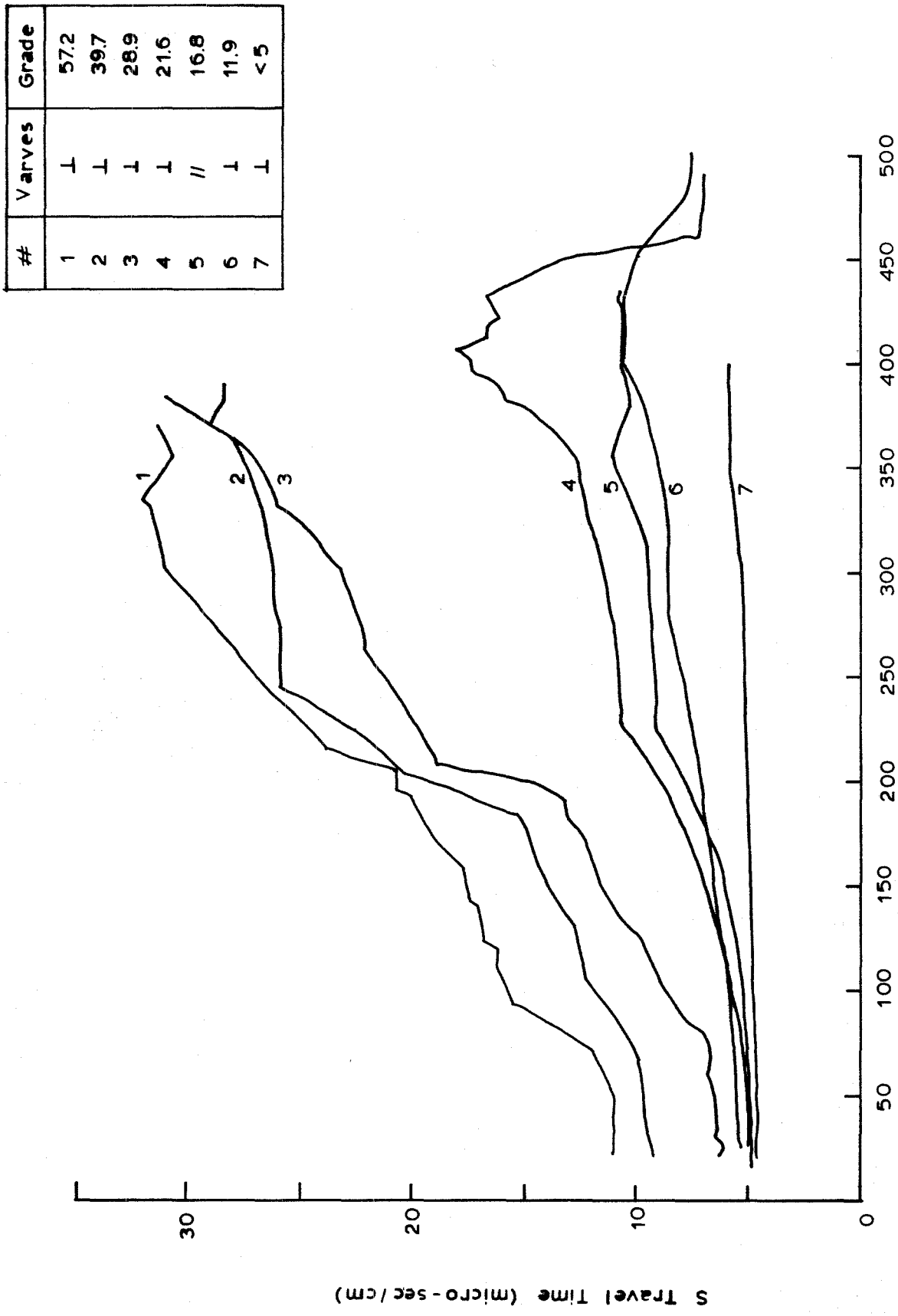

#	Varves	Grade
1	⊥	57.2
2	⊥	39.7
3	⊥	28.9
4	⊥	21.6
5	//	16.8
6	⊥	11.9
7	⊥	<5

Figure 3.38 S-wave Travel Time vs. Temperature for Oil Shale Samples of Different Grades

to bedding of 14.2 an the 4.6 fold increase in shear-wave travel time corresponds to a 21.2 fold decrease in shear modulus. These extreme variations in modulii indicate that richer grades of oil shale will show such large reductions in elastic moduli that their contributions to the load carrying capabilities to a pillar may be negligible.

Some large-strain data on the effective moduli of oil shale at elevated temperatures should be obtained in order to evaluate the linearity of oil shale elastic properties at high temperatures and the applicability of the severe degradation of moduli observed in the small-strain ultrasonic measurements. In order to illustrate the large variations in effective modulii, the constrained and shear modulii calculated from the measured travel times for a 21.6 gpt sample (curves no. 4 in Figures 3.37 & 3.38) are illustrated as functions of temperature in Figure 3.39. The dependence of the maximum change in effective moduli upon oil shale grade is illustrated in Figure 3.40. Figure 3.40 serves to further illustrate the severe thermal degradation of elastic properties which could occur in oil shale material of grades greater than 20 gpt when heated to temperatures approaching 400^{o}C. The only benefit which might be expected from this observed degradation of elastic properties would be the limitation of large-stress concentrations potentially resulting from the large thermal coefficients of expansion characteristic of the rock.

A more detailed discussion of the approach and techniques for acoustic properties determination is given in Appendix 6.5.

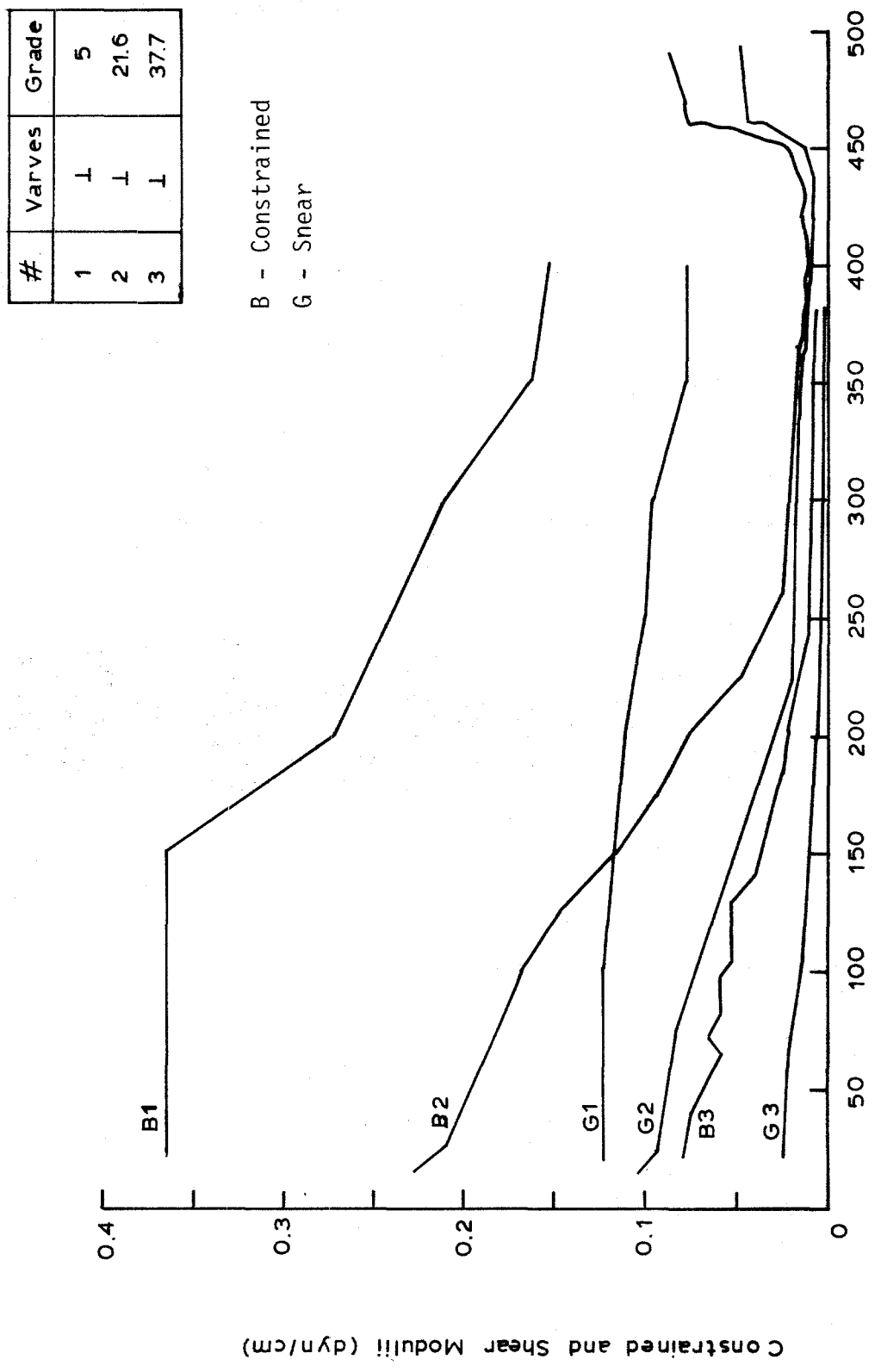

Figure 3.39 Constrained and Shear Modulii vs. Temperature for Oil Shale Samples of Different Grades

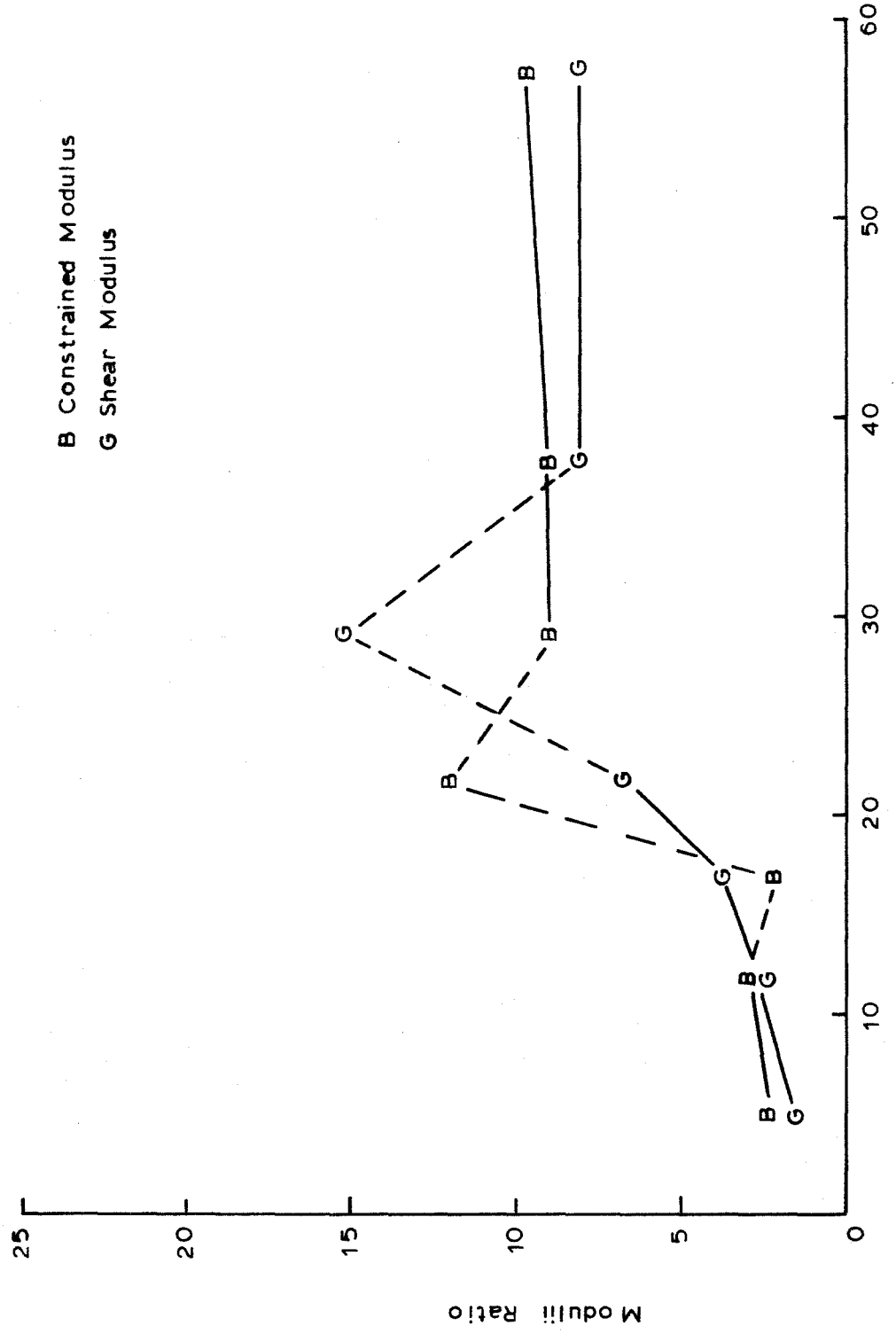

Figure 3.40 Ratio of elastic moduli at 25 °C to 300 °C as a function of oil shale grade.

3.3.4 Thermal expansion

The reproducability of the thermal expansion data is indicated by the upper two curves in Figure 3.41, where the sample elongation in percent is given as a function of temperature for two essentially identical samples of oil shale heated at different rates. Curve No. 1 gives thermal expansion data which was obtained simultaneously with thermal-conductivity measurements at a heating rate of four degrees centigrade per minute, and curve No. 2 is for a heating rate of two degrees centigrade per minute. Both thermal expansion curves show consistent and essentially linear expansion up to 200°C. At just over 200°C, both curves show a slight drop which is probably related to some type of thermal relaxation mechanism taking place in the heated kerogen. Above 200°C the thermal expansion data is possibly perturbed to some extent by creep effects taking place in the sample. Most samples have been loaded at a 100 psi normal stress, with the exception of two samples which were tested at 50 psi.

Experiments have been conducted for thermal expansion both perpendicular to the varves (bedding) and along the varves. Data from samples at the two orientations are also shown in Figure 3.41. As would be expected, the sample oriented for measurement of thermal expansion perpendicular to the varves (Curve No. 3) shows greater thermal expansion than is observed in the direction of the varves (Curve No. 4). Also, as would be expected, the thermal expansion perpendicular to the varves displays greater non-linearity than does thermal expansion along the varves. As

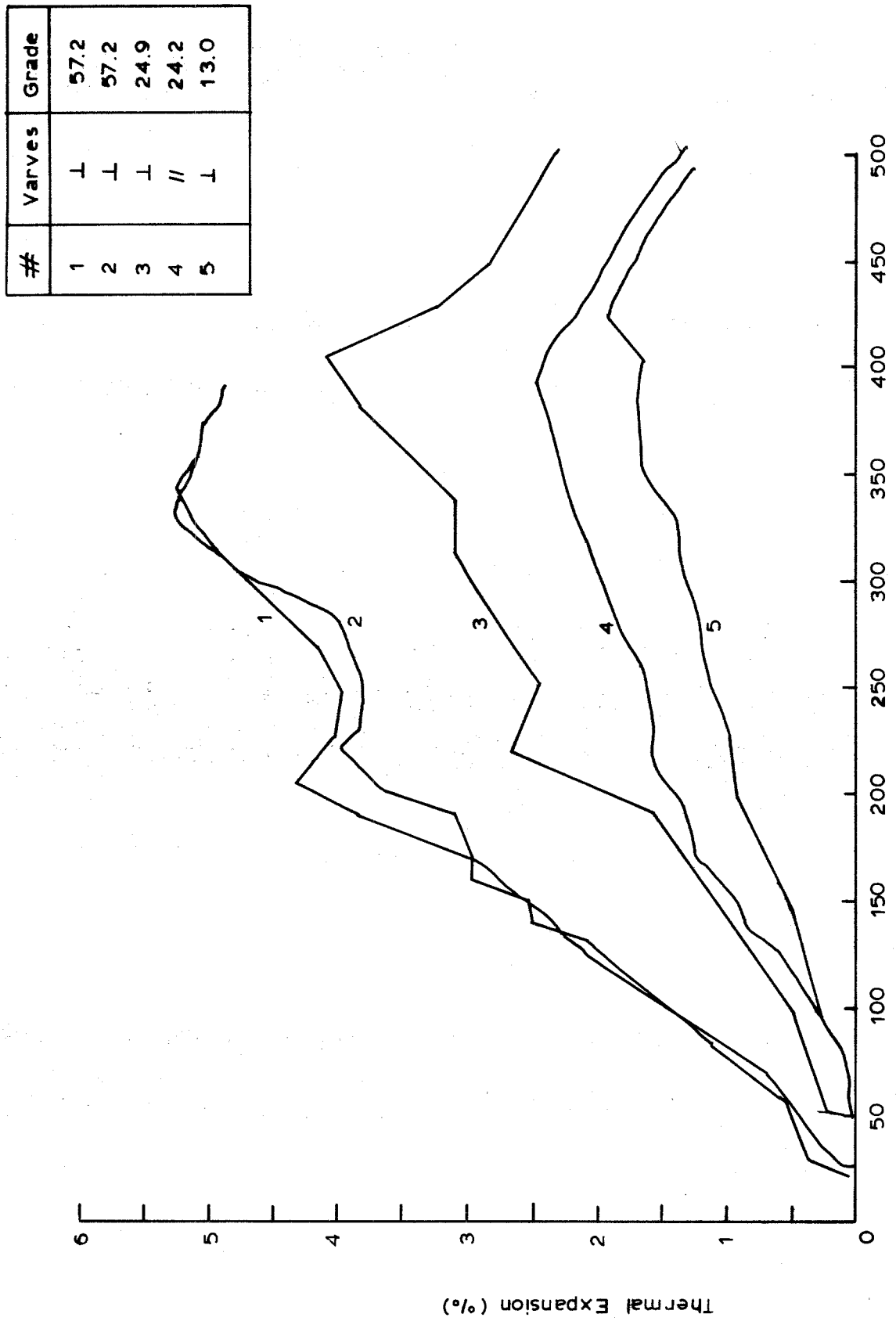

#	Varves	Grade
1	⊥	57.2
2	⊥	57.2
3	⊥	24.9
4	//	24.2
5	⊥	13.0

Figure 3.41 Thermal Expansion vs. Temperature for Oil Shale Sample of Different Grades

shown in Figure 3.41, all samples, and especially the richer samples, show a marked knee or stress relaxation occurring at just over 200°C. The sample shortening occurring for all curves at temperatures around 400°C is definitely related to creep occurring within the loaded samples. The thermal expansion data can be reasonably well represented by two linear curves. One curve, or coefficient of expansion, describes well sample behavior below 200°C and a second can describe sample behavior above 200°C. Additional data on the importance of creep effects in the thermal expansion of samples in the temperature range from 200 to 400°C will be needed before the absolute value of thermal expansion behavior in this temperature range can be defined. Up to 200°C, the thermal expansion is consistently related to oil shale grade and sample orientation. The best value for the effective linear thermal coefficients of expansion acting over the two temperature ranges for samples of various grades and orientations are tabulated in Table 3.14.

3.3.5 Electrical properties

A simplified block diagram of the a.c. electrical impedance is given in Figure 3.42. The measurement sequence is cyclic and the a.c. impedance is obtained over the frequency range 10 Hz to 10^6 Hz. Upon a signal from the microprocessor, the frequency synthesizer applies a sine wave signal simultaneously to the oil shale and to the reference channel of the gain phase meter. The gain phase meter determines the relative attenuation and phase shift of the signal as it passes through the shale. The time it takes to perform this measurement depends upon the frequency,

TABLE 3.14

EFFECTIVE LINEAR THERMAL COEFFICIENTS
OF EXPANSION FOR VARIOUS SAMPLES (%/^{o}C)

	Below 200^{o}C		Above 200^{o}C	
Grade (gallons/ton)	$\perp$	//	$\perp$	//
13.0	$.629 \times 10^{-2}$		$.425 \times 10^{-2}$	
24.9	1.24×10^{-2}	$.804 \times 10^{-2}$	1.03×10^{-2}	$.607 \times 10^{-2}$
37.7	1.28×10^{-2}		$.700 \times 10^{-2}$	
57.2	2.21×10^{-2}		1.39×10^{-2}	

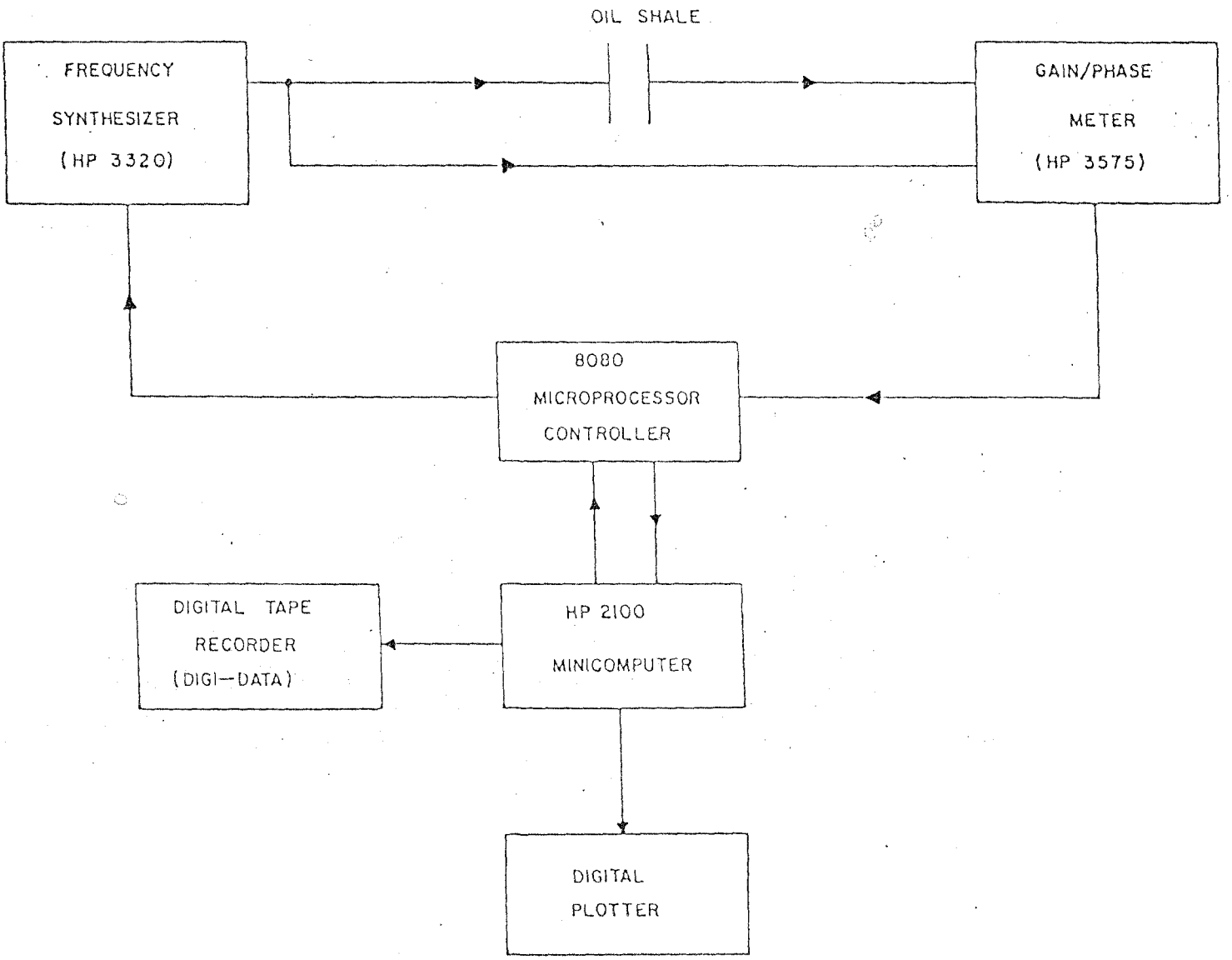

ELECTRICAL IMPEDANCE BLOCK DIAGRAM

FIGURE 3.42

being considerably shorter at higher frequencies. After an appropriate settling time, the microprocessor transmits the attenuation and phase shift to the microcomputer which in turn stores the data on magnetic tape for subsequent processing. The computer then sends a signal to the microprocessor indicating that the data acquisition cycle is completed, and the measurement cycle repeats.

From the attenuation and phase, the equivalent electrical resistance and capacitance of the sample are computed. The system response is automatically subtracted out of the raw data during analysis. From the sample geometry and the resistance and capacitance, the dielectric constant and the loss tangent are calculated. These material dependent "constitutive" parameters are more general than the geometry dependent electrical impedance parameters. (41) The dielectric constant is a measure of the fraction of energy in the electric field energy stored in the material while the loss tangent is a measure of the fraction of energy in the electrical field dissipated by the material. These two parameters commonly characterize the dielectric properties of a material, although numerous other equivalent parameter sets could also be used (41)

Figures 3.43 & 3.44 depict the behavior of the dielectric constant of 66.7 gpt shale as a function of temperature and frequency. Similar behavior was observed for other grades. The dielectric constant is seen to decrease from a relatively high value at low frequencies (412) to a lower value at high frequencies. In addition, the dielectric constant is seen to

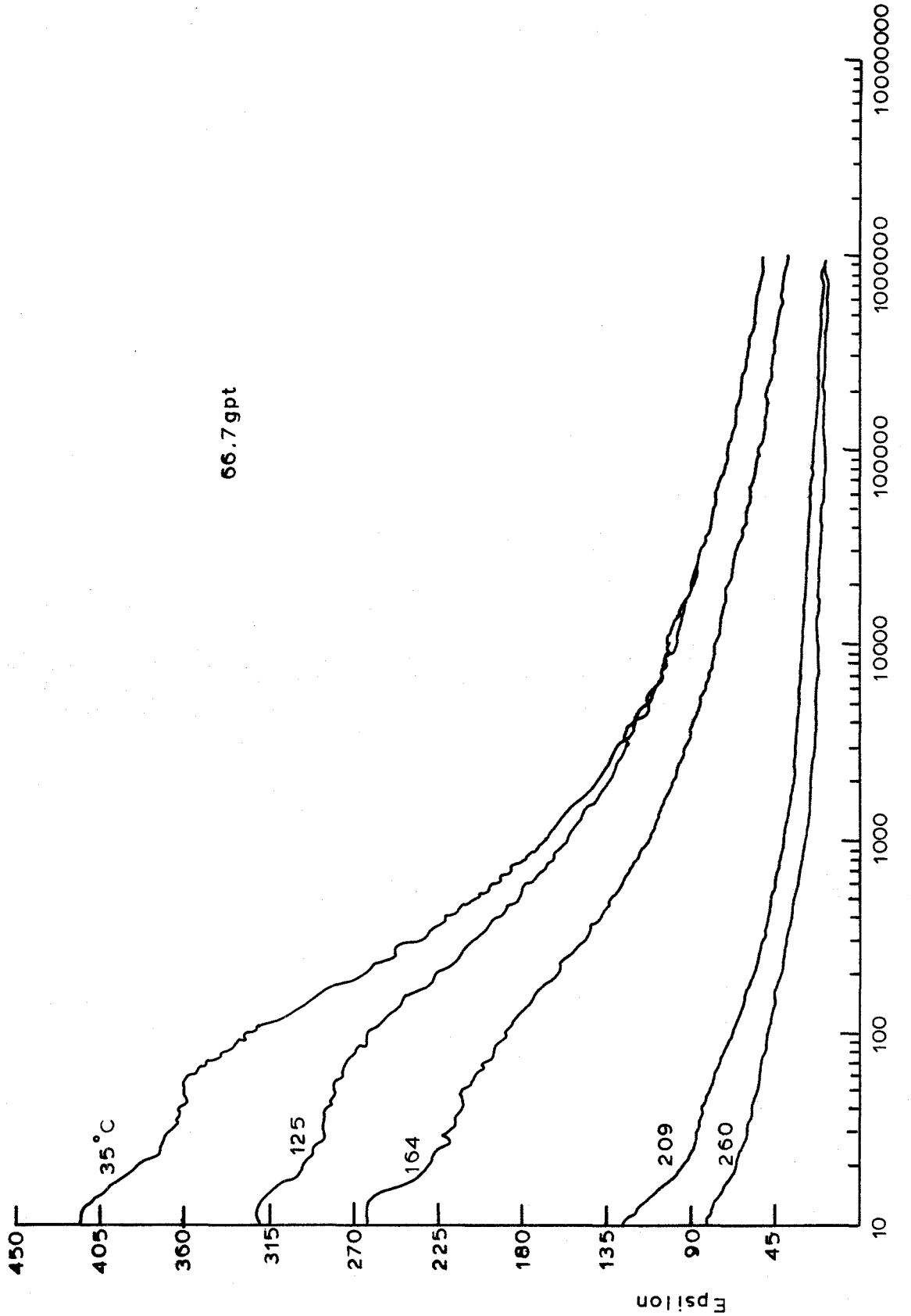

Figure 3.43 Low Temperature Dielectric Constant of 66.7 gpt Oil Shale

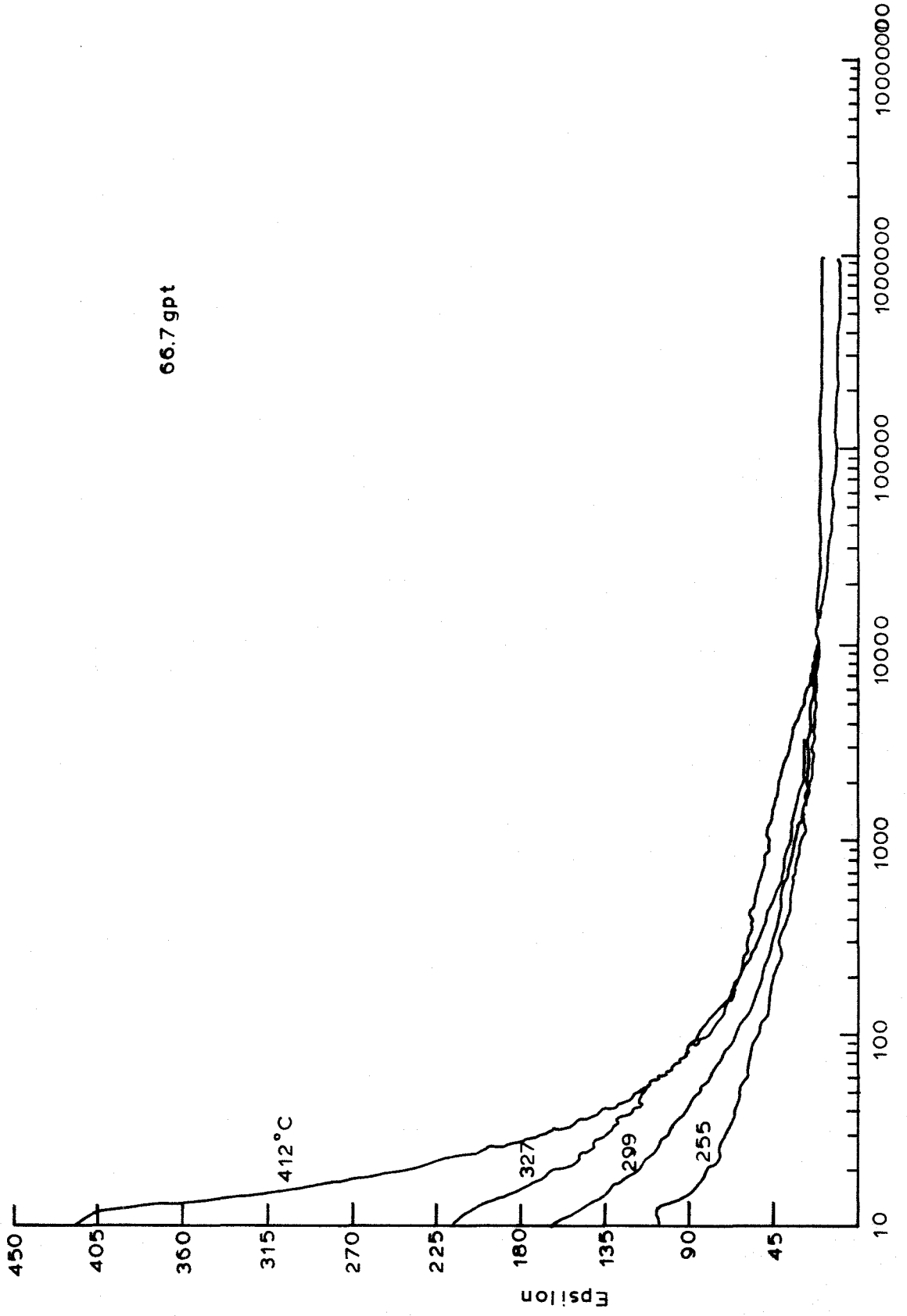

Figure 3.44 High Temperature Dielectric Constant of 66.7 gpt Oil Shale

initially decrease with increasing temperature. However, at about 250° C the dielectric constant is seen to gegin increasing again, especially at lower frequencies. At temperatures where significant amounts of organic decomposition occur, the dielectric constant attains values approaching the low temperature values. However, the falloff with frequency is more rapid. The origins of this effect are as yet not well understood. Pore pressure effects and capillary water in the shale could possibly play a role in this effect. This possibility is indicated by the shift in the baseline slope on the DTA at about 250°C.

Typical data showing the variation of the dielectric parameters with frequency are shown in Table 3.15 for a 37 gpt oil shale sample. The dielectric constant E' shows the frequency dependence characteristic of water-bearing sedimentary rocks and minerals; [42] a sharp decrease in dielectric constant at low frequencies, and relative insensitivity to frequency at higher values, are typical for all the samples studied. The high values of the dielectric constant found for the oil shale samples may be explained in terms of the Maxwell-Wagner theory for interfacial polarization. [43] The presence of semi-conducting clay particles which give rise to a membrane effect, might also account for the large values of dielectric constant. [44] The data shown in Table 3.8 also reveal a sharp increase in the a.c. conductivity with increasing frequency. This behavior is consistant with previously published work on the electrical properties of limestone, marl and dolomite, [42] which show that

Table 3.15

Dielectric Analysis of Green River Oil Shale

(37.0 gpt)

Frequency (c/s)	Resistivity (ohms-cm)	Capacitance farads	ε'	ε''	$\tan\delta$	A.C. Conductivity (mho-cm^{-1})
10	0.100×10^{11}	0.161×10^{-10}	18.54	1.831	0.098	0.102×10^{-10}
50	0.442×10^{10}	0.164×10^{-10}	18.90	0.829	0.043	0.231×10^{-10}
100	0.236×10^{10}	0.164×10^{-10}	18.91	0.776	0.041	0.432×10^{-10}
1000	0.480×10^{9}	0.150×10^{-10}	17.21	0.382	0.022	0.212×10^{-9}
4000	0.369×10^{8}	0.142×10^{-10}	16.28	1.240	0.076	0.276×10^{-8}
10,000	0.963×10^{7}	0.134×10^{-10}	15.35	1.901	0.124	0.106×10^{-7}
52,000	0.113×10^{7}	0.108×10^{-10}	12.39	3.113	0.251	0.102×10^{-6}
94,000	0.808×10^{5}	0.552×10^{-11}	6.35	2.410	0.380	0.126×10^{-5}

the less the water-content and/or the higher the resistivity of the material, the greater is the decrease in the resistivity with increasing frequency. The water content of oil shale is variable; it, however, seldom exceeds 6-10%, which is well within the limits observed for sedimentary rocks which exhibit similar dielectric behavior.

The nature of dispersion observed in oil shale for the loss tangent, tan is shown by a typical curve, Figure 3.45 for a 26 gpt sample. The presence of a broad peak at low frequencies (<1000 Hz) is interpreted in terms of interfacial polarization effects. The occurance of secondary maxima in tan at higher frequencies which is observed only at higher temperatures is also significant. The peak maxima show a pronouced dependance on temperature, shifting to higher frequencies with increasing temperature. It is possible to extract activation energies for dipole relaxation processes from such temperature dependent behavior. In materials as heterogeneous and complex as oil shale, the wide range of relaxation times significantly complicates the interpretation of these data. The dependence of the magnitude of tan on temperature also indicate that at high temperatures where tan δ shows values of $>$ 1, the conduction is primarily ohmic, wheras at low temperatures (tan δ $<$ 1), the conduction is by displacement mechanisms. This behavior is consistent with the observed changes in the resistency of oil shale with temperatures; changes in the resistivity over five orders of magnitude are commonly observed for the oil shale samples.

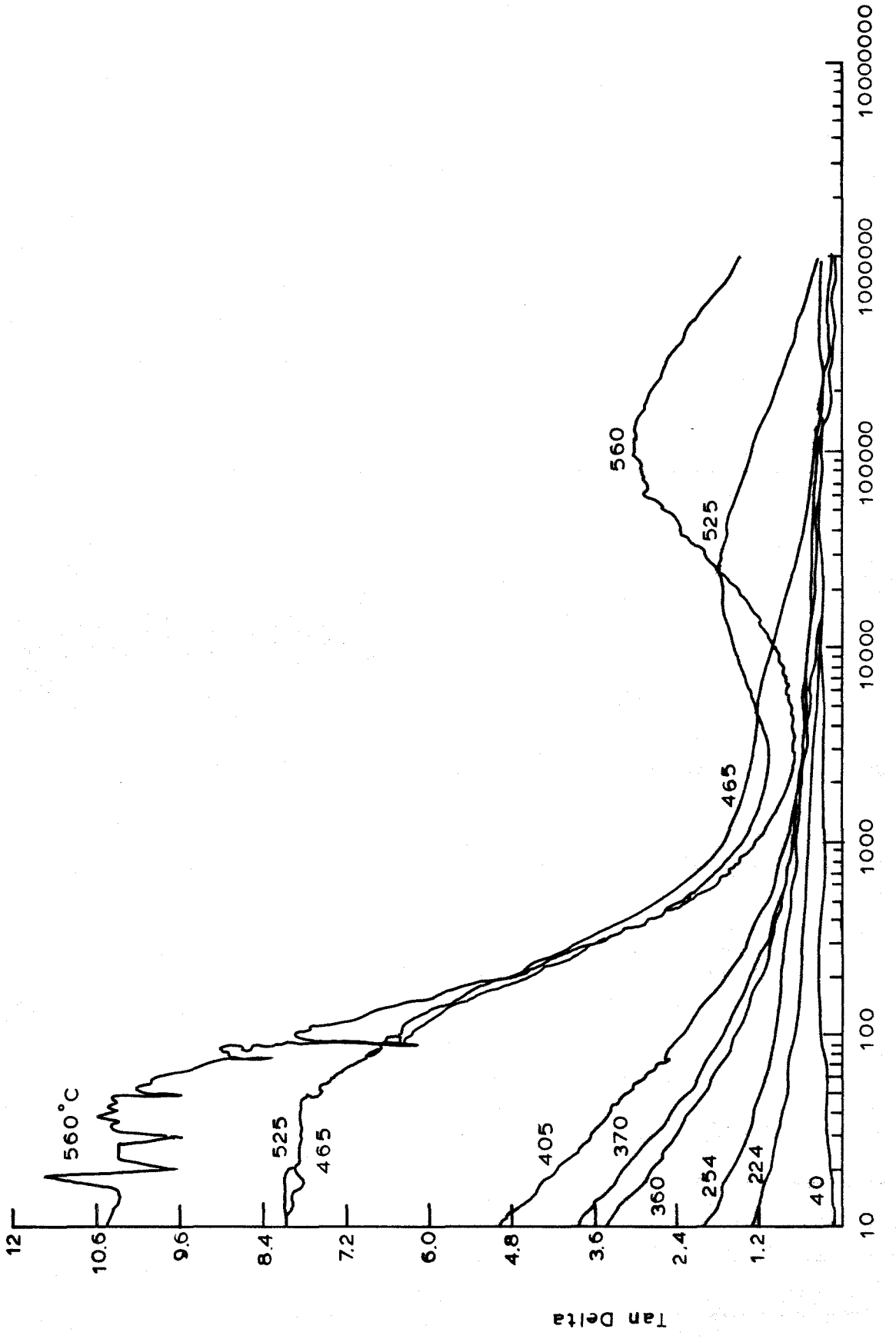

Figure 3.45 Temperature Dependent Loss Tangent versus Frequency for 26.0 gpt Oil Shale

Figure 3.46 shows the loss tangent versus frequency for a 29.8 gpt shale. The same major features are observed as were observed for the 26 gpt sample. A secondary peak in the loss tangent appears at the temperatures where organic decomposition begins to occur as indicated by the DTA curve. However, the temperatures at which this secondary peak begins to occur is lower on the higher grade of shale.

Figure 3.47 shows the temperature dependence of the dielectric constant of oil shale for different grades ranging from 7.5 to 60 gpt. The sharp changes in the values at temperatures in the range 100 - 150°C are possibly correlated with the loss of capillary water and change in the pore structure of the oil shale samples. The pronounced increase in the dielectric constant at temperatures above 270°C probably arises from the onset of the decomposition of the organic matter. The thermal behavior of the samples as shown by their DTA carried out simultaneously under the same conditions, exhibits remarkably similar trends and points towards a common origin for the observed effects.

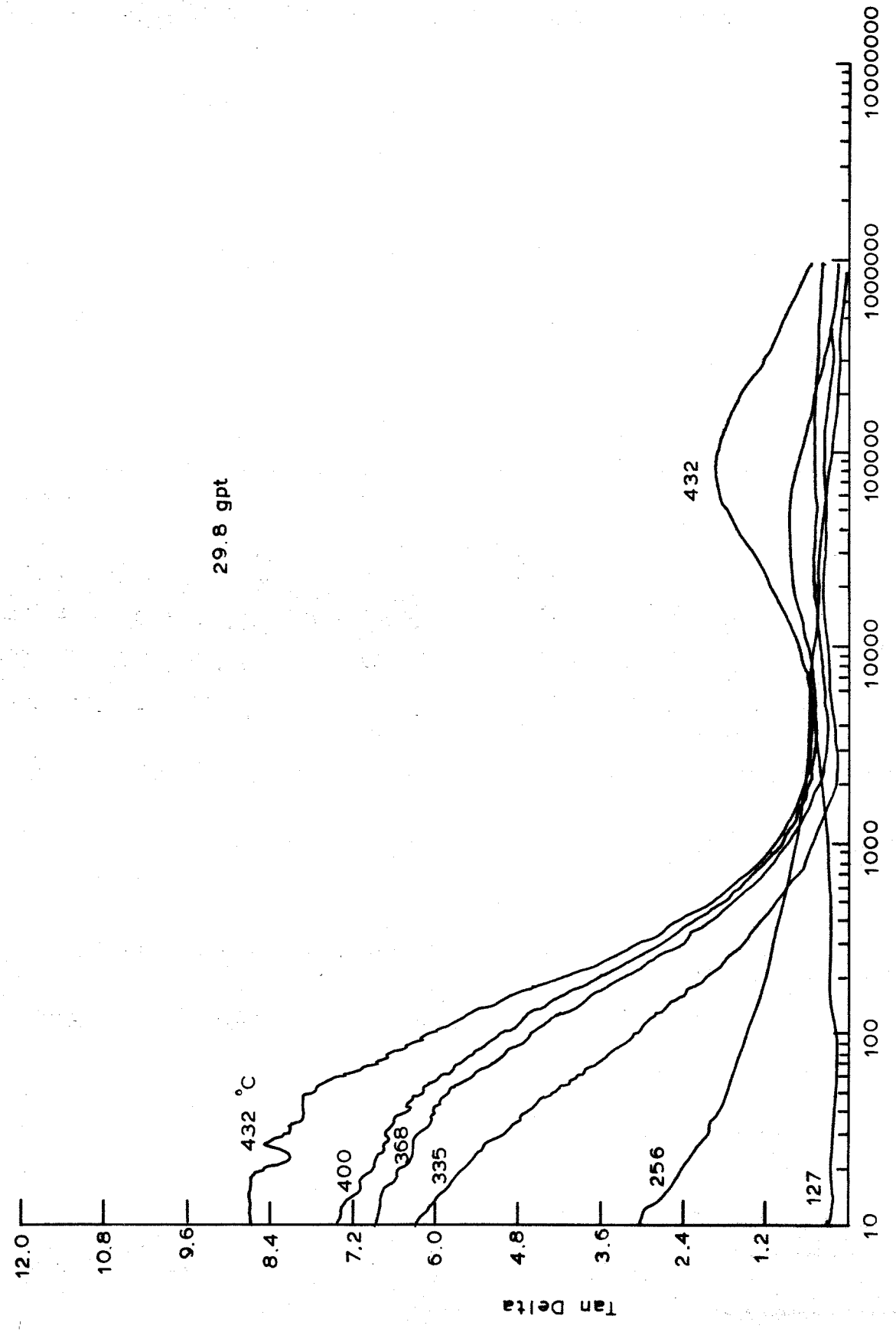

Figure 3.46 Temperature Dependent Loss Tangent for 29.8 gpt Oil Shale

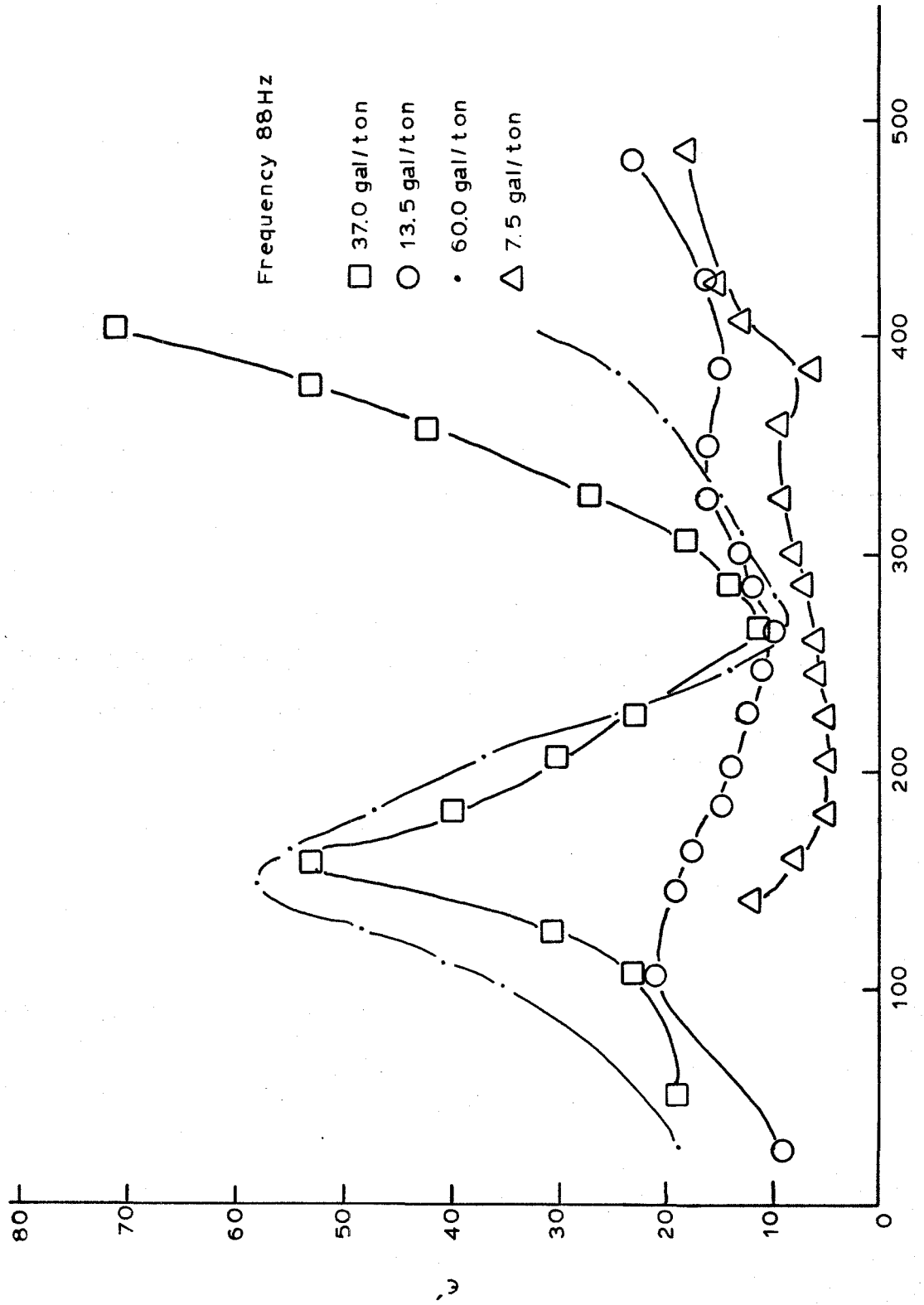

Figure 3.47 Low Frequency Dielectric Constant versus Temperature for Various Grades of Oil Shale

3.4 Mathematical Modeling

The mathematical modeling was undertaken with the approach of sequentially developing more complicated models and using the previous models as a basis for checking results. Following is a summary of the models developed to date and their results.

3.4.1 Verification Model

The simplified pillar system is depicted in Figure 3.48. The element which was studied is shown as a disk of radius "R" and unit height, which has an internal temperature distribution which varies with time "t" and radial position "r". Heat is transferred from the radial surface of the disk to an ambient with a temperature "Ta". Rate of convective heat transfer is governed by the convection coefficient "H". No heat is transferred across the axial surface of the disk.

Also shown in Figure 3.48 is a plan view of the disk as divided into washer-shaped elements for the finite-difference formulation. Energy balances performed on each element yield the descriptive equations which are used in the finite-difference solution. The equations are depicted in simplified finite-difference form in Figure 3.49.

Thermal patterns resulting from numerical solution of the equations in Figure 3.49 are to be used to verify the predictions of the finite-element model. Before this could be done with any confidence, it was first necessary to demonstrate that the finite-difference model was correct within the limitations imposed by the assumtions cited above. Verification of the finite-difference model was accomplished by neglecting

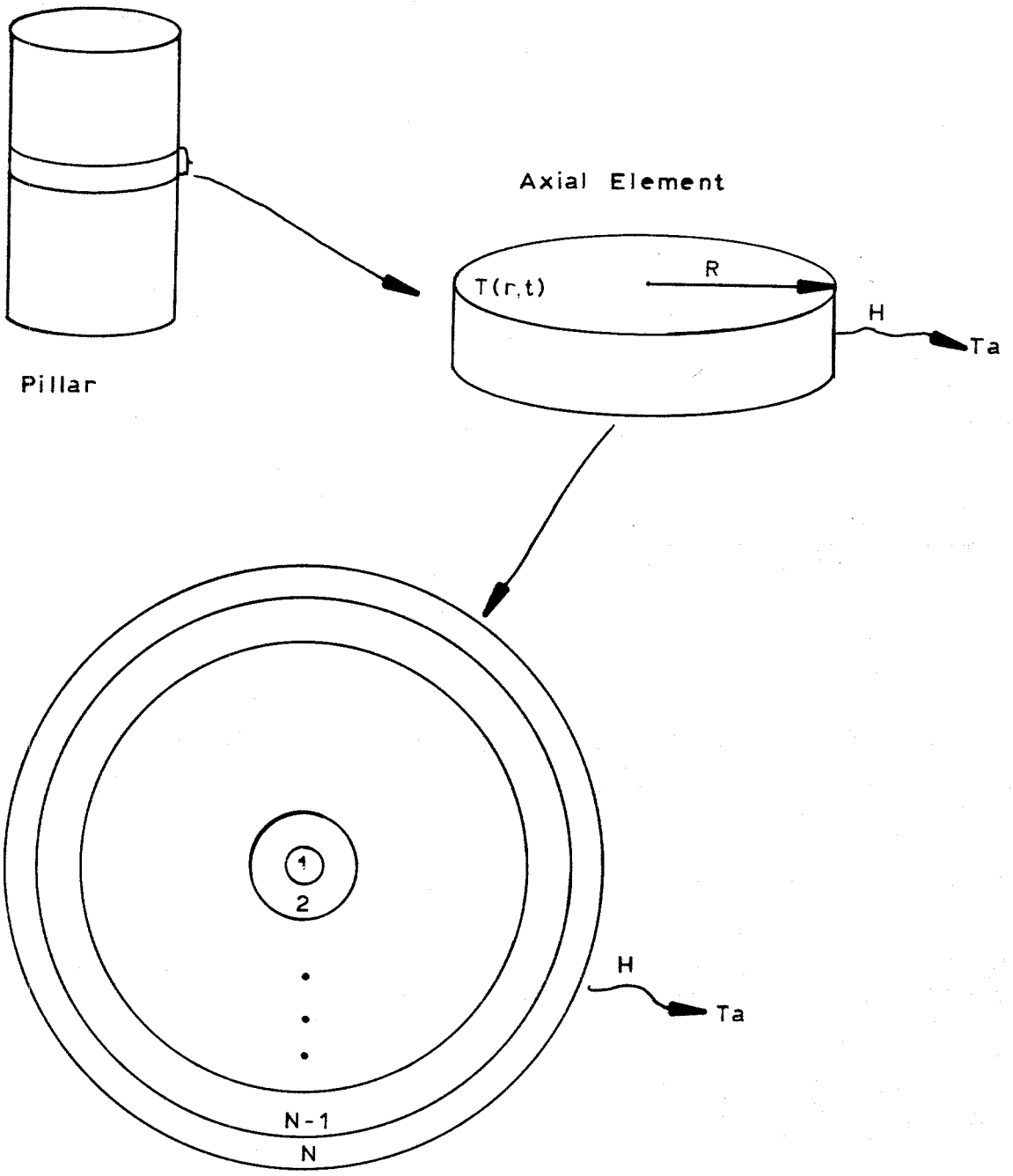

SIMPLIFIED PILLAR SYSTEM

FIGURE 3.48

Figure 3.49

HEAT-BALANCE EQUATIONS, FINITE DIFFERENCE FORM

1.) CENTER NODE

$$\rho CV(1)\left[\frac{T'(1)-T(1)}{\Delta t}\right]= KA(2)\left[\frac{T(2)-T(1)}{\Delta r}\right]$$

2.) INTERMEDIATE NODES

$$\rho CV(J)\left[\frac{T'(J)-T(J)}{\Delta t}\right]= -KA(J)\left[\frac{T(J)-T(J-1)}{\Delta r}\right] + KA(J+1)\left[\frac{T(J+1)-T(J)}{\Delta r}\right]$$

3.) SURFACE NODES

$$\rho CV(N)\left[\frac{T'(N)-T(N)}{\Delta t}\right]= -KA(N)\left[\frac{T(N)-T(N-1)}{\Delta r}\right] - HA(N+1)\,(T(N)-Ta)$$

BOUNDARY CONDITIONS

Conditions in r are implied in (1) and (3)
Initial Condition: At $t=0$, $T(J)=Ti$

LEGEND

ρ	Density, Lb./Ft.^{3}
C	Specific Heat, Btu./Lb. °F.
V(J)	Volume of Node J, Ft.^{3}
T'(J)	Temperature of Node J at Time $t+\Delta t$, °F.
T(J)	Temperature of Node J at Time t, °F.
Δt	Time Increment, Hr.
K	Thermal Conductivity, Btu./Ft. Hr. °F.
Δr	Increment of Radial Distance, Ft.
A(J)	Surface Area of Node J in the Radial Direction, Ft.^{2}
H	Convection Coefficient, Btu./Ft.^{2} Hr. °F.
Ta	Ambient Temperature, °F.
Ti	Initial Temperature, °F.

thermal-property variations and taking the limit of the equations in Figure 3.49 as radial and time increments approached zero. The result was the differential equation and the boundary conditions depicted in Figure 3.50. This system has an analytical solution involving Bessel functions of the first kind, as shown in Figure 3.51. The analytical solution was used to check the finite-difference solution for the special care of constant thermal properties.

Figure 3.52 is a listing of the general finite-difference program which was coded in the FORTRAN language and run on the DEC-10 system at the Colorado School of Mines. The program consists of a driver segment, SHAL, and two subroutines, PROP and PMAP. SHAL sets up the problem parameters, performs the heat-transfer calculations, and terminates at the specified problem time. PROP calculates values for the thermal properties at each time step. PMAP calls for printing of the problem parameters and of the temperature distribution within the pillar increment at specified time steps.

When the program was run for comparison with the analytical solution, PROP was modified to provide constant property values to SHAL. On other runs, the equations of Tihen, Carpenter, and Sohns of the Laramie Energy Research Center were used to calculate values of oil-shale thermal conductivity. Shaw's equation was used to calculate specific heat as a function of temperature. Density was assumed constant in all cases.

Several runs were made with fixed thermal properties to provide data for comparison with the analytical solution.

Figure 3.50

HEAT-BALANCE EQUATIONS, DIFFERENTIAL FORM

$$\frac{\partial T}{\partial t} = \frac{K}{\rho C}\left[\frac{\partial^2 T}{\partial r^2} + \frac{1}{r}\frac{\partial T}{\partial r}\right]$$

BOUNDARY CONDITIONS

1. At $t=0$, $T=Ti$
2. At $r=R$, $-\frac{K\partial T}{\partial r} = H(T-Ta)$
3. At $r=0$, $\frac{\partial T}{\partial r} = 0$

LEGEND

T = Temperature, °F.
r = Radial Distance, Ft.
K = Thermal Conductivity, Btu./ Hr. Ft. °F.
ρ = Density, Lb./ $Ft.^3$
C = Specific Heat, Btu./ Lb. °F.
t = Time, Hr.
Ti = Uniform Initial Temperature, °F.
H = Unit Surface Conductance (Convection Coefficient), Btu./ Hr. $Ft.^2$ °F.
A = Area Exposed to the Ambient, $Ft.^2$
Ta = Uniform Ambient Temperature, °F.

Figure 3.51

ANALYTICAL SOLUTION WITH BESSEL FUNCTIONS

$$\frac{T(r,t)-Ta}{Ti-Ta} = 2Bi \sum_{n=1}^{\infty} \frac{EXP(-a\lambda_n^2 t)\ Jo(\lambda_n r)}{(\lambda_n^2 R^2 + Bi^2)\ Jo(\lambda_n R)}$$

Bi = Biot Number (HR/K)

a = Thermal Diffusivity ($K/\rho C$)

λ = Zeros of the equation

$$(\lambda R)\, J_1(\lambda R) - Bi\, Jo(\lambda R) = 0$$

Jo = Bessel Function of the first kind of order 0

J_1 = Bessel Function of the first kind of order 1

T(r,t) = Temperature at Radius r and Time t, °F.

r = Radial Distance, Ft.

R = Outer Radius of Cylinder, Ft.

t = Time, Hr.

H = Convection Coefficient, Btu./Ft.^{2} Hr. °F.

K = Thermal Conductivity, Btu./Ft. Hr. °F.

ρ = Density, Lb./Ft.^{3}

C = Specific Heat, Btu./Lb. °F.

Ta = Ambient Temperature, °F.

BESSEL FUNCTION DEFINITION

$$Jp(X) = \sum_{K=0}^{\infty} \frac{(-1)^K\ (X/2)^{2K+P}}{K!\ \ (K+P)!}$$

FIGURE 3.52 PROGRAM LISTING

```
C    ************************************************************
      COMMON T(100),TP(100),R(100),AR(100),AZ(100),RO(100),
     1CP(100),AK(100),ALP(100),DT,TIME,TMAX,ITER,IMAX,H,G,NR,
     2TA,PD,HITE,DR,ICK,TI,DC(100),TRGT,RBAR(100),TB(100),FCTR
      OPEN(UNIT=2,FILE='SHALL.DAT',ACCESS='SEQIN')
      PI=3.141596
      READ(2,52)NRUN
      DO 8 J(1)=1,NRUN
      READ(2,50)PD,HITE,G
      READ(2,52)TI,TA,H,TRGT,FCTR
      READ(2,51)TMAX,IMAX,NR,ICK,KPT
50    FORMAT(8F10.3)
51    FORMAT(F10.3,5I10)
52    FORMAT(8I10)
      ANR=NR-1
      DR=PO/(2.*ANR)
      R(1)=0.0
      R(2)=DR/2.
      AR(1)=0.0
      AK(1)=0.0
      DO 1 J=3,NR
      R(J)=R(J-1)+DR
      R(NR+1)=R(NR)+DR/2.
      AR(NR+1)=2.*PI*R(NR+1)*HITE
      AK(NR+1)=0.0
      T(NR+1)=TA
      DO 2 J=1,NR
      RBAR(J)=2.*(R(J+1)**3-R(J)**3/(3.*(R(J+1)**2-R(J)**2))
      AR(J)=2.*PI*R(J)*HITE
      AZ(J)=PI*(R(J+1)**2-R(J)**2)
      V(J)=AZ(J)*HITE
      TP(J)=TI
 2    T(J)=TI
C
      ITER=0
      TINF=0.0
      IPT=KPT
      CALL PROP
      CALL PMAP(IFLAG)
      GO TO 5
C
 3    DO 4 J=1,NR
 4    T(J)=TP(J)
      CALL PROP
 5    TIME=TIME+DT
      ITER=ITER+1
      IP(1)=T(1)*(1.-ALP(1)*DT)+T(2)*ALP(1)*DT
      DO 6 J=2,NR
 6    TP(J)=T(J)*(1.-DT*(AL(J)+ALP(J)))+DT*(T(J-1)*AL(J)+T(J+1)*ALF(J))
      IF(ITER-IPT)3,7,7
 7    CALL PMAP(IFLAG)
      IPT=IPT+KPT
      IF(IFLAG)3,3,8
 8    CONTINUE
      STOP
      END
```

```
C
      SUBROUTINE PMAP(IFLAG)
      COMMON T(100),TP(100),P(100),AR(100),AZ(100),V(100),RO(100),
     1CP(100),AK(100),AL(100),ALP(100),DT,TIME,TMAX,ITER,IMAX,H,G,NR,
     2TA,PD,HITE,DR,ICK,TI,DC(100),TRGT,RBAR(100),TB(100),FCTR
      IF(TIME)1,1,2
 1    WRITE(3,50)
      WRITE(3,51)PD,HITE,G,TI,TA,H,NR
      WRITE(3,52)
      WRITE(3,66)
      WRITE(3,55)(J,J=1,NR)
      WRITE(3,56)(R(J),J=1,NR),R(NR+1)
      WRITE(3,67)(RBAR(J),J=1,NR)
      WRITE(3,68)(AR(J),J=1,NR)
      WRITE(3,69)(V(J),J=1,NR)
      WRITE(3,71)FCTR
      IFLAG=0
 2    TMIN=TINF*60
      WRITE(3,54)ITER,TIME,TMIN
      WRITE(3,55)(J,J=1,NR)
      WRITE(3,57)(TP(J),J=1,NR),T(NR+1)
      WRITE(3,70)(TB(J),J=1,NR)
      IF(ICK)4,4,3
 3    WRITE(3,60)(RO(J),J=1,NR)
      WRITE(3,61)(CP(J),J=1,NR)
      WRITE(3,62)(AK(J),J=1,NR)
      WRITE(3,63)(AL(J),J=1,NR)
      WRITE(3,64)(ALP(J),J=1,NR)
      WRITE(3,65)(DG(J),J=1,NR)
 4    IF(TIME-TMAX)5,7,7
 5    IF(ITER-IMAX)6,7,7
 6    IF(TB(1)-TRGT)8,7,7
 7    IFLAG=1
C
C************FORMATS*****************************************************
C
50    FORMAT(1H1,    'ONE DIMENSIONAL MODEL FOR HEAT TRANSFER IN AN OIL
     1 SHALE PILLAR',/,1H ,40('-'))
51    FORMAT(1H ,'PROBLEM PARAMETERS ARE: PILLAR DIAMETER=',F8.2,'FT',
     1/1H,T26,'PILLAR HEIGHT=',F8.2,'FT',
     2/1H,T26,'FISCHER ASSAY=',F7.2,' GPT',
     3/1H ,T26,'INITIAL TEMPERATURE=',F7.1,'F',
     4/1H ,T26,'AMBIENT TEMPERATURE=',F7.1,' F',
     5/1H ,T26,'CONVECTION COEFFICIENT=',F8.2,' BTU/HR.SQFT.F',
     6/1H ,T26,'NUMBER OF NODES=',15/)
52    FORMAT(1H ,'IN THE FOLLOWING PRINTOUT, TIME=ELAPSED PROBLEM TIME',
     1/1H ,T29,'J=RADIAL INDEX',
     2/1H ,T29,'R=RADIAL DISTANCE TO NODE J (FT)',
     3/1H ,T29,'T=TEMPERATURE OF NODE J (F)',
     4/1H ,T29,'RD=DENSITY (LB/CUFT)',
     5/1H ,T29,'CP=SPECIFIC HEAT (BTU/LB.F)',
     4/1H ,T29,'AK=THERMAL CONDUCTIVITY (BTU/HR.FT,F)',
     4/1H ,T29,'AL=DIFFUSIVITY CONSTANT (1/HR)',
     4/1H ,T29,'ALP=DIFFUSIVITY CONSTANT (1/HR)',
     4/1H ,T29,'DT=STABLE TIME STEP FOR NODE J (HR)',
     4/1H ,4 ('-')/)
```

```
54     FORMAT(/1H ,'ITERATION',I5,T18,'TIME=',F8.2,' HOURS OR',F8.1,
      1' MINUTES')
55     FORMAT(1H ,T4,'J=',15I7)
56     FORMAT(1H ,T4,'R=',15F7.2)
57     FORMAT(1H ,T4,'T=',15F7.1)
60     FORMAT(1H ,T3,'RC=',15F7.1)
61     FORMAT(1H ,T3,'CP=',15F7.3)
62     FORMAT(1H ,T3,'AK=',15F7.3)
63     FORMAT(1H ,T3,'AL=',15F7.3)
64     FORMAT(1H ,T2,'ALP=',15F7.3)
65     FORMAT(1H ,T3,'DT=',15F7.2)
66     FORMAT(1H ,'GEOMETRICAL PARAMETERS')
67     FORMAT(1H ,T1,'RBAR=',15F7.2)
68     FORMAT(1H ,T3,'AR=',15F7.2)
69     FORMAT(1H ,T4,'V=',15F7.2/)
70     FORMAT(1H ,T1,'TBAR=',15F7.1)
71     FORMAT(1H ,'****CONDUCTIVITIES MULTIPLIED BY',F7.3,'****'/)
C
 8    RETURN
      END
C
C*C*C*C*C*C*C*C*C*C*C*C*C*C*C*C*C*C*C*C*C*C*C*C*C*C*C*C*C*C*C*C*C*C*C*C*C*C*C*C*C*C*C*C*C*C*C
C
      SUBROUTINE PROP
      COMMON T(100),TP(100),R(100),AR(100),AZ(100),V(100),RO(100),
     1CP(100),AK(100),AL(100),ALP(100),DT,TIME,TMAX,ITER,IMAX,H,G,NR,
     2TA,PO,HITE,DR,ICK,TI,DC(100),TRGT,RBAR(100),TB(100),FCTR
      DIMENSION C(6),D(6)
      DATA(C(K),K=1,6)/1,8081,-3.698E-02,1.980E-03,3.056E-04,-5.184E-06,
     1-1.872E-05/
      DATA(D(K),K=1,6)/1.8246,-4.4844E-02,-2.309E-04,3.652E-04,0.0,
     11.067E-05/
      DATA(RO(K),K=1,100)/100*140.4/
      CPRAK(ZW)=0.172+0.001*(0.067+0.00162*G)*(ZW+460.)
      CPRET(ZT)=0.174+0.000051*(ZT+460.)
     1NRAW(TW)=(C(1)+C(2)*G+C(3)*TW+C(4)*G*G+C(5)*TW*TW+C(6)*G*TW)
     1*0.578176
      INRET(IT)=(D(1)+D(2)*G+D(3)*IT+D(4)*G*G+D(5)*TT*TT+D(6)*G*TT)
     1*0.578176
      TBAR(L)=(T(L)*(RBAR(L)-R(L))+T(L-1)*(R(L)-RBAR(L-1)))/
     1(RBAR(L)-RBAR(L-1))
      DO 7 J=1,NR
      IF (T(J)-500.)1,1,2
 1    CP(J)=CPRAW(T(J))
      GO TO 3
 2    CP(J)=CPRET(T(J))
 3    IF(J-1)7,7,4
 4    TB(J)=TBAR(J)
      TM1=(TB(J)-32.)/1.8
      IF(T(J)-500.)5,5,6
 5    AK(J)=INRAW(TM1)*FCTR
      GO TO 7
 6    AK(J)=TNRET(TM1)*FCTR
```

```
 7      CONTINUE
        DO 6 J=1,NR
        ZAL=1./(RO(J)*CP(J)*V(J)*DR)
        AL(J)=ZAL*AK(J)*AR(J)
 8      ALP(J)=ZAL*AK(J+1)*AR(J+1)
        ALP(NR)=R*AR(NR+1)/(RO(NR)*CP(NR)*V(NR))
        CHK=1.0E+06
        DO 10 J=1,NR
        DC(J)=1./(AL(J)+ALP(J))
        IF(CHK-DC(J))10,10,9
 9      CHK=DC(J)
10      CONTINUE
        OT=CHK



C @*@*@*@*@*@*@*@*@*@*@*@*@*@*@*@*@*@*@*@*@*@*@*@*@*@*@*@*@*@*@*@*@*@*
        RETURN
```

Temperature-averaged property values were used in these cases, and the convection coefficient was selected to comply with the constraints of the Bessel-function solution.

Figures 3.53 & 3.54 present the results of typical runs of two values of the convection coefficient. In each case, pillar diameter is 18 feet, thermal conductivity is 0.730 Btu/hr. ft. ^{o}F, specific heat is 0.247 Btu/lb. ^{o}F, density is 140.4 lb/ft^{3}, initial temperature is 0.0^{o}F, ambient temperature is 1000^{o}F, and the pillar increment is divided into 10 elements. Convection coefficients of 1.014 and 4.056 Btu/hr. ft^{2}^{o}F were used to generate the data shown.

In both cases, excellent agreement was obtained between the analytical solution and the fixed-property numerical solution. These results were considered to comprise ample verification of the numerical approach, at least when fixed thermal properties are used in the predictive equations.

Two additional runs were then performed to determine the effects of allowing thermal conductivity and specific heat to vary with temperature. The equations of Tihen, Carpenter, and Sohns were used to predict thermal conductivities as functions of temperature for 20-gallon-per-ton oil shale, and Shaw's equations were used to calculate specific heats as functions of temperature for the same shale. The PROP subroutine of the numerical model was programmed so that the equations for raw oil shale were used at temperatures below 500^{o}F and the equations for retorted shale were used at temperatures between 500 and 1000^{o}F. This technique involved a slight extrapolation of Tihen's equations beyond their

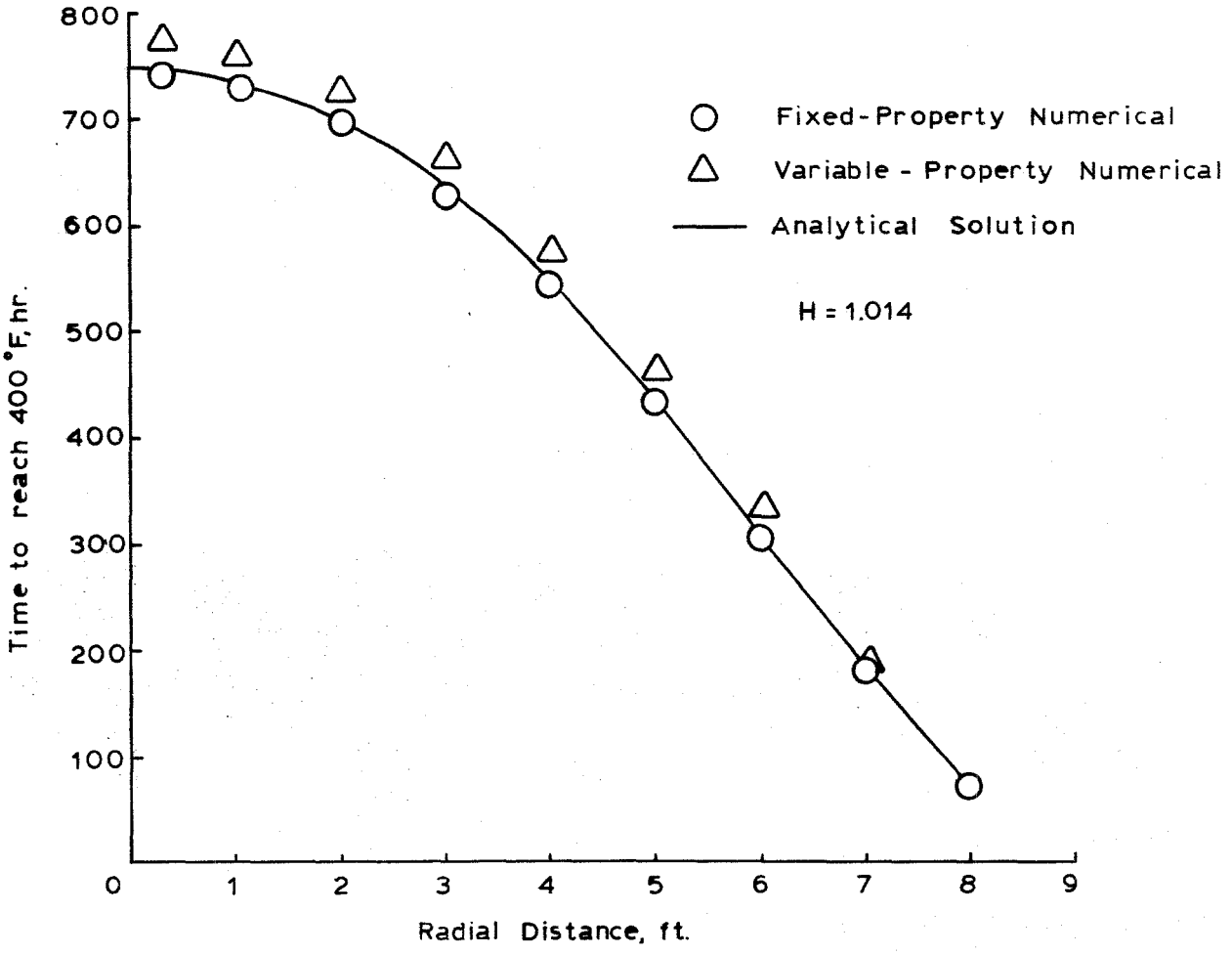

Figure 3.53 Comparison of Analytical Solution, Fixed-Property Numerical Solution, and Variable-Property Numerical Solution, H = 1.014 Btu./Ft.^{2} Hr. °F.

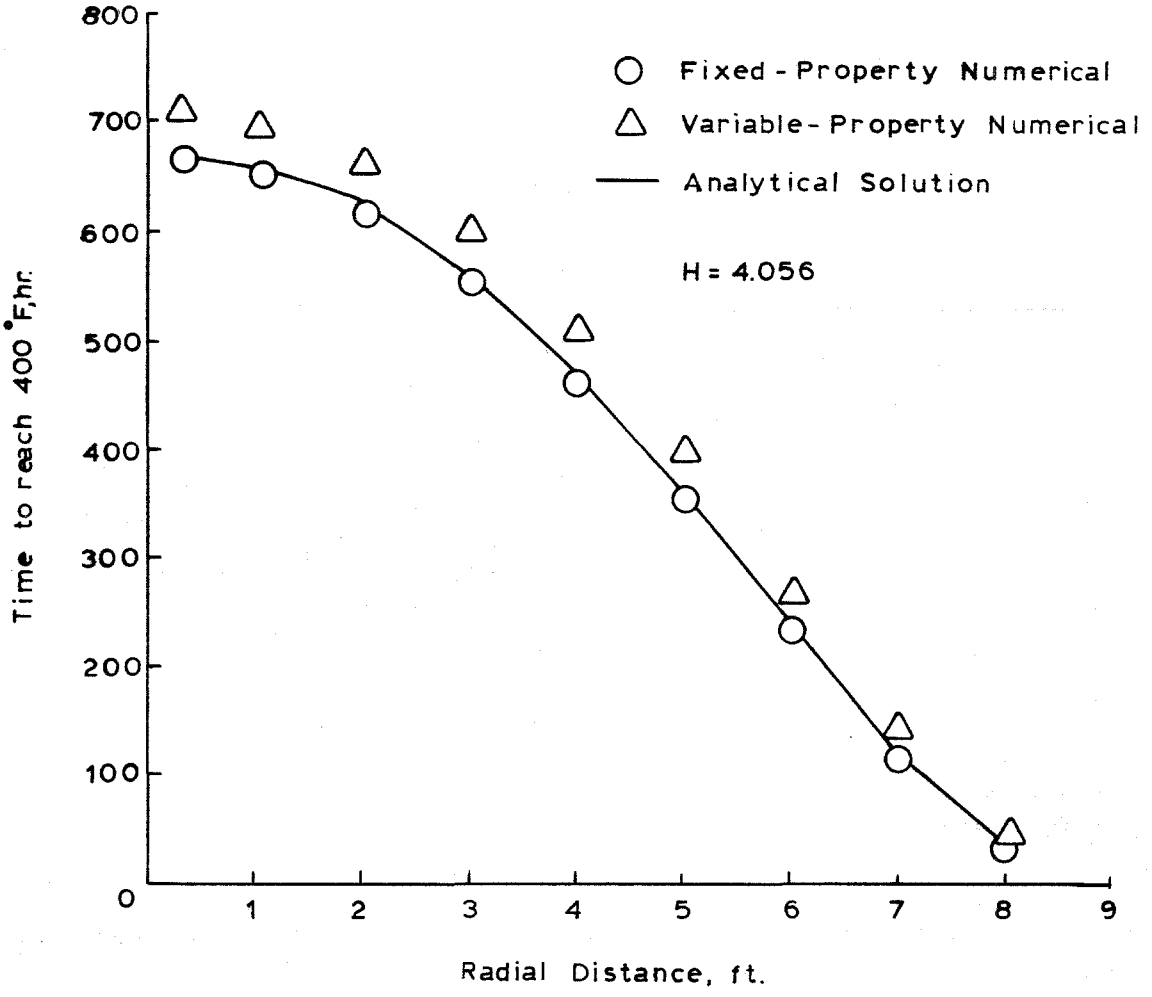

Figure 3.54 Comparison of Analytical Solution, Fixed - Property Numerical Solution, and Variable - Property Numerical Solution, H = 4.056 Btu./Ft.^{2} Hr. °F.

reliable temperature range of 100 to 900°F. Use of Shaw's equations in this manner required gross extrapolation of the correlations beyond their reliable temperature range of 150 to 450°F.

Curves generated by the variable-property runs are included in Figures 3.53 and 3.54 to permit comparison with the analytical solution and the fixed property solution. General observations include:

- At points near the pillar surface, variable-property predictions agreed quite well with both analytical and fixed-property numerical solutions.

- Agreement between the variable-property predictions and the other solutions was better near the surface of the pillar than at the center.

- Overall agreement was better for the higher convection coefficient of H = 4.056 (Figure 3.54) than for the lower coefficient of H = 1.014 (Figure 3.53)

These effects are believed to be related to the relative importance of convective heat transfer, which affects heat flow at the surface, and conductive heat transfer, which controls heat flow within the pillar.

Within the pillar, the rate of conductive heat transfer is determined by the thermal properties. At the pillar surface, heat transfer is strongly affected by the magnitude of the

convection coefficient. Thus, near the pillar surface, variations in thermal conductivity or specific heat will be dampened by the convection coefficient, and similar thermal behavior will be predicted over a broad range of thermal properties. The higher the convection coefficient, the more pronounced the dampening effect, up to the point at which the convection coefficient is so large that conduction becomes the controlling heat transfer mechanism. As will be shown later, control of heat transfer by conduction occurs at convection coefficients substantially larger than 4.056.

The fact that the variable-property solution deviates from the analytical and fixed-property solutions does not indicate an error in the methodology employed. Rather, it demonstrates that thermal properties which vary with temperature do affect the thermal behavior of a body. This result was expected and in fact the deviation between variable-property behavior and fixed-property behavior was less than anticipated. Since rather arbitrary values were used for the fixed thermal properties, it is anticipated that these properties could be "tuned" to force the fixed-property solution within acceptable limits of accuracy.

Upon completion of the verification runs, the variable-property numerical model was used for some preliminary studies of the effects of heat-transfer parameters on thermal behavior of the hypothetical pillar. The three parameters studied were thermal conductivity (K), convection coefficient (H), an ambient temperature (Ta). Results of each study are discussed below.

Thermal Conductivity

Figure 3.55 depicts the results of three runs which were made to evaluate the effects of thermal-conductivity variation on heat flow into the hypothetical pillar. In the base case, thermal conductivities were used as calculated from the equations of Tihen, et al. In the other two runs, these same conductivities were multiplied by either 0.75 or 1.25 to simulate errors of ± 25% in the thermal conductivity correlation. General observations include:

- Simulated errors in the magnitude of K had little effect on heat flow near the pillar surface.

  Effect of these errors increased near the center of the pillar.

  Absolute errors in the heat flow calculations were lower near the pillar surface, but relative errors remained fairly constant over the entire radius.

  Negative errors in K had a greater effect on heat flow calculations than did positive errors. For example, an error of -25% in K produced a 32% error in the time required for the pillar center to reach 400°F. An error of + 25% caused an error of only 20% in the time required to reach 400°F.

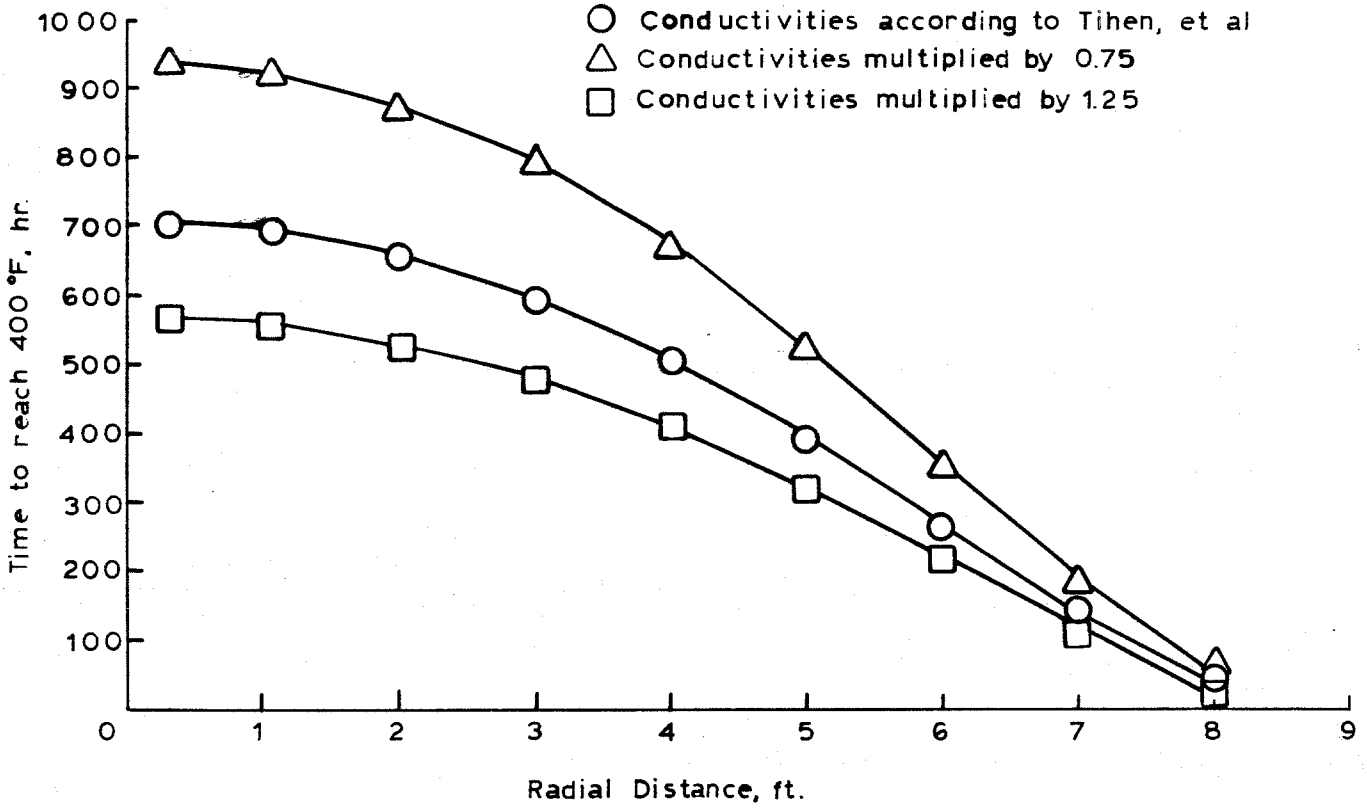

Figure 3.55 Effect of Thermal Conductivity Variation on Heat Flow, Variable - Property Numerical Solution

It is believed that these observations may be specific to the magnitude of the convection coefficient which was used in the runs depicted. In each run, a convection coefficient of 5 was assumed for heat transfer at the surface of the pillar. At this low level, overall heat transfer to the pillar is largely controlled by surface convection and is less dependent on thermal conduction within the pillar. Reducing the thermal conductivity by 25% shifts control from convection towards conduction and makes the calculations more dependent on conductivity. Increasing thermal conductivity by 25% does not change the dominant position of surface convection and hence has a lesser effect on the calculations. Additional evidence of this effect is presented in the next section.

Convection Coefficient

Figure 3.56 depicts the results of three runs which were made to evaluate the effects of convection-coefficient variation on heat flow. In each case, thermal conductivity values were used as calculated from the Tihen correlations. All other parameters were the same except that convection coefficients of 1, 5, and 25 were assumed at the surface.

The results shown are significant in that they indicate that a very large change in H has a relatively small effect on propogation of the thermal wave through the pillar. For example, increasing the coefficient by a factor of five (from H = 1 to H = 5) decreased the time required for the pillar center to reach 400°F by only about 10%. An additional five-fold increase (from H = 5 to H = 25) produced a change of only 11% in the time required for the center to reach 400°F.

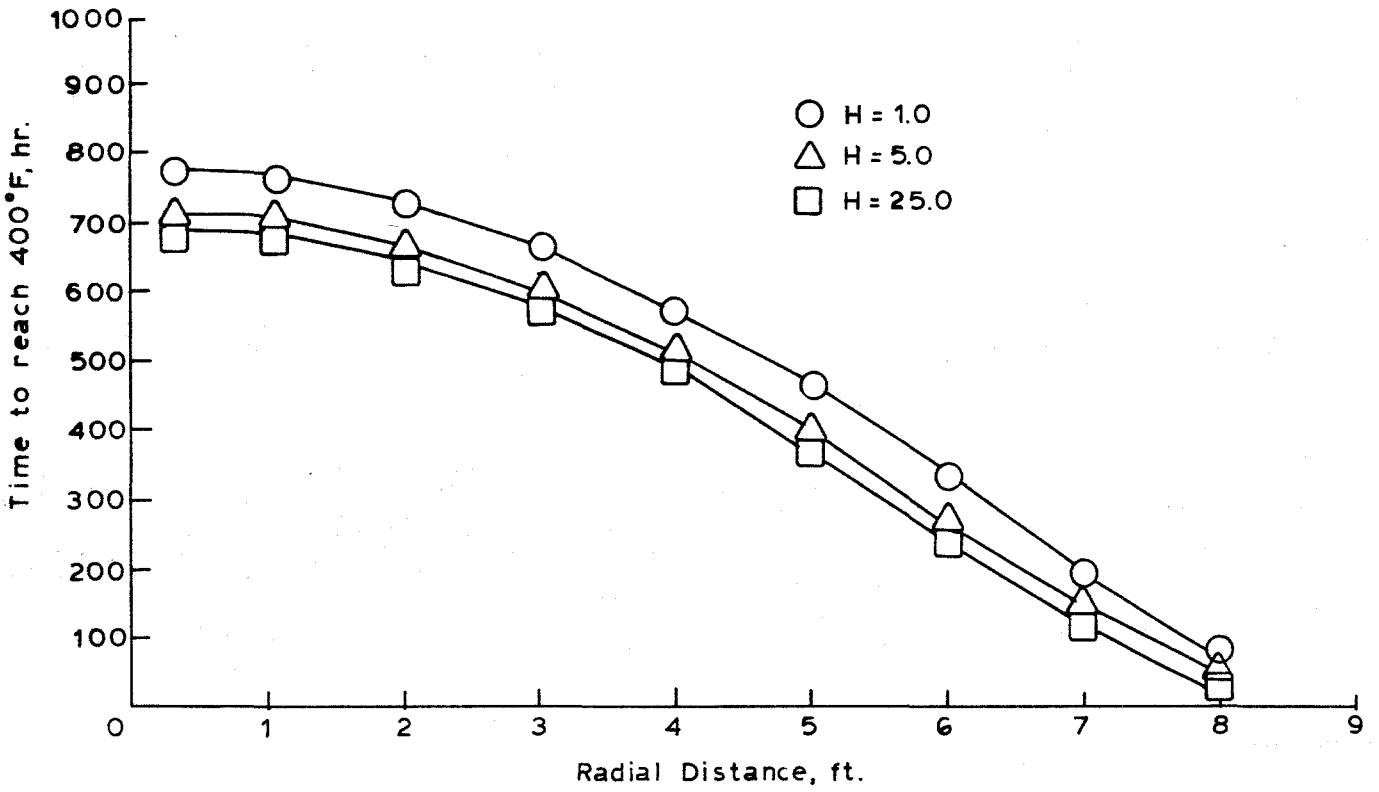

Figure 3.56 Effect of Convection Coefficient on Heat Flow, Variable-Property Numerical Solution

These results emphasize the relative importance of the convective and conductive heat transfer mechanisms. Between H = 1 and H = 5, convection is the controlling mechanism, and varying H has a small but significant effect. Above H = 5, conduction becomes the controlling mechanism, and large increases in H do not cause significant increases in heat flow.

Ambient Temperature

In oil-shale retorting, the ambient temperature,Ta, is the temperature of the gas stream or rubble adjacent to the outer surface of the pillar. Figure 3.57 depicts the results of three model runs which were made to evaluate the effect of Ta on heat flow. The temperatures studied were selected arbitrarily, but they could corresond to conditions within an in-situ retort. An ambient temperature of 500°F is probably a good value for the gas stream during the preheat period. A Ta of 750°F is a good value for the retorting period, and a Ta of 1000°F is a good average value for the gas-stream temperature during passage of the combustion front.

As shown in Figure 3.38, Ta has a large effect on heat flow, and the effect is roughly linear. That is, a doubling of Ta (from 500 to 1000°F) reduces the time for the pillar center to reach 400°F by approximately one-half (from 1384 hours to 706 hours). The effect is more pronounced near the pillar surface. For example, doubling Ta reduces the time required for a point one foot from the pillar surface to reach 400°F by a factor of six.

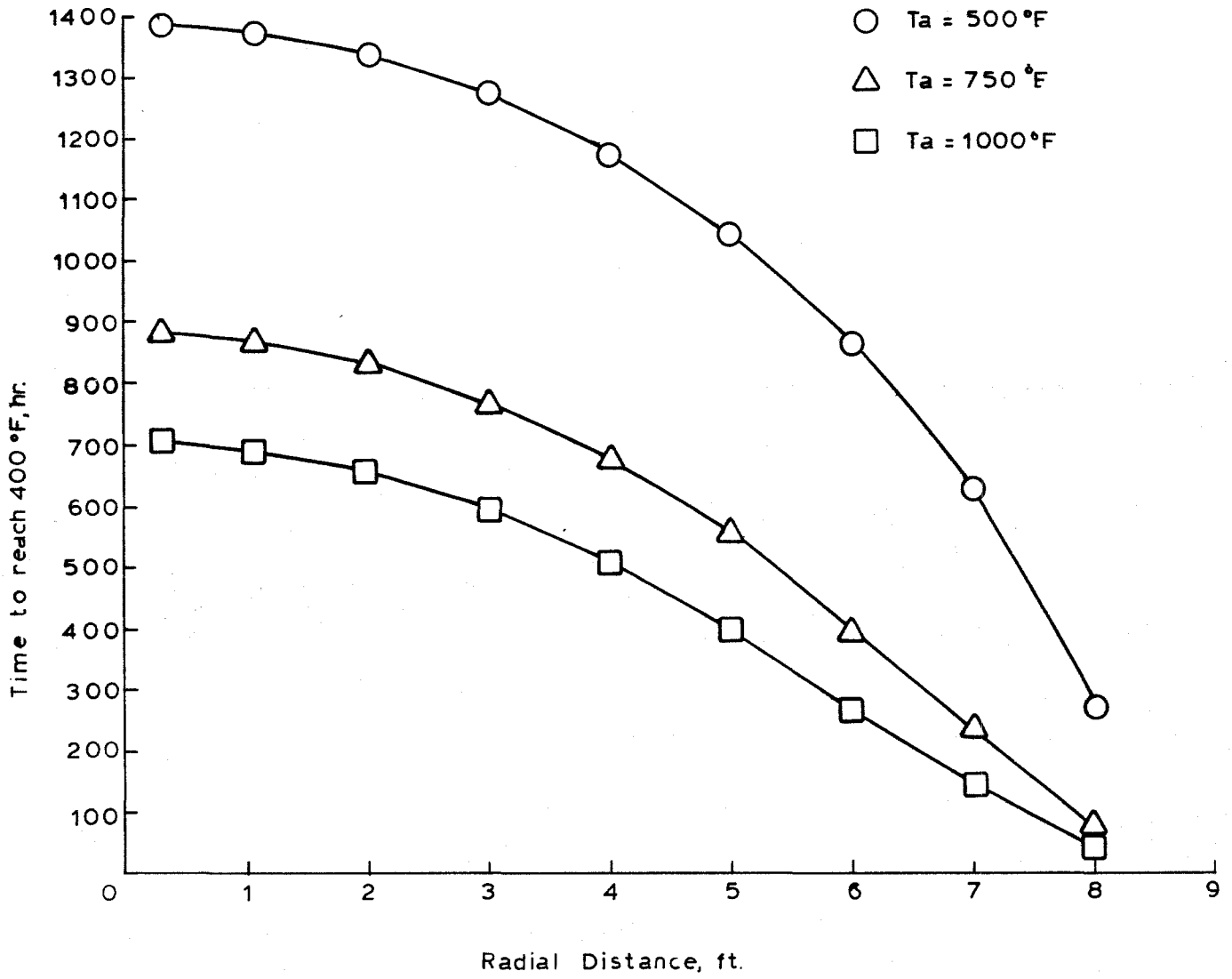

Figure 3.57 Effect of Ambient Temperature on Heat Flow, Variable - Property Numerical Solution

3.4.2 Preliminary retort model

Figure 3.58 depicts the temperature profiles in a cross section of a room-and-pillar retort. The conditions studied were:

- The center pillar is 100 feet square.
- The barrier wall is 50 feet thick.
- Fischer assay of the solid shale is 20 gallons per ton.
- The contained rubble is ignited at time zero and immediately attains a temperature of 1000°F. This temperature is maintained over the time of the analysis.
- Heat is transferred from the rubble to the solid shale with a convection coefficient of 5.0 Btu/hr ft^2 °F.
- All adjacent retorts in the retort plant are ignited simultaneously, and all are operated with the same burn progression.

The figure is a "snapshot" of the temperature profiles 565 hours (23.5 days) after the rubble was ignited.

Simultaneous operation of adjacent retorts is not likely to be encountered in commercial operation because of potential safety problems. The case was run because the barrier wall is subjected to maximum heat input under these conditions and is

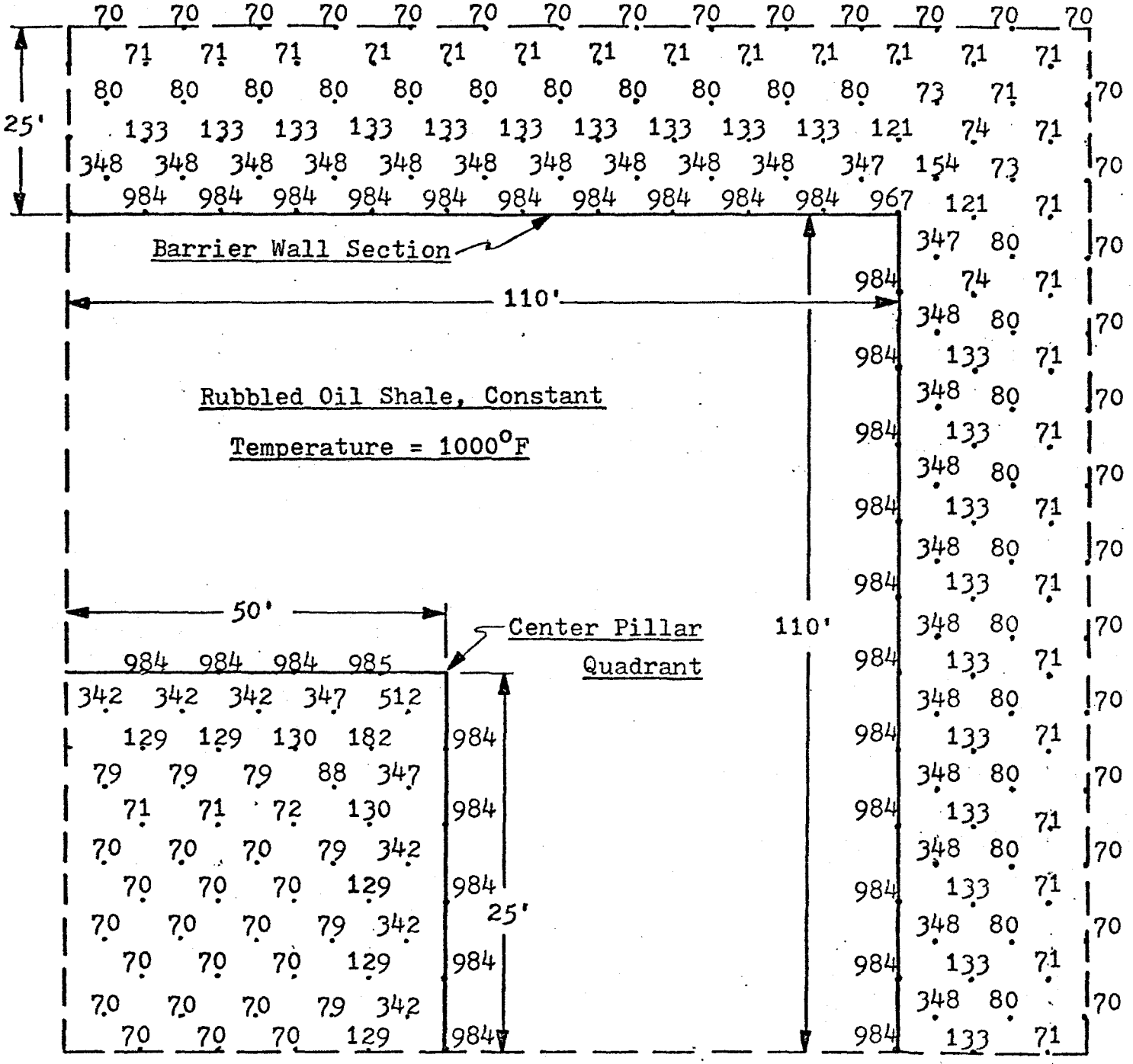

Thermal Profiles in a Room and Pillar Oil Shale Retort

Time = 565 hours after ignition

Convection coefficient = 5.0 Btu/hr ft^2 ^oF

Temperatures in ^oF

Figure 3.58

most likely to encounter failure. The modeled system also enjoys considerable symmetry which reduces computation time and expense. Because of the planes of symetry (which are denoted by dashed lines in the figure), it is only necessary to describe one quadrant of the retort. The other quadrants have identical temperature profiles. It is also necessary to model only one-half of the barrier wall thickness. The other half is the mirror image of the half shown.

As shown in figure 3.58, after 565 hours of heating, the outer surfaces of the center pillar and of the barrier wall have been heated to 984 - 1000°F, and it is safe to assume that shale near the surfaces will be fully retorted. Five feet into the solid shale, temperatures have not risen above 350°F, and negligible retorting has occurred. Ten feet in from the surface, shale is warm (ca 130°F) but no retorting has occured. Fifteen feet in, th shale is essentially at initial formation temperature (70°F).

3.4.3 Fenix and Scisson retort model

Using similar assumptions, a second series of runs in more detail were accomplished. Retort configuration that was modeled with finite-difference techniques is shown in Figure 3.59. The designated geometry is again a product of the earlier USBM project performed by Fenix and Scisson. [45] Geometry corresponds to their "Room and Pillar, Vertical Drill and Blast" method of retort development. The retort module comprises a square center pillar of solid shale surrounded by a square annulus filled with shale rubble which in turn is surrounded by a

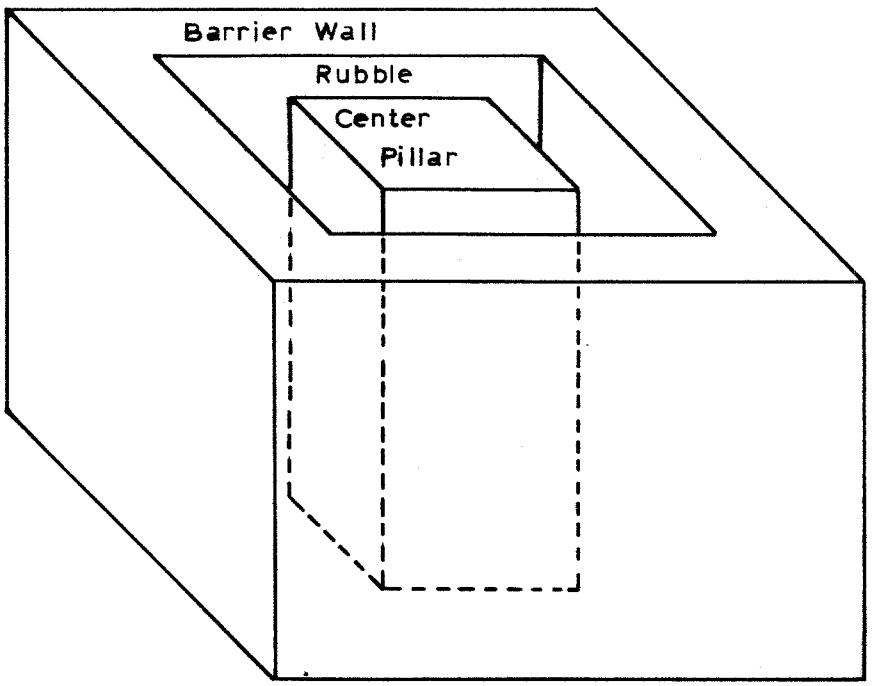

RETORT CONFIGURATION

FIGURE 3.59

barrier wall of solid shale which separates the module from identical modules in the same retort plant. A portion of the overall plant is shown in plan view in Figure 3.60. The drawing is scaled for a center-pillar width (P_c) of 100 feet, and overall rubble width (S) of 200 feet, and a barrier-pillar thickness (P_b) of 50 feet. Planes of geometric symmetry are indicated in the figure, and are denoted by dashed lines. In the first series of model runs, it was assumed that all retort modules in the plant burn at the same time and that progression of the combustion isotherm is identical in all modules. The above assumptions provide a highly symmetric geometry for modeling purposes. Such symmetry is depicted in Figure 3.61 where it is shown that the numerous planes allow a reduced model of a wedge-shaped area to simulate the entire module. Temperature histories in the non-modeled areas can be predicted by rotating the wedge about the center point of the module. It is recognized that this simplified system is unlikely to be reproduced in commercial practice, but it is being considered at present because of its simplicity and because it represents a "worst case" with respect to heating of the support pillars.

The retort rubble is burned by igniting the upper surface of the retort and forcing the combustion front to travel down along the retort axis by injecting preheated air through headers above the module. In the worst case imaginable, the entire rubbled volume would ignite instantaneously and would continue to burn

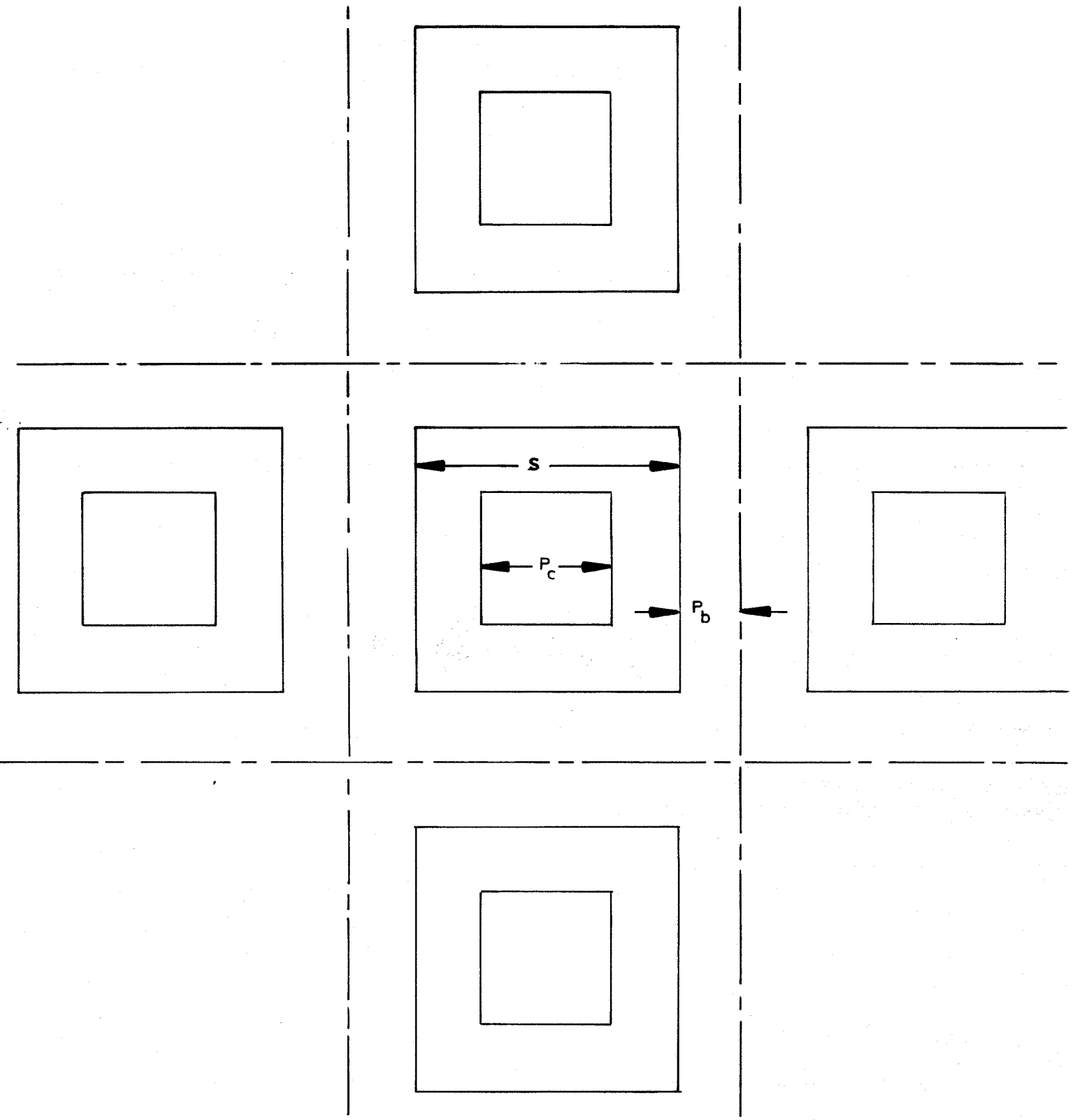

RETORT PLANT

FIGURE 3.60

To Scale for: S = 200

P_c = 100

P_b = 50

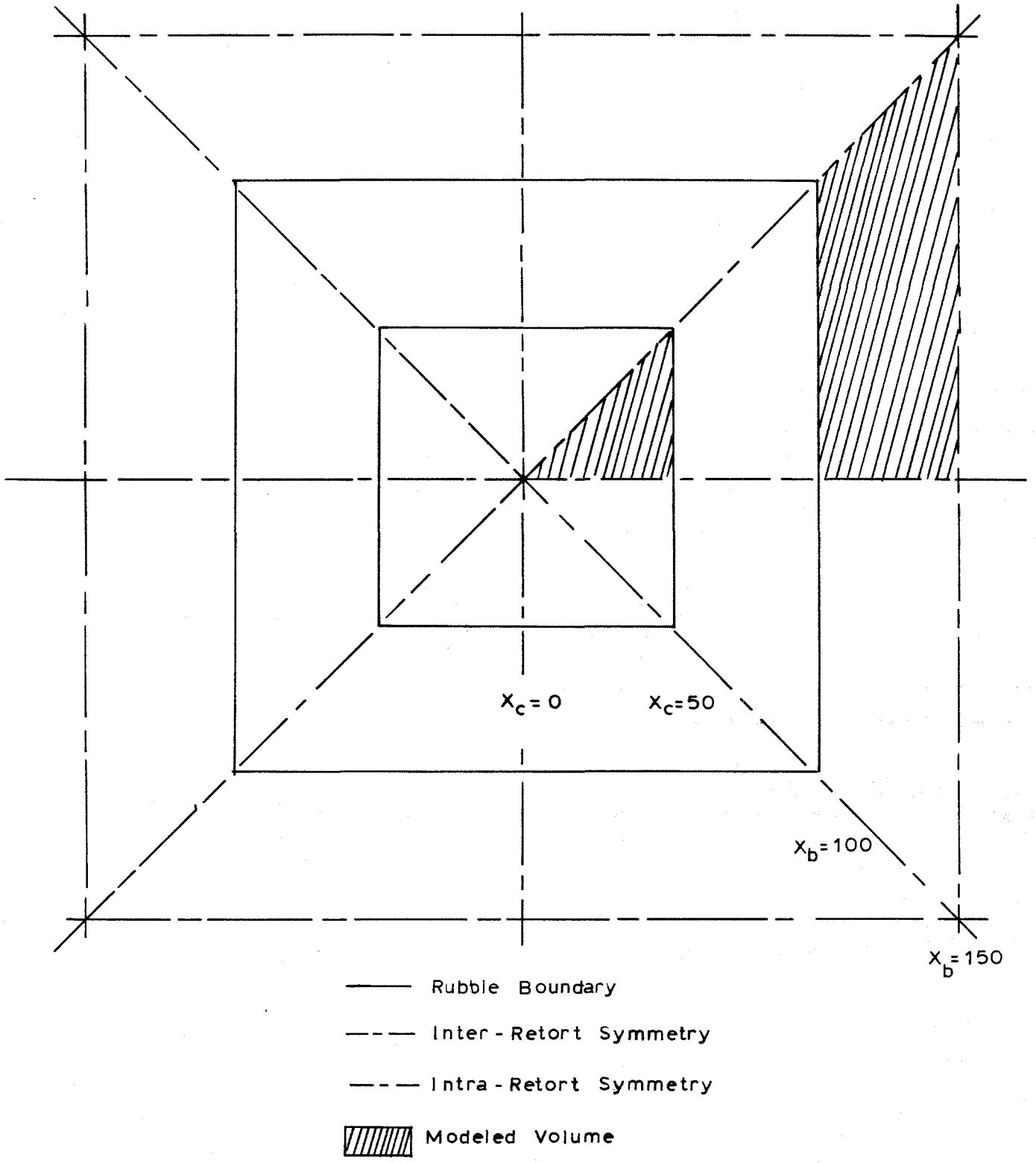

Figure 3.61 View of Single Retort Showing Plane Symmetry

for an undefined time. In this situation, the support pillars (both center and barrier) would be exposed to hot gases at a temperature of approximately 1400°F for very long times, and deep penetration of heat into the solid shale would occur. A model run was made to simulate this case, and results are shown in Figure 3.62. The ambient temperature to which the solid-shale surfaces are exposed is indicated by the row of squares along the top axis of the plot. As shown, at time zero, this temperature rises instantaneously to 1400°F and remains constant at this level for 800 hours. The temperature of the outer surface of the center pillar T(50) also rises rapidly and approaches the ambient temperature assymptotically. After 800 hours of exposure, the pillar surface is at a temperature of approximately 1370°F. The temperature of the pillar five feet in from the exposed surface is indicated by T(45) in the plot. As shown, this temperature rises much more slowly than the surface temperature, and after 800 hours of rubble combustion, the five-foot point is still at a temperature of only about 450° -- below the temerature at which significant kerogent pyrolysis would occur. Five feet further in from T(45), the shale temperature never exceeds about 180° -- somewhat warm to the touch but much too cool for kerogen conversion. After 800 hours, the temperature 15 feet in from the surface T(35) is essentially still at initial formation temperature.

In a more realistic retorting method, the top of the rubble would be ignited, and the retorting wave would proceed down the axis in an orderly manner. As time passed, rubble distant from

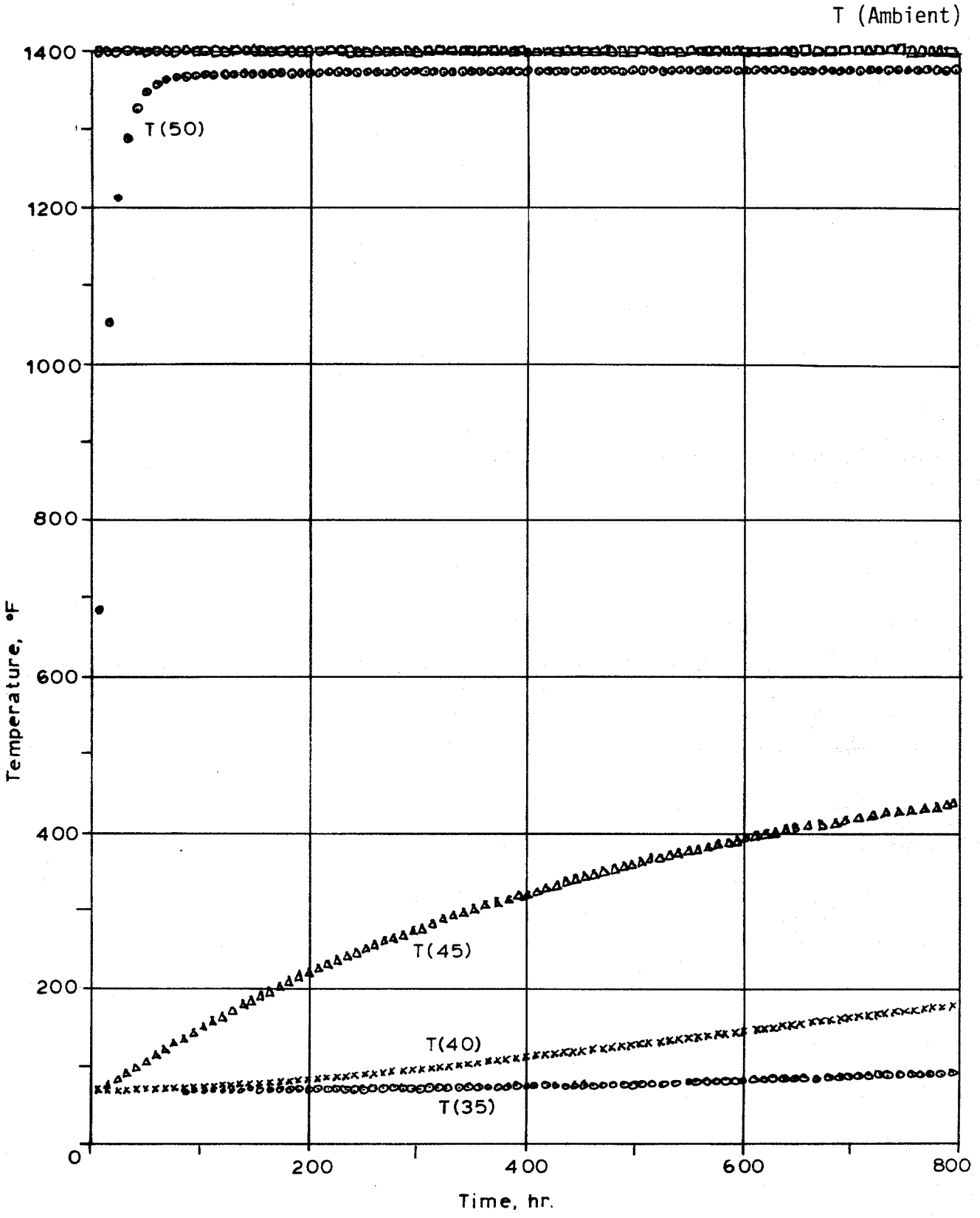

Figure 3.62 Center Pillar Temperatures for Rubble Fixed at 1400 °F

the upper retort surface would gradually be heated to pyrolysis temperatures and then to combustion temperatures. After the combustion wave passed, the retorted shale would gradually cool to the temperature of the incoming gas. Don Fausett has modeled such behavior, based on measurement made in the NTU retort at Laramie. He has provided a mathematical correlation in which temperature at any location along the retort axis may be determined as a function of time, maximum combustion temperature, width of the combustion zone, temperature drop across the combustion zone, initial formation temperature, and two empirical parameters called alpha and gamma. Behavior of this function for a 200-foot-high retort is given in Figure 3.63 for two values of the empirical parameters. The value alpha=0 produces a well-behaved temperature history which is probably a realistic prediction of thermal characteristics of an actual operating retort. In essence, the figure is a snapshot of the temperature profile in the retort at a time midway between start of the burn and termination of gas flow. The maximum temperature of 1400^{o} occurs at the midpoint of the retort axis (x=100). The shale at the lower end of the retort is still close to initial formation temperature, and the shale near the top of the retort has already cooled to the temperature of the incoming gas.

Figure 3.64 is a plot of the temperature history of the center point of the retort axis, given Dr. Fausett's hypothetical progression. As shown, the point is well below the maximum temperature for much of the retorting cycle. (The curve is the mirror-image of the curve plotted in Figure 3.63) This more-

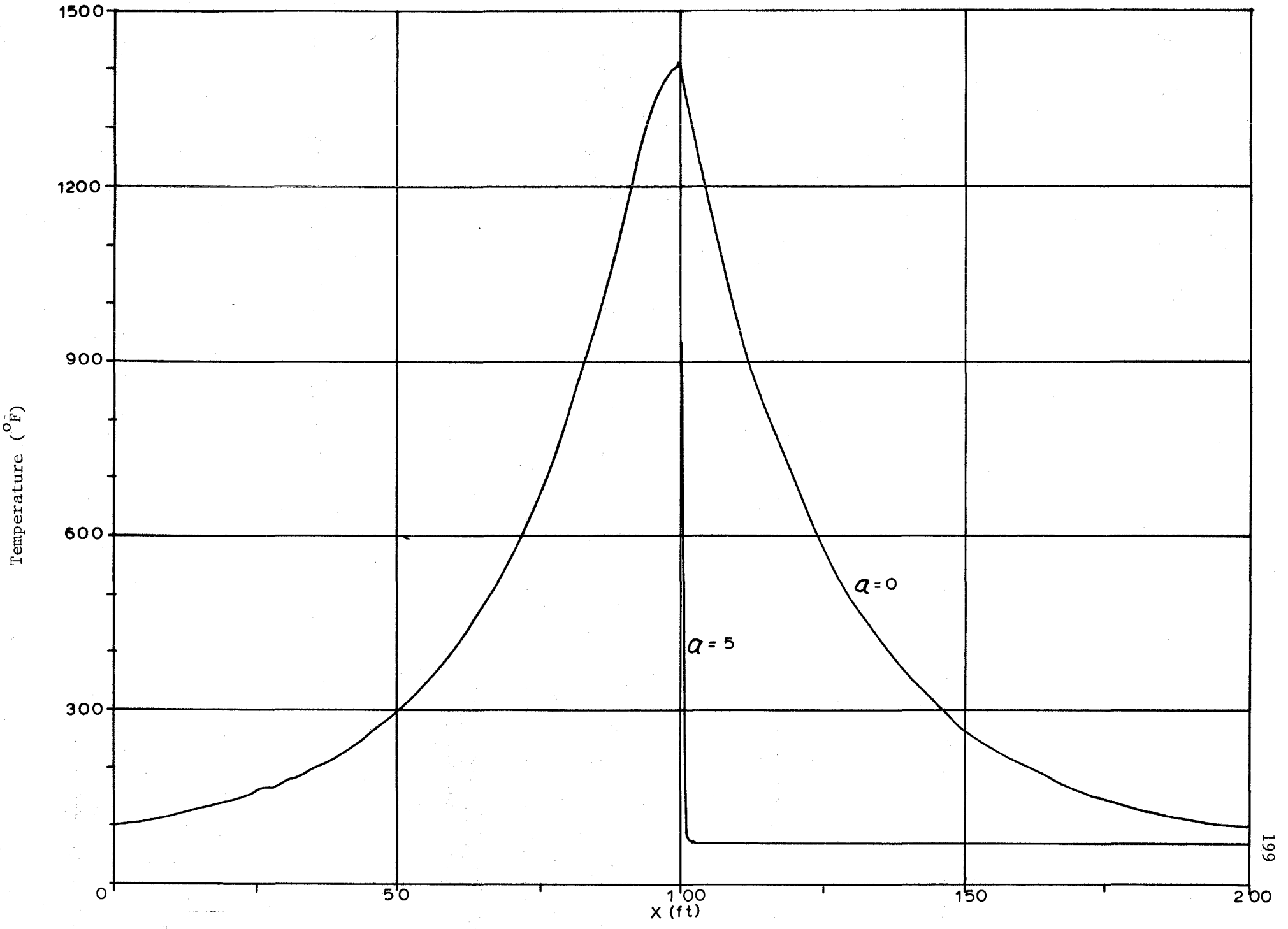

Figure 3.63 Temperature Profile Halfway Through Burn, Alpha = 0.0, Gamma = 0.077 and Alpha = 5.0, Gamma = 5.077

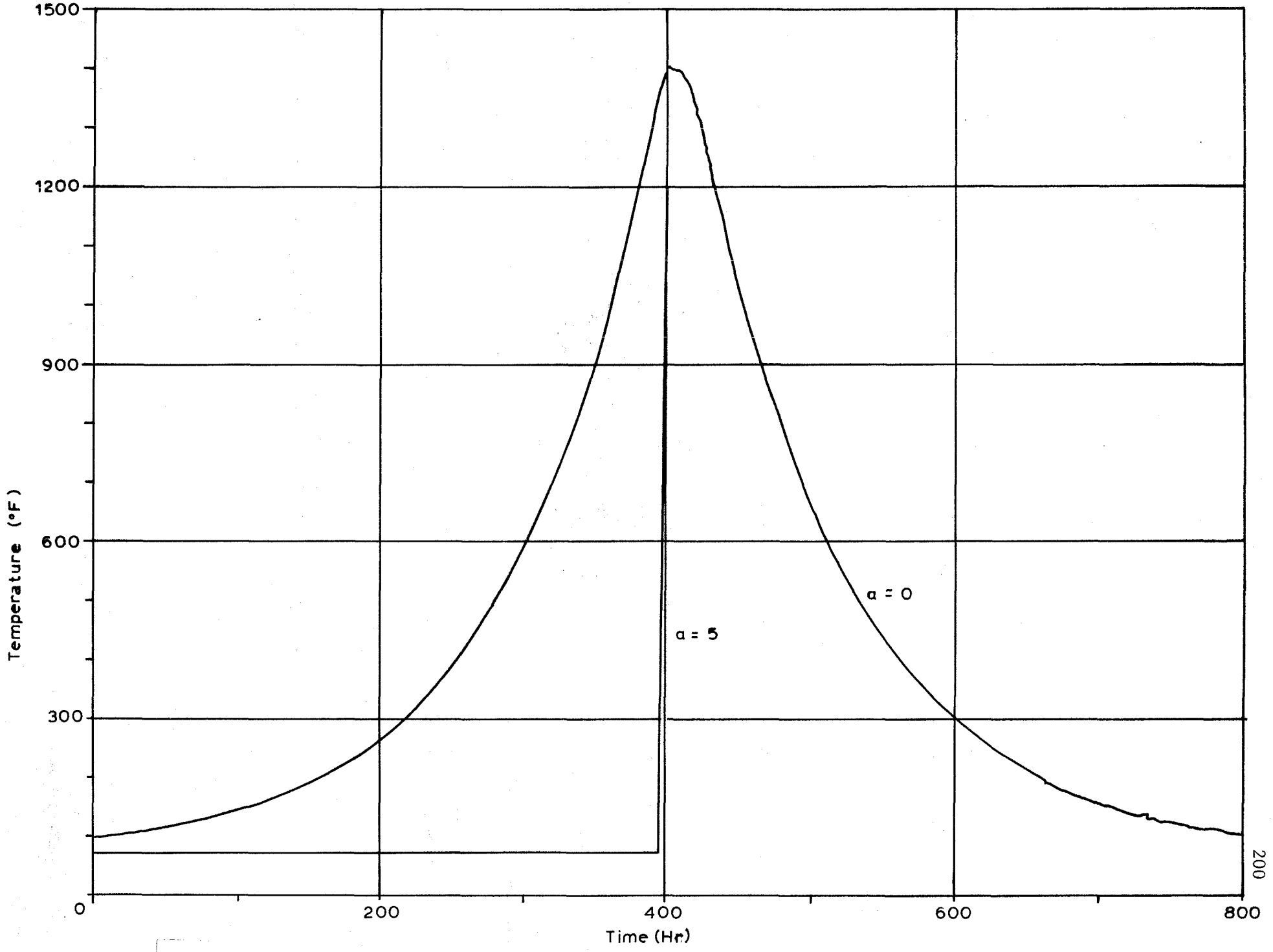

Figure 3.64 Temperature History at Midpoint of 200 ft. Retort, Alpha = 0.0, Gamma = 0.077 and Alpha=5.0, Gamma = 5.077

realistic scenario was also examined with the model. Results are shown in Figure 3.65. The plot is similar to that of figure 3.62 in that it includes a plot of the ambient temperature (TA), the center-pillar surface temperature ((T(50)), the temperature five feet into the center pillar (T(45)), the temperature ten feet in (T(40)), and the pillar temperature fifteen feet in from the surface (T(35)). However, the temperature histories are very different from the eariler predictions. The surface temperature follows the ambient temperature quite closely, but it is at 1400^{o}F for only a very short time. The temperature five feet in rises initially in response to the high initial ambient temperature, but once the combustion wave has passed, T(45) decays slowly towards initial formation temperature. It never exceeds 200^{o}. Effect of the combustion wave is scarcely noticeable ten feet into the pillar, and it is undetectable at a distance of 15 feet.

All of the calculations from which Figures 3.62 & 3.65 were derived, were performed with a convection coefficient of H=10. This is a very high value and is only truly applicable to turbulent flow in small pipes. Because of the large cross-sections and low gas-flow rates that will be encountered in actual retorts, much smaller values of H would be more appropriate. The true value remains to be determined, but it is quite likely that it will be closer to H=1 than H=10. To estimate the effect of convection-coefficient magnitude on pillar heating, a series of runs was made to model temperatures five feet in from the center-pillar surfaces as a function of

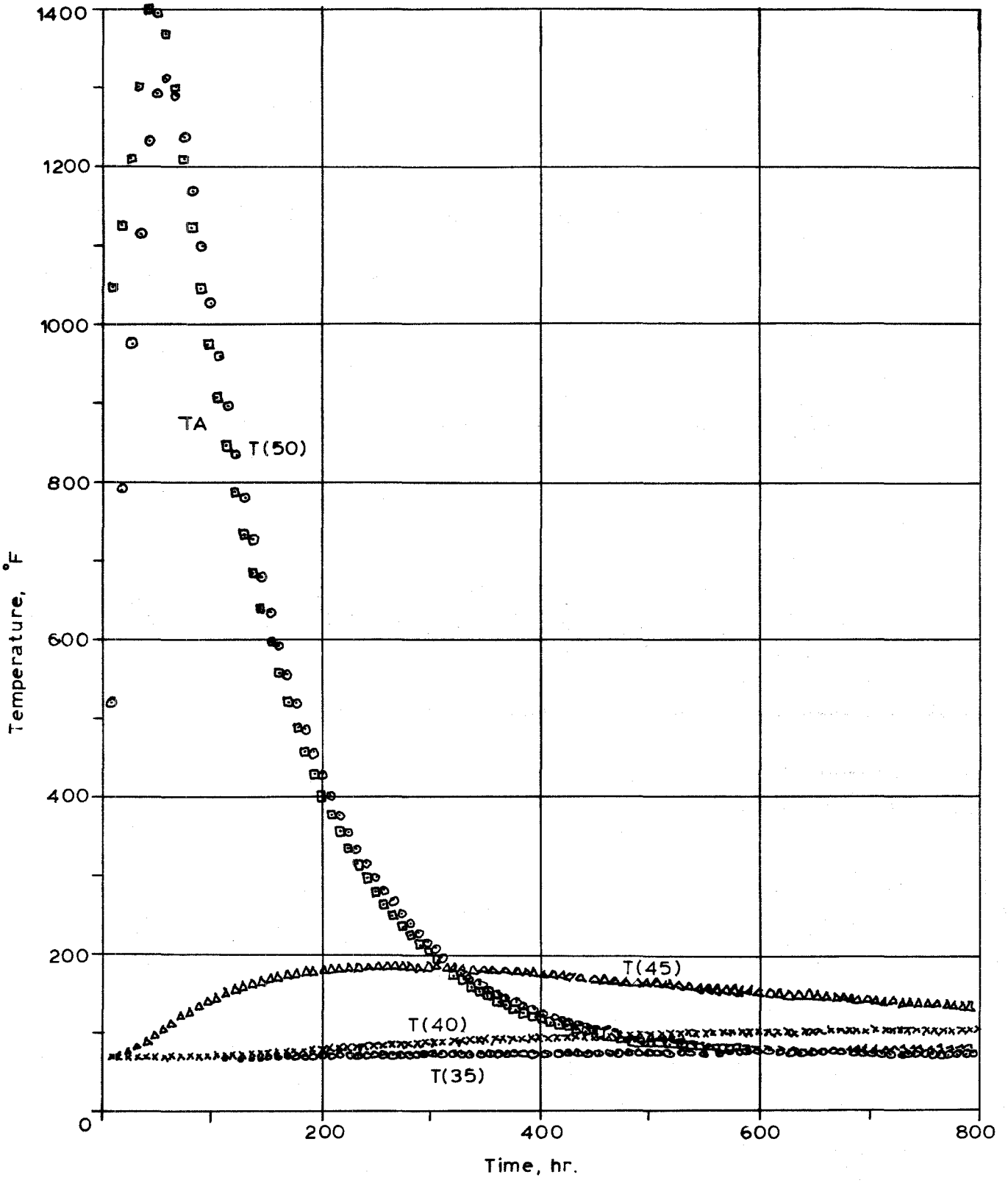

Figure 3.65 Center Pillar Temperatures for Variable Rubble Temperature

convection coefficient. Results are shown in Figure 3.66. The H=10 curve corresponds to the T(45) behavior shown in Figure 3.65. As shown in the Figure, decreasing H to H=5 has a slight effect on temperature history. However, decreasing it to H=1 has a pronounced effect, and decreasing it to H=0.5 results in a prediction that T(45) will never exceed 150°F.

3.4.4 Thermal Analysis of In-Situ Heater Test

As discussed previously in section 2.6, an in-situ heater test was performed in the floor of an existing oil shale mine to produce data regarding temperature profiles and vertical expansion due to heating of oil shale rock. The objective was to utilize the data obtained to confirm the validity of the models developed to explain the temperatures and stresses occurring in a pillar during in-situ retorting.

A temperature distribution for a model simulating the insitu heater test was determined using the ANSYS[1] finite element program and the temperature dependent thermal property data from section 3.3. The distributions were calculated for an axially symmetric model with the same progression of heater temperatures as in the insitu test.

Transient temperature distributions were determined over a 12 hour period for each heater cycle. Because the thermal properties were temperature dependent, an iterative procedure was used in the calculations.

[1]Swanson Analysis Systems, Inc.

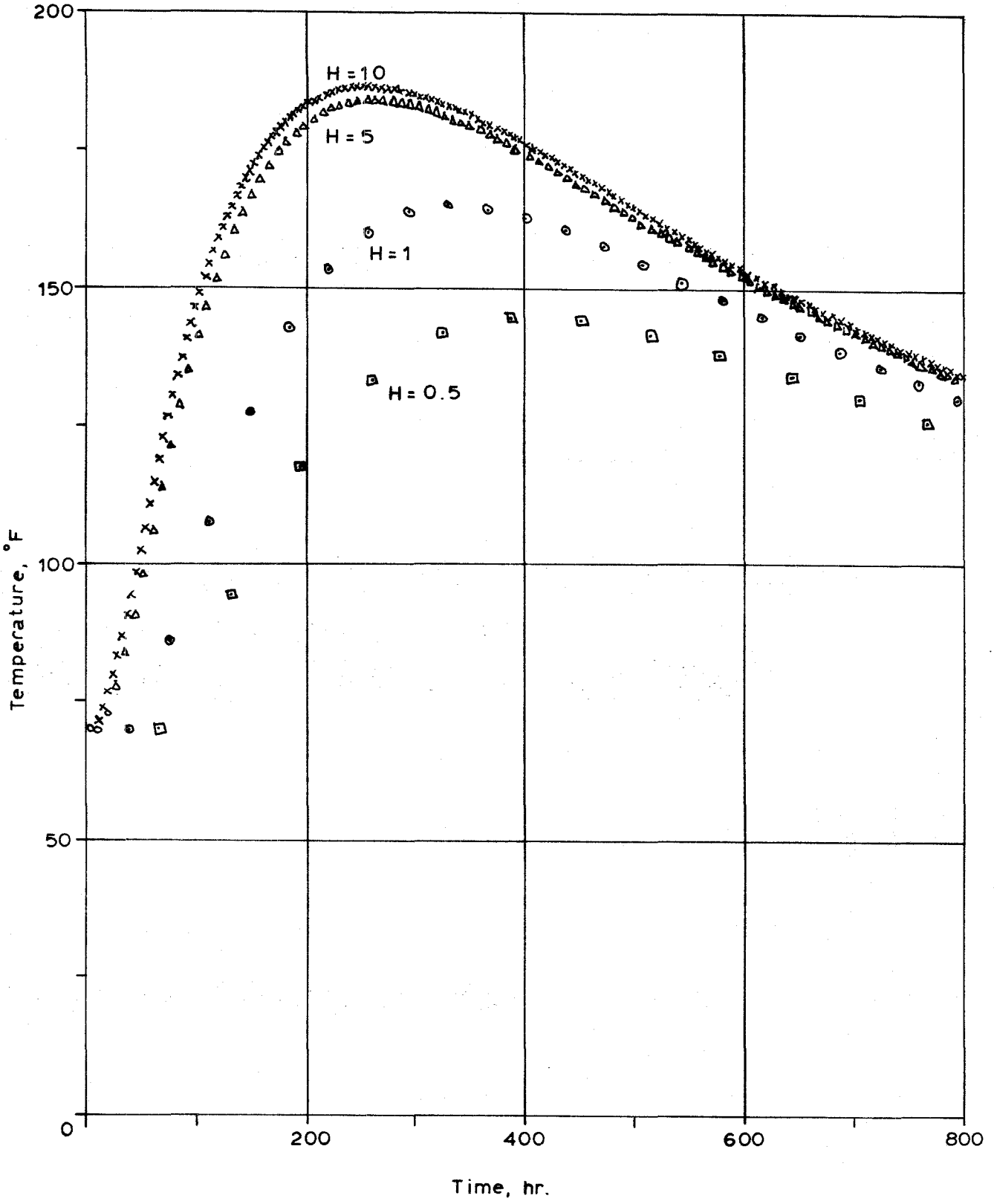

Figure 3.66 Center Pillar Temperatures for Various Convection Coefficients

The finite element model was axially symmetric about the heater hole axis as shown in figure 3.67 The geometry of the model was designed so that the nodal points would be in vertical lines coincident with the thermocouple sensors locations of the insitu test. The nodal points along these lines are half way between the location of the insitu thermo couples so that the calculated temperatures for the sensor locations are the average of the two bracketing temperatures in the model. This geometry was necessary so that the temperatures could be applied at nodel points along the heater hole boundary.

The boundary conditions for the model were zero heat transfer along the outside vertical and bottom boundaries and air convection heat transfer along the top boundary (which would be the mine floor). The temperature dependent thermal properties (in MKS units) are given in table 3.16. The values were taken from graphs in the interim report and input as tables in the program.

Because the insitu heater test was only successful for six cycles, only six simulated temperature cycles were calculated for the model. In the first cycle the top most heaters in the hole were simulated by applying temperatures of 100, 500, 500 and 100 °C at nodal points 6, 12, 18, and 24 inches respectively down the hole. In the succeeding cycles the sequence was shifted down 6 inches for each cycle with the previously heated nodal points reduced to 50 degrees C. A transient optimization was used to simulate a 12 hour period for each cycle. Ten iterations were

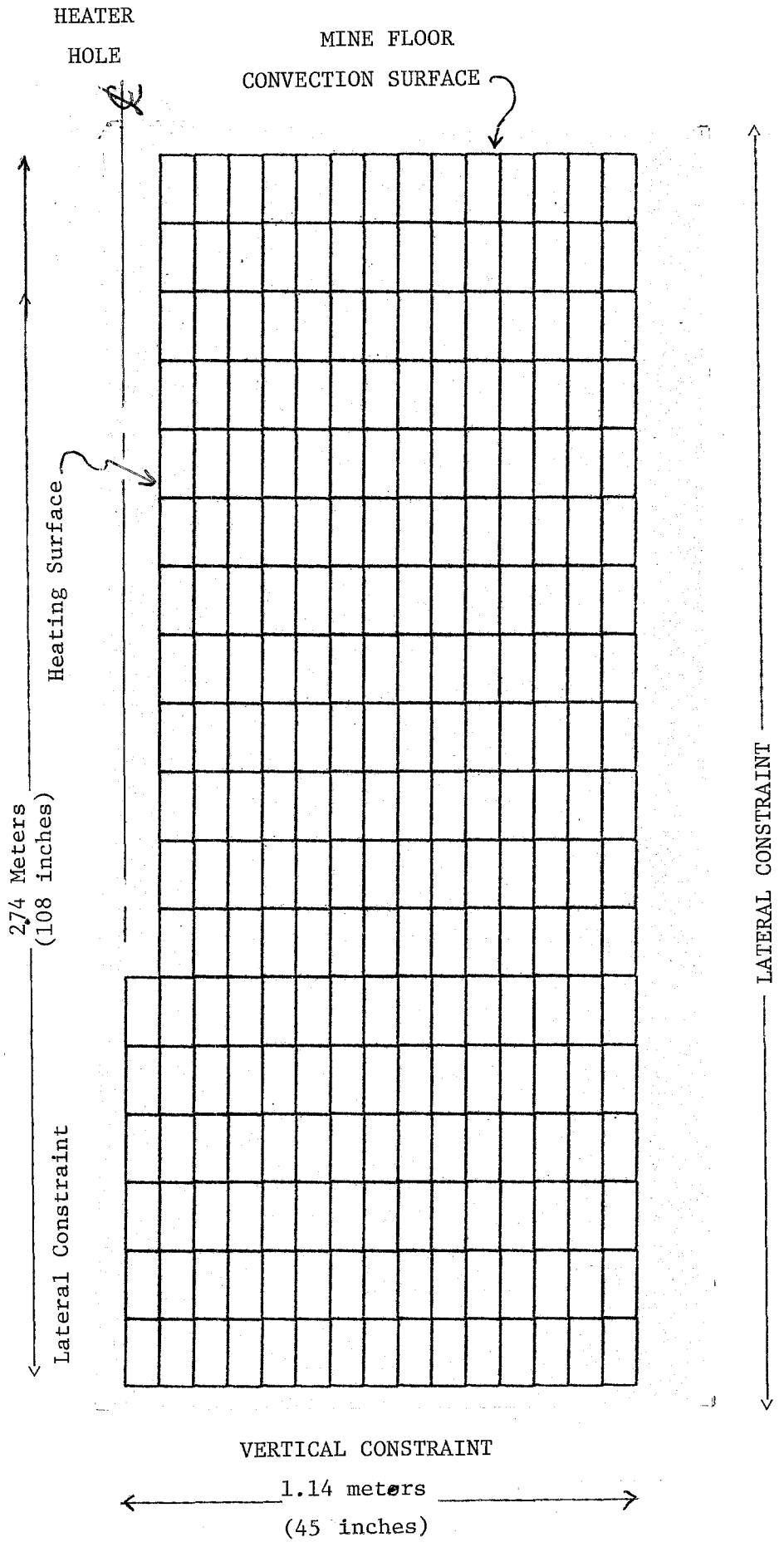

Figure 3.67 Mesh for Thermal and Stress Distribution In-situ Heater Test

TABLE 3.16 THERMAL MATERIAL PROPERTIES

USED IN MODELING IN SITU HEATER TEST

	Thermal Transmissivity W/M^{o}C		Heat Capacity	Air Convection Coefficient
Temp ^{o}C	Horizontal	Vertical	J/Kg ^{o}C	
0	1.39	1.21	1470	0.31
50	1.25	1.09	1425	4.65
100	1.12	0.97	1380	6.88
150	0.99	0.87	1335	7.83
200	0.88	0.77	1290	8.16
250	0.78	0.68	1245	8.33
300	0.68	0.60	1200	8.62
350	0.60	0.52	1155	9.11
400	0.53	0.46	1110	9.74
450	0.46	0.40	1065	10.20
500	0.40	0.35	1020	10.05

Density = 2265 $\frac{Kg}{M^3}$

required for a convergent solution in each thermal load cycle.

The results shown in figures 3.68 through 3.73 indicate good correlation between the insitu temperatures and the temperatures predicted by the computer study. The maximum rock temperatures increase with increasing hole depth, and the heaters do not raise the temperature of the rock much more than 12 to 18 inches away from the hole are of similar shape for both the measured and calculated valves. The small variation in actual values is probably caused by localized changes in rock properties that the computer cannot model because of the absence of physical data on every inch of the material tested. The core from the mine floor indicated a grade of about 20 gal/ton, but the mine floor has been exposed to the atmosphere for 15 years and may have suffered some change in thermal properties from those measured in the laboratory for shale of similar grade. There were no thermocouple readings for exact temperature determination in the previously heated hole areas. Because of lack of this information, a 50°c residual temperature was assumed. Inputing better data in this area might have resulted in even closer agreement in the temperature profile trailing the high temperature test.

3.4.5 Surface Displacement over Heater Test Area

Using the temperature distributions calculated for the heater test cycles, and the temperature dependent elastic properties determined previously in the project, the vertical

FIGURE 3.68

COMPARISON OF MEASURED AND CALCULATED
TEMPERATURE DISTRIBUTION AT
6 AND 12 INCHES FROM HEATER HOLE

FIRST CYCLE

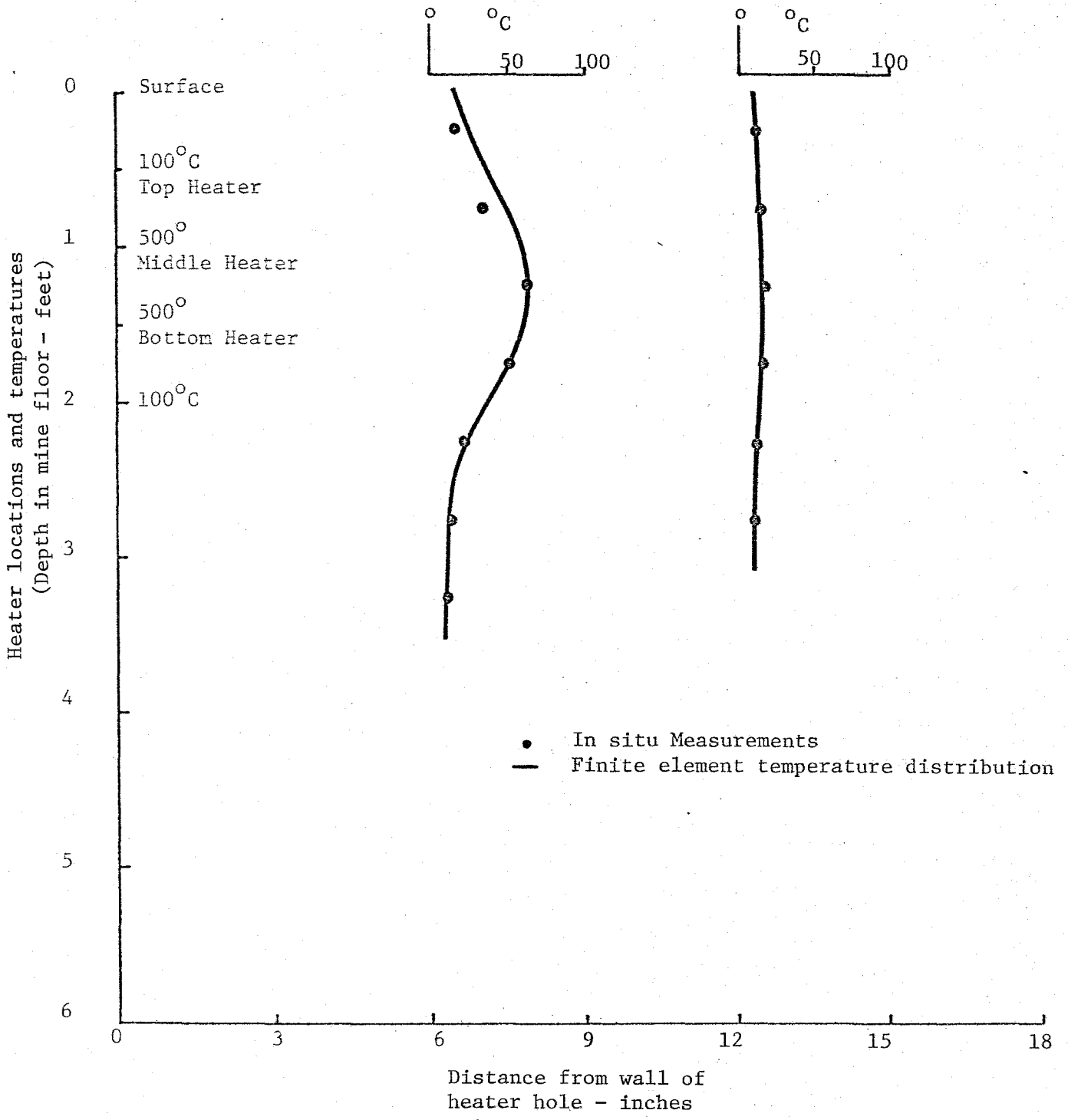

FIGURE 3.69

COMPARISON OF MEASURED AND CALCULATED
TEMPERATURE DISTRIBUTION AT
6 and 12 INCHES FROM HEATER HOLE

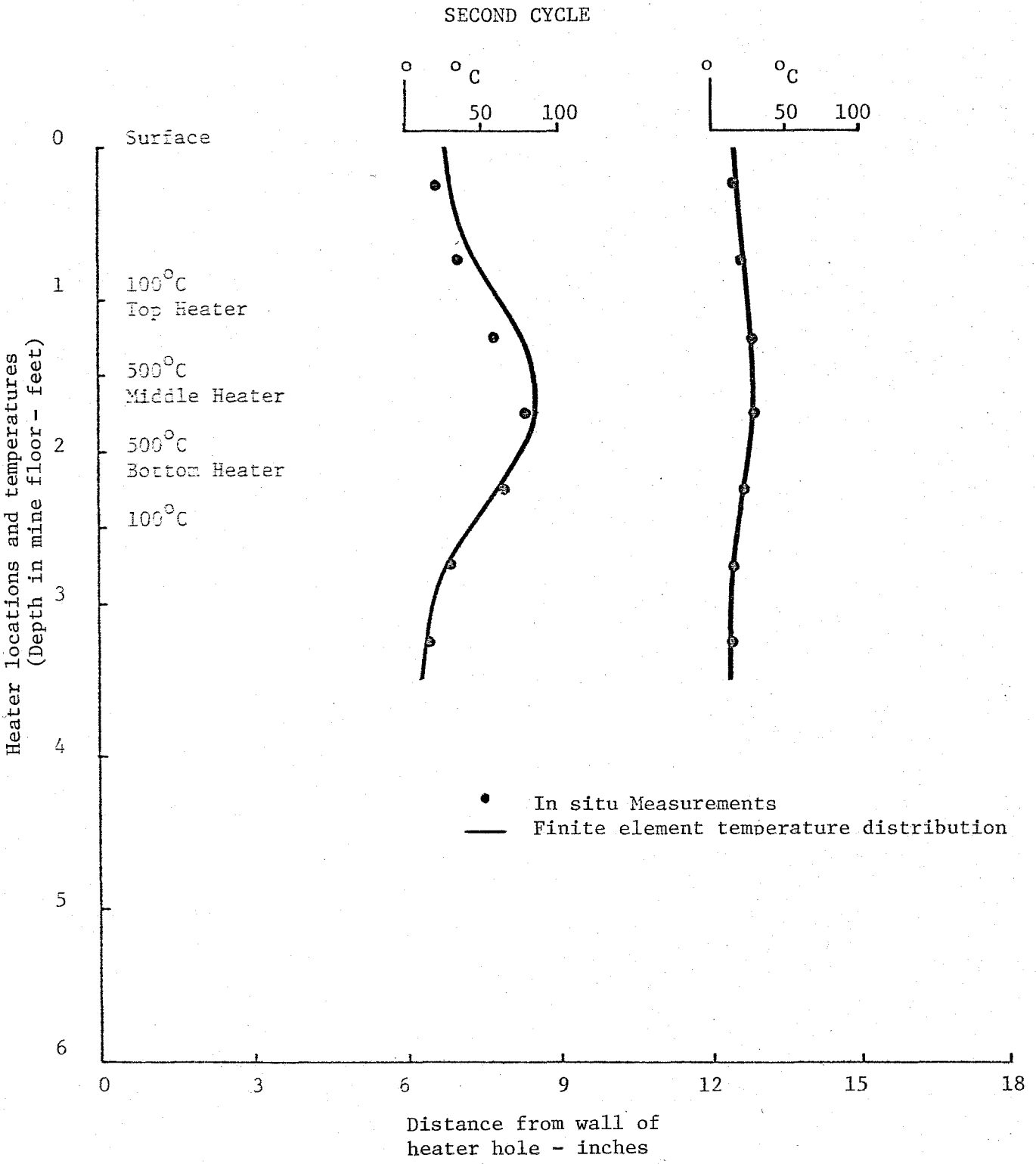

FIGURE 3.70

COMPARISON OF MEASURED AND CALCULATED
TEMPERATURE DISTRIBUTION AT
6 and 12 INCHES FROM HEATER HOLE

THIRD CYCLE

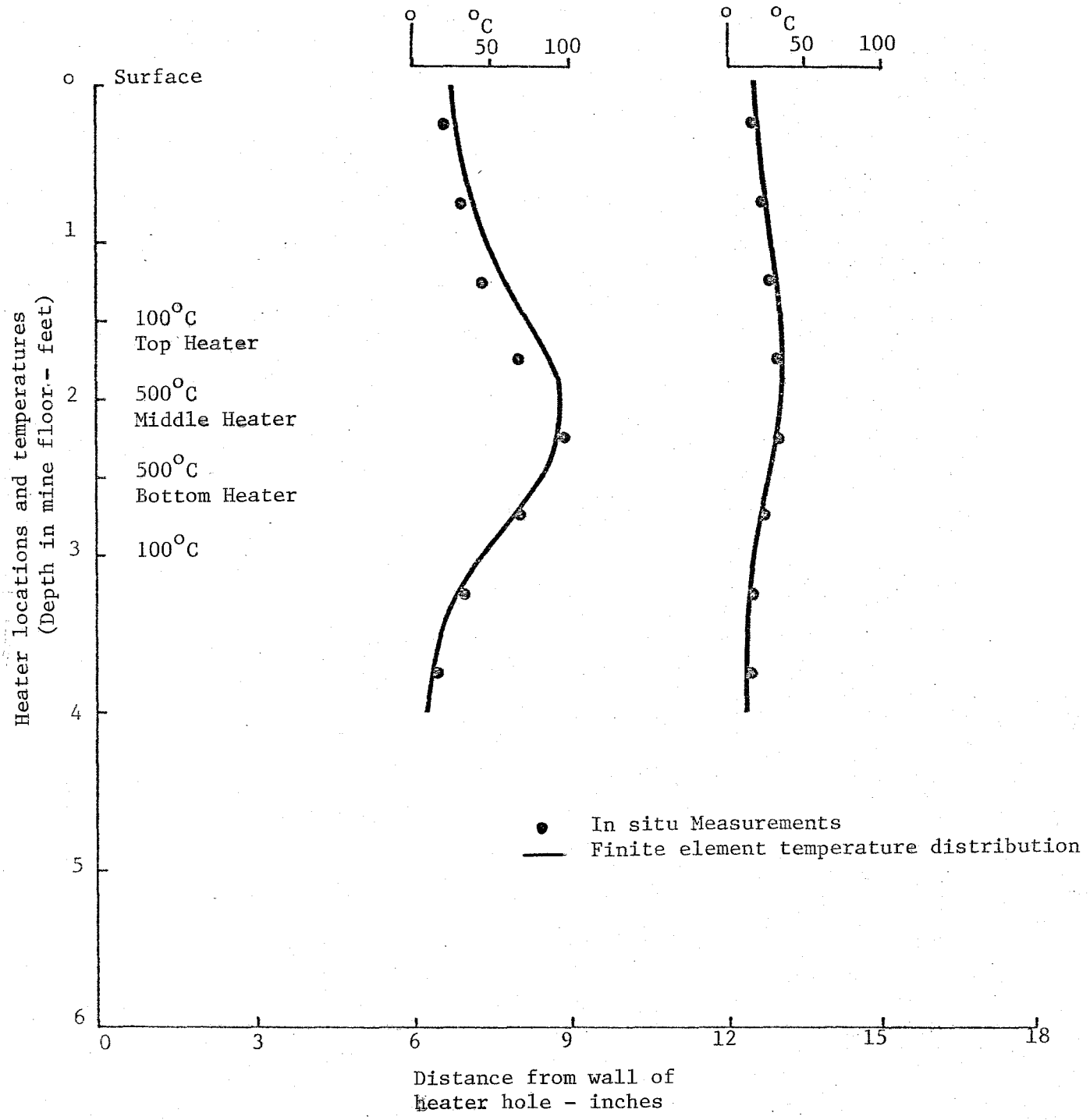

FIGURE 3.71

COMPARISON OF MEASURED AND CALCULATED
TEMPERATURE DISTRIBUTION AT
6 AND 12 INCHES FROM HEATER HOLE

FOURTH CYCLE

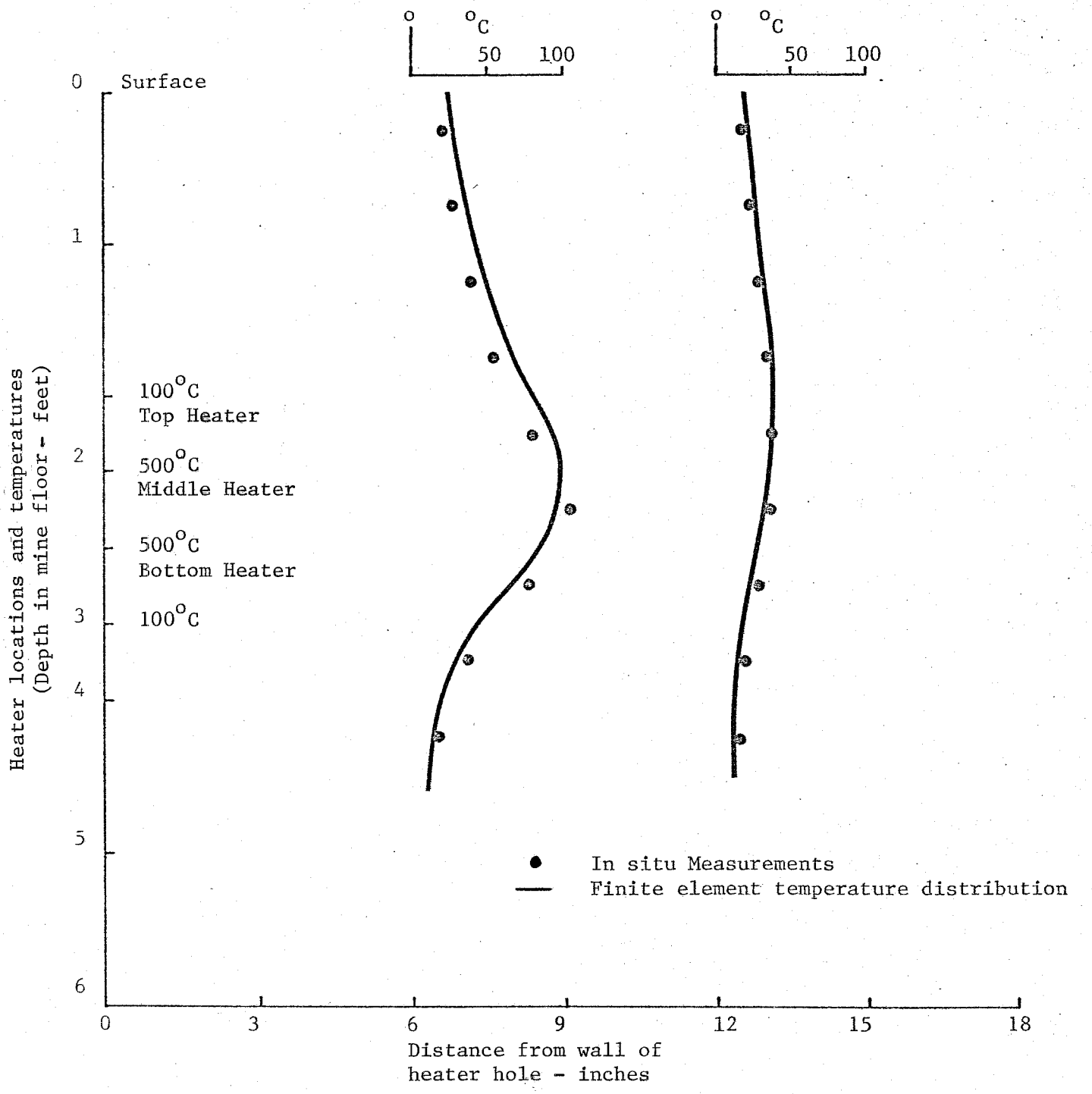

FIGURE 3.72

COMPARISON OF MEASURED AND CALCULATED
TEMPERATURE DISTRIBUTION AT
6 AND 12 INCHES FROM HEATER HOLE

FIFTH CYCLE

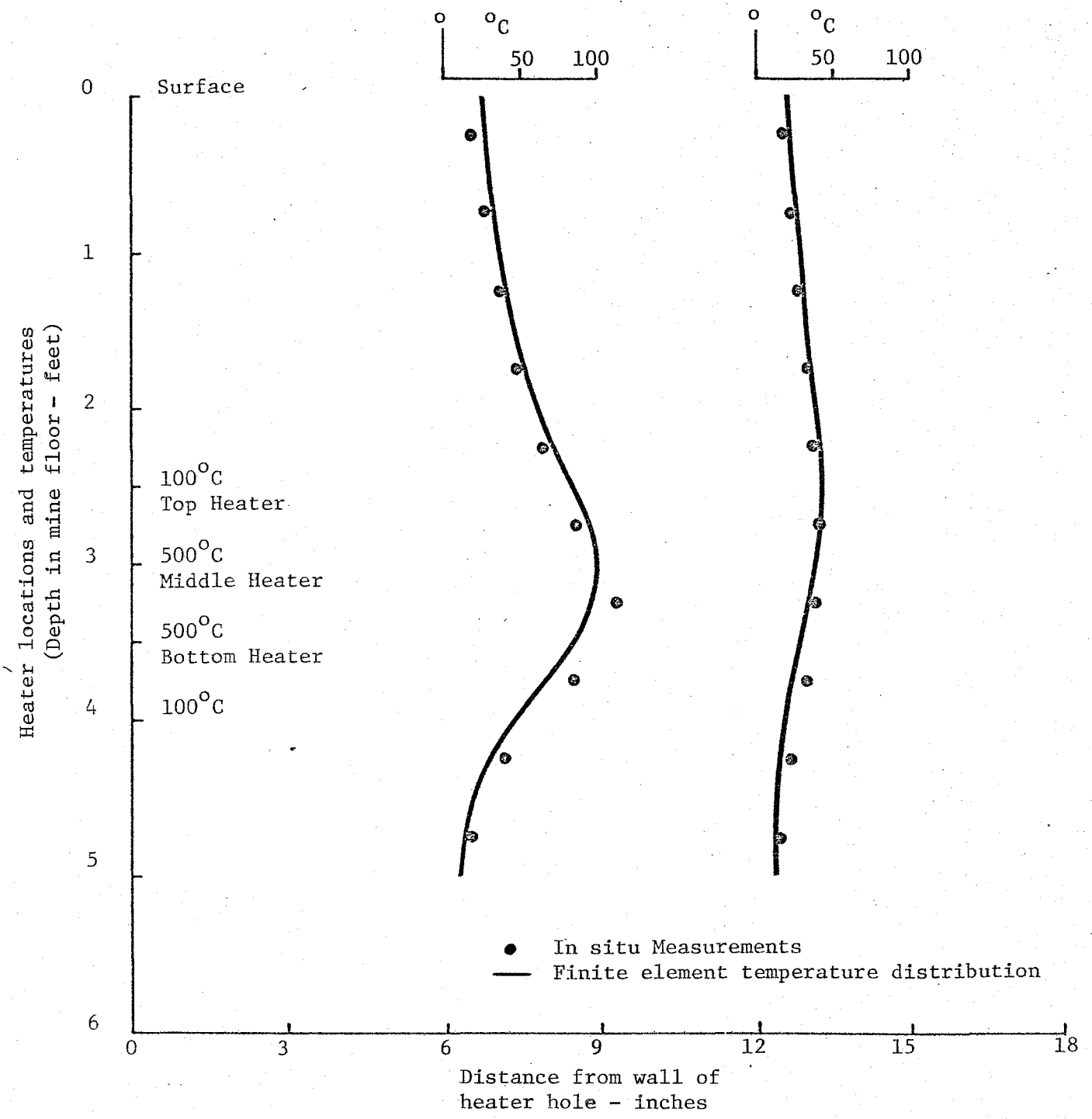

FIGURE 3.73

COMPARISON OF MEASURED AND CALCULATED
TEMPERATURE DISTRIBUTION AT
6 AND 12 INCHES FROM HEATER HOLE

SIXTH CYCLE

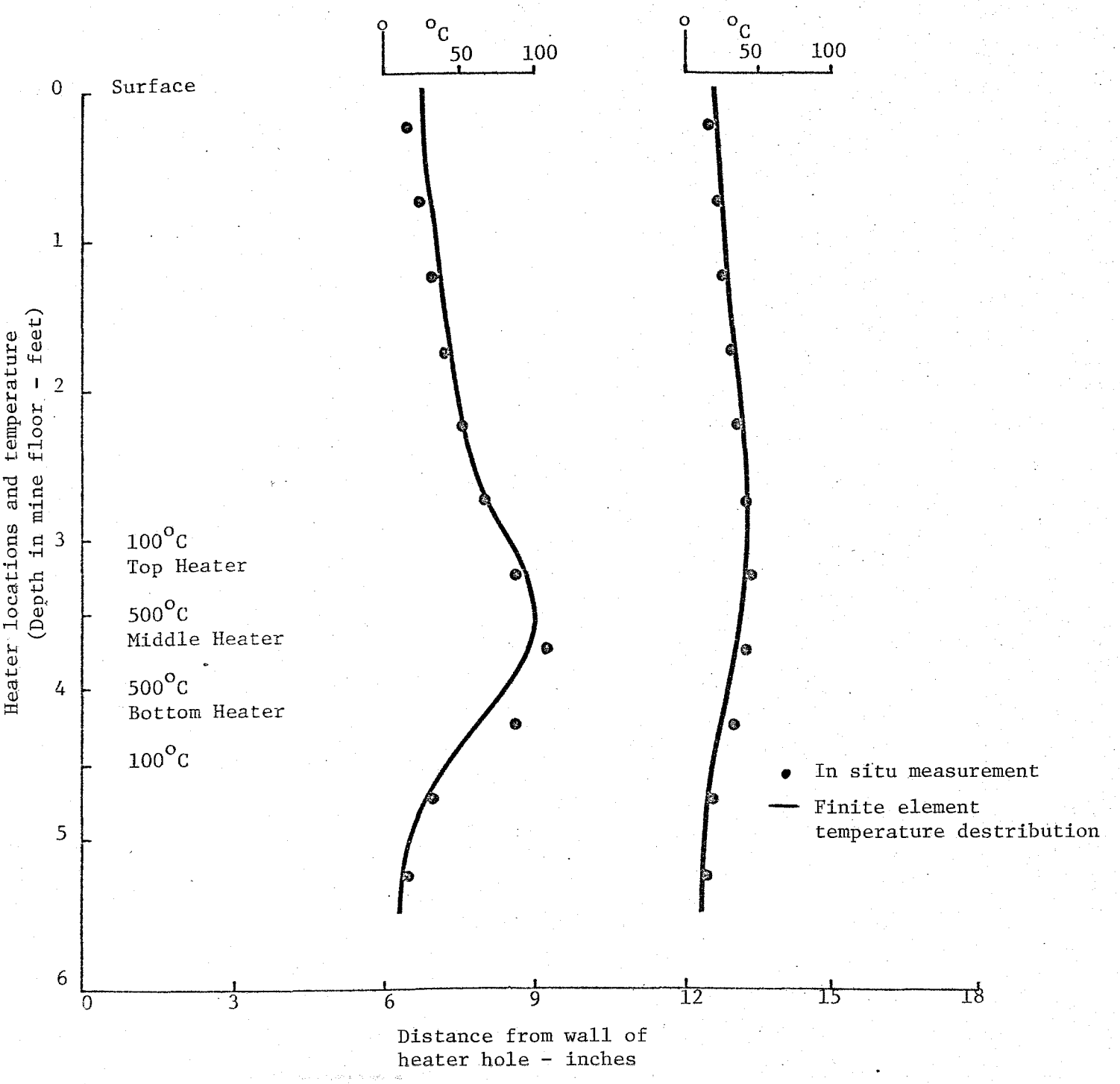

surface displacements due to thermal expansion over the heater test area were calculated. Figure 3.74 is a plot of the theoretical surface displacement that would occur over the heater test area if the thermal expansion were a completely reversable process (i.e. expansion upon heating - contracting upon cooling). Only the first six cycles were plotted to show the trend as the heat source moves down away from the floor surface. The surface displacement near the heater hole decreases from a maximum of 0.0015M as the heat source becomes more remote. Farther away from the hole the displacements slowly increase. Thus influence of the heat on thermal expansion becomes less localized and a more general phenomena as the heat influences a larger and larger volume of material.

No quanitative comparisons are possible with the load cell data from the frame over test area because the displacement of the load cells are interdependent through the flexure of the frame. However, some qualitative comparisons are possible. Figure 3.75 illustrates the comparison between the theoretical calculation of surface displacement and that of the load cell on the frame at a distance of 9 inches from the heater hole center. Theory says that the displacement should decline fairly steadily with time as the heat source moves away from the surface with time. The load cell measurements demonstrate phenomena not accounted for in theory, as these data increase in value with time to a maximum and then begin a slow decline. One explanation for this difference in behavior is irreversible expansion of the

FIGURE 3.74

VERTICAL SURFACE DESPLACEMENT VERSUS DISTANCE FROM HEATER HOLDE CENTER

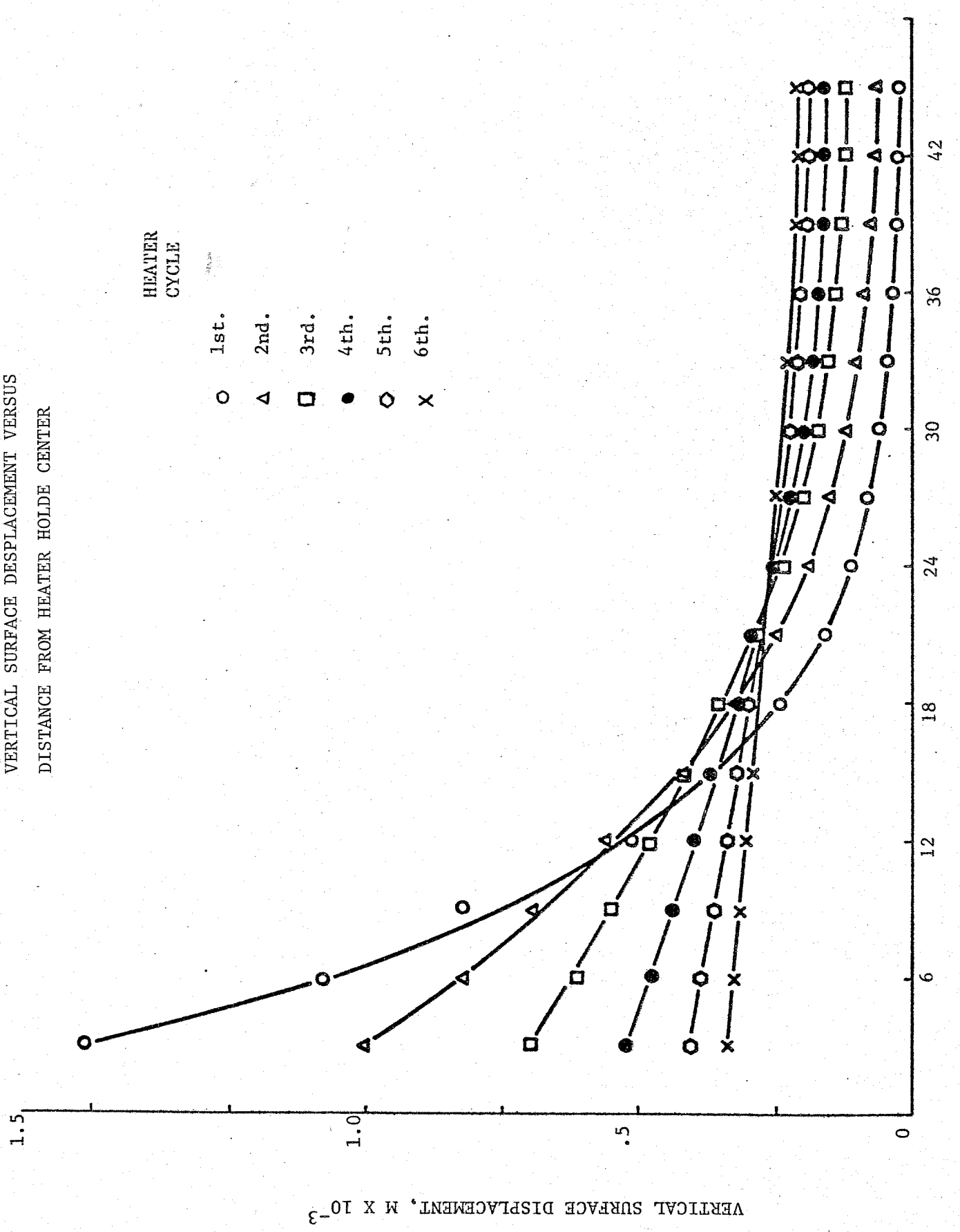

FIGURE 3.75

COMPARISON OF MEASURED AND PREDICTED SURFACE DISPLACEMENT 9" FROM HEATER HOLE CENTER

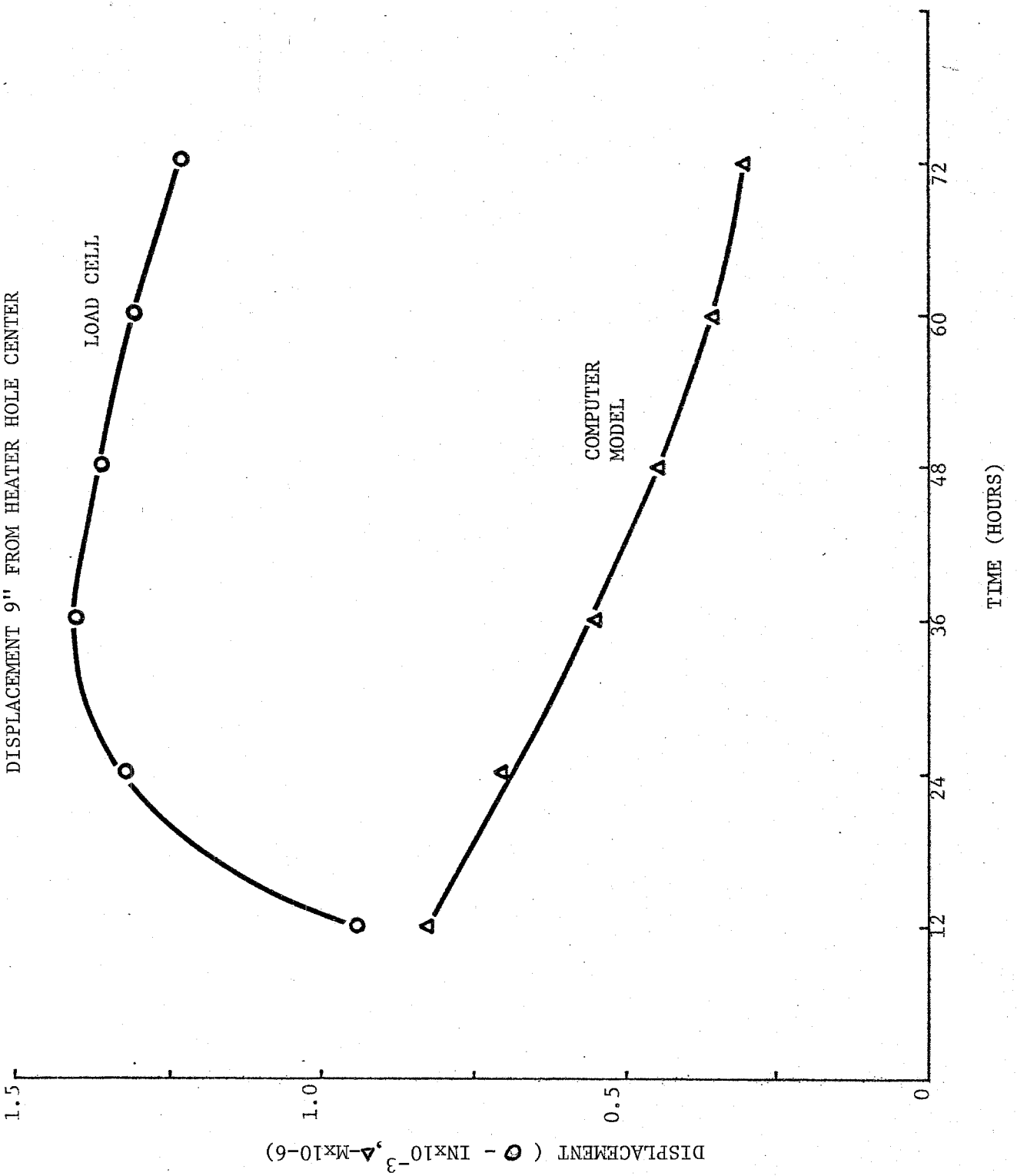

oil shale (exfoliation?) above a certain temperature brought about by physical alteration of the composition of the shale. Because of the lack of constraint, the effect of this irreversible expansion is probably more pronounced near the surface of the oil shale. The load cells show the greatest increase while the heat source is closest to the surface (12 & 24 hours) and then level off and start to slowly decline as the heat source is moved deeper (36 & 48 hours). The total expansion at this point near the hole is probably part reversable - part irreversable.

Figure 3.76 shows a similar comparison but at a distance of 19.5 inches from the heater hole center. The load cell data at this point shows a similar pattern with time with the expansion predicted by the model. Probably at this distance from the heater hole the rock temperatures were low enough that no irreversable thermal expansion occured.

Although the comparisons between the load cell data and the model have been on a selected basis (most of the load cell data showed either no change or no comparable pattern), the conclusions drawn are probably reasonable. The apparent irreversable expansion of the oil shale close to the heat source is the most significant effect observed.

FIGURE 3.76

COMPARISON OF MEASURED AND PREDICTED SURFACE DISPLACEMENT 19.5" FROM HEATER HOLE CENTER

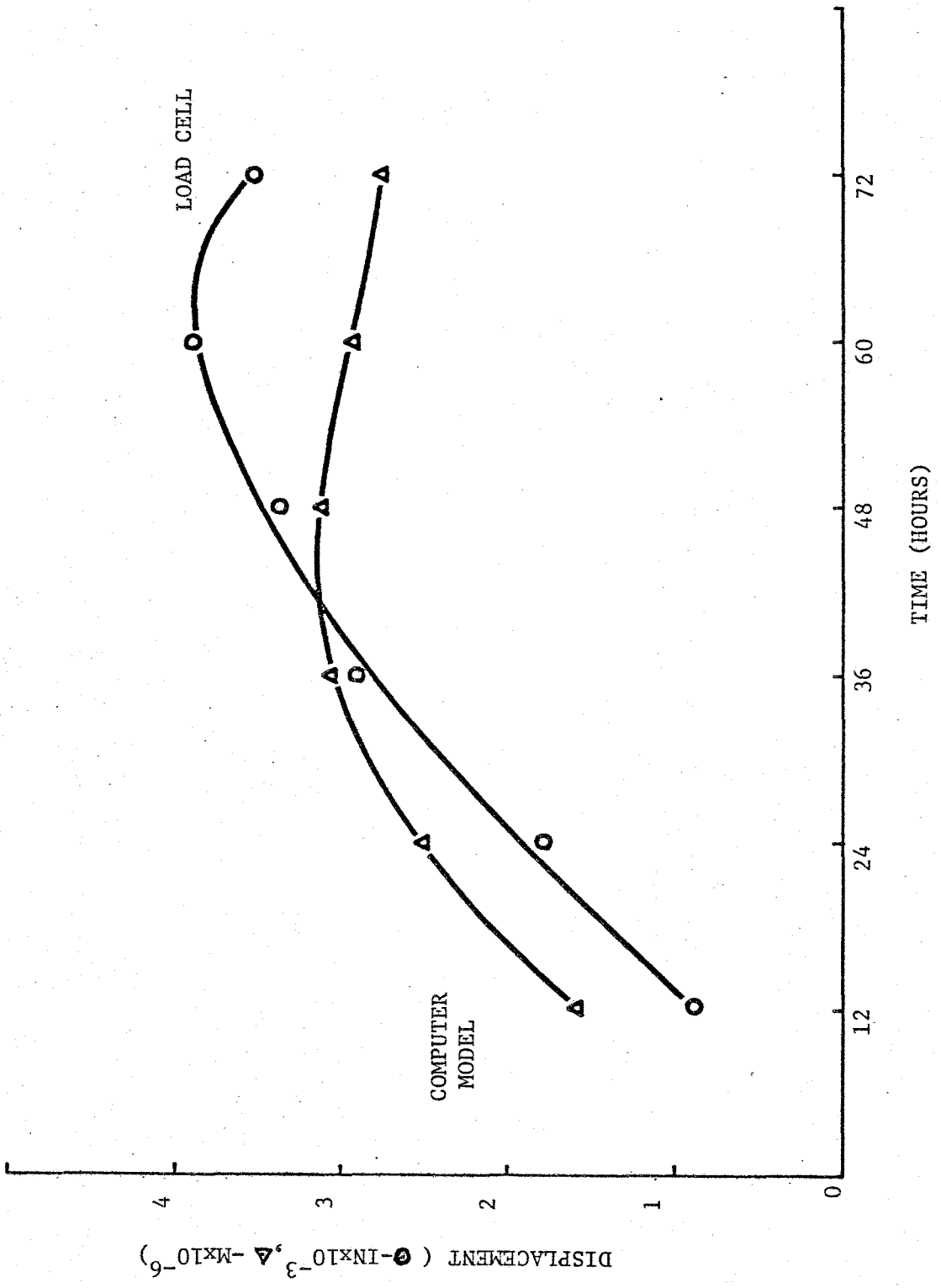

3.4.6 In Situ Retort Pillar Thermal Stress

A plane strain finite-element analysis of the thermal stress induced in an insitu retort pillar was performed using temperature dependent thermal and mechanical properties of oil shale. The pillar model, the same as has been previously investigated, was 100 feet square and 200 feet high. The pillar center line is an axis of symmetry meaning that the same constraint and heat loads are applied to both sides of the pillar. The model is constrained along this axis of symmetry to allow no horizontal displacement and along the bottom to allow no vertical displacement. The loading along the side of the pillar simulated the lateral loading of the rubblized oil shale. A uniform pressure of 1000 psi (6.895×10^6 N/m^2) was applied across the top of the pillar. The actual load on the top of a pillar would not be uniform, but even including the roof layer in the model would not reproduce the actual pillar loads as determined in field studies.(Obert & Duvall p548). The pillar was also subjected to gravity acceleration of 32.2 ft/sec^2 (9.8 $^{m}/_{sec^2}$).

Analysis Program and Model

The analysis of the model was done with the ANSYS[1] program which is a versatile multifunctional finite element analysis program that allows sequential coupled thermal and static analysis with wide flexibility in the range of input variables. The programs were run on the CDC cybernet system. The thermal and static options in the program were used in the analysis.

[1]Swanson Analysis Systems Inc.

The thermal analysis was made using the temperature dependent specific heat and thermal transmissivity properties of oil shale developed earlier in the project. The finite element model containing 400 elements (Figure 3.77) was constructed in such a way as to have geometrically increasing element sizes moving away from the side of the pillar. This was necessary so that the elements in the area of the very high temperature gradient near the side of the pillar would be small enough to allow a convergent solution without having a model with a very large number of elements.

Thermal Analysis for 120 Hour Temperature Cycle

The thermal run was made to determine the transient temperature distribution in the pillar after 120 hours (5 days) with a temperature of 500° C along the retort side of the pillar. Keeping the temperature at 500° C for 120 hours at each node was to simulate a burn rate of 0.5 inches per hour along the retort wall. Originally the temperature of 500°C was to be applied successively at each node and the resulting temperature distribution determined. However, as 12 iterations were required for convergence of each temperature load step, it became apparent that using the 40 load steps (40 nodes) this procedure would require, would use up about one hour of CP time and be very expensive. Instead the temperature was applied along the whole boundary in one step.

This simplification would not affect the temperature penetration into the pillar but would result in a larger thermal expansion as determined in the static analysis. This simplified

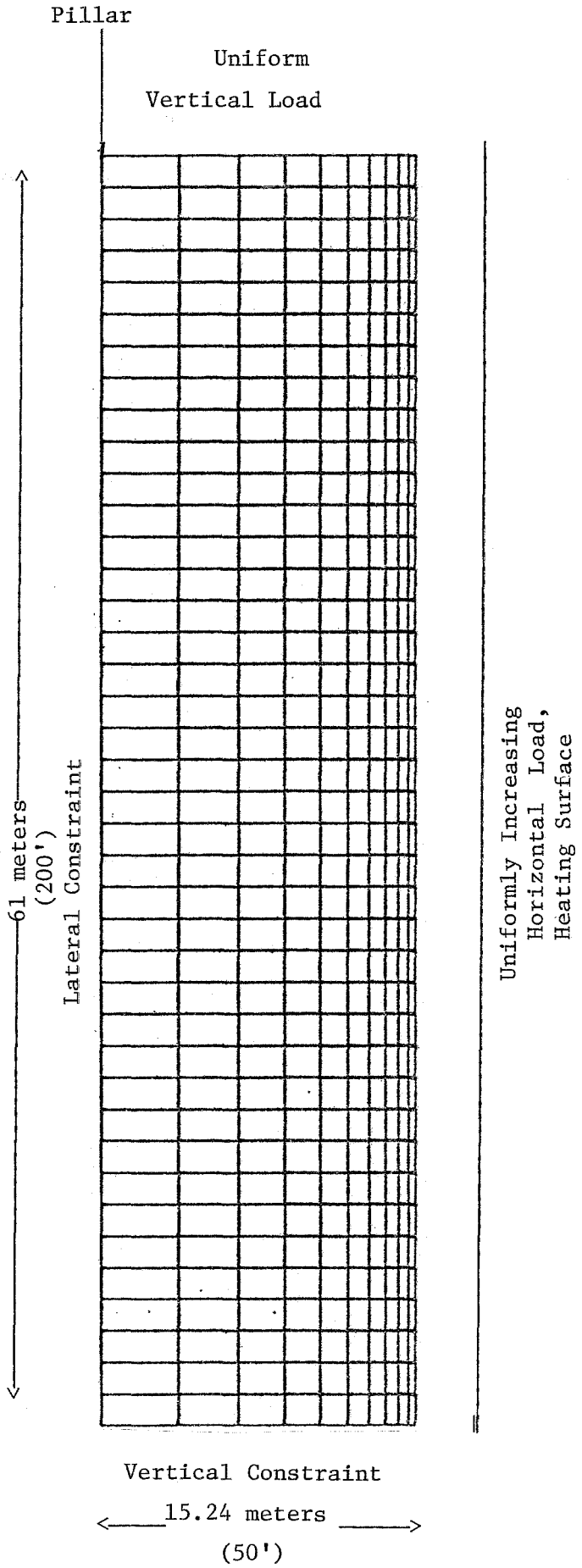

MESH FOR THERMAL AND STRESS DETERMINATIONS IN RETORT PILLAR

FIGURE 3.77

analysis would result in thermal expansion greater than might be shown by doing the analysis in a sequential manner. This comes about because in the sequential analysis the thermal effect would pass up the side of the pillar as a wave instead of an overall heating of the pillar side. Elements no longer affected by the high temperatures would lose part or all of their expansion. Thus the method used would represent a worse case in terms of thermal expansion than a pillar would probably experience from retorting.

The program used a two dimensional isoparametric element. The temperature distribution (T) for each element was determined from a numerical solution to the equation:

$$\rho C_p \frac{\partial T}{\partial t} = K_{xx} \frac{\partial^2 T}{\partial x^2} + K_{yy} \frac{\partial^2 T}{\partial y^2}$$

Where

ρ = density

C_p = specific heat

K = thermal conductivity

These temperature dependent properties were presented previously in the section on the insitu heater test.

Nodal point temperatures computed in the thermal analysis were recorded on tape for use in the static analysis. This temperature distribution is shown in Figure 3.78. The contour values are given in table 3.17 . The temperature gradient is so steep that the individual contours are not distinguishable. The temperature is at the ambient ($10^{o}C$) about 1 meter into the pillar.

Static Analysis for 120 Hour Temperature Cycle

As was discussed earlier the pillar model was loaded on top with a uniform load and along the side with a linearly increasing load downward to simulate the lateral force from the rubblized shale (Figure 3.79). The broken shale was assumed to have a density of $100\#/ft^3$ and an angle of internal friction of 50 degrees. The load was descretized and applied at the nodal points. The program used a two dimensional isoparametric element (Wilson, et al) in the solution of the displacements and stresses. Temperature dependent mechanical properties used are given in Table 3.18. The program linearly interpolates for the property values at the specific nodal temperatures previously determined in the thermal run.

Stress determinations were made without thermal effects, and with thermal effects. Contour plots of the horizontal stress (Tx), vertical stress (Ty) and shear stress (t xy) are presented for the two cases along with plots of the exaggerated displacements in figures 3.80, 3.81, 3.82, and 3.83, (no thermal effects) and 3.84, 3.85, 3.86, and 3.87, (thermal effects) at 120 hours. Tables 3.19 and 3.20 give the respective contour stress

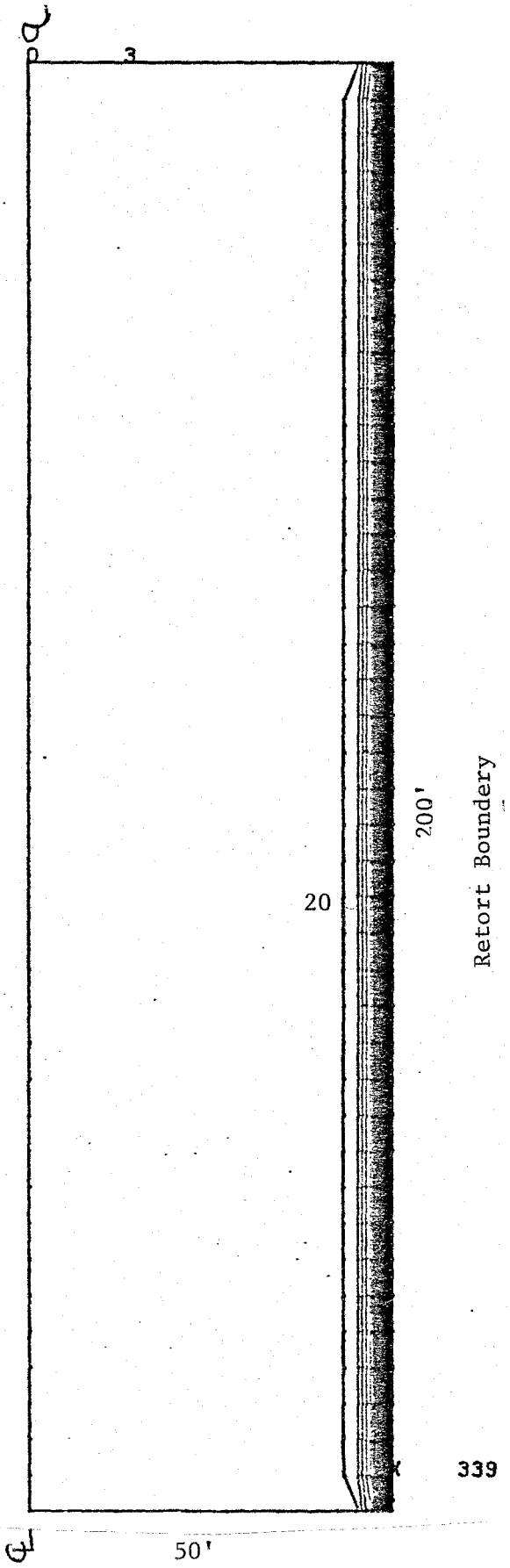

TEMPERATURE CONTOURS IN OIL SHALE PILLAR AT 120 HOURS (CONTOUR INTERVAL 20°C)

FIGURE 3.78

TABLE 3.17

TEMPERATURE CONTOUR LINE VALUES (^{o}C)AT 120 HRS.

0	20.000	40.000	60.000	80.000
100.00	120.00	140.00	160.00	180.00
200.00	220.00	240.00	260.00	280.00
300.00	320.00	340.00	360.00	380.00

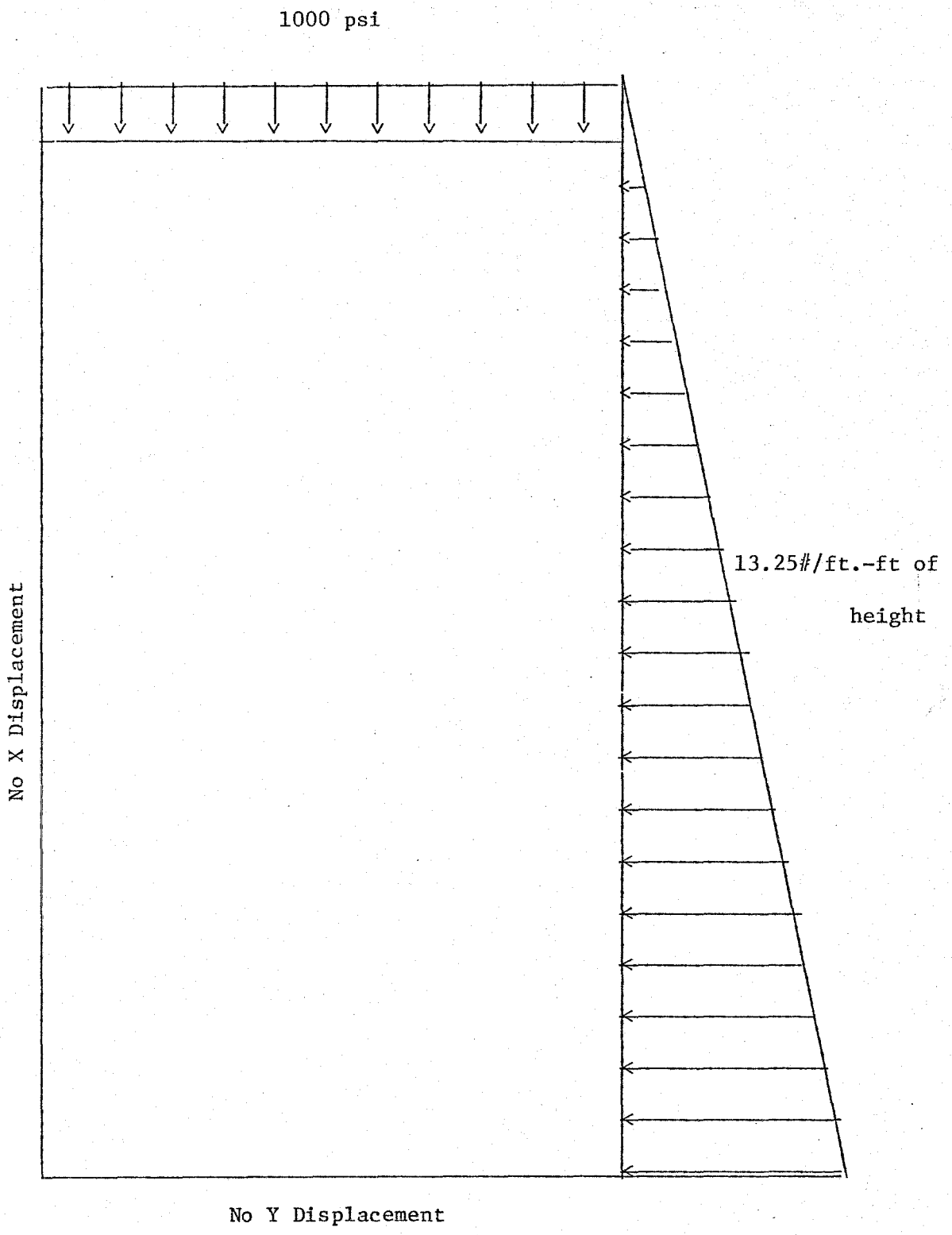

Figure 3.79 Boundary Loads for Oil Shale Pillar

TABLE 3.18

Temperature Dependent Mechanical Properties

Temp ^{o}C	Modulus $N/M^2 \times 10^9$	Poissons Ratio
10	13.9	0.22
20	13.9	0.22
140	9.4	0.47
260	7.3	0.01
380	3.4	0.47
500	3.2	0.32

Temp ^{o}C	Incremental Thermal Expansion Coefficients	
	X	Y
10	0	0
50	0	0
100	0.0003	0.0003
150	0.0006	0.0007
200	0.0007	0.0010
250	0.0006	0.0010
300	0.0007	0.0010
350	0.0007	0.0009
400	0.0006	0.0010
450	0.0004	0.0006
500	0.0003	0.0005

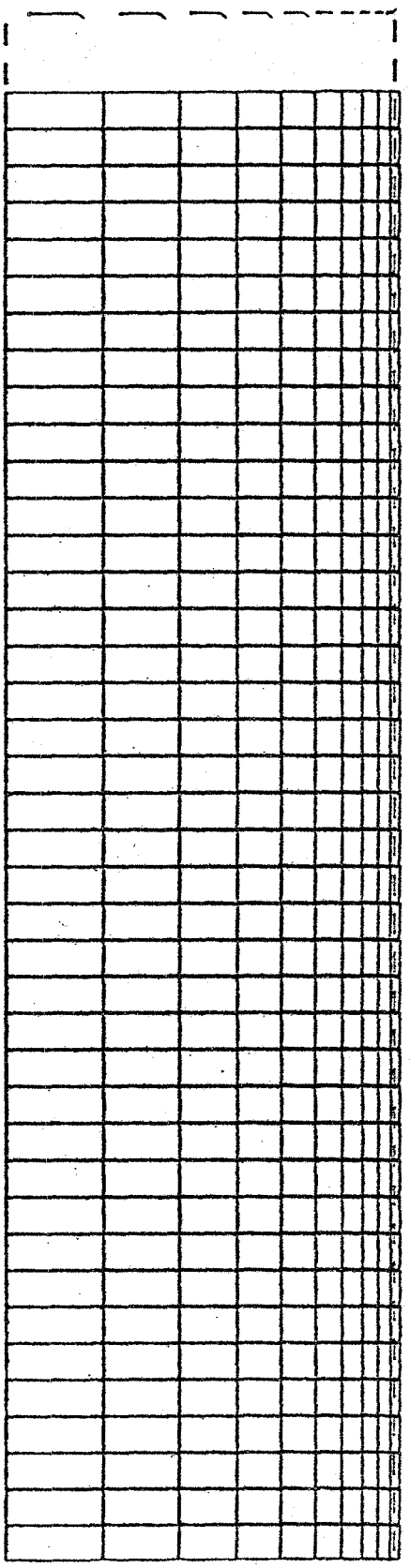

Figure 3.80 Exagerated Displacement - No Thermal Loads

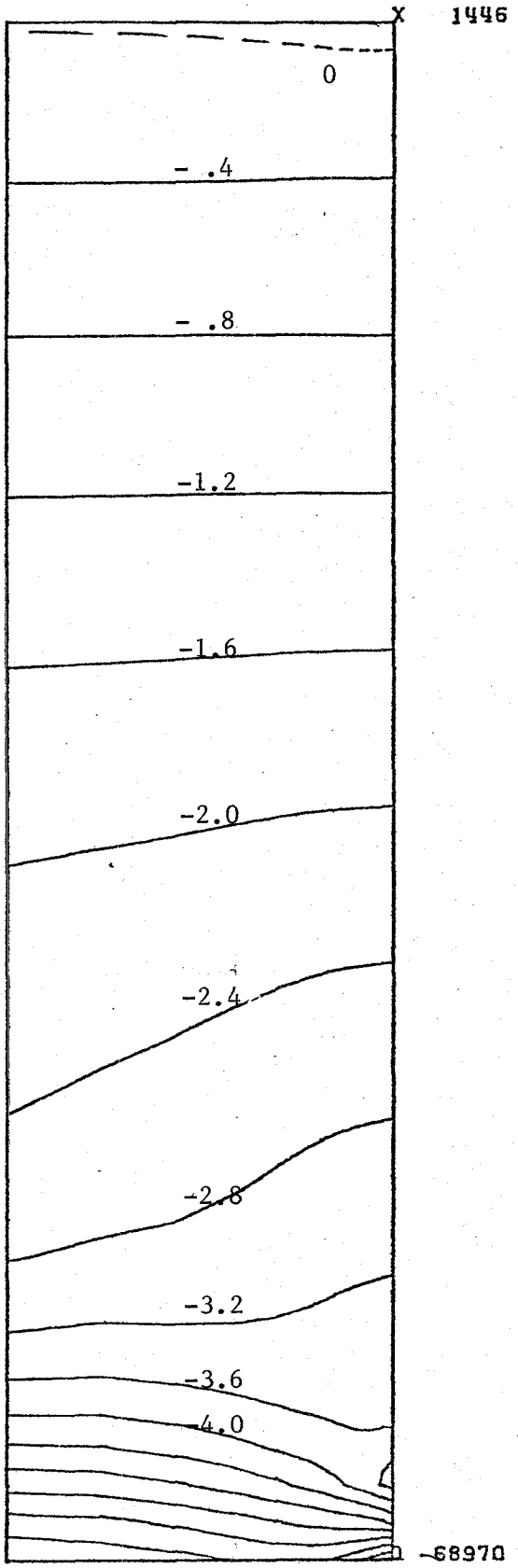

HORIZONTAL STRESS (σ_x, NO THERMAL LOAD)

FIGURE 3.81

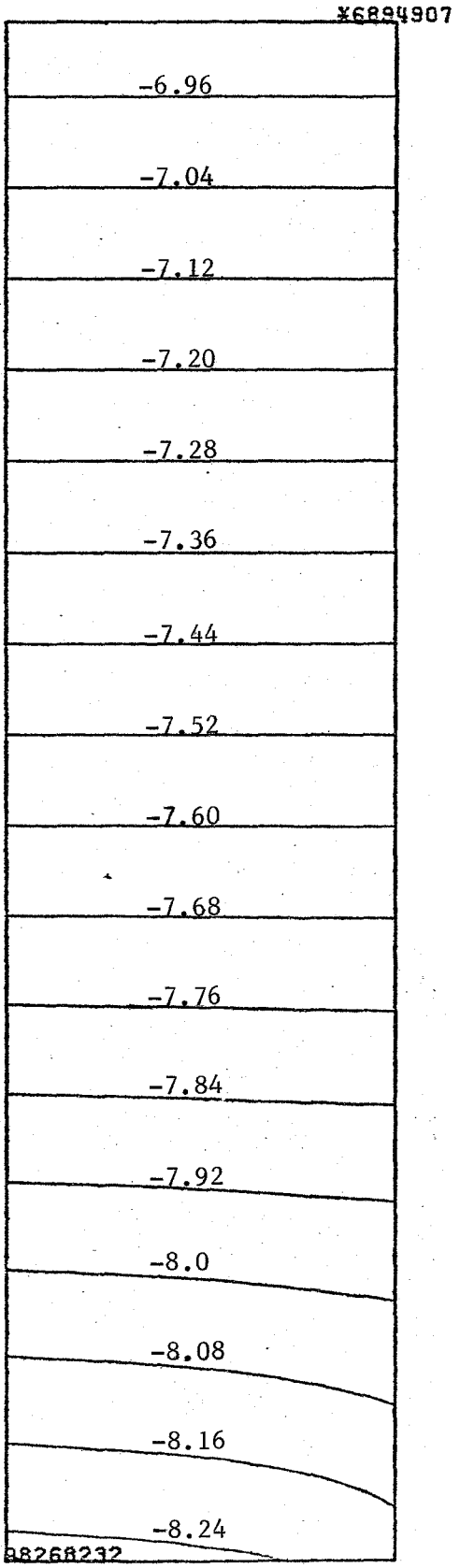

VERTICAL STRESS (σy, NO THERMAL LOAD)

FIGURE 3.82

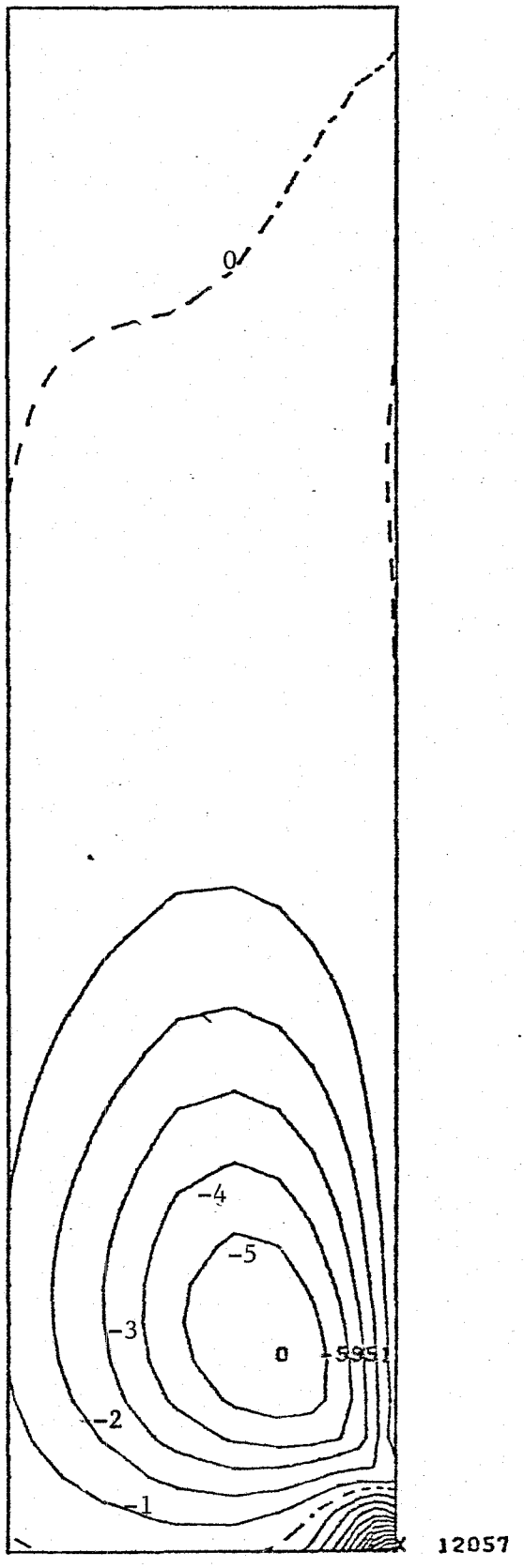

SHEAR STRESS (τ_{xy}, NO THERMAL LOAD)

FIGURE 3.83

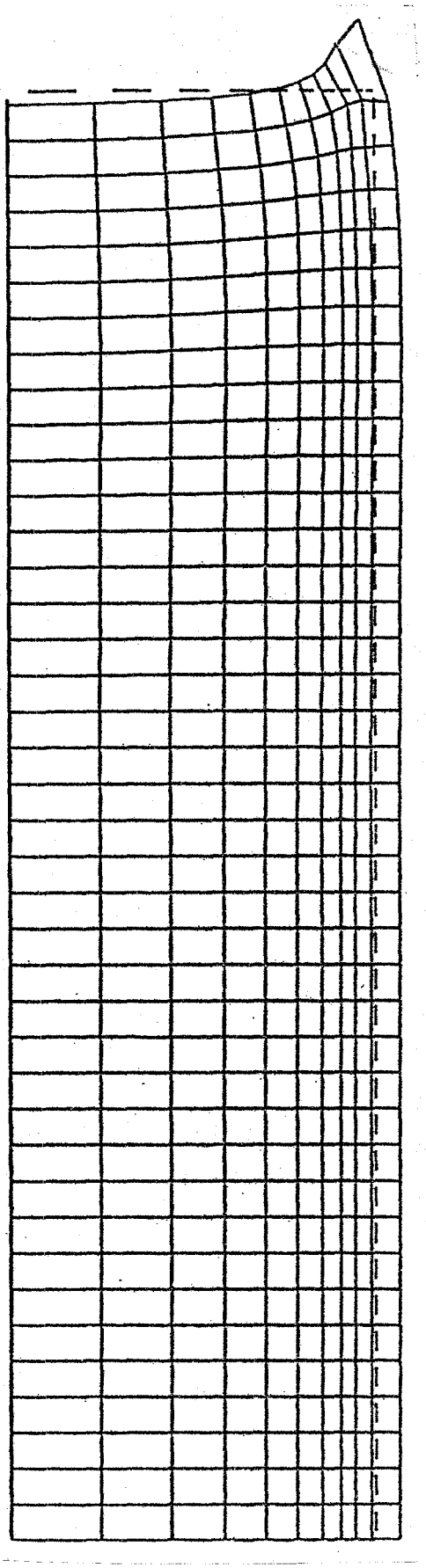

Figure 3.84 Exagerated Displacement - Thermal Loads at 120 hours

TABLE 3.19

(No Thermal Load)

σ_x contour line values (Fig. 3.81)

10^4 N/M^2

-7.2	-6.8	-6.4	-6.0	-5.6
-5.2	-4.8	-4.4	-4.0	-3.6
-3.2	-2.8	-2.4	-2.0	-1.6
-1.2	-0.8	-0.4	0	0.4

σ_x Contour line values (Fig. 3.82)

10^6 N/M^2

-8.32	-8.24	-8.16	-8.08	-8.00
-7.92	-7.84	-7.76	-7.68	-7.60
-7.52	-7.44	-7.36	-7.28	-7.20
-7.12	-7.04	-6.96		

τ_{xy} Contour values (Fig. 3.83)

10^3 N/M^2

-6.	-5.	-4.	-3.	-2.
-1.	0	1.	2.	3.
4.	5.	6.	7.	8.
9.	10.	11.	12.	13.

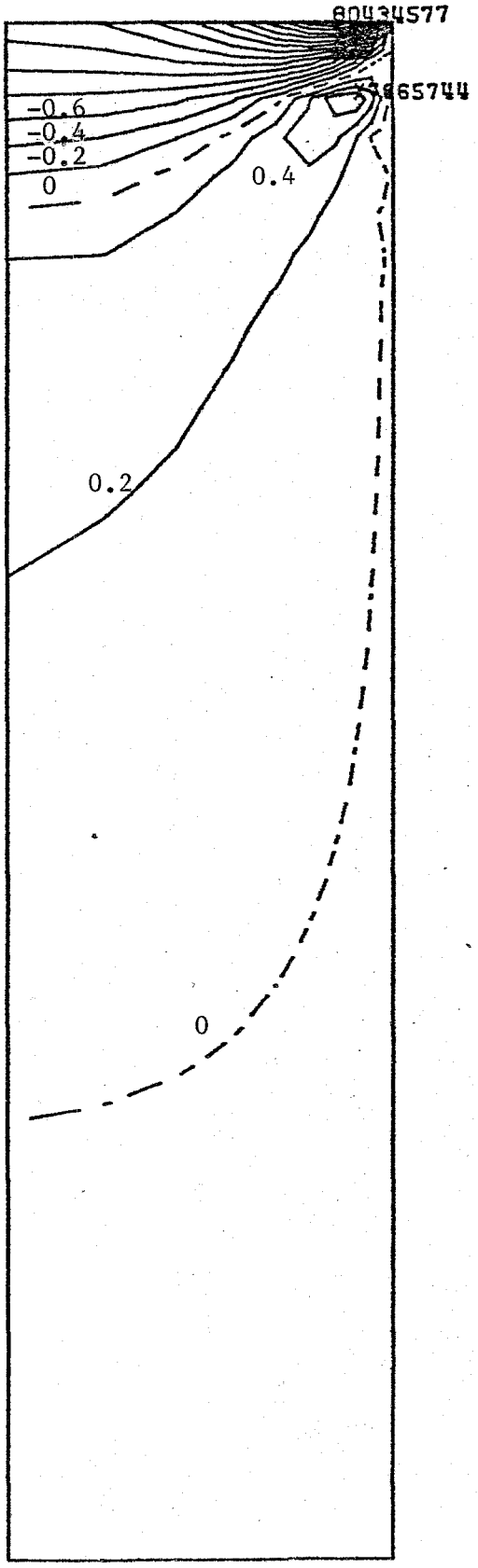

HORIZONTAL STRESS (σ_x) WITH THERMAL LOADS AT 120 HOURS

FIGURE 3.85

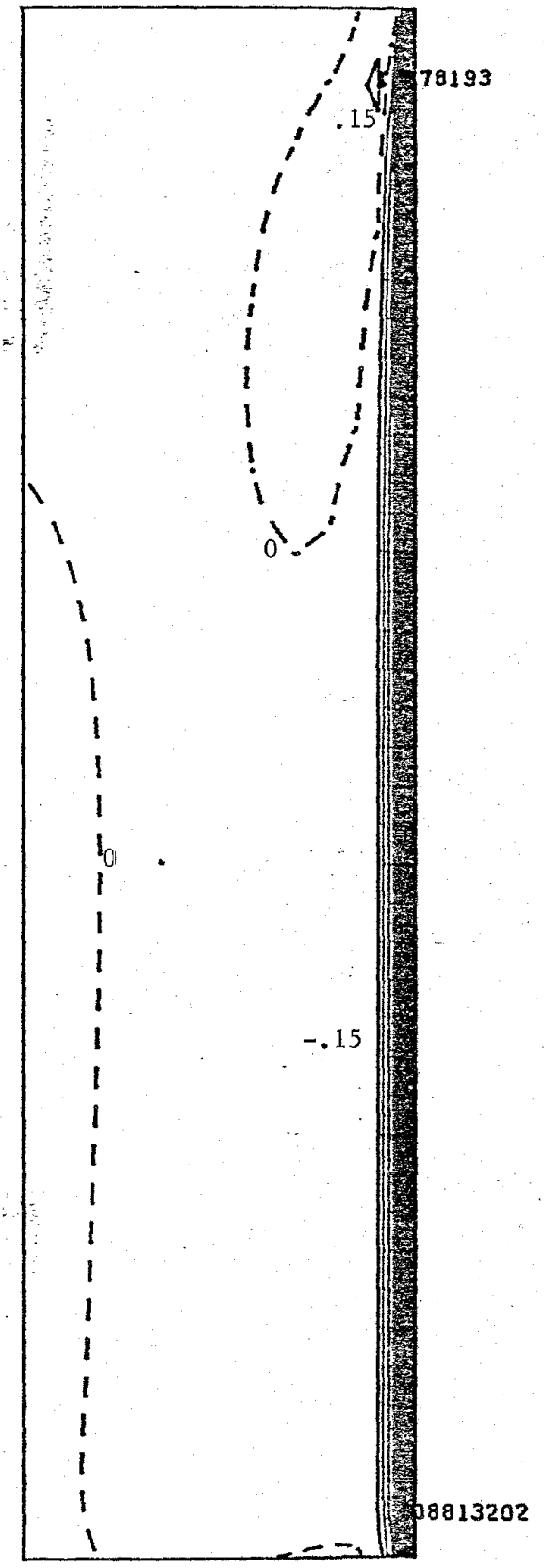

VERTICAL STRESS (σ_y) WITH THERMAL LOADS AT 120 HOURS

FIGURE 3.86

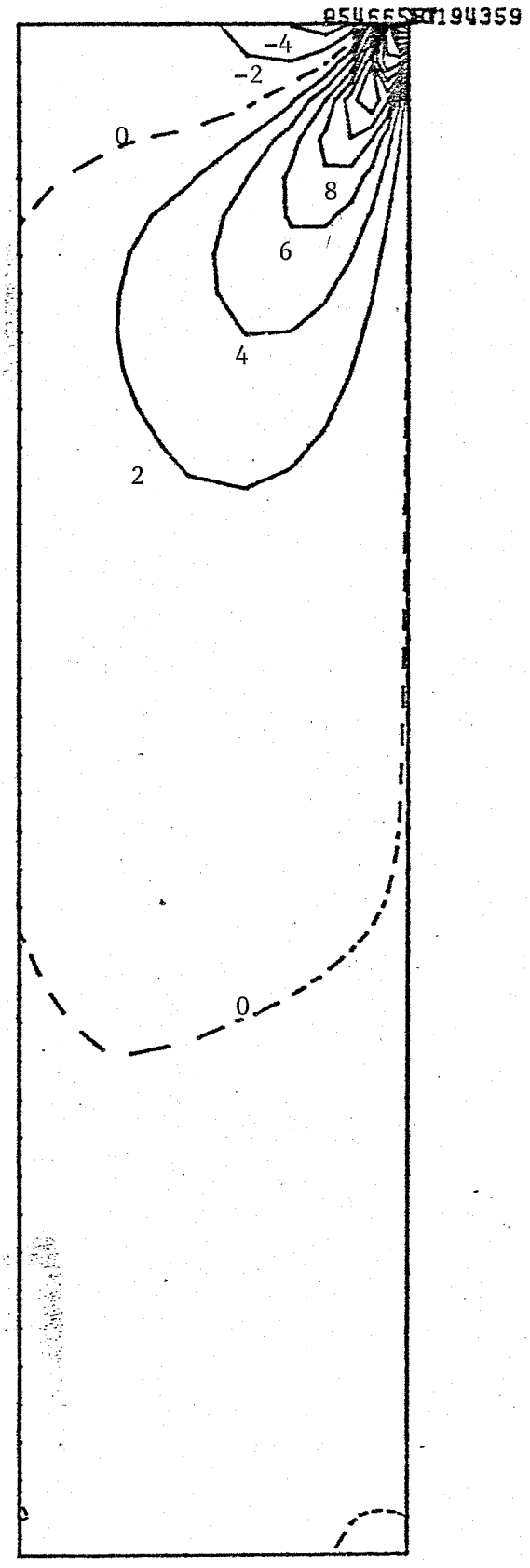

SHEAR STRESS (τ_{xy}) WITH THERMAL LOADS AT 120 HOURS

FIGURE 3.87

TABLE 3.20

(With Thermal Load at 120 hours)

σ_x Contour line values (Fig. 3.85)

10^7 N/M^2

-3.2	-3.0	-2.8	-2.6	-2.4
-2.2	-2.0	-1.8	-1.6	-1.4
-1.2	-1.0	-0.8	-0.6	-0.4
-1.2	-1.0	-0.8	-0.6	-0.4
-0.2	0	0.2	0.4	0.6

σy Contour line values (Fig. 3.86)

10^8 N/M^2

-2.10	-1.95	-1.80	-1.65	-1.50
-1.35	-1.20	-1.05	-0.90	-0.75
-0.60	-0.45	-0.30	-0.15	0
0.15	0.30	0.45	0.60	0.75

τ_{xy} Contour line values (Fig. 3.87)

-6.	-4.	-2.	0	2.
4.	6.	8.	10	12.
14.	16.	18.	20.	22.
24.	26.	28.	30.	32.

values in $^{N}/_{M}^{2}$. The first determination shows a generally uniform stress pattern through the pillar with the only concentrations resulting from the side load of the rubblized shale.The determination that includes temperature effects predictably shows the large vertical displacement and resulting high vertical compressive stress concentration along the edge of the pillar resulting from the high thermal gradient along that edge. If the pillar were a high strength material, the stress distribution would be realistic. However the high temperature triaxial strength tests done earlier in the project demonstrated the rapid loss of strength with temperature rise for the oil shale. Thus the highly stressed skin of the pillar would fail and there would be a redistribution of stress until equilibrium with the strength of the shale was achieved.

Figure 3.88 is a comparison plot of the thermally induced vertical stress (σ_y) the temperature, and temperature dependent triaxial vertical compressive strength through the horizontal center of the pillar. The compressive stress is close to zero out to about one meter of the edge of the pillar then it rises to about 20×10^7 N/M^2 (29,000 psi). The compressive strength line crosses this stress line about 1/2 meters (19 inches) in to the pillar. Although the size of the elements used would not allow too precise a determination of this distance, the pillar edge would probably not fail very far into the pillar based on this determination. Reduction of pillar support area would be on the order of 3%. The value of σ_y for no temperature effect is also shown and is well below the strengths determined for the vertical

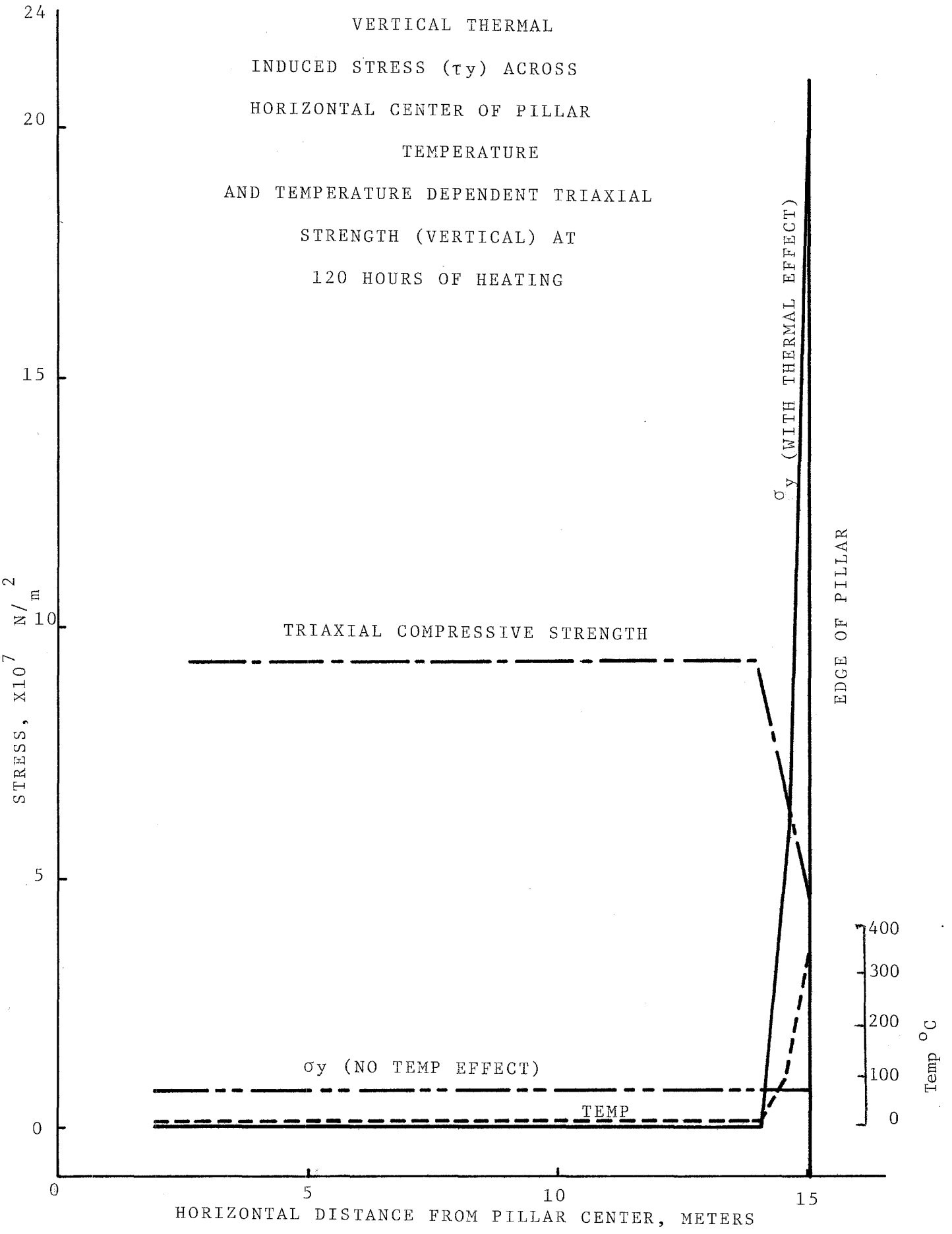
VERTICAL THERMAL
INDUCED STRESS (τy) ACROSS
HORIZONTAL CENTER OF PILLAR
TEMPERATURE
AND TEMPERATURE DEPENDENT TRIAXIAL
STRENGTH (VERTICAL) AT
120 HOURS OF HEATING
STRESS, X10^7 N/m^2
24
20
15
10
5
0
TRIAXIAL COMPRESSIVE STRENGTH
σy (WITH THERMAL EFFECT)
EDGE OF PILLAR
σy (NO TEMP EFFECT)
TEMP
400
300
200
100
0
Temp °C
0
5
10
15
HORIZONTAL DISTANCE FROM PILLAR CENTER, METERS

FIGURE 3.88

load of 1000 psi. The horizontal stress (σ_x) is not plotted, but it is in compression all along this line and of small value (20,000 N/M^2).

Thermal and Static Analysis at 800 Hours of Temperature

The previous thermal analyses of the pillar using finite differences indicated that little change took place in the pillar temperature distributions after 800 hours of heating. A thermal stress analysis was done at this time point to approximate a steady state situation in the pillar.

Figure 3.89 illustrates the temperature distribution at this time. The contour values are presented in Table 3.21. The thermal gradient is still very steep but extends farther into the pillar than at 120 hours. The temperature in the pillar is at the ambient value at about 4 meters (7.5 feet) into the pillar. This agrees fairly well with the previous work that indicated very little temperature change at 10 feet into the pillar at 800 hours.

Figures 3.90 through 3.93 show the exaggerated displacement, ox, oy and txy for 800 hours of heating. The contour values are shown in Table 3.22. The patterns are similar to the contours at 120 hours only the high σy values are deeper into the pillar. Figure 3.94 presents the vertical stress (σy) at the mid-pillar horizontal plane. Comparison of these values with the values at 120 hours (Fig. 3.88) shows that the maximum value of the compressive s tress near the pillar edge is lower than the 120

TABLE 3.21

Temperature Contour Line Values (^{o}C) at 800 Hours

		25.000	50.000	75.000
100.00	125.00	150.00	175.00	200.00
225.00	250.00	275.00	300.00	325.00
350.00	375.00	400.00	425.00	450.00

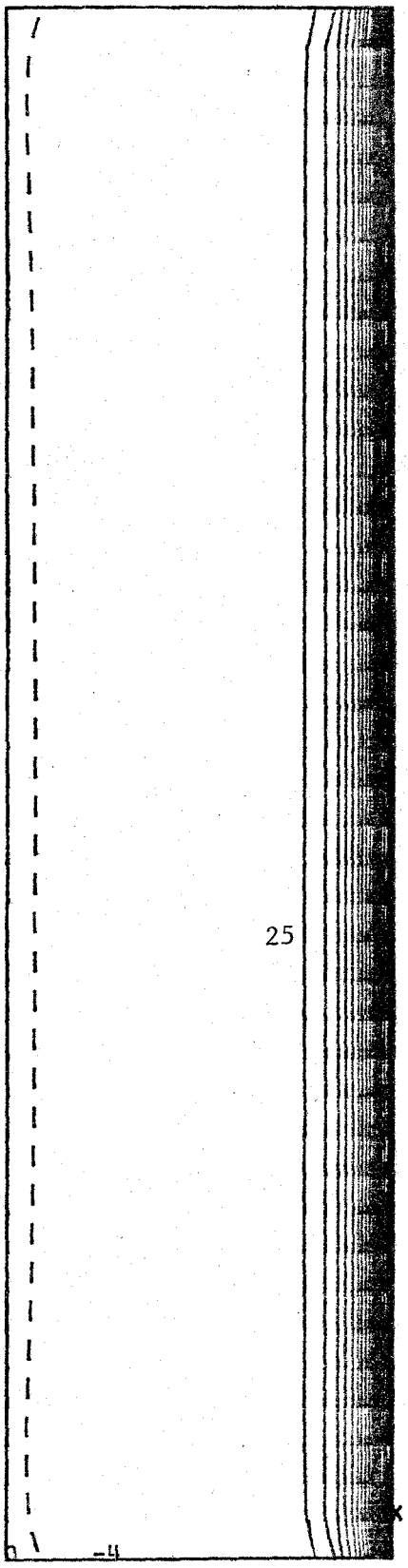

Figure 3.89 Temperature Distribution in Retort Pillar at 800 hours

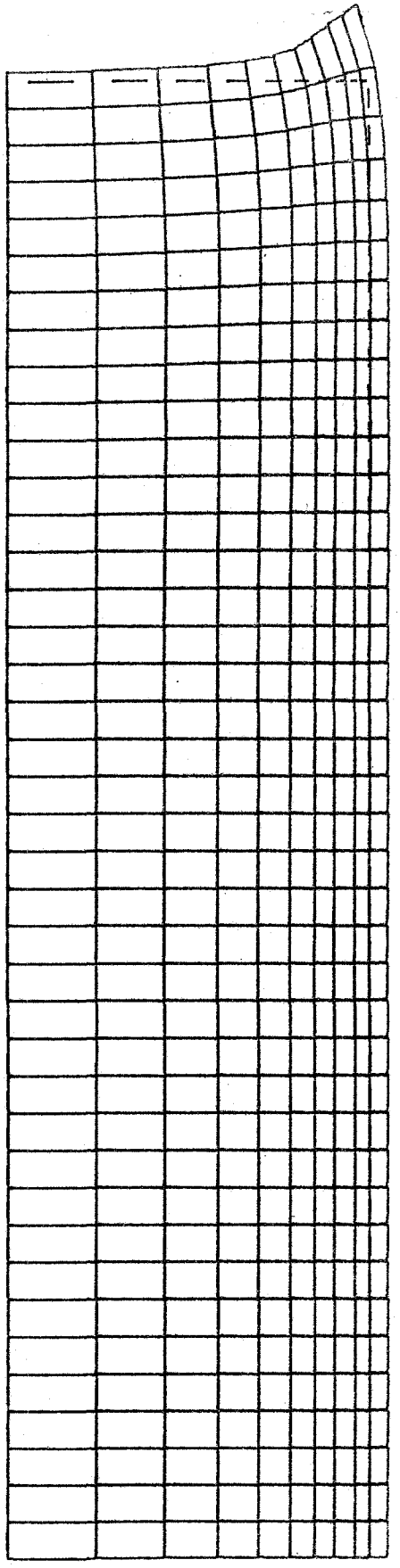

Figure 3.90 Exagerated Displacement in Retort Pillar at 800 hours

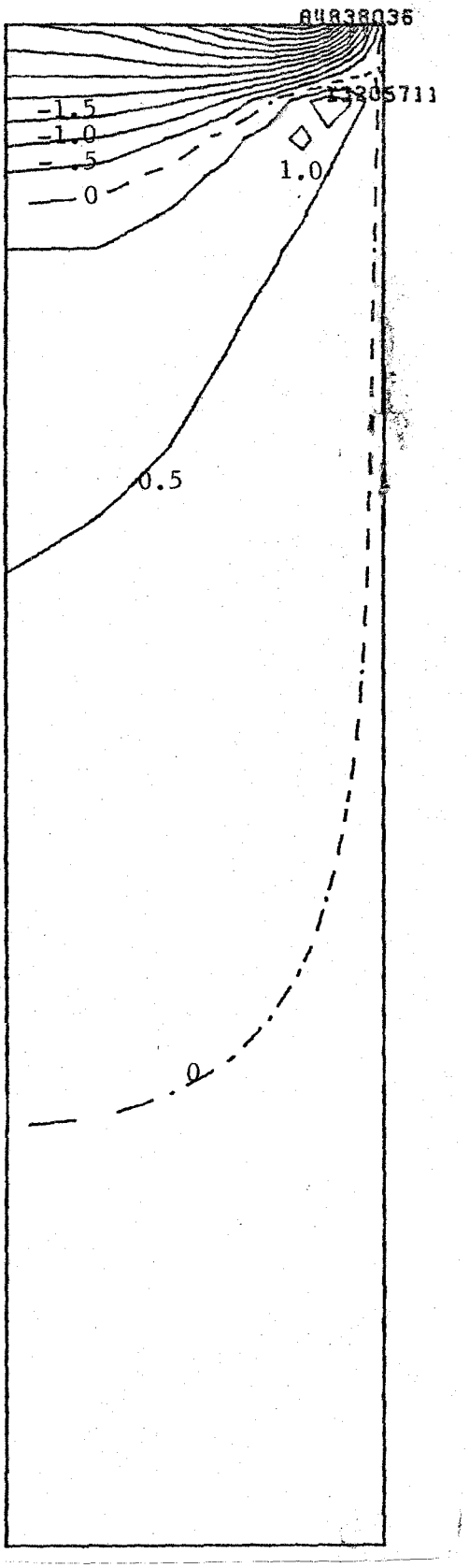

HARIZONTAL STRESS (σx) DISTRIBUTION IN RETORT PILLAR AT 800 HOURS

FIGURE 3.91

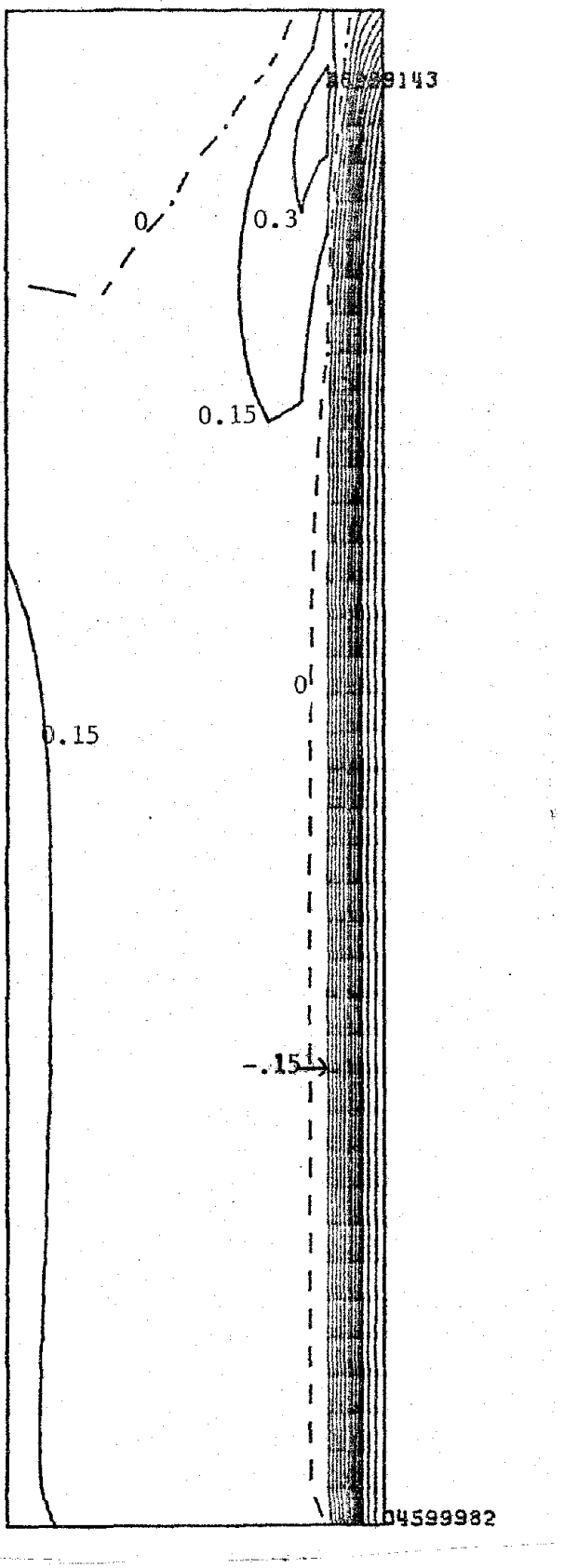

VERTICAL STRESS (σy) DISTRIBUTION IN RETORT PILLAR AT 800 HOURS

FIGURE 3.92

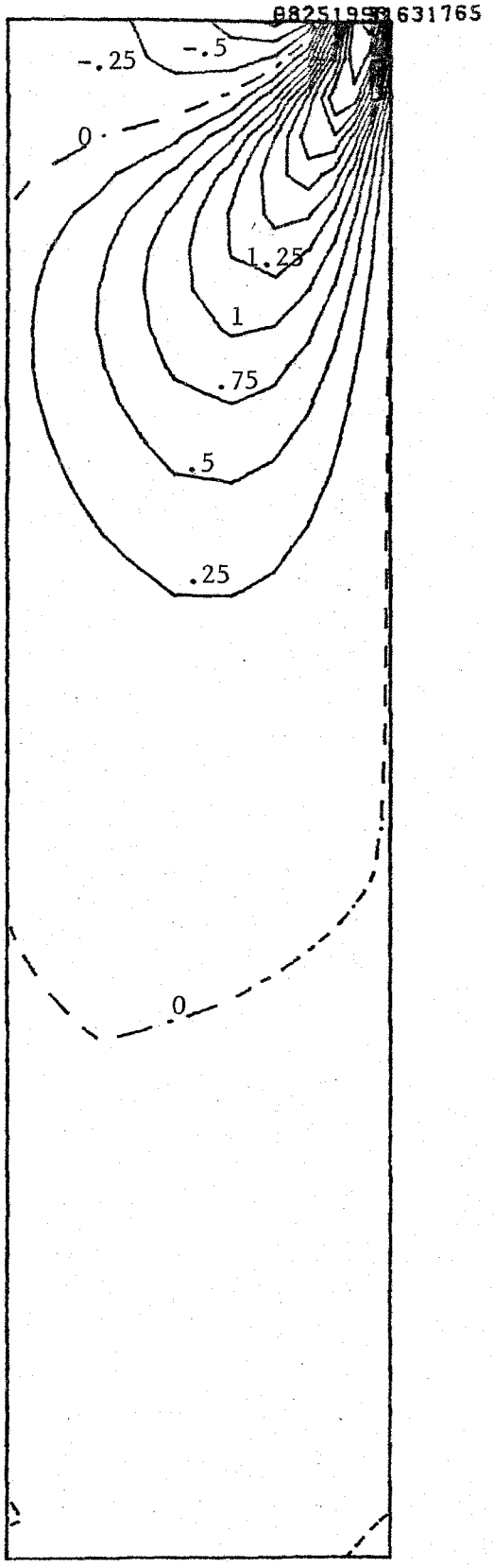

Figure 3.93 Shear Stress (τ_{xy}) in Retort Pillar at 800 hours

TABLE 3.22

(With Thermal Load at 800 Hours)

σ_x contour line values (Fig. 3.91)

10^7 N/M^2

-7.0	-6.5	-6.0	-5.5	-5.0
-4.5	-4.0	-3.5	-3.0	-2.5
-2.0	-1.5	-1.0	-0.5	0
0.5	1.0	1.5	2.0	2.5

σ_y Contour line values (Fig. 3.92)

10^8 N/M^2

-1.95	-1.80	-1.65	-1.50	-1.35
-1.20	-1.05	-0.90	-0.75	-0.60
-0.45	-0.30	-0.15	0	0.15
0.30	0.45	0.60	0.75	0.90

τ_{xy} Contour line values (Fig. 3.93)

-1.25	-1.00	-0.75	-0.50	-0.25
0	0.25	0.50	0.75	1.00
1.25	1.50	1.75	2.00	2.25
2.50	2.75	3.00	3.25	3.50

FIGURE 3.94

VERTICAL THERMAL INDUCED STRESS (σy) ACROSS HORIZONTAL CENTER OF PILLAR, TEMPERATURE AND TEMPERATURE DEPENDENT TRIAXIAL STRENGTH (VERTICAL) AT 800 HOURS OF HEATING

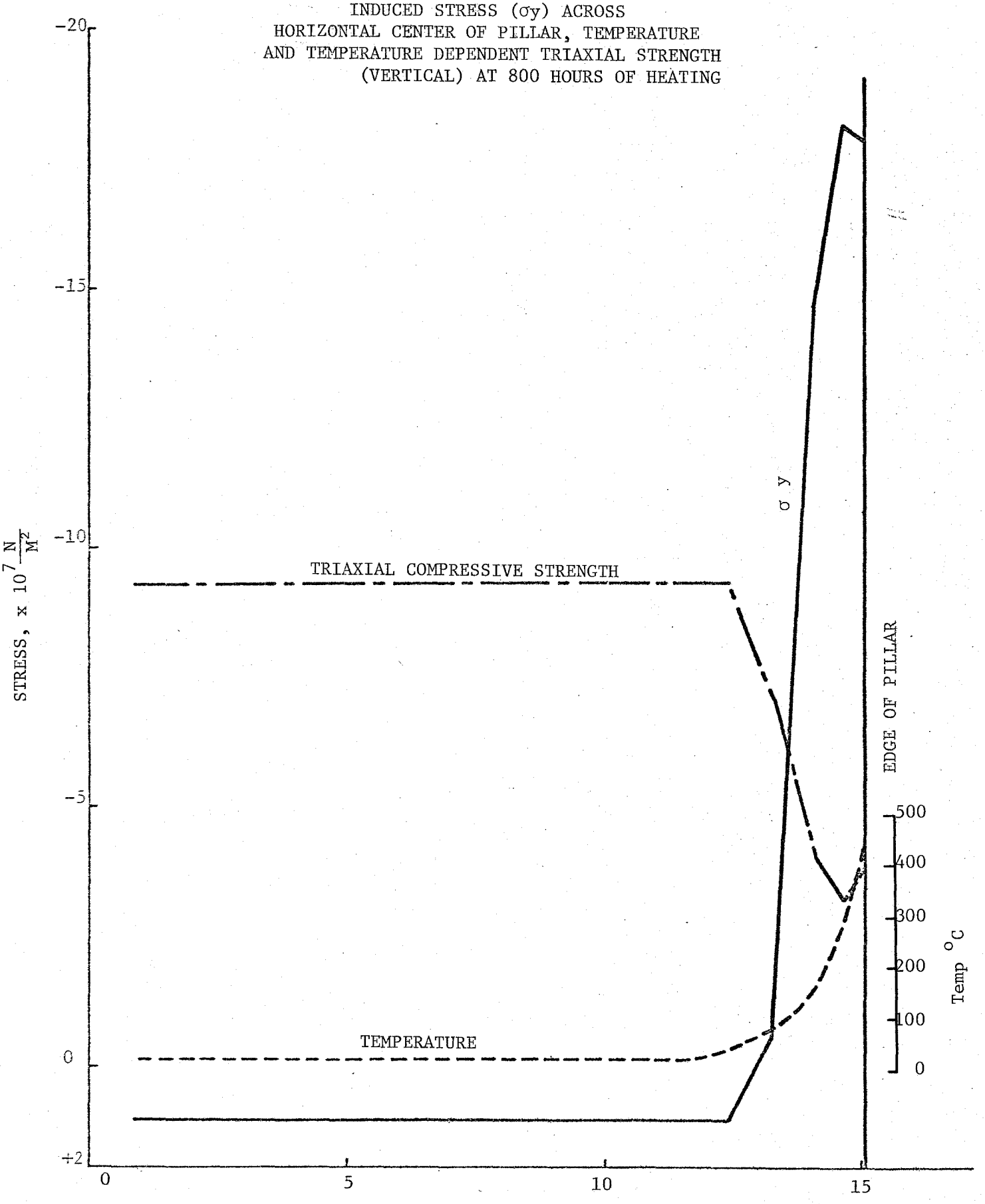

hour case, that the thermal induced compressive stress extends into the pillar edge about 2.5 times farther than in the 120 hour case, and that the rest of the pillar is in tension as a result of this high skin stress on the pillar. The intersection of the stress with the temperature dependent triaxial compressive strength occurs at about 1.5 meters (5') into the pillar. On this basis failure probably would not extend more than 5 or so feet into the pillar. This would mean a reduction in pillar support area of about 10%.

4.0 CONCLUSIONS

The major conclusions of the work accomplished on USBM Contract H0262031 can be summarized as follows:

1. It was determined that both Anvil Points and Logan Wash can provide samples with classic oil shale mineralogy with oil yields covering the range of interest and without significant concentrations of nahcolite and dawsonite minerals. The sample collection for this research program was undertaken at the Logan Wash site because of convenience, experience and the fact that Logan Wash was an active in-situ retorting facility.

Typical Green River oil shale was represented by obtaining samples from Logan Wash. X-ray diffraction did not detect any nacholite or dawsonite in the samples collected. Chemical analysis detected water-soluble sodium from nacholite or halite, but at very low concentrations.

2. To determine whether the heating atmosphere affects oil shale strength, tests were conducted under both nitrogen flushed and oxygen available atmospheres. No discernable effect of heating atmosphere was found on the indirect tensile strength for the full range of kerogen contents and temperatures investigated. For the compressive strength, initially an approximately 25% increase was observed for the samples heated in air over those heated in nitrogen. However, in further tests where all samples were encased in

a vented aluminum case and restrained so as to present axial exfoliation, strengths were not significantly different. These results led to the conclusion that the heating atmosphere did not have a significant bearing on the strength of oil shale.

3. Heating time was also found to have little or no effect on oil shale strength after the time required for thermal equilibrium to occur in the sample. All samples for the physical property testing in this research program were heated for at least 16 hours prior to testing.

4. Compressive strength was found to be highly sensitive to temperature with a major loss of strength occurring in heating to only 140°C. For heating beyond 380°C to 500°C, a strength regain was found to occur particularly for vertical cores at all grades investigated. The horizontal cores showed a similar strength behavior for 15 gpt grade, but the data including all grades were not conclusive to confirm the occurrence of strength regain at higher temperatures. The strength regain beyond 380°C for vertical cores was attributed to significant loss of kerogen taking place in heating to this temperature and the resultant change in the physical behavior of oil shale.

5. Increased grade was seen to cause a consistent reduction in sample strength both for horizontal and vertical

cores. The rate of reduction in compressive strength was greater at lower grades. The strength of vertical cores was more sensitive to grade than that for horizontal cores.

6. Confining pressure was found to be very effective in increasing sample strength for all temperature and grade levels investigated. Moreover, as the compressive strength became very low at higher temperatures, a greater proportionate effect of confining pressure was observed.

7. On the average, the horizontal cores yielded higher compressive strengths than vertical cores. This finding which was contrary to expectations was believed to be a result of variation in varve structure of oil shale samples. A vertical core containing a rich band of kerogen would be more succeptible to premature failure than a horizontal core having a similar rich band. The profound effect of varve structure on the strength of vertical cores was evident in many failed samples as the presence of one or more rich bands contributed to excessive sample deformation and subsequent premature failure.

8. The entire triaxial strength data obtained from laboratory tests was analyzed through regression techniques to develop equations to mathematically represent the oil shale strength in terms of grade, temperature and confining pressure. The data fitting procedure employed was a

stepwise regression technique, starting with simple single variables and then progressing by adding more complicated components until the increase in the quality of the fit did not compensate for the increase in the complexity of the equation. The strength equations formulated for the vertical and horizontal cores contained identical functions of the variables with only difference being in the coefficients. The multiple correlation coefficients were .76 an .864 for the vertical and horizontal cores, respectively. These correlation coefficients are considered to be reasonably good given the inherent variability of oil shale strength as a result of variation in mineralogy and varve structure.

9. The F-value statistics as calculated from the regression analysis showed the confining pressure to be the least significant of all these variables. For the vertical cores, the temperature contributed the largest effect, followed by grade. This sequence was reversed for the horizontal cores, regression results showing the grade to be the most significant variable affecting strength.

10. The Brazilian tensile strengths showed a similar sensitivity to temperature as did the compressive strength with a major loss of tensile strength occurring in heating only to 140°C. For vertical cores, a gradual reduction of strength was seen to occur with increasing grade. No

consistent effect of grade on strength was present for the horizontal cores.

11. At a temperature of 20°C, the tensile strength of vertical cores was more than 50% higher than the horizontal cores. However, for temperatures above 140°C, the horizontal cores showed a consistently higher strength than vertical cores. Furthermore, at high temperatures (380°C), the vertical cores virtually lost all of their tensile strength. In some instances, high temperatures resulted in sample failure before any noticeable load could be applied to the sample.

12. Using stepwise regression techniques, equations were also developed to explain the tensile strength behavior of oil shale with varying grade and temperature. The multiple correlation coefficients for the vertical and horizontal cores were .96 and .83 respectively.

13. The F-value statistics determined from the regression analysis showed that the temperature by far had the largest effect on the tensile strength of oil shale. With its very low F-value, grade was shown to have very little effect on tensile strength.

14. As expected, the measured elastic properties, the Young's modulus and the Poisson's ratio showed a large

degree of variation. Similar to compressive strength, a major reduction of Young's modulus was found to occur in heating only to 140°C. Increasing grade resulted in a continous reduction of Young's modulus. The confining pressure appeared to have no discernable effect on Young's modulus.

15. The regression equations developed for the Young's modulus had relatively low multiple correlation coefficients as a result of large variation in data. The confining pressure did not enter the regression equations, confirming the experimentally derived conclusions that the Young's modulus for oil shale was not affected by the confining pressure.

16. The data for Poisson's ratio showed extreme variability, thus not allowing the development of any regression equations with resonable correlation coefficients.

17. The thermal conductivity was found to be dependent on grade, but not highly dependent on temperature, except while shale is actively retorting. The thermal conductivity decreased with increasing temperature and increasing grade.

18. The thermal diffusivity decreased with increasing temperature and increasing grade.

19. It became evident that the thermal expansion of oil shale during heating can exert considerable expansive forces. Thermal expansion has been characterized as a dual slope function up to the temperature at which plastic deformation of the shale became significant. Thermal expansion was essentially meaningless above that temperature.

20. The dielectric constant decreased with increasing frequency and attained relatively high low-frequency values over 400°C.

21. The loss tangent decreased with increasing frequency and increased with increasing temperature.

22. At temperatures where significant organic matter decomposition occurred, the loss tangent began to exhibit secondary peaks at a frequency of around 10^5 Hz.

23. Anomolies in the ultrasonic travel times recorded on the thermal samples during heating correlated well with observed physical and chemical changes in oil shale during heating.

24. The changes in thermal, electrical, and acoustic properties correlated well. It is possible that these correlations can be used to develop sensors for retort diagnostics and to investigate potential retort locations.

25. A one dimensional finite-difference numerical model has been developed for heat transfer into an oil shale pillar. The model has been verified by comparison with analytical solution.

26. The results of the finite-element structural analysis regarding the effect of thermal stress on oil shale pillar strength indicated that during retorting a very high vertical compressive stress will be generated at the edge of the pillar. Comparison of this induced stress with the temperature dependent triaxial compressive strength led to the conclusion that at 120 hours of retort heating, about three percent of the pillar support area would be lost. For 800 hours of heating, the corresponding loss for pillar support area would be approximately 10 percent. It should be noted that the thermal properties used in the finite-element analysis were for unstressed oil shale as determined in laboratory physical property tests. As the thermal conductivity and heat capacity would be expected to be lower for fractured oil shale, the thermal stresses calculated from the model should represent a worst case situation.

27. A temperature distribution for a model simulating the in-situ heater test was determined using the ANSYS finite-element program and the temperature dependent thermal property data from laboratory experiments. A good correlation was found between the in-situ temperatures and those predicted by the computer analysis.

28. No quantitative comparisons were possible between the computer model results and the displacement data from the in-situ heater test because the displacement measurements made with load cells were interdependent through the flexure of the test frame. It was possible to make some qualitative comparisons, however, showing good correlation between the field data and the computer study.

29. The in-situ heater test further confirmed the conclusion that the oil shale is an excellent insulator.

30. The degree of support that the rubblized shale would provide to the pillars can not be determined from the work done so far. A simplified graduated constant load condition was used for the horizontal pillar load. This provided some constraint on the pillars, but in a real situation the area between pillars would be full of rubble and any horizontal pillar displacement would result in some increase in the constraint load against the pillar. Before

further modeling is done, the properties of cohesion and the internal friction angle for the unburned and burned rubblized shale should be determined along with the expansion characteristics of the burned rubble

31. Subsidence was not evaluated because the preliminary creep tests on shale at elevated temperature indicated that creep would have a major effect on pillar displacement. The thermo elastic analysis of the pillars indicated an upward displacement rather than the downward displacement that occurs in a coal pillar. Effective analysis of subsidence will require better information on the creep of shale with rising temperature.

32. Kerogen recovery from the pillars between the retorts would probably be very low. The depth of penetration at temperature sufficient to retort the shale (370-425°C) would be less than one foot at 800 hours of heating. Based on this depth the kerogen recovery from the pillars would be less than 2 percent. Joints and fractures in the pillar might result in some additional recovery.

5.0 REFERENCES

1. Sladek, T.A., 1974, Recent Trends in Oil Shale -- Part 1: History, nature and reserves, Mineral Ind. Bull., V17, No. t, 20 p.

2. Cook, W.C., 1970, Thermal analysis of oil shales: Colorado School of Mines Quart., v. 65, no. 4, October, p. 133-140

3. Stanfield, K.E., and others, 1951, Properties of Colorado oil shale USBM R.I. 4825

4. Hendrickson, T.A., 1974, Synthetic Fuels Data Handbook, 1975 edition: Cameron Engineers, Denver, Colorado, p. 44.

5. Smith, J.W., and Young, N.B., 1969, Determination of dawsonite and nahcolite in Green River formation oil shales: USBM R.I. 7286, 20 p.

6. Smith, J.W., and others, 1972, estimating nahcolite and dawsonite content of Colorado oil shale from oil-yield assay data: USBM R.I. 7689, 24p

7. Tisot, P.R., and Sohns, H.W., 1971, Structural deformation of Green River oil shale as it relates to in-situ retorting; USBM R.I. 7576, 27p

8. Tisot, P., 1967, Alterations in the structure and physical properties of Green River oil shale by thermal treatment: J. Chem. Eng. Data, July.

9. Harak, A.E., and others, 1970, Preliminary design and operation of a 150-ton oil shale retort: Colorado School of Mines Quart., v. 65, No. 4, October, p. 41-56

10. Carpenter, H.C., and Sohns, H.W., 1974, Development of technology for in-situ oil shale processes: Colorado School of Mines Quart., v. 69, no. 2, April, p. 143-170

11. Schlinger, W.C., and Jesse, D.R., 1967, Hydrotorting--Use of hydrogen for improved recovery of shale oil: Colorado School of Mines Quart., v. 62, no. 3, July, p. 133-40

12. Tihen, S., and others, 1968, Thermal conductivity and thermal diffusivity of Green River oil shale: NBS Special Publication

13. Sladek, T.A., 1968. Determination of low-temperature thermal conductivities for several grades of oil shale: Master of Science thesis, Colorado School of Mines, Golden, Colorado.

14. Sladek, T.A., 1971, A determination of the composition and temperature dependencies of thermal conductivity factors for Green River oil shale: Ph. D. thesis, Colorado School of Mines, Golden, Colorado.

15. Prats, M., and O'Brien, S., 1975, The thermal conductivity and diffusivity of Green River oil shales: J. Petroleum Tech., January, p. 97

16. Dubow, J., Nottenburg, R., and Collins, G., 1976, Thermal and electrical conductivities of oil shale: Paper to be presented at ACI Fall Meeting, 1976.

17. Collins, G., and DuBow, J., 1976, Electrical and thermal conductivities of Green River oil shale: Progress report, Laramie Energy Research Center, Energy Research and Development Administration, January

18. Pratt, A., 1969, Heat transmission in low conductivity materials, in Thermal Conductivity, Academic Press

19. Allred, V.D., 1966, Kinetics of oil shale pyrolysis: Chem. Eng. Prog., v. 62, no. 8, Aug, pp. 55-60. Reprinted in Colorado School of Mines Quart., v. 62, no. 3, July, 11967, pp. 91-109

20. Fausett, D.W., and others, 1974, Second-order effects in the kinetics of oil shale pyrolysis: USBM R.I. 7889, 21p.

21. McKee, R.H., and Lyder, E.E., 1921, The thermal decomposition of shales. I--Heat Effects: Ind. and Engr. Chem. J., v. 13, no. 7, July, p. 613-8.

22. _____, 1921, The thermal decomposition of oil shales. II-Determination of the heat of reaction involved in their thermal decomposition: Ind. and Engr. Chem. J., v. 13, no. 8, August, p. 678-84.

23. Maier, C.G., and Zimmerley, 1924, The chemical dynamics of the transformation of the organic matter to bitumen in oil shale: Univ. Utah Bull., v. 14, no. 7, January, p. 62-81.

24. Cummins, J.J., and Robinson, W.E., 1972, Thermal degradation of Green River kerogen at 150° to 350°C: Rate of product formation: USBM R.I. 7620, 15 p.

25. Hendrickson, T.A., ed., 1974, Synthetic fuels data handbook, 1975 edition: Cameron Engineers, Denver, Colorado.

26. Stanfield, K.E., and Frost, I.C., 1949, Method of Assaying oil shale by a modified Fischer retort: USBM R.I. 4477, 13 p.

27. Brobst, D.A., and Tucker, J.D., 1973, x-ray mineralogy of the Parachute Creek Member, Green River formation, in the Northern Piceance Creek Basin, Colorado: U.S. Geol. Survey. Prof. Paper 803, 53 p.

28. Fahey, J.J., 1962, Saline minerals of the Green River formation; with a section on x-ray powder data for saline minerals of the Green River formation, by M.E. Mrose: U.S. Geol. Survey Prof. Paper 405, 50 p.

29. Smith, J.W., and Young, N.B., 1969, Determination of dawsonite and nahcollite in Green River formation oil shales: U.S. Bureau of Mines R.I. 7286, 20 p.

30. Allred, V.D., 1964, Some Characteristic Properties of Colorado Oil Shale which may Influence In-Situ Processing: CSM Quart., Vol. 59, No. 3, July, pp. 47-76.

31. Bae, J.H., 1969, Some Effects of Pressure on Oil Shale Retorting: S.P.E. Journal, vol. 9, No. 3, September, pp. 287-292.

32. Campbell, W.G., and others, 1970, Evaluation of Oil Shle Fracturing Experiments Near Rock Springs, Wyoming: USBM R.I. 7397, 21 p.

33. Carpenter, H.C., 1975, Fracturing Oil Shale for In-Situ Retorting Experiments: Meeting of the A.I. Ch. E., Los Angeles, November 20.

34. Olinger, B., 1977. "Oil Shale Under Dynamic Stress." LA-6901-PR, Los Alamos Scientific Laboratory, p. 9.

35. Thill, R., Bur, T., and Hjelmstad, K., 1974. "Elastic Response to Ultrasonic Pulse," in Bureau of Mines Test Procedures for Rocks, Inf. cir. 8628, edited by Lewis, W. and Tandanand, S.

36. Peselnick, L., and R.M. Stewart. 1975. "A sample Assembly for Velocity Measurements in Rocks at Elevated Temperatures and Pressures." J. Geophys. Res., 80, p. 3765.

37. Schreiber, E., O.L. Anderson, and N. Soga. 1973. "Elastic Constants and Their Measurement." McGraw-Hill, New York, pp. 35-81.

38. Papadakis, E.P. 1967. J. Acoust. Soc. Am. 42, pp. 1045-1051.

39. Spetzler, H. 1970. "Equation of State of Polycrystalline and Single-Crystal MgO to 8 Kilobars and 800°K." J. Geophys. REs., 75 (11), pp. 2073-2087.

40. Spencer, J.W. and A.M. Nur. 1976. "The Effects of Pressure, Temperature and Pore Water on Velocities on Westerly Granite." J. Geophys. REs., 81 (5), pp. 899-904.

41. Hippel, A. von, Dielectrics and Waves, MIT Press, 1954

42. Parkhomenko, E.I., "Electrical Properties of Rocks", Plenum Press, New York, Chapter IV, p. 200, 1967.

43. Cole, R.H., In "Progress in Dielectrics", vol. 3, J. Wiley and Sons, New York, pp. 47-100, 1961.

44. Keller, G.V., and Licastro, P.H., Geol. Survey Bull. 1052-H, 1959.

45. Fenix and Scisson, Inc., 1976, Phase I report on technical and economic feasibility of in-situ shale-oil recovery, USBM Contract S0241073: Fenix and Scisson, Inc., Tulsa, Oklahoma.

46. Smith, J.W., 1963, Stratigraphic change in organic composition demonstrated by oil specific gravity-depth correlation in Tertiary Green River oil shales, Colorado: Bull. Am. Assoc. Petrol. Geol., v. 47, May, p. 804-13.

47. Smith, J.W. and Milton C., 1966, Dawsonite in the Green River formation of Colorado: Econ. Geol., v. 61, no. 6, September - October, p. 1029-42.

6.0 APPENDICES

6.1 Glossary

1. Fischer Assay - Technique for determining the kerogen content of an oil shale sample.

2. In Situ Retorting - The pyrolysis of oil shale underground for the removal of kerogen from an in-place fracture rock mass.

3. Leached Zone - Considered that portion of the oil shale horizon not containing significant concentrations of nahcolite or dawsonite.

4. Retorting Isotherm - Refers to the temperature level at various distances into the retort wall or pillar.

5. Saline Mineral Zone - Refers to that portion of the oil shale horizon containing significant concentrations of nahcolite or dawsonite.

6. Sample Characterization - The process of identifying a sample of oil shale based on its kerogen and mineral content.

7. Structural Degradation Temperature - That temperature at which a sample of oil shale begins to lose the ability to support a load, the sample having essentially no strength above this temperature.

8. Structural Transition Temperature - See structural degradation temperature.

9. Transient Line Probe Method - Method of determining thermal conductivity using a line source within the sample. Not considered accurate for layered or macro-heterogeneous materials.

6.2 Status of Current In-Situ Projects

6.2.1 Introduction

As part of the Phase I assessment of the current and projected needs of the oil shale industry, organizations active in the design or development of in situ retorting techniques were contacted. Their input was solicited as to the pertinent variables that should be investigated and the respective levels of those variables. Also reviewed were various retort configurations and system layouts to include size of chambers, chamber separation, pillars, depth, burn rate, duration of temperature, and time during which extraction continues. The discussions confirmed the need for the work planned for this investigation and will be very helpful in the model selection and evaluation portions.

Often a company, for proprietary reasons, could not provide us with much information, but in all cases considerable interest was shown in the potential results of the investigation. Following is a brief summary of the information gained from the more communicative organizations.

6.2.2 DOE Oil Shale Projects

The Department of Energy is conducting several research projects related to in situ retorting of oil shale.

The Laramie Energy Research Center has designed and constructed a 150-ton batch type retort to determine the retorting characteristics of a column of mine-run, ungraded oil shale ranging in size from fines to 5-ton pieces. The results of 10 experimental runs are reported in [A.E. Horak, L. Dockter, A. Long, and H.W. Sohns, "Oil Shale Retorting in a 150-Ton Batch-

Type Pilot Plant," U.S. Bureau of Mines Report of Investigations 7995, 1974, 31 pp.]

The University of Wyoming is conducting a research project under an ERDA contract to develop mathematical models of in situ oil shale retorting. The results being sought include: modification and extension of existing kinetic models for kerogen decomposition; incorporation of fracturing techniques into the overall retorting model; development of mathematical models to describe the time-temperature profiles and oil yields in forward combustion retorting; and development of a control system to optimize the retorting process.

Application of the in situ recovery process to oil shale has been tested by the Laramie Energy Research Center during field experiments near Rock Springs, Wyoming. The results of those tests demonstrate that a self-sustaining combustion zone can be created in an oil shale bodey, that this zone can be moved through the oil shale, and that the process will produce shale oil [E.L. Burwell, T.E. Sterner, and H.C. Carpenter, "U.S. Bureau of Mines Report of Investigations 7783, 1973, 41 pp; H.E. Carpenter, "In Situ Oil Shale Processing Research in the Rock Springs, Wyoming, Area," presented at the American Nuclear Society meeting in San Francisco, California, November 20, 1975.]

Several private companies have submitted proposals to ERDA for in situ field experiment projects. Among those companies are Occidental, Tally Frac, Geokinetics, and Equity. Negotiations are presently underway to determine the precise nature of the experiments to be conducted. The status of those projects will be monitored as they progress.

The Colorado School of Mines under an ERDA contract is conducting a research project to formulate and develop a boundary layer model for the description of oil shale retorting processes. The boundary layer model differs from other mathematical models in several respects: it does not assume a constant rate of propagation of the combustion zone during retorting; it permits inclusion of an eqution for fuel (carbon residue) concentration in the mathematical description of the combustion process; it is not necessary to subdivide the retorting model into a chemical-kinetics model and a thermal model because the equations describing species concentrations and temperature distribution are solved simultaneously; and it is possible to compute "influence coefficients" which express the sensitivity of measurable combustion properties to questionable input data.

6.2.3 Oil Shale Activities at Lawrence Livermore Laboratory

A meeting was held on October 31, 1976, at Lawrence Livermore Laboratory (LLL) near Livermore, California, between D.W. Fausett, T.A. Sladek and several LLL staff members. LLL is a large research and development facility operated by the University of California for the Energy Research and Development Administration. LLL was established in 1952 by the Atomic Energy Commission and was operated for the AEC until AEC's non-regulatory activities were aabsorbed by ERDA at the time of its creation.

LLL employs nearly 6,000 technical, administrative and clerical personnel. Of this total, 10 engineers and scientists are in oil shale related work, with most of their activities

concentrating on development of in situ technology. In 1975, LLL proposed to ERDA a massive six-year development program entitled "Rubble In Situ Extraction" (acronym RISE) which would have culminated in a field demonstration of modified in situ retorting. The overall program would have cost approximately $80 million.

RISE has not yet been funded by ERDA, but LLL is proceeding with research in several areas which were included in the RISE proposal. Many of LLL's activities can be of utility to this program, and it is important that we maintain communication with the LLL oil shale staff regarding project progress.

Most of LLL's oil shale work is being performed by members of the Earth Sciences Group, with additional projects performed by the Organic Materials Group. Following are synopses of some of the more pertinent projects.

6.2.3.1 Pilot-Plant Studies

LLL has built and operated two modernized NTU retorts which can be used to simulate in situ retorting. Both units are cylindrical. The smaller unit has a bed diameter of one foot and bed height of 5 feet. It is well instrumented with thermowells and gas-sampling ports around the retort periphery at several axial locations. The larger unit has a bed diameter of 4 feet and a bed height of 20 feet. Instrumentation and sampling capabilities are similar to those of the smaller unit. Both units are equipped with a "traveling" thermocouple which can monitor bed emperature at any location along the retort axis during operation. The retorts are being modified for adiabatic operation and will be computer controlled.

LLL's experience with these retorts could help this program by providing wall-temperture data as functions of time for several retorting mechanisms.

6.2.3.2 Mathematical Modeling

LLL is developing a thermochemical model of retorting in a rubble-filled retort chimney. The model includes thermal conduction, gas-to-solid thermal convection, mass transport, axial dispersion, and chemical transformation of kerogen and carbonate minerals. Unfortunately, the model is for rubble only. Thermal, chemical, and physical changes in the retort wall are neglected, and the wall is treated as a zero-heat-flux boundary.

Although the LLL model is not directly applicable to the pillar program, it may still be useful in two ways. At a minimum, model predictions of wall temperatures, in conjunction with LLL's pilot-retort results, would provide thermal histories for use in this program. In addition, the one-dimensional LLL code could provide a starting point for development of our specialized comprehensive pillar model. Both possibilities were discussed with the LLL staff. They were receptive and encouraging of a cooperative effort.

6.2.3.3 Mechanical Properties

LLL is studying the behavior of oil shale rubble beds under axial loading. Prior work was principally theoretical, but some room-temperature tests of bed loading have been performed. Additional testing at elevated temperatures is planned and may include bed-permeability studies under triaxial loading.

LLL plans to sponsor some studies of the rock mechanics of solid oil shale at elevated temperatures. Work will be done by Texas A&M University and will involve one grade of shale. LLL may be able to provide us with a chunk of the shale for our physical-test program. Results would provide a cross-check for both studies.

6.2.3.4 Heating of Oil Shale Blocks

Three studies are being conducted which may be of use to this program. First is a study of the thermal behavior of large blocks of shale during retorting. This project is being conducted to investigate some thermal anomalies observed by the LERC staff during retorting of large shale pieces in the 150-ton NTU at Laramie. LERC reported that center temperatures in a large (7000-pound) block increased much more rapidly than would be expected if thermal conduction were the only heat-transfer path into the block. At first, it was suspected that oxygen was diffusing into the block and causing oxidation to occur in the interior, with subsequent generation of excess heat and rapid temperature rise near the center. Further investigation revealed that "observed" center temperatures were false and resulted for shorting of the thermocouples at the block surface. As part of this project, LLL investigated a pressure pulse phenomenon observed during block retorting. The pulse was found to be related to rapid burning of shale oil and/or gas at the block surface when the block was heated in air. No pulsation was detected when the blocks were heated in nitrogen. This may have relevance to retorting of pillar material in our study. Surface combustion may be sporadic, and this may complicate our modeling effort.

The second project is an investigation of reactions between shale char (residual carbon) and CO_2 in the retort gas stream. Results were reported at the 9th. Oil Shale Symposium in Golden in 1976. The third project is to study the effects of block size on oil yield. Several investigators have reported that large blocks suffer in oil yield during retorting, and LLL is investigating mechanisms which may be responsible. This work is just beginning.

6.2.3.5 Summary

LLL has several projects proposed and underway which may be of significant value to the pillar program. Included are pilot-plant retorting tests, mathematical modeling, bed-strength tests, rock mechanics, and block-heating tests. Exchange of information between the groups would be of mutual benefit and has the potential for substantial time and cost savings for our program. Potential cooperative efforts should be pursued.

6.2.4 Fenix and Scisson Models

Under USBM funding, Fenix and Scisson of Tulsa, Oklahoma, has completed "Technical and Economic study of an Underground Mining, Rubblization, and In Situ Retorting System for Deep Oil Shale Deposits." Several major questions arose related to the behavior of oil shale at elevated temperatures as a result of that study.

Several modified in situ systems were investigated, but two were considered as having the greatest potential:

1. Room and Pillar-Vertical Drill and Blast,
2. Tunnel Boring-Horizontal Ring Drill and Blast

A base 50,000BPD facility was assumed, requiring multiple fired retorts. The retort rubblization and firing was staggered to reduce the likelihood of excessively large temperature anomalies causing surface disruption. The possibility of restabilization of the burned retorts was also investigated as a possible means of increasing resource recovery. Their chamber sizes were on the order of 180 to 220 feet square with a central pillar of 40 to 80 feet square. Separation between chambers was initially set at 30 to 50 feet. They were very interested in possible recovery from these barrier walls and pillars. For design purposes, they assumed a depth of 1000 feet.

When asked about burn rates they said that $\frac{1}{2}$" per hour to 4"per hour was assumed for their work. Apparently, ERDA is considering rates of up to 8" per hour. They envisaged maintaining production from a chamber for up to 6 months, indicating long term recoveries from walls and pillars could be a significant factor.

They seemed quite enthusiastic that this study was being pursued and promised full cooperation throughout the program.

6.2.5 Oil Shale Activities at Occidental Petroleum

Occidental Petroleum (Oxy) has substantial oil shale holdings in the Piceance Basin and has been active in development of in situ retorting since acquiring the Garrett Research and Development Company several years ago. Oxy, through subsidiary Occidental Oil Shale, Inc., is perhaps the most active in situ oil shale company in the private sector and is certainly the most visible, having released numerous publications of general interest on in situ retorting. Unfortunately, very little

technical information has been released and very little is anticipated. Oxy is a private corporation and does not hold any major government contracts in oil shale development. Oxy has spent over $30 million of its own funds on oil shale in the last five years. In order to protect this investment and to assure a favorable competitive position, Oxy chooses to maintain a proprietary position with respect to data generated in its tests.

Oxy did respond to ERDA Fossil Energy Program Opportunity Notice No. 2 which was issued in February, 1976, for in situ oil shale demonstration programs. Oxy was one of four companies selected by ERDA for negotiation of final development contracts. Proposal review and contract negotiations are continuing, and Oxy chooses not to endanger its position in the negotiations by releasing details of its proposed demonstration program. Richard D. Ridley, Executive Vice President and Manager of Operations, Occidental Oil Shale, Inc., did state retorts, each with a capacity of 500-2000 barrels per day (BPD), and will have a net capacity of 5,000-10,000 BPD. The proposed plant will be located at the Oxy's present site along Logan Wash on the southern fringe of the Piceance basin. The program will consist of a relatively short engineering and design phase followed by construction and operation of the retorts. Mr. Ridley did not provide an overall time estimate for the demonstration program.

Oxy will proceed with its demonstration program regardless of the outcome of the PON solicitation. To date, Oxy has built and fired four in situ retorts which ranged in size from the small initial unit which contained 3,000 to 4,000 tons of shale and yielded 1,200 barrels of oil to the largest unit which had a

capacity of 500 barrels per day and which yielded over 30,000 barrels of crude shale oil. The latest retort was first fired in December, 1975, and burned to completion in June, 1976. Much of the rubble in the retort was quite lean with oil yields in the 10-15 gallon-per-ton range. Shale oil produced from this retort was submitted to applications testing in an undisclosed area. The next step is the demonstration plant which, according to Oxy, will "prove conclusively the economics of the process, provide a practical demonstration that Oxy's approach is acceptable from an environmental point of view, and show the extent to which it can employ poorer quality shale rock on a large scale."

All of Oxy's field experiments have been conducted at Logan Wash in low-quality shale with oil yield in the area of 15 gallons per ton. All have used the modified or mine-assisted approach in which 10-30% of the shale in the retort region is mined, and the remaining shale is rubbled by controlled blasting to produce a pseudo-NTU retort in situ. Shale at the top of the rubble pile is ignited, and an air-gas mixture is fed to the top of the pile to carry the flamefront vertically downwards through the pile. Crude shale oil produced as the front progresses trickles through the rubble pile and collects in a sump from which it is pumped to the surface for processing and disposition. Retort gases are a mixture of combustion products, atmospheric nitrogen, and some hydrocarbons. Gas heating value is quite low.

Oxy has considered alternatives to combustion retorting, such as the gas-recycle mode of operation which would produce higher quality oil and gas. Use of spent retorts as gas scrubbers has

also been considered as a method for reducing gaseous emissions from the retorting operation. This possibility should be of interest to our present program, since passage of hot or cold gases through a burned-out retort would affect the thermal history of the barrier walls and hence would affect their strength and stability.

Oxy has conducted a number of studies pertinent to our program, but results are propriety. Included are "some" mechanical-property measurements at elevated temperatures but not under confining pressure. No thermal-property data have been measured. Particle-size distribution has been estimated in the pilot retorts. A mathematical model of the retort was developed with existing property data from Laramie and was verified by the field tests. Mr. Ridley was pessimistic that we would be allowed to use our data in Oxy's model, but he would entertain a formal request for a cooperative effort in that area. Included in Oxy's PON proposal was some study of rock mechanics in cooperation with the Bureau of Mines Denver Mining Research Center.

Oxy estimates that a commercial plant based on modified in situ retorting at the Logan Wash site could produce shale oil with a market price of approximately $12 per barrel. At this level, the product would be competitive with new domestic crude petroleum and with OPEC crude. This estimate was based on retorting of lean, 10-20 gallon-per-ton shale. Costs for richer shales should be substantially lower, but Mr. Ridley was not sure that modified retorting could utilize the rich deeply-buried shales near the depocenter of the basin.

The possiblity of acquiring samples from the area of Occidental's retorting operation was discussed and will be evaluated against other sources or as a possible co-source of sample.

6.2.6 Activities at Western Oil Shale Corp.

The Western Oil Shale Corportion (WESTCO) had submitted an in situ plan to ERDA, but is no longer under consideration for demonstration funding. WESTCO is, however, still proceeding on their own but at a reduced scale. They displayed considerable interest in our proposed testing program and offered to supply us with their retort model geometry and operating conditions providing the corporate members agreed. Contact will be maintained throughout the contract.

6.2.7 Equity Oil Company

Equity Oil Company is one of the organizations under consideration for a field demonstration in situ retort. They were very enthusiastic about our work and offered to send us their retort plans and provide us with the pertinent retort parameters. Equity will also send us copies of the background information they have collected.

Equity Oil's process is closer to true in situ and they anticipate using lower temperatures to generate a better quality of shale oil. Much valuable information for model design and process evaluation should result from mutual cooperation between our organizations.

6.2.8 Other and Future Sources of Information

The pursuance and maintenance of technical communication with industries and agencies involved with in situ retorting of oil

shale is ongoing. As mentioned, communication is often one-sided as proprietary restrictions limit transfer of technology.

Often contact with individual organizations or attendance at technical meetings results in additional oil shale related projects being revealed. As related work becomes apparent, we will make contact with the organizations involved and try to set up the most mutually beneficial transfer of data or results.

1. Agapito, J. F., 1972, Pillar design in competent bedded formations: Ph.D. Thesis, Dept. of Mining Engr., Colorado School of Mines.

2. Agapito, J. F., 1974, Rock mechanics applications to the design of oil shale pillars: Mining Engr., v. 26, no. 5, p. 20-5.

3. Alexander, J. D., and others, 1962, Factors affecting fuel availability and composition during in situ combustion: Jour. of Petr. Tech., October, p. 1154-62.

4. Allred, V. D., and Merril, L. S., Jr., 1964, Ignition characteristics of Colorado oil shale: ACS Div. Fuel Chem. Preprints, v. 8, no. 1, Papers presented at 147th National Meeting, Philadelphia, April 5-10.

5. Allred, V. D., 1964, Some characteristic properties of Colorado oil shale which may influence in-situ processing: CSM Quart. v. 59, no. 3, July, p. 47-76.

6. Allred, V. D., 1965, Countercurrent combustion: a process for retorting oil shale: Chem. Engr. Prog. Symp. Series No. 54, 61, p. 60.

7. Allred, V. D., 1967, Shale oil developments -- Kinetics of oil shale pyrolysis: CSM Quart. v. 62, no. 3, July, p. 91-109.

8. Allred, V. D., 1966, Kinetics of oil shale pyrolysis: Chem. Eng. Prog., v. 62, no. 8, August, p. 55-60.

9. Allsman, P. T., 1968, A simultaneous caving and surface restoration system for oil shale mining: CSM Quart. v. 63, no. 4, October, p. 113-126.

10. American Institute of Mining and Metallurgical Engineers, 1974, Proceedings of the first five Oil Shale Symposia: 1964-1968 (held at the Colorado School of Mines and published in the CSM Quarterlies): Golden, Colo., 912 p.

11. Atkins, J. O., and Peng, S. S., 1974, Compression testing of rock in simulated lunar environment: U. S. Bur. Mines RI 7983, 21 p.

12. Atwood, M. T., 1973, The production of shale oil: Chemtech, October, p. 617-21.

13. Austin, A. C., 1971, Structure contours and overburden on the top of the Mahogany zone, Green River Formation, in the northern part of the Piceance Creek basin, Rio Blanco County, Colorado: U. S. Geol. Survey Misc., Field Studies Map MF-309.

14. Bae, J. H., 1969, Some effects of pressure on oil shale retorting: S.P.E. Journal, v. 9, no. 3, September, p. 287-92.

15. Barnes, A. L., and Ellington, R. T., 1968, A look at in-situ oil shale retorting methods based on limited heat transfer contact surfaces: CSM Quart., v. 63, no. 4, October, p. 83-108.

16. Barnes, A. L., and Rowe, A. M., 1968, A feasibility study of in situ retorting process for oil shale: Soc. Pet. Engrs. J., v. 8, no. 3, September, p. 231-40.

17. Beck, B. L., and others, 1971; Analytical laboratory techniques for oil shale: ACS Div. Fuel Chem. Preprints, v. 15, no. 1, Papers presented at Los Angeles, March 29 - April 2.

18. Belser, C., 1955, Apparatus for producing oil from oil shale in situ: U. S. Patent 2,725,939, December 6.

19. Berry, V. J., Jr. and Parrish, D. R., 1960, a theoretical analysis of heat flow in reverse combustion: AIME Trans., v. 219, p. 124-31.

20. Blackburn, C. O., 1924, Investigation of oil shale kerogen by the fractionation of the primary bitumen in high vaccum and by organic extractions: CSM Quart., v. 19, no. 2, April, p. 7-46.

21. Bradley, B. T., and others, 1975, Laboratory and in situ mechanical behavior studies of fractured oil shale pillars: Rock Mechanics, v. 7, p. 101-20.

22. Braun, R. L., and Rothman, A. J., 1974, Oil shale pyrolysis: Kinetics and Mechanism of oil production: UCRL - 75974, Preprint, August 19, see also: Fuel, v. 54, April, p. 129-31.

23. Brobst, D. A., and Tucker, J. D., 1973, X-ray mineralogy of the Parachute Creek Member, Green River formation, in the northern Piceance Creek Basin, Colorado: U. S. Geol. Survey Prof. Paper 803, 53 p.

24. Brown, J. W., and Repsher, R. C., 1972, Detection of rubble zones in oil shale by the electrical resistivity technique: U. S. Bur. Mines RI 7674, 17 p.

25. Burwell, E. L., and others, 1970, Shale oil recovery by in situ retorting -- a pilot study: J. Pet. Tech., v. 22, December, p. 1520-4.

26. Burwell, E. L., and Jacobsen, I. A., Jr., 1974, Usable gas from oil shale during retorting: Effects of oxygen content, pressure, and oil shale grade: U. S. Bureau of Mines Technical Progress Report 85, November, 8 p.

27. Burwell, E. L. and others, 1973, In situ retorting of oil shale -- results of two field experiments: USBM RI 7783, 41 p.

28. Burwell, E. L., and others, 1974, Permeability changes and compaction of broken shale during retorting: USBM RI 7860, 16 p.

29. Campbell, W. G., and others, 1970, Evaluation of oil shale fracturing experiments near Rock Springs, Wyo.: USBM RI 7397, 21 p.

30. Cane, R. F., 1943, Some thermochemical properties of the torbanite of the Glen Davis deposit: Royal Society of New South Wales Jour. and Proc., v. 76, December, p. 190-202.

31. Cane, R. F., 1951, The mechanism of the pyrolysis of torbanite: Chapter in Oil shale and cannel coal, edited by George Sell. The Institute of Petroleum, London, v. II, p. 592-604.

32. Carlson, A. J., 1937, Inorganic environment in kerogen transformation: Univ. Calif. Publ. Eng., v. 3, no. 6, April, p. 295-342.

33. Carpenter, H. C., 1975, Fracturing oil shale for in situ retorting experiments: Meeting of the A. I. Ch. E., Los Angeles, November 20.

34. Carpenter, H. C., 1975, In situ oil shale processing research in the Rock Springs, Wyoming, Area: Meeting of the American Nuclear Society, San Francisco, November 20.

35. Carpenter, H. C., and Lombard, D. B., 1967, Recovering oil by retorting a nuclear chimney in oil shale: J. Pet. Tech., v. 19, no. 6, p. 727-34.

36. Carpenter, H. C., and others, 1970, Oil shale research related to proposed nuclear projects: Proc. Symp. on engineering with nuclear explosives, Las Vegas, Nevada, Jan. 14-16, 1970, v. 2, Conf-700101, May, p. 1364-75.

37. Carpenter, H. C., and others, 1972, Evaluation of an in-situ retorting experiment in Green River oil shale: J. Pet. Tech., v. 24, January, p. 21-6.

38. Carpenter, H. C., and Sohns, H. W., 1968, Application of aboveground retorting variables to in-situ oil shale processing: CSM Quart., v. 63, no. 4, October, p. 71-82.

39. Carpenter, H. C., and Sohns, H. W., 1974, Development of technology for an in-situ oil shale processes: CSM Quart., v. 69, no. 2, April, p. 143-170.

40. Cieslewicz, W. J., 1967, Present trends in Estonian-Russian work on oil shale: CSM Quart., v. 62, no. 3, July, p. 141-65.

41. Cieslewicz, W. J., 1971, Selected topics of recent Estonian-Russian oil-shale research and development: CSM Quart., v. 66, no. 1, January, 154 pp.

42. Cook, W. C., 1970, Thermal analysis of oil shales: CSM Quart., v. 65, no. 4, October, p. 133-140.

43. Couch, E. J., and Franz, F. S., 1962, Die Bedeutung des Wärmetransportes für in-situ-verbrennungsvorgänge: Erdöl und Kuhle - Erdgas - Petrochemie, v. 15, no. 7, July, p. 515-19.

44. Culbertson, W. J., and others, 1970, Disposal and uses of oil shale ash: CSM Quart., v. 65, no. 4, October p. 89-131.

45. Cummins, J. J., and Robinson, W. E., 1972, Thermal degradation of Green River Kerogen at 150° to 350°C: Rate of product formation U. S. Bur. Mines RI 7620, 15 p.

46. Cummins, J. J., and others, 1974, Thermal degradation of Green River kerogen at 150° to 350°C: Composition of products: U. S. Bur Mines RI 7924, 18 p.

47. Dannenberg, R. O., and Matzick, A., 1960, Bureau of Mines gas-combustion retort for oil shale, a study of the effects of process variables: U. S. Bur. Mines RI 5545, 73 p.

48. Decora, A. W., 1975, The outlook and status of in situ oil shale research; Meeting of the American Nuclear Society, San Francisco, November 20.

49. Decora, A. W., and Carpenter, H. C., 1976, Multi-purpose utilization of oil shale: UNITAR-IIASA Conference on Future Supply of Nature-Made Petroleum and Gas, Laxenburg, Austria, July 5-16.

50. Dimitriyer, A., and others, 1972, The physical properties of rocks at high temperatures: NASA IT-684, June.

51. Dinneen, G. U., 1965, Effect of retorting temperature on the composition of shale oil: Chem. Eng. Prog. Symp. Series No. 54, 61, p. 42.

52. Di Ricco, L., and Barrick, P. L., 1956, Pyrolysis of oil shale: Ind. and Eng. Chem., v. 48, no. 8, August, p. 1316-19.

53. Dockter, L., 1975, Combustion of oil shale carbon residue: Meeting of the A. I. Ch. E., Los Angeles, November 20.

54. Dockter, L., and others, 1971, Retorting ungraded oil shale as related to in-situ processing II: A.C.S. Preprints, Div. Fuel Chemistry, v. 15, no. 1, p. 2-11.

55. Dockter, L., and others, 1976, A mathematical model of oil shale retorting: First Rocky Mountain Fuel Symposium, Brigham Young University, Provo, Utah, January.

56. Dougan, P. M., and others, 1970, The potential for in-situ retorting of oil shale in the Piceance Creek basin of northwestern Colorado: CSM Quart., v. 65, no. 4, October, p. 57-72.

57. Dryden, J. R., 1972, Method for producing retorting channels in shale deposits: U. S. Patent 3,696,8666, October 10.

58. Duvall, J. J., and Jensen, H. B., 1975, Simulated in-situ retorting of oil shale in a controlled-state retort: CSM Quart., v. 70, no. 3, July, p. 187-205.

59. Dyni, J. R., and others, 1971, Nahcolite analyses of three drill cores from the saline facies of the Green River formation in northwest Colorado: U. S. Geol. Survey open-file rept., 13 p.

60. Dyni, J. R., and others, 1971, Thermal method for quantitative determination of nahcolite in Colorado oil shale: U. S. Geol. Surv. Prof. Paper 750B, p. B184-98.

61. Engler, C., 1913, Die Chemie und Physik des Erdöls: Vol. I of Des Erdöl: seine Physik, Chemie, Geologie, Technologie und sein Wirtschaftsbetrieb, by C. Engler and J. V. Höfer: Verlag von S. Hirzel, Leipzig, p. 30-31.

62. Fahey, J. J., 1962, Saline minerals of the Green River formation; with a section on X-ray powder data for saline minerals of the Green River formation, by M. E. Mrose: U. S. Geol. Survey Prof. Paper 405, 50 p.

63. Fausett, D. W., 1974, Mathematical study of an oil shale retort: Ph.D. Thesis, Dept. of Math., Univ. of Wyoming.

64. Fausett, D. W., 1975, A mathematical model of an oil shale retort: CSM Quart., v. 70, no. 3, July, p. 273-313.

65. Fausett, D. W., George, J. H., and Carpenter, H. C., 1974, Second-order effects in the kinetics of oil shale pyrolysis: U. S. Bur. Mines RI 7889, 21 p.

66. Feldmann, H., and Huebler, J., 1964, Hydrogasification of oil shale in a continuous flow reactor: Am. Chem. Soc., Div. Fuel Chem., v. 8, no. 1, Papers for meeting of April 5-10, p. 90-105. see also: Ind. and Eng. Chem. -- Proc. Res. and Dev., no. 2, April, p. 155-62.

67. Finncane, D., and others, A perturbation analysis of second order effects in the kinetics of oil shale pyrolysis: to be published.

68. Frost, C. M., 1972, Refining of crude shale oil produced by in-situ retorting: Am. Chemical Society Preprints, Div. Fuel Chemistry, v. 16, no. 1, p. 73-87.

69. Gary, J. H., 1965, Is thermal recovery the answer to economic production of shale oil: World Oil, August 1, p. 98-101.

70. Gavin, M. J., 1924, Oil shale -- A historical, technical, and economic study: U. S. Bur. Mines Bull. 210.

71. Gejrot, C., 1965, Development of the Swedish shale oil industry: Chem. Prog. Symp. Series No. 54, 61, p. 7.

72. George, J. H., and Harris, H. G., 1975, Mathematical modeling of in situ oil shale retorting: Presented at SIAM-SIGNUM 1975 Fall Meeting, San Francisco, Calif., December 3-5 (to appear LA SIAM J. of Num. Anal.)

73. Gosik, R. J., 1969, Thermal effects of heat losses from an insulated oil-shale sample: Master of Engineering Report, Colorado School of Mines, 69 p.

74. Grant, B. F., 1964, Sinclair retorts oil shale in place in series of tests: Oil & Gas J., v. 62, no. 29, July 20, p. 84-6.

75. Grant, B. F., 1964, Retorting shale underground -- Problems and possibilities: CSM Quart., v. 59, no. 3, July, p. 39-46.

76. Guthrie, B., 1964, Oil from rock -- the gas combustion process: CSM Quart., v. 59, no. 3, July, p. 7-18.

77. Harak, A. E., and others, 1970, Preliminary design and operation of a 150-ton oil shale retort: CSM Quart., v. 65, no. 4, October, p. 41-56.

78. Harak, A. E., and others, 1971, Some results from the operation of a 150-ton oil shale retort: U. S. Bur. Mines Tech. Prog. Rept. 30, January, 14 p.

79. Harak, A. E., and others, 1974, Oil shale retorting in a 150-ton batch-type pilot plant: U. S. Bur Mines RI 7995, 31 p.

80. Heady, H. H., 1952, Differential thermal study of Colorado oil shale: Am. Mineral, v. 37, p. 804-11.

81. Hendrickson, T. A., ed., 1975, Synthetic fuels data handbook, 1975 edition: Cameron Engineers, Denver.

82. Hermance, J., and others, 1972, Electrical properties of basalt: Relation of laboratory to in-situ measurements: J. Geophys. Res., v. 77, p. 1424.

83. Hill, G. R., and Dougan, P., 1967, The characteristics of a low-temperature in-situ shale oil: CSM Quart., v. 62, no. 3, July, p. 75-90.

84. Hill, G. R., and others, 1966, Direct production of low pour point high gravity shale oil: Am. Chem. Soc. -- Div. Fuel Chem., v. 10, no. 2, papers for meeting of March 22-31, p. 59-65. see also: Ind. and Eng Chem. -- Prod. Res. and Dev., v. 6, no. 1, March, p. 52-9.

85. Hooker, V., and Duvall, W. I., 1971, Stress investigations in Rock quarries: U. S. Bur. Mines RI 7589, 12 p.

86. Huang, J., 1971, Effective thermal conductivity of porous rocks: J. Geophys, Res., v. 76, p. 6420.

87. Hubbard, A. B., and Robinson, W. E., 1950, A thermal decomposition study of Colorado oil shale: U. S. Bur. Mines RI 4744.

88. Hull, W. Q., and others, 1951, Liquid fuels from oil shale: Ind. and Eng. Chem., v. 43, no. 1, January, p. 2-15.

89. Hutt, J., and Berg, J., 1968, Thermal and electrical conductivities of sandstone rocks and ocean sediments: Geophysics, v. 33, p. 489-500.

90. Jacobsen, I. A., Jr., and Burwell, E. L., 1976, Effects of space velocity on quality and quantity of gas from oil shale retorting: U. S. ERDA Report of Investigations LERC/RI-75/1, June, 27 p.

91. Jensen, H. B., and others, 1971, Characterization of a shale oil produced by in situ retorting: ACS Div. Fuel Chem. Preprints, v. 15, no. 1, Papers presented at Los Angeles, March 29 - April 2.

92. Johnson, D. R., and Smith, J. W., 1970, Bureau of Mines apparatus for thermal analysis: simultaneous DTA-TG-EGA for oil shale and solid fuels: U. S. Bur. Mines RI 7429, 17 p.

93. Johnson, D. R., and others, 1974, Thermal characteristics of shortite: U. S. Bur. Mines RI 7862, 9 p.

94. Johnson, W. F., and others, 1975, In situ retorting of oil shale rubble: A model of heat transfer and product formation in oil shale particles: CSM Quart., v. 70, no. 3, July, p. 237-72.

95. Jones, D. G., and Dickert, J. J., Jr., 1965, Composition and reactions of oil shale of the Green River formation: Chem. Eng. Prog. Symp. Series, v. 61, no. 54, p. 34-41.

96. Jones, J. F., and others, 1966, Pyrolysis of oils derived from coal and oil shale in fluidized bed of catalysts: Am. Chem. Soc. -- Div. Fuel Chem., v. 10, no. 2, papers for meeting of March 22-31, p. C79-87.

97. Jukkola, E. E., and others, 1953, Thermal decomposition rates of carbonates in oil shale: Ind. and Eng. Chem., v. 45, no. 12, December, p. 2711-14.

98. Karrick, L. C., 1922, Some factors affecting products from destructive distillation of oil shales: U. S. Bur. Mines RI 2324, 5 p. (see also Chem. Age, v. 30, March 1922, p. 112-14).

99. Karrick, L. C., 1923, Effects of temperature and time of reaction in distilling oil shales on the yields of properties of crude oils: U. S. Bur. Mines RI 2456, 8 p.

100. Knapp, R. H., and Aris, R., 1972, On the equations for the movement and deformation of a reaction front: Arch. Rational Mech. Anal., v. 44, no. 3, p. 165-77.

101. Lekas, M. A., 1966, Economics of producing shale oil, the nuclear in-situ retorting method: CSM Quart., v. 61, no. 3, July, p. 91-114.

102. Lekas, M. A., and Carpenter, H. C., 1965, Fracturing oil shale with nuclear explosives for in-situ retorting: CSM Quart., v. 60, no. 3, July, p. 7-30.

103. Lesser, H. A., and others, 1967, Conduction heating of oil shale formations: CSM Quart., v. 62, no. 3, July, p. 111-112. see also: Soc. Petr. Engrs. J., v. 6, no. 4, December, 1966, p. 372-82.

104. Linden, H. R., 1965, Conversion of solid fossil fuels to high-heating value pipeline gas. Chem. Eng. Prog. Symp. Series, no. 54, v. 61, p. 76-103.

105. Lindroth, D. P., 1974, Thermal diffusivity of six igneous rocks at elevated temperatures and reduced pressures: U. S. Bur. Mines RI 7954, 33 p.

106. Lorenz, P. B., 1973, Radioactive tracer pulse method of evaluating fracturing of underground oil shale formations: U. S. Bur. Mines RI 7791, 33 p.

107. Maier, C. G., and Zimmerly, S. R., 1924, The chemical dynamics of the transformation of the organic matter to bitumen in oil shale: University of Utah Bulletin, no. 14, p. 62-81.

108. Mains, C. J., and Matzick, A., 1953, Theoretical considerations of heat transfer in the gas-flow oil-shale retort: U. S. Bur Mines RI 4995, August, 11 p.

109. Mallon, R. G., and Miller, W. C., 1975, Thermal behavior of oil shale blocks heated in air: CSM Quart., v. 70, no. 3, p. 221-36.

110. Marshall, P. W., 1974, Colony Development Operation room-and-pillar oil shale mining: CSM Quart., v. 69, no. 2, April, p. 171-84.

111. Matic, D., and Mijatovic, I., 1965, Retorting of Yugoslav (Aleksinac) oil shale by gas combustion retort: Chem. Eng. Prog. Symp. Series No. 54, 61, p. 15.

112. Matzick, A., and others, 1960, Experiments in crushing Green River oil shale: U. S. Bur. Mines RI 5563, 64 p.

113. McKee, R. H., and Lyder, E. E., 1921, The thermal decomposition of shales, I - Heat effects: Ind. and Eng. Chem., v. 13, no. 7, July, p. 613-18.

114. McKee, R. H., and Lyder, E. E., 1921, The thermal decomposition of oil shales. II - Determination of the heat of reaction involved in their thermal decomposition: Ind. and Eng. Chem., v. 13, no. 8, August, p. 678-84.

115. Melton, N. M., and Cross, T. S., 1967, Fracturing oil shale with electricity: CSM Quart., v. 62, no. 3, July, p. 45-62. see also: J. Pet. Tech., v. 20, no. 1, January, p. 37-41.

116. Merrill, R. H., 1954, Design of underground mine openings oil shale mine, Rifle, Colorado: U. S. Bur. Mines RI 5089, 56 p.

117. Meyer, W. C., and Yen, T. F., The effects of bio-leaching on Green River oil shale: ACS Div. Fuel Chem. Preprints, v. 19, no. 2, Papers presented at 167th National Meeting, Los Angeles, April 1-5.

118. Miller, J. S., and Howell, W. D., 1967, Explosive fracturing tested in oil shale: CSM Quart., v. 62, no. 3, July, p. 63-74.

119. Miller, J. S., and Johansen, R. T., 1974, Fracturing oil shale with explosives for in situ recovery: ACS Div. Fuel Chem. Preprints, v. 19, no. 2, Papers presented at 167th National Meeting, Los Angeles, April 1-5.

120. Miller, J. S., and Nicholls, H. R., 1973, Methods and evaluation of explosive fracturing in oil shale: U. S. Bur. Mines RI 7729, 22 p.

121. Mityurev, A. K., 1962, Mechanism and kinetics of thermal decomposition of Baltic shales: Chem. and Tech. of Combustible Shales and their Products, June, p. 205-21.

122. Mityurev, A. K., 1962, Fundamentals of theory of thermal decomposition of solid fuel: Chem. and Tech. of Combustible Shales and their Products, June, p. 222-46.

123. Murphy, W. I. R., 1960, In-situ shale-oil production problems: Univ. Calif. Radiation Lab (Livermore, Calif.) and San Francisco Operations Office: U. S. Atomic Energy Commission, Plowshare Series, UCRL-5678, Part IV, 1960, p. 80-101.

124. Nevans, T. D., 1966, Gaseous and particulate emissions from shale oil operations: ACS Div. Fuel Chem. Preprints, v. 10, no. 1, Papers presented at 151st Annual Meeting, Pittsburgh, March 22-31.

125. Obert, L., and Merrill, R. H., 1958, Oil shale mine, Rifle, Colorado: a review of design factors: U. S. Bur. Mines RI 5429, 13 p.

126. Pforzheimer, H., 1974, Paraho-New prospects for oil shale: Chem. Eng. Prog., v. 70, no. 9, September, p. 62-5.

127. Poulson, R. E., and others, 1974, Characteristics of synthetic crude from crude shale oil produced by in situ combustion retorting: ACS Div. Fuel Chem. Preprints, v. 19, no. 2, Papers presented at 167th National Meeting, Los Angeles, April 1-5.

128. Powell, R., 1971, Thermal comparator methods, in Thermal Conductivity, v. 2: Academic Press, R. Tye, editor.

129. Prats, M., and O'Brien, S., 1975, Thermal conductivity and thermal diffusivity of Green River oil shale: J. Pet. Tech., January, p. 97-106.

130. Ramey, H. J., Jr., 1971, In situ combustion: Proceedings of the Eighth World Petroleum Congress, vol. 3, Applied Science Publ. Ltd., Essex, England, p. 253-62.

131. Rand, W. P., 1933, Generation of oil in rocks by shearing pressures: IV - V. Further studies of effects of heat on oil shales: Am. Assoc. Petroleum Geologists Bull., v. 17, p. 1229-50. (Petroleum Research Corp. Microfilm Card 48 0 26.).

132. Reed, J. J., 1966, Rock mechanics applied to oil shale mining: CSM Quart., v. 61, no. 3, July, p. 45-54.

133. Ridley, R. D., 1974, In-situ processing of oil shale: CSM Quart., v. 69, no. 2, April, p. 21-24.

134. Robinson, W. E., and Cook, G. L., 1971, Compositional variations of the organic material of the Green River oil shale - Colorado No. 1 core: U. S. Bur. Mines RI 7492, 32 p.

135. Robinson, W. E., and Cook, G. L., 1973, Compositional variations of organic material from Green River oil shale Wyoming No. 1 core: U. S. Bur. Mines RI 7820, 32 p.

136. Robinson, W. E., and Cummins, J. J., 1960, Compositions of low-temperature thermal extracts from Colorado oil shale: Jour. Chemical Engineering Data, v. 5, p. 74-80.

137. Robinson, W. E., and Hubbard, A. B., 1951, Study of preheating oil shale: U. S. Bur. Mines RI 4787, April, 13 p.

138. Robinson, W. E., and others, 1963, Oxidation of Colorado oil shale: U. S. Bur. Mines RI 6166, 33 p.

139. Rogers, M. P., 1974, A bibliography of Bureau of Mines publications dealing with oil shale and shale oil 1917-1974: U. S. ERDA, Laramie Energy Research Center, OSRD 59, December, 44 p.

140. Rose, C. K., and Utter, S., 1955, Cutting action of rotary bits in oil shale: U. S. Bur. Mines RI 5174, 24 p.

141. Rothman, A. J., 1975, Research and development of rubble in situ extraction of oil shale (RISE) at Lawrence Livermore Laboratory: CSM Quart., v. 70, no. 3, July, p. 159-78.

142. Sarapuu, E., 1965, Underground electrocarbonization of oil shale: CSM Quart., v. 60, no. 3, July, p. 198-205.

143. Shaw, A. J., 1947, Specific heat of Colorado oil shales: U. S. Bur. Mines RI 4151, 9 p.

144. Shell Oil Company, 1974, In situ recovery of shale oil: U. S. Patent 3,804,169 (see September 1974 Synthetic Fuels for description).

145. Shell Oil Company, 1974, In situ recovery of shale oil: U. S. Patent No. 3,804,172 (see September 1974 Synthetic Fuels for description).

146. Shul'man, A. I., and Proskuryakov, V. A., 1968, Study of the kinetics of the isothermal decomposition of Leningrad shale kerogen at the stage of bituminization. (Transl. from Russian): Khim. Teknol. Goryuch. Slantsev Prod. Ikh Pererab, p. 278-94.

147. Silver, R. S., 1953, Theoretical treatment of combustion in fuel beds I - Gas composition and heat release: Fuel, v. 32, p. 121-37.

148. Silver, R. S., 1953, Theoretical treatment of combustion in fuel beds II - Temperature attained in combustion: Fuel, v. 32, p. 138-50.

149. Sinel'nikov, A. S., 1962, Processing of shale in USSR: Chem. and Tech. of Combustible Shales and Their Products, June, p. 3-20.

150. Sipprelle, E. M., and Teichman, H. L., 1950, Roof studies and mine structure stress analysis, Bureau of Mines oil-shale mine, Rifle, Colorado. Trans. AIEM, v. 187, October, p. 1031-6.

151. Skinner, E. H., and others, 1974, In situ determination of rock behavior by overcore stress relief method, physical property measurements, and initial deformation method: U. S. Bur. Mines RI 7962, 87 p.

152. Sladek, T. A., 1969, Determination of low-temperature thermal conductivities for several grades of oil shale: M.S. Thesis, Colorado School of Mines, 51 p.

153. Sladek, T. A., 1970, A determination of composition and temperature dependencies of thermal conductivity factors for Green River oil shale: Ph.D. Thesis, Colorado School of Mines, 99 p.

154. Sladek, T. A., 1974, Recent trends in oil shale -- Part 1: History, nature and reserves, Mineral Ind. Bull., v. 17, no. 6, 20 p.

155. Sladek, T. A., 1975, Recent trends in oil shale -- Part 2: Mining and shale oil extraction processes: Mineral Ind. Bull, v. 18, no. 1, January, 21 p.

156. Sladek, T. A., 1975, Recent trends in oil shale -- Part 3: Shale oil refining and some oil shale problems: Mineral Ind. Bull., v. 18, no. 2, March.

157. Smith, J. W., 1956, Specific gravity-oil yield relationships of two Colorado oil-shale cores: Ind. Eng. Chem., v. 48, p. 441-4.

158. Smith, J. W., 1962, Analytical method for study of thermal degradation of oil shale: U. S. Bur. Mines RI 5932, 17 p.

159. Smith, J. W., 1969, Theoretical relationship between density and oil yield for oil shares: U. S. Bur. Mines RI 7248, April, 14 p.

160. Smith, J. W., 1968, Oil yields of Green River oil shale from Colorado Corehole No. 1: U. S. Bur. Mines RI 7071.

161. Smith, J. W., and others, 1968, Characteristics of Green River oil shales at Bureau of Mines Wyoming Corehole No. 1: U. S. Bur. Mines RI 7172.

162. Smith, J. W., and others, 1972, Oil yields and characteristics of Green River Formation oil shares at Wasco Ex-1, Unitah County, Utah: U. S. Bur. Mines R.I. 7693.

163. Smith, J. W., and Trudell, L. G., 1968, Wyoming Corehole No. 1 -- A potential site for production of shale oil in place: CSM Quart., v. 63, no. 4, October, p. 55-69.

164. Smith, J. W., and Young, N. B., 1969, Determination of dawsonite and nahcolite in Green River formation oil shales: U. S. Bur. Mines RI 7286, 20 p.

165. Snyder, P. W., Jr., and others, 1974, An evaluation of in-situ oil shale retorting: Paper presented at the NSF Workshop on In-situ Oil Shale Retorting, La Jolla, California, September 3-7.

166. Sohns, H. W., and Carpenter, H. C., 1966, In situ oil shale retorting: Chem. Eng. Prog., v. 62, no. 8, August, p. 75-8.

167. Sohns, H. W., and others, 1951, Heat requirements for retorting oil shale: Ind. and Engr. Chem., v. 43, no. 1, January, p. 33-6.

168. Somerton, W. H., and Boozer, G. D., 1960, Thermal characteristics of porous rocks at elevated temperatures: Pet. Tech. Jour., v. 12, p. 77-81.

169. Stanfield, K. E., and Frost, I. C., 1949, Method of assaying oil shale by a modified Fischer retort: U. S. Bur. Mines RI 4477, 13 p.

170. Stanfield, K. E., and others, 1951, Properties of Colorado oil shale: U. S. Bur. Mines RI 4825, 27 p.

171. Stanfield, K. E., and others, 1954, Oil yields of sections of Green River oil in Colorado, Utah, and Wyoming, 1945-52: U. S. Bur. Mines RI 5081.

172. Stanfield, K. E., and others, 1960, Oil yields of sections of Green River oil shale in Colorado, 1954-57: U. S. Bur. Mines RI 5614.

173. Stanfield, K. E., and others, 1964, Oil yields of sections of Green River oil shale in Utah, 1952-62: U. S. Bur. Mines RI 6420.

174. Stanfield, K. E., 1966, Progress report on Bureau of Mines-Atomic Energy Commission corehole, Rio Blanco County, CSM Quart., v. 61, no. 3, July, p. 33-44.

175. Stanfield, K. E., and others, 1967, Oil yields of sections of Green River oil shale in Colorado, 1957-63: U. S. Bur. Mines RI 7051.

176. Sterner, T. E., and others, 1975, Evaluation of in situ oil shale experiments by hot-film logging: U. S. ERDA Report of Investigations LERC/RI-75/1.

177. Stout, N. D., and others, 1976, Pyrolysis of oil shale: The effects of thermal history on oil yield: LLL Preprint UCRL-77831, April 27.

178. Thomas, G. W., 1963, A theoretical analysis of forward combustion in petroleum reservoirs: Ph.D. Dissertation, Dept. of Petroleum Eng., Standord Univ.

179. Thomas, G. W., 1966, Some effects of overburden pressure on oil shale during underground retorting: Soc. Pet. Engr. J., v. 6, no. 1, March, p. 1-8.

180. Thring, M. W., 1952, Physics of fuel bed combustion: Fuel, v. 31, p. 355-64.

181. Thurmala, M., and Clark, E., 1967, Dynamic Rock Mechanics: Society of Mining Engineers, New York, p. 697.

182. Tihen, S. S., and others, 1968, Thermal conductivity and thermal diffusivity of Green River oil shale: Proc. 7th Conf., NBS Spec. Publ. No. 302, September, p. 529-535.

183. Tisot, P. R., 1967, Alterations in structure and physical properties of Green River shale by thermal treatment: J. Chem. Eng. Data, v. 12, no. 3, July, p. 405-11.

184. Tisot, P. R., and Murphy, W. I. R., 1960, Physiocochemical properties of Green River oil shale, particle size and particle size distribution of inorganic constituents: J. Chem. Eng. Data, v. 5, no. 4, p. 558-62.

185. Tisot, P. R., and Murphy, W. I. R., 1963, Physical structure of Green River oil shale from Colorado: U. S. Bur. Mines RI 6184, 24 p.

186. Tisot, P. R., and Murphy, W. I. R., 1965, Physical structure of Green River oil shale: Chem. Eng. Prog. Symp. Series No. 54, 61, p. 25.

187. Tisot, P. R., and Sohns, H. W., 1970, Structural response of rich Green River oil shales to heat and stress and its relationship to induced permeability: Chem. Eng. Data, v. 15, no. 3, p. 425-34.

188. Tisot, P. R., and Sohns, H. W., 1971, Structural deformation of Green River oil shale as it relates to in-situ retorting: U. S. Bur. Mines RI 7576, 27 p.

189. Tissot, B., 1969, Premieres donnees sur les mecanismes et la cinetique de la formation du petrole dans les sediments, simulation d'un schema reactionnel sur ordinateur: Rev. Inst. Francais Petr., v. 24, no. 4, p. 470-501.

190. Tyler, A. L., 1975, Excess heat generation in retorting oil shale in air: CSM Quart., v. 70, no. 3, p. 207-20.

191. Vulis, L. A., 1961, Thermal regimes of combustion. (Transl. from Russian by Morris D. Friedman): McGraw-Hill Book Co., Inc., New York, p. 193-245.

192. Warren, J. E., 1960, Reverse combustion: Ph.D. Thesis, Dept. of Petroleum and Natural Gas Engr., Pennsylvania State Univ.

193. Weichman, B., 1974, The superior process for development of oil shale and associated minerals: CSM Quart., v. 69, no. 2, April, p. 25-44.

194. Weil, S. A., and others, 1974, Hydrogasification of oil shale: ACS Div. Fuel Chem. Preprints, v. 19, no. 2, Papers presented at 167th National Meeting, Los Angeles, April 1-5.

195. Weitkamp, A. W., and Gutberlet, L. C., 1970, Application of a microretort to problems in shale pyrolysis: Ind. and Eng. Chem., Process Design Dev., v. 9, no. 3, p. 386-95.

196. Williams, F. A., 1965, Combustion theory: Addison-Wesley Publ. Co., Inc., Reading, Mass., p. 95-136.

197. Williamson, D. R., 1964, Oil shales, Part 4: Retorting and other beneficiation of oil shales: CSM Mineral Ind. Bull., v. 7, no. 6, November, 13 p.

198. Wise, R. D., and others, 1971, Heat content of some Green River oil shales: U. S. Bur. Mines RI 7482, March, 16 p.

199. Yen, T. F., 1974, A new structural model of oil shale kerogen: ACS Div. Fuel Chem. Preprints, v. 19, no. 2, Papers presented at 167th National Meeting, Los Angeles, April 1-5.

200. Young, N. B., and Smith, J. W., 1970, Dawsonite and nahcolite analyses of Green River formation oil-shale section, Piceance Creek Basin, Colorado: U. S. Bur. Mines RI 7455, 22 p.

201. Young, D. K., and others, 1974, Stepwise oxidation of bioleached oil shale: ACS Div. Fuel Chem. Preprints, v. 19, no. 2, Papers presented at 167th National Meeting, Los Angeles, April 1-5.

202. Zambas, P. G., and others, 1972, Large-scale experimentation in oil shale: Soc. Mining Engineers, AIME, Trans., v. 252, no. 3, p. 283-89.

203. Zimsmeister, G., and Ong-Oh, A., 19 , Heat conduction in materials with thermal properties dependent on temperature history: Advances in Heat Transfer, v. 8.

6.4 Measurement of Thermal Transport Properties by a Transient Method *

6.4.1 Introduction

The thermal transport properties of an isotropic material are completely defined by any two of the three parameters: conductivity (K), diffusivity (k), and heat capacity (c_p). As these three parameters are related by the equation:

$$K = \rho c_p k$$

where ρ is the density, knowledge of any of two can be utilized to calculate the third.

The parameters defining thermal transport in a material are usually measured independently. The Transient Method presented here determines directly from the temperature data of a continuously heated sample both the diffusivity and heat capacity of the sample and from them deduces the conductivity.

The method offers several important advantages. The thermal transport properties are obtained from a unique sample. Compared to steady-state methods, the transient method is fast, automatic, and can provide data on a continuous basis during sample heating. The transient-thermal-analysis method enables the thermal transport behavior of chemically reactive samples (with endo or exothermic chemical reactions) to be determined.

* Excerpted from Christophe Petit's M.S. Thesis, Civil Engineering Dept., Colorado State University

6.4.2 Fundamental Formulae

For a homogeneous isotropic solid whose thermal conductivity is independent of temperature, we have

$$\frac{\partial^2 T}{\partial x^2} + \frac{\partial^2 T}{\partial y^2} + \frac{\partial^2 T}{\partial z^2} - \frac{1}{k}\frac{\partial T}{\partial t} = 0$$

where $k = \frac{K}{\rho c_p}$ is the diffusivity

and K, ρ, and c_p are respectively the conductivity, density and heat capacity. We assume there is no heat production.

This equation is the equation of conduction of heat which, for one-dimensional flow becomes:

$$\frac{\partial^2 T}{\partial x^2} - \frac{1}{k_x}\frac{\partial T}{\partial t} = 0 \qquad (6.4.1)$$

where k_x is the diffusivity in the x-direction.

In the case of linear flow of heat in a solid bounded by two parallel planes, the rate of heat gain per unit volume is

$$\frac{\partial Q}{\partial t} = \rho\, c_p \frac{\partial T}{\partial t} \qquad (6.4.2)$$

The flux of heat at a point across any surface is

$$q = - K \frac{\partial T}{\partial x} \qquad (6.4.3)$$

where $\frac{\partial T}{\partial x}$ denotes the differentiation of T in the direction of outward normal x.

If q is known for two parallel planes, then the heat Q, gained (or lost) for the region between the planes may be calculated, and a measurement of the temperature change in the region can be used with Equation (6.4.2) to calculate c_p, the heat capacity.

6.4.3 Basis of the Transient Method

The stack used for the transient method is shown in Figure 6.4.1. The principal feature of this method involves heating the upper and lower stack heaters at a linear temperature heating rate and then monitoring the five temperatures at the interfaces heater-pyrex, pyrex-sample and at the center of the sample. As compared to the steady state method, it is not necessary to maintain a temperature gradient across the sample. One-dimensional heat flow is assumed through the sample and the two pyrex reference disks surrounding it.

The method of data analysis basically involves two independent operations, one for determining diffusivity and the other for determining heat capacity.

Starting from the equation for linear heat flow (6.4.1)

$$\frac{\partial^2 T}{\partial x^2} - \frac{1}{k}\frac{\partial T}{\partial t} = 0$$

and knowing the boundary conditions for the sample, initial temperature distribution and constant heating rate V along the two parallel surfaces, an equation can be derived which relates x-coordinate, temperature, heating rate V and diffusivity of the sample. Knowledge of heating rate and temperature in the middle of the sample, for example, provides a value for diffusivity.

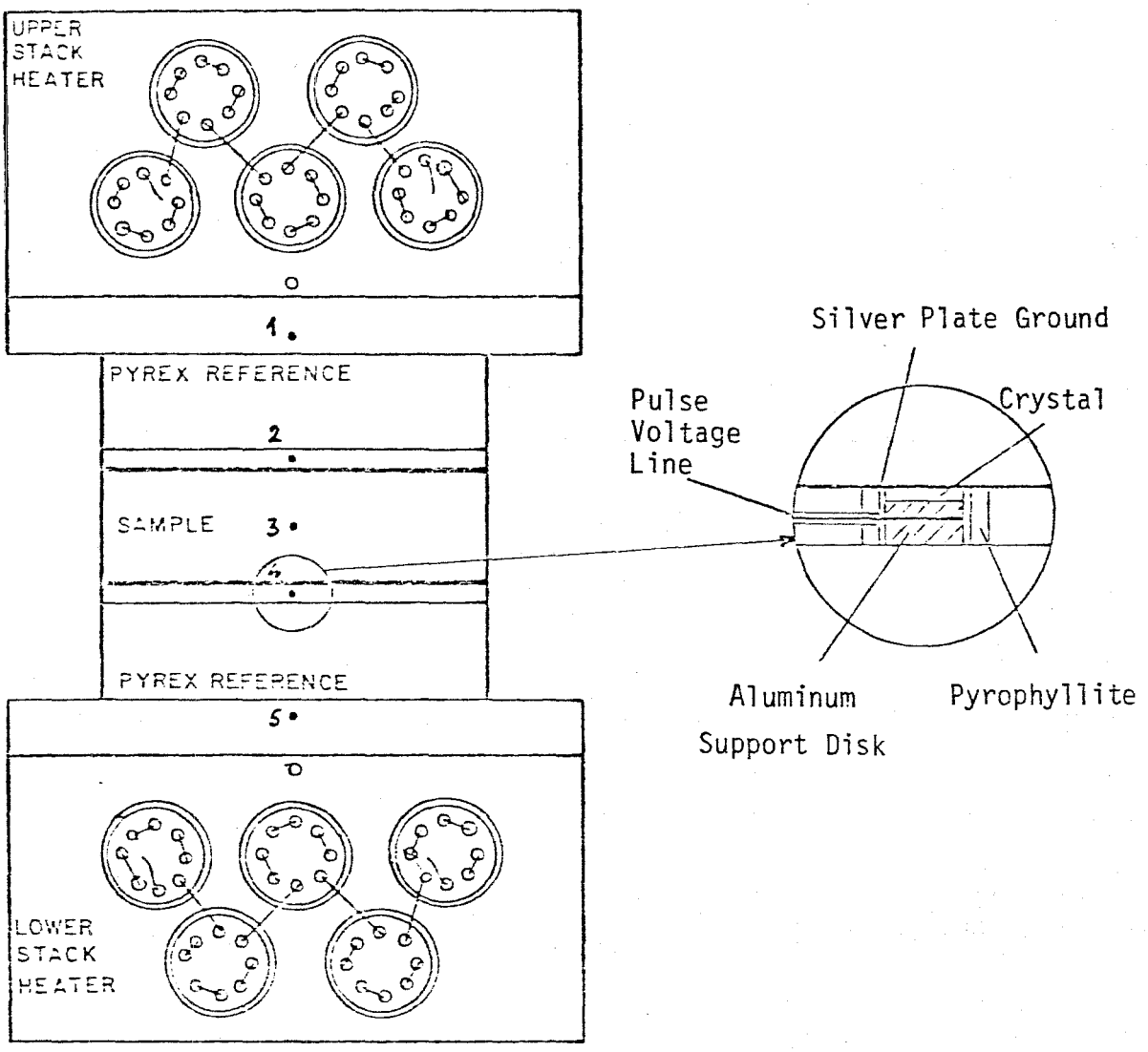

Figure 6.4.1 Experimental stack for measurement of ultrasonic and thermal properties of rocks during transient heating.

This relation between temperature, heating rate, diffusivity and x-coordinate can be used to derive a temperature distribution within the pyrex disks where diffusivity and heating rate are known. Knowledge of this distribution provides the derivative $\frac{\partial T}{\partial x}$ near the interface with the sample and permits the computation of heat flux entering the sample (Equation 6.4.3) Equating this flux to the heat gain of the sample (Equation 6.4.2) we get:

$$-K\left[\left(\frac{\partial T}{\partial x}\right)_1 + \left(\frac{\partial T}{\partial x}\right)_2\right] = \rho c_p \ell \frac{\partial T}{\partial t} \qquad (6.4.4)$$

Where K is the pyrex conductivity

$\left(\frac{\partial T}{\partial x}\right)_1$ and $\left(\frac{\partial T}{\partial x}\right)_2$ are the derivatives of temperature distribution within the pyrex, along their interface with the sample.

ℓ, ρ are the thickness and density of the sample.

$\frac{\partial T}{\partial t}$ is the heating rate of the sample.

The heat capacity c_p is then known and the conductivity K can be derived by the equation

$$K = \rho c_p k$$

6.4.3.1 Simplification of the General Problem of Conduction

The linear flow of heat in a solid bounded by two parallel planes at temperatures $T_1(t)$ and $T_2(t)$ and with the initial temperature distribution $f(x)$ has been treated by Carslaw

and Jaeger (1959). The equations for this case are:

$$\frac{\partial T}{\partial t} = k \frac{\partial^2 T}{\partial x^2} \qquad (0 < x < \ell)$$

$$T = T_1(t), \quad \text{when} \quad x = 0$$

$$T = T_2(t), \quad \text{when} \quad x = \ell$$

$$T = f(x), \quad \text{when} \quad t = 0$$

let us define u and w such that: $T = u + w$

where

$$\frac{\partial u}{\partial t} = k \frac{\partial^2 u}{\partial x^2} \qquad (0 < x < \ell)$$

$$u = 0, \quad \text{when} \quad x = 0 \quad \text{and} \quad x = \ell$$

$$u = f(x), \quad \text{when} \quad t = 0$$

and

$$\frac{\partial w}{\partial t} = k \frac{\partial^2 w}{\partial x^2} \qquad (0 < x < \ell)$$

$$w = T_1(t), \quad \text{when} \quad x = 0$$

$$w = T_2(t), \quad \text{when} \quad x = \ell$$

$$w = 0, \quad \text{when} \quad t = 0$$

u can be written (Carslaw and Jaeger, 1959)

$$u = \frac{2}{\ell} \sum_1^{\infty} e^{-kn^2\pi^2 t/\ell 2} \sin \frac{n\pi x}{\ell} \int_0^{\ell} f(x') \sin \frac{n\pi x'}{\ell} \, dx'$$

The boundary conditions for w being functions of the time we may use Duhamel's Theorem and derive the solution from the case where the surface temperatures are constant (Carslaw and Jaeger, 1959)

$$w = \frac{2k\pi}{\ell^2} \sum_1^\infty n\, e^{-kn^2\pi^2 t/\ell^2} \sin \frac{n\pi x}{\ell} \int_0^t e^{kn^2\pi^2\lambda/\ell^2} [T_1(\lambda)-(-1)^n T_2(\lambda)]\, d\lambda$$

Let us simplify the expressions of u and w with the hypothesis of the transient method:

$$u = \frac{2}{\ell} \sum_1^\infty e^{-at} \sin \frac{n\pi x}{\ell} \int_0^\ell f(x') \sin \frac{n\pi x'}{\ell}\, dx'$$

where

$$a = \frac{kn^2\pi^2}{\ell^2}$$

$f(x')$ is the temperature distribution at $t = 0$, let us assume it is a linear distribution

$$f(x') = \frac{T_2' - T_1'}{\ell} x + T_1'$$

T_1' and T_2' are the initial temperatures along the parallel surfaces (1) and (2) of the specimen. ℓ is the thickness of the specimen.

Thus,

$$\int_0^{\ell} f(x') \sin \frac{n\pi x'}{\ell}\, dx' = \frac{T_2' - T_1'}{\ell} \int_0^{\ell} \underbrace{x' \sin \frac{n\pi x'}{\ell}\, dx'}_{A} + T_1' \int_0^{\ell} \underbrace{\sin \frac{n\pi x'}{\ell}\, dx'}_{B}$$

Integrating by parts, we get for A,

$$A = -\left[\frac{x'\ell}{n\pi} \cos \frac{n\pi x'}{\ell}\right]_0^{\ell} + \frac{\ell}{n\pi} \int_0^{\ell} \cos \frac{n\pi x'}{\ell}\, dx'$$

$$= -\frac{\ell^2}{n\pi} \cos n\pi + \left(\frac{\ell}{n\pi}\right)^2 \sin n\pi$$

$$= -\frac{\ell^2}{n\pi} \cos n\pi$$

and,

$$B = -\frac{\ell}{n\pi} \left[\cos \frac{n\pi x'}{\ell}\right]_0^{\ell} = \frac{\ell}{n\pi} (1 - \cos n\pi)$$

whence,

$$u = \frac{2}{\ell} \sum_1^{\infty} e^{-at} \sin \frac{n\pi x}{\ell} \left(\frac{T_2' - T_1'}{\ell}\right) \left(-\frac{\ell^2}{n\pi} \cos n\pi\right)$$

$$+ \frac{2}{\ell} \sum_1^{\infty} e^{-at} \sin \frac{n\pi x}{\ell}\, T_1' \frac{\ell}{n\pi} \left(1 - \cos n\pi\right)$$

$$u = \frac{2}{\pi}(T_1' - T_2')\left(\sum_{\substack{1 \\ n=\text{even}}}^{\infty} \frac{1}{n} e^{-at} \sin\frac{n\pi x}{\ell} - \sum_{\substack{1 \\ n=\text{odd}}}^{\infty} \frac{1}{n} e^{-at} \sin\frac{n\pi x}{\ell}\right)$$

$$+ \frac{4}{\pi} T_1' \sum_{\substack{1 \\ n=\text{odd}}}^{\infty} \frac{1}{n} e^{-at} \sin\frac{n\pi x}{\ell}$$

Finally,

$$u = \frac{2}{\pi} T_2' \sum_{1}^{\infty} \frac{(-1)^{n-1}}{n} e^{-at} \sin\frac{n\pi x}{\ell} + \frac{2}{\pi} T_1' \sum_{1}^{\infty} \frac{1}{n} e^{-at} \sin\frac{n\pi x}{\ell}$$

where $a = \frac{kn^2\pi^2}{\ell^2}$

Note:

The exponential e^{-at} appears in both terms of the expression of u. It is interesting to get an idea of its value. Considering the typical values:

$$k = .4 \times 10^{-6} \text{ m}^2/\text{sec}$$

$$\ell = 1.5 \text{ cm}$$

and restricting the summation to $n=1$ as e^{-at} rapidly decreases for increasing n, we get

$$a = \frac{kn^2\pi^2}{\ell^2} = \frac{.4 \times 10^{-6} \times 1 \times \pi^2}{1.5^2 \times 10^{-4}} = .018$$

e^{-at}, and consequently u, are thus negligible shortly after the beginning of the experiment.

$$w = \frac{2k\pi}{\ell^2} \sum_1^\infty n\, e^{-at} \sin \frac{n\pi x}{\ell} \int_0^t e^{a\lambda} \left[T_1(\lambda) - (-1)^n T_2(\lambda)\right] d\lambda$$

$$\text{Where } a = \frac{kn^2\pi^2}{\ell^2}$$

Let us consider separately the two cases: n odd and n even.

n odd

$$(-1)^n = -1 \Rightarrow T_1(\lambda) - (-1)^n T_2(\lambda) = T_1(\lambda) + T_2(\lambda) = T_1' + T_2' + 2V\lambda$$

Where T_1' and T_2' are the initial temperatures at $x = 0$ and $x = \ell$, and V is the heating rate calculated for each time interval Δt. Thus,

$$w_{odd} = \frac{2k\pi}{\ell^2} \sum_{\substack{1 \\ n=odd}}^\infty n\, e^{-at} \sin \frac{n\pi x}{\ell} \int_0^t \underbrace{e^{a\lambda} \left[T_1' + T_2' + 2V\lambda\right] d\lambda}_{A}$$

$$\text{knowing that } \int \lambda e^{a\lambda} = \frac{\lambda}{a} e^{a\lambda} - \frac{e^{a\lambda}}{a^2}$$

$$A = 2V \int_0^t \lambda\, e^{a\lambda}\, d\lambda + (T_1' + T_2') \int_0^t e^{a\lambda}\, d\lambda$$

$$= 2V \left[\frac{\lambda}{a} e^{a\lambda} - \frac{e^{a\lambda}}{a^2}\right]_0^t + (T_1' + T_2') \left[\frac{e^{a\lambda}}{a}\right]_0^t$$

$$= 2V \left[\frac{t}{a} e^{at} - \frac{e^{at}}{a^2} + \frac{1}{a^2}\right] + (T_1' + T_2') \left[\frac{e^{at}}{a} - \frac{1}{a}\right]$$

Thus,

$$w_{odd} = \frac{2k\pi}{\ell^2} \sum_{\substack{1 \\ n=odd}}^{\infty} n \sin \frac{n\pi x}{\ell} \left[2V \left(\frac{t}{a} - \frac{1}{a^2} + \frac{e^{-at}}{a^2} \right) + (T_1' + T_2') \left(\frac{1}{a} - \frac{e^{-at}}{a} \right) \right]$$

Finally,

$$w_{odd} = \frac{4V}{\pi} \left[\sum_{\substack{1 \\ n=odd}}^{\infty} \frac{t}{n} \sin \frac{n\pi x}{\ell} - \frac{\ell^2}{k\pi^2} \sum_{\substack{1 \\ n=odd}}^{\infty} \frac{1}{n^3} \sin \frac{n\pi x}{\ell} + \frac{\ell^2}{k\pi^2} \sum_{\substack{1 \\ n=odd}}^{\infty} \frac{1}{n^3} \sin \frac{n\pi x}{\ell} e^{-at} \right]$$

$$+ \frac{2}{\pi} (T_1' + T_2') \left[\sum_{\substack{1 \\ n=odd}}^{\infty} \frac{1}{n} \sin \frac{n\pi x}{\ell} - \sum_{\substack{1 \\ n=odd}}^{\infty} \frac{1}{n} \sin \frac{n\pi x}{\ell} e^{-at} \right]$$

n even

$$(-1)^n = 1 \Rightarrow T_1(\lambda) - (-1)^n T_2(\lambda) = T_1(\lambda) - T_2(\lambda) = H$$

The temperature difference between the two parallel surfaces, H, is not a known function of time. For the derivation it can be assumed that H was constant between 0 and t. Thus,

$$w_{even} = \frac{2k\pi}{\ell^2} \sum_{\substack{1 \\ n=even}}^{\infty} n e^{-at} \sin \frac{n\pi x}{\ell} \int_0^t H e^{a\lambda} \, d\lambda$$

$$= \frac{2k\pi}{\ell^2} H \sum_{\substack{1 \\ n=even}}^{\infty} n e^{-at} \sin \frac{n\pi x}{\ell} \frac{1}{a} (e^{at} - 1)$$

Finally,

$$w_{even} = \frac{2}{\pi} H \sum_{\substack{1 \\ n=even}}^{\infty} \frac{1}{n} \sin \frac{n\pi x}{\ell} (1 - e^{-at})$$

We have shown earlier that $e^{-at} << 1$.

Noting that: $T_1' + T_2' + 2Vt = T_1 + T_2$ and, $H = T_1 - T_2$.

w can be written:

$$w = \frac{2}{\pi} (T_1 + T_2) \sum_{\substack{1 \\ n=odd}}^{\infty} \frac{1}{n} \sin \frac{n\pi x}{\ell} + \frac{2}{\pi} (T_1 - T_2) \sum_{\substack{1 \\ n=even}}^{\infty} \frac{1}{n} \sin \frac{n\pi x}{\ell}$$

$$- \frac{4\ell^2 V}{k\pi^3} \sum_{\substack{1 \\ n=odd}}^{\infty} \frac{1}{n^3} \sin \frac{n\pi x}{\ell}$$

This expression can be simplified noting that:

$$\frac{2}{\pi} T_1 \sum_{\substack{1 \\ n=odd}}^{\infty} \frac{1}{n} \sin \frac{n\pi x}{\ell} = T_1 \left(1 - \frac{x}{\ell}\right)$$

$$\frac{2}{\pi} T_2 \left(\sum_{\substack{1 \\ n=odd}}^{\infty} \frac{1}{n} \sin \frac{n\pi x}{\ell} - \sum_{\substack{1 \\ n=even}}^{\infty} \frac{1}{n} \sin \frac{n\pi x}{\ell} \right) = T_2 \frac{x}{\ell}$$

We saw that u is negligible; whence T = w and

$$T = T_1 - (T_1 - T_2) \frac{x}{\ell} - \frac{4\ell^2 V}{k\pi^3} \sum_{\substack{1 \\ n=odd}}^{\infty} \frac{1}{n^3} \sin \frac{n\pi x}{\ell} \qquad (6.4.5)$$

when $x = \frac{\ell}{2}$, $\sum_{\substack{1 \\ n=odd}}^{\infty} \frac{1}{n^3} \sin \frac{n\pi}{2} = .96895$

and

$$T\Big|_{\ell/2} = \frac{T_1 + T_2}{2} - .125\,\frac{\ell^2 V}{k} \qquad 6.4.6$$

In order to compute the heat capacity we need to know $\frac{\partial T}{\partial x}$ in the references along (1) and (2) (see Introduction of § 6.4.3), let us use the expression of T found before (Equation 6.4.5):

$$\frac{\partial T}{\partial x} = \frac{T_2 - T_1}{\ell} - \frac{4V\ell}{k\pi^2} \sum_{\substack{1 \\ n=\text{odd}}}^{\infty} \frac{1}{n^2} \cos \frac{n\pi x}{\ell}$$

Thus, when $x = \ell$

$$\frac{\partial T}{\partial x}\Big|_{x = \ell} = \frac{T_2 - T_1}{\ell} - \frac{4V\ell}{k\pi^2} \sum_{\substack{1 \\ n=\text{odd}}}^{\infty} \frac{1}{n^2} \cos n\pi$$

$$\sum_{\substack{1 \\ n=\text{odd}}}^{\infty} \frac{1}{n^2} \cos n\pi = -\,1.19064$$

Whence,

$$\frac{\partial T}{\partial x}\Big|_{x = \ell} = \frac{T_2 - T_1}{\ell} + .4825\,\frac{V\ell}{k} \qquad 6.4.7$$

6.4.3.2 Application to the Transient Method Stack

The introduction of section 6.4.3 gave the basic principles for determining the thermal parameters. The corresponding formulae are derived here. The five thermocouples used for the Transient Method are numbered from one to five (see Figure 6.4.1). At regular intervals of time, the five temperatures are read. Equation (6.4.6) can be applied to the sample:

$$T_3 = \frac{T_2 + T_4}{2} - .125 \frac{\ell^2 V}{k}$$

ℓ, the sample thickness and V, the heating rate are known; then

$$k = .125 \frac{\ell^2 V}{.5 (T_2 + T_4) - T_3} = \frac{\ell^2 V}{4 (T_2 + T_4) - 8T_3} \qquad (6.4.8)$$

For given experimental conditions the diffusivity is inversely proportional to the temperature lag of the sample.

Using a prime (') to express the reference caracteristics and properties, Equation (6.4.4) becomes

$$\rho c_p \ell V = -K' \left[\left(\frac{\partial T}{\partial x} \right)_2 + \left(\frac{\partial T}{\partial x} \right)_4 \right]$$

With $\frac{\partial T}{\partial x}$ calculated in the reference at the interface with the sample by Equation (6.4.7)

$$\left(\frac{\partial T}{\partial x} \right)_2 = \frac{T_2 - T_1}{\ell'} + .4825 \frac{V' \ell'}{k'}$$

$$\left(\frac{\partial T}{\partial x} \right)_4 = \frac{T_4 - T_5}{\ell'} + .4825 \frac{V' \ell'}{k'}$$

Finally, we get for the heat capacity,

$$c_p = \frac{K'}{\rho \ell V} \left[\frac{T_1 - T_2 + T_5 - T_4}{\ell'} - .965 \frac{V' \ell'}{k'} \right] \qquad (6.4.9)$$

The conductivity is then calculated by

$$K = \rho c_p k \qquad (6.4.10)$$

NOTES

1. For more accuracy, two different values of heating rate are computed for each temperature interval. V', the heating rate of the pyrex, can be derived as the average heating rate along its parallel surfaces:

$$V' = \frac{\Delta T_1 + \Delta T_2 + \Delta T_4 + \Delta T_5}{\Delta t}$$

Where ΔT represents the temperature increase along the pyrex surfaces (Figure 6.4.1) during the last time interval Δt. The heating rate of the sample, V, is more accurately described when manually controlling the heating by considering the temperature at the middle of the sample. An "equivalent temperature" of the sample can be expressed, assuming a parabolic temperature distribution during heating (see Note 4):

$$T = \frac{T_2 + T_4}{2} - .67\left(\frac{T_2 + T_4}{2} - T_3\right)$$

and

$$V = \frac{\Delta T}{\Delta t}$$

2. In order to check the accuracy of the Transient Method, this method has been used to compute the thermal parameters of pyrex 7740. The results are shown in Figures 6.4.2, 6.4.3 and 6.4.4 simultaneously, with results obtained by conventional methods. The diffusivity values agree quite well with data given in the Thermophysical Properties Research Center Journal (1977). The slope of the conductivity curve is somewhat smaller than the one obtained by steady-state measurements.

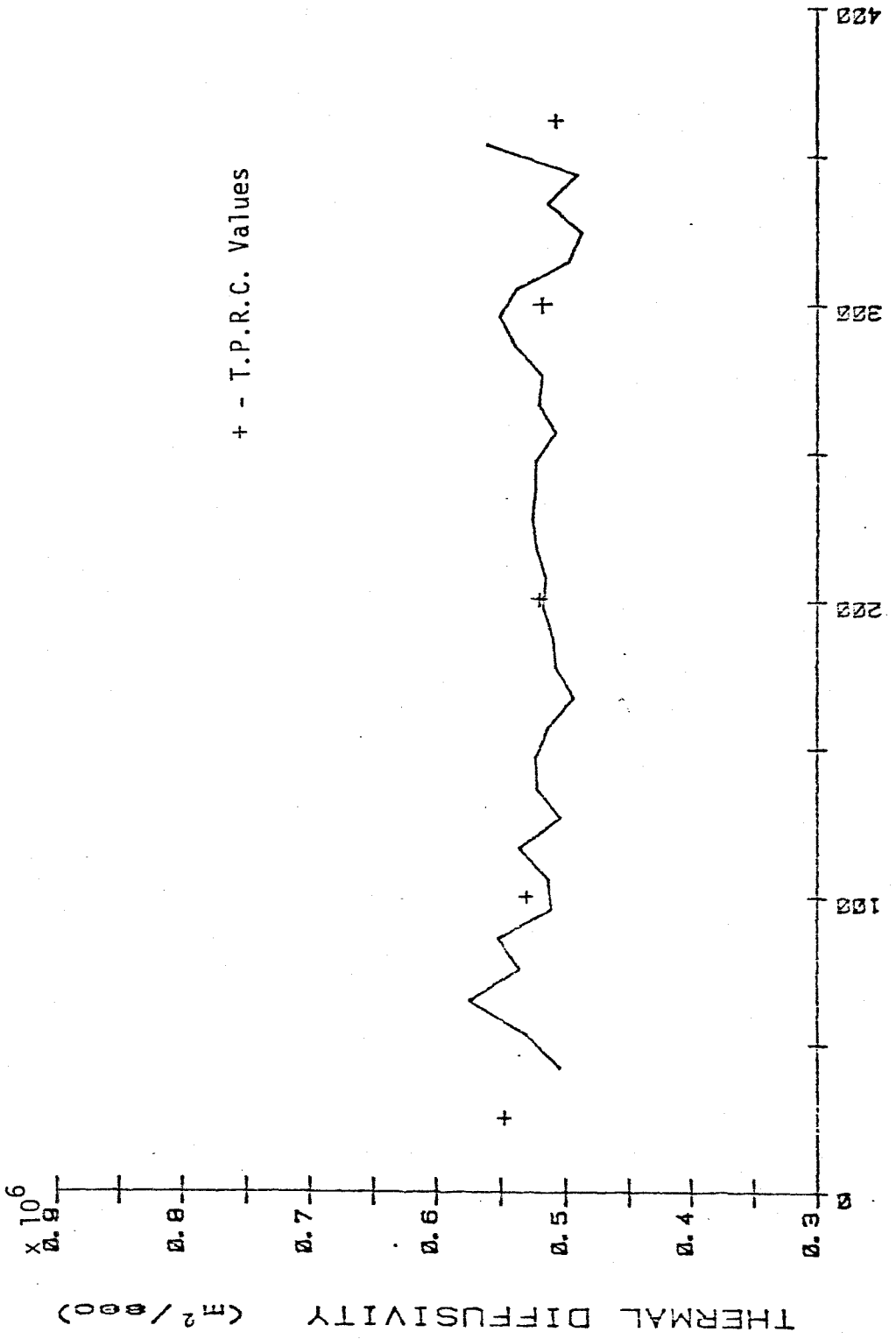

Figure 6.4.2 Thermal diffusivity vs. temperature for Pyrex 7740 measured by the Transient Method.

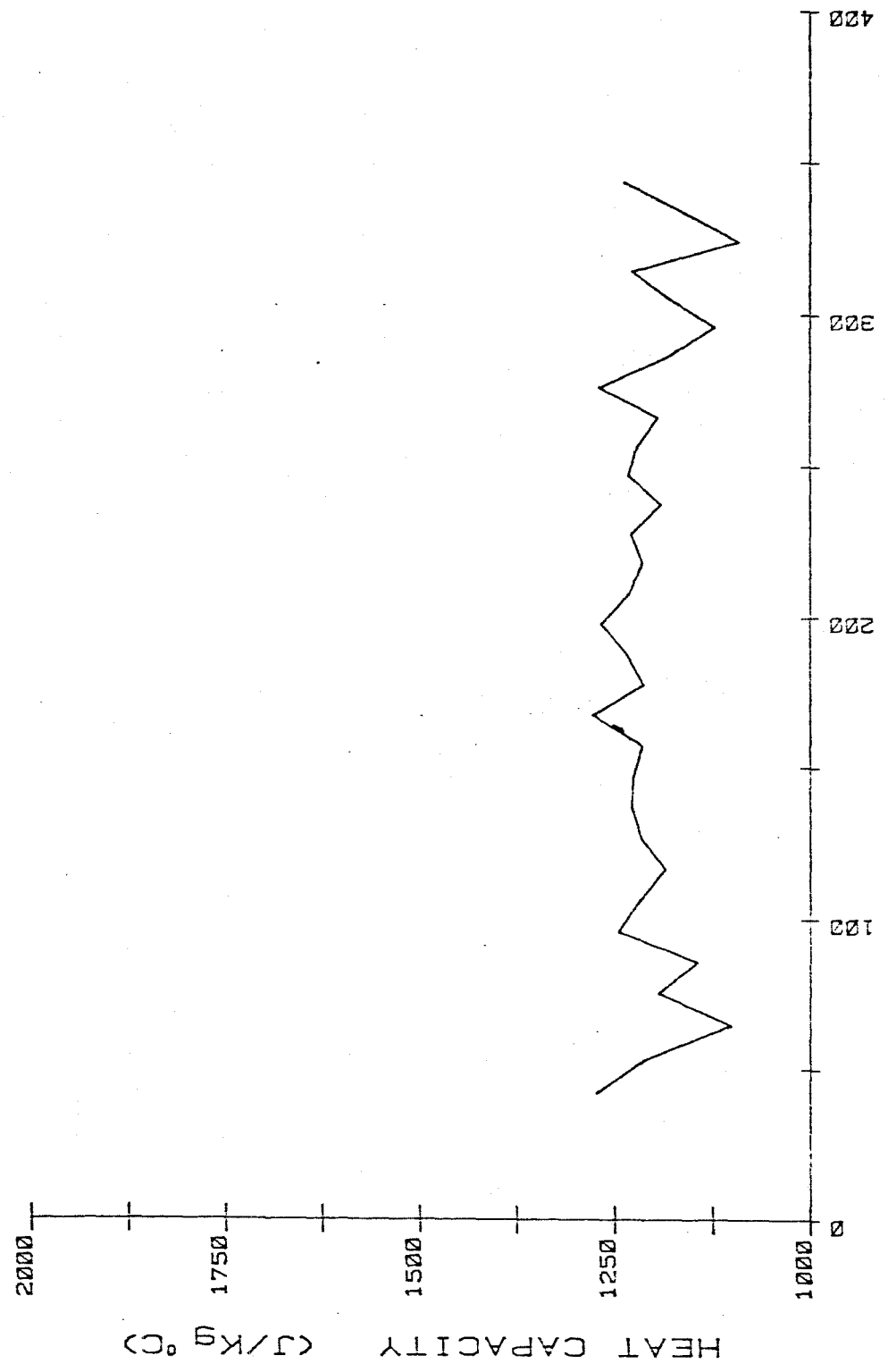

Figure 6.4.3 Heat capacity vs. temperature for Pyrex 7740 measured by the Transient Method.

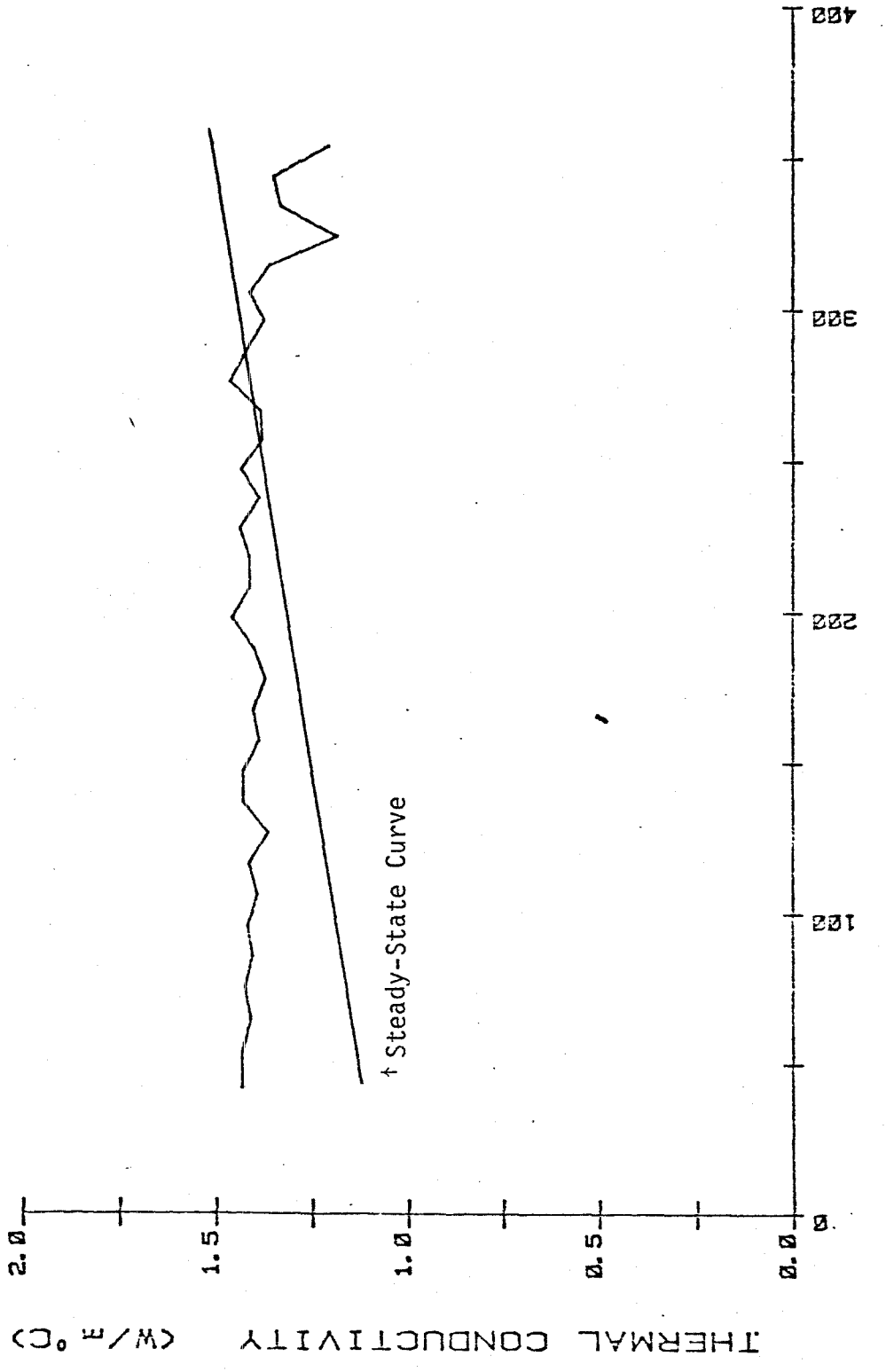

Figure 6.4.4 Thermal conductivity vs. temperature for Pyrex 7740 measured by the Transient Method.

Pyrex 7740 reference disks were employed for this experiment. The diffusivity and conductivity values used in the analysis were respectively the Thermophysical Properties Research Center and steady-state curves.

$$k = (.55 - .000125\ T)\ 10^{-6} \qquad (m^2/sec)$$

$$k = 1.07 + .00126\ T \qquad (W/m°C)$$

The same values have been used for all the experiments with oil shale samples.

3. In the analysis of the thermal parameters k and c_p, the only data needed for Equations (6.4.8) and (6.4.9) are the five temperatures of the stack monitored simultaneously and the current heating rate V. Thus, no cumulative error is possible with this transient method.

4. Looking at the equation for the linear heat flow:

$$\frac{\partial^2 T}{\partial x^2} - \frac{1}{k}\frac{\partial T}{\partial t} = 0$$

we see that, assuming constant heating rate and diffusivity, the expression of T is of the second order with respect to x and the temperature distribution during heating can be considered parabolic.

5. The heat capacity derived by transient analysis actually represents an apparent heat capacity. Peaks in the variation with respect to temperature correspond to the different ends or exothermic reactions and changes of phase occurring during heating.

6.5 Measurement of Elastic Properties by a Pulse Transmission Method *

6.5.1 Introduction

Two basically different techniques have been used to measure the velocity of both longitudinal and shear waves in rocks and other materials. The more sophisticated one is based upon the determination of the ultrasonic frequencies at which continuous sinusoidal waves propagate repetitively across the sample with constructive interference (Schreiber, et al., 1973). This technique includes variations referred to as "pulse-echo-overlap" (Papadakis, 1967), ultrasonic interferometry (Spetzler, 1970) and resonance-frequency methods. The second, and simpler technique, involves the precise measurement of pulse transmission times of characteristic waves across a sample of known dimensions (Peselnick and Stewart, 1975). This technique requires that two ultrasonic transducers (a sender and a receiver) be in contact with the sample, but has the advantage of using first arrivals and, thus, not being perturbed by reflections in the sample and any supporting apparatus. The interferometric technique has the advantage that only one transducer can be used (as both sender and receiver) and the disadvantage that sample geometry and transducer bonding are critical. The relative precisions of the two techniques are typically 1 in 100 for pulse transmissions and 1 in 10,000 for the interferometric or resonance techniques. This is due to the higher accuracy obtained in the measurement of the frequency at which constructive interference occurs compared to the measurement of delay times in the pulse transmission technique. In addition, these techniques have the advantage of being non-destructive, thus permitting numerous, repetitive measurements

* Excerpted from Christophe Petit's M.S. Thesis, Civil Engineering Dept., Colorado State University

to be made while other parameters, such as confining pressure, pore pressure, temperature, etc., are being varied. It is also important to remember when computing the elastic moduli that the equations have been derived for isotropic materials.

The traditional piezoelectric crystals used for ultrasonic measurements (quartz and barium titanate) are restricted in that they have low piezoelectric Curie points (250^{o}) and cannot be used directly for high temperature measurements. These materials can only be used for high temperature studies if appropriate buffer rods are incorporated into the sample assembly (Spetzler, 1970). More recently the capabilities of lithium niobate ($LiNbO_3$) as a high temperature piezoelectric transducer have been demonstrated (Spencer and Nur, 1976). If measurements at both high temperature and high pressure (1 to 10 kb) are desired, it is necessary to incorporate the lithium niobate transducers in a pressure resistant probe such that the transducers see a lower pressure (Spencer and Nur, 1976). For the measurements made on shale, however, the maximum uniaxial and confining stresses are low enough (less than 1 kb) that such encapsulation is not necessary. The very high temperature capabilities of lithium niobate, on the other hand, make it very attractive for making active measurements during the actual retorting of oil shale samples.

6.5.2 Stress-Strain Relations and Equations of Motion for an Isotropic Linearly Elastic Solid

A basic assumption of the theory of linear elasticity is that the components of stress are linear functions of the components of strain. For an isotropic solid, the stress-strain relations along the principal axes are:

$$\sigma_i = \lambda\Delta + 2G\varepsilon_i \qquad (i = 1, 2, 3)$$

Where $\Delta = \varepsilon_1 + \varepsilon_2 + \varepsilon_3$ is the volumetric strain and λ and G are the Lame's constants; G is called the shear modulus.

Two other parameters, related to λ and G, are widely used. Young's modulus E is the ratio of stress to strain for uniaxial stress

$$E = \frac{\sigma_i}{\varepsilon_i}$$

Poisson's ratio ν is defined, in the case of isotropic material, as the ratio of lateral expansion to longitudinal contraction

$$\nu = -\frac{\varepsilon_2}{\varepsilon_1}$$

The general stress-strain relations are easily deduced for any orthogonal system of axes (O_x, O_y, O_z)

$$\sigma_x = \lambda\Delta + 2G\varepsilon_x \qquad \sigma_y = \lambda\Delta + 2G\varepsilon_y \qquad \sigma_z = \lambda\Delta + 2G\varepsilon_z$$

$$\tau_{xy} = G\gamma_{xy} \qquad \tau_{yz} = G\gamma_{yz} \qquad \tau_{zx} = G\gamma_{zx}$$

Where $\Delta = \varepsilon_x + \varepsilon_y + \varepsilon_z$

$$\gamma_{xy} = \frac{\partial v}{\partial x} + \frac{\partial u}{\partial y} \qquad \gamma_{yz} = \frac{\partial w}{\partial y} + \frac{\partial v}{\partial z} \qquad \gamma_{xz} = \frac{\partial w}{\partial x} + \frac{\partial u}{\partial z}$$

u, v, w being respectively the displacements in the x, y, and z directions.

The components of rotation are defined as follows:

$$\omega_x = \frac{1}{2}\left(\frac{\partial w}{\partial y} - \frac{\partial v}{\partial z}\right) \qquad \omega_y = \frac{1}{2}\left(\frac{\partial u}{\partial z} - \frac{\partial w}{\partial x}\right) \qquad \omega_z = \frac{1}{2}\left(\frac{\partial v}{\partial x} - \frac{\partial u}{\partial y}\right)$$

(6.5.1)

The equations of motion are derived by equating the resulting force on a parallelepiped in any direction to its mass times the component of acceleration in that direction.

Let us consider a parallelepiped with its faces normal to the principal axes (x, y and z) as shown in Figure 6.5.1.

The resulting force in the negative x-direction is:

$$\sigma_x + \frac{\partial \sigma_x}{\partial x} dx \; dy \; dz - \sigma_x \; dy \; dz + \tau_{yx} + \frac{\partial \tau_{yx}}{\partial y} dy \; dx \; dz - \tau_{yx} \; dx \; dz$$

$$+ \tau_{zx} + \frac{\partial \tau_{zx}}{\partial z} dz \; dx \; dy - \tau_{zx} \; dx \; dy = \rho \; dx \; dy \; dz \; \frac{\partial^2 u}{\partial t^2}$$

Finally,

$$\frac{\partial \sigma_x}{\partial x} + \frac{\partial \tau_{yx}}{\partial y} + \frac{\partial \tau_z}{\partial z} = \rho \frac{\partial^2 u}{\partial t^2}$$

and,

$$\frac{\partial \tau_{xy}}{\partial x} + \frac{\partial \sigma_y}{\partial y} + \frac{\partial \tau_{zy}}{\partial z} = \rho \frac{\partial^2 v}{\partial t^2}$$

$$\frac{\partial \tau_{xz}}{\partial x} + \frac{\partial \tau_{yz}}{\partial y} + \frac{\partial \sigma_z}{\partial z} = \rho \frac{\partial^2 w}{\partial t^2}$$

These equations of motion may be expressed in terms of strains, using the stress-strain relations:

$$\rho \frac{\partial^2 u}{\partial t^2} = (\lambda + G) \frac{\partial \Delta}{\partial x} + G \nabla^2 u \qquad (6.5.2)$$

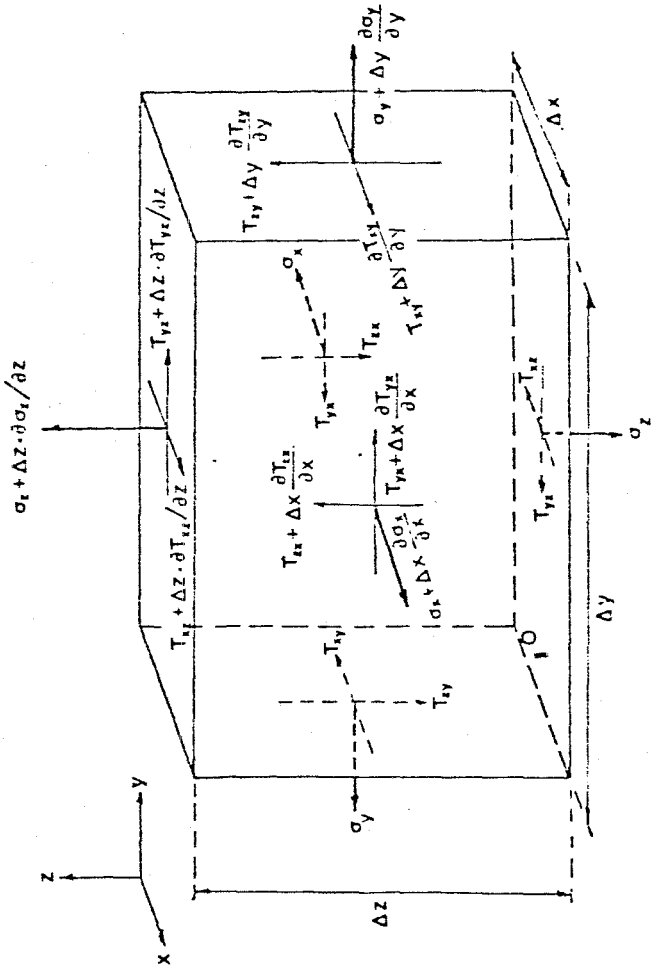

Figure 6.5.1 Three-dimensional stress state

$$\rho\frac{\partial^2 v}{\partial t^2} = (\lambda + G)\frac{\partial \Delta}{\partial y} + G\nabla^2 v \qquad (6.5.3)$$

$$\rho\frac{\partial^2 w}{\partial t^2} = (\lambda + G)\frac{\partial \Delta}{\partial y} + G\nabla^2 w \qquad (6.5.4)$$

6.5.3 Pulse Propagation Method Formulae

Differentiating (6.5.2), (6.5.3) and (6.5.4) partially with respect to x, y, z, respectively, and adding the results, gives

$$\frac{\partial^2 \Delta}{\partial t^2} = \frac{\lambda + 2G}{\rho}\nabla^2 \Delta$$

For a 1-D wave, this equation becomes:

$$\frac{\partial^2 u}{\partial t^2} = \frac{\lambda + 2G}{\rho}\frac{\partial^2 u}{\partial x^2}$$

Which is the equation of a compression wave with a velocity of propagation.

$$C_p = \left(\frac{\lambda + 2G}{\rho}\right)^{\frac{1}{2}} = \left[E\,(1 - \nu)/(1 + \nu)(1 - 2\nu)\rho\right]^{\frac{1}{2}}$$

$$\text{or } C_p = \left(\frac{B}{\rho}\right)^{\frac{1}{2}} \qquad (6.5.5)$$

where $B = \lambda + 2G$ is called the constrained modulus

Differentiating (6.5.3) and (6.5.4) partially with respect to z and y,

respectively, subtracting the results and dividing by two gives:

$$\rho \frac{\partial^2}{\partial t^2}\left[\frac{1}{2}\left(\frac{\partial w}{\partial y} - \frac{\partial v}{\partial z}\right)\right] = G \nabla^2\left[\frac{1}{2}\left(\frac{\partial w}{\partial y} - \frac{\partial v}{\partial z}\right)\right]$$

this becomes knowing (6.5.1), for a 1-D wave

$$\frac{\partial^2 \omega_x}{\partial t^2} = \frac{G}{\rho} \nabla^2(\omega_x)$$

Which is the equation of a shear wave with a velocity of propagation

$$C_s = \left(\frac{G}{\rho}\right)^{\frac{1}{2}} \tag{6.5.6}$$

Equations (6.5.5) and (6.5.6) can be used to derive expressions for the different elastic moduli as functions of appropriate wave velocities and the material density. For isotropic materials

$$E = C_s^2 \rho \left[3 (C_p/C_s)^2 - 4\right] / \left[(C_p/C_s)^2 - 1\right]$$

$$\nu = \frac{1}{2}\left[(C_p/C_s)^2 - 2\right] / \left[(C_p/C_s)^2 - 1\right]$$

$$B = \rho C_p^2 \tag{6.5.7}$$

$$G = \rho C_s^2 \tag{6.5.8}$$

In the present study, we are interested in the variations of the constrained and shear moduli, B and G, which are only functions of C_p and C_s respectively.

Comparing the expressions of C_p and C_s, we get:

$$C_p^2 = \frac{\lambda + 2G}{\rho} > C_s^2 = \frac{G}{\rho}$$

The compression wave (or P-wave) arrival is seen first on the transmitted signal, the shear wave (or S-wave) arrival is detected later where the signal starts having a higher amplitude due to the larger amount of energy carried in the shear wave. A clear and instantaneous change in the slope of the curve corresponds to that arrival (see Figure 6.5.2).

Different studies have shown that the dynamic values of Young's modulus are generally greater than the static values (Rinehart, et al., 1961; Barker, et al., 1975). This is due to the fact that the changes in stress associated with ultrasonic pulse propagation are too small to produce non-linear material response. The observation that velocities increase with stress at low values of stress shows that the velocities of wave propagation reflect the degree of porosity and microcracking of rocks. The ultrasonic methods are only limited when the elastic response is extremely non-linear and the very small strain characteristics of ultrasonic measurements are not representative of the strains experienced in a particular application.

Ultrasonic measurement of longitudinal and shear wave velocities made simultaneously with thermal measurements provide a solid and valuable basis for interpreting the chemical and microstructural causes of changes in the different properties during heating and retorting of oil shale. In addition, correlations between the various types of simultaneous data will provide both guidelines and a much needed data base for eventually making geophysical field measurements during in situ retorting operations

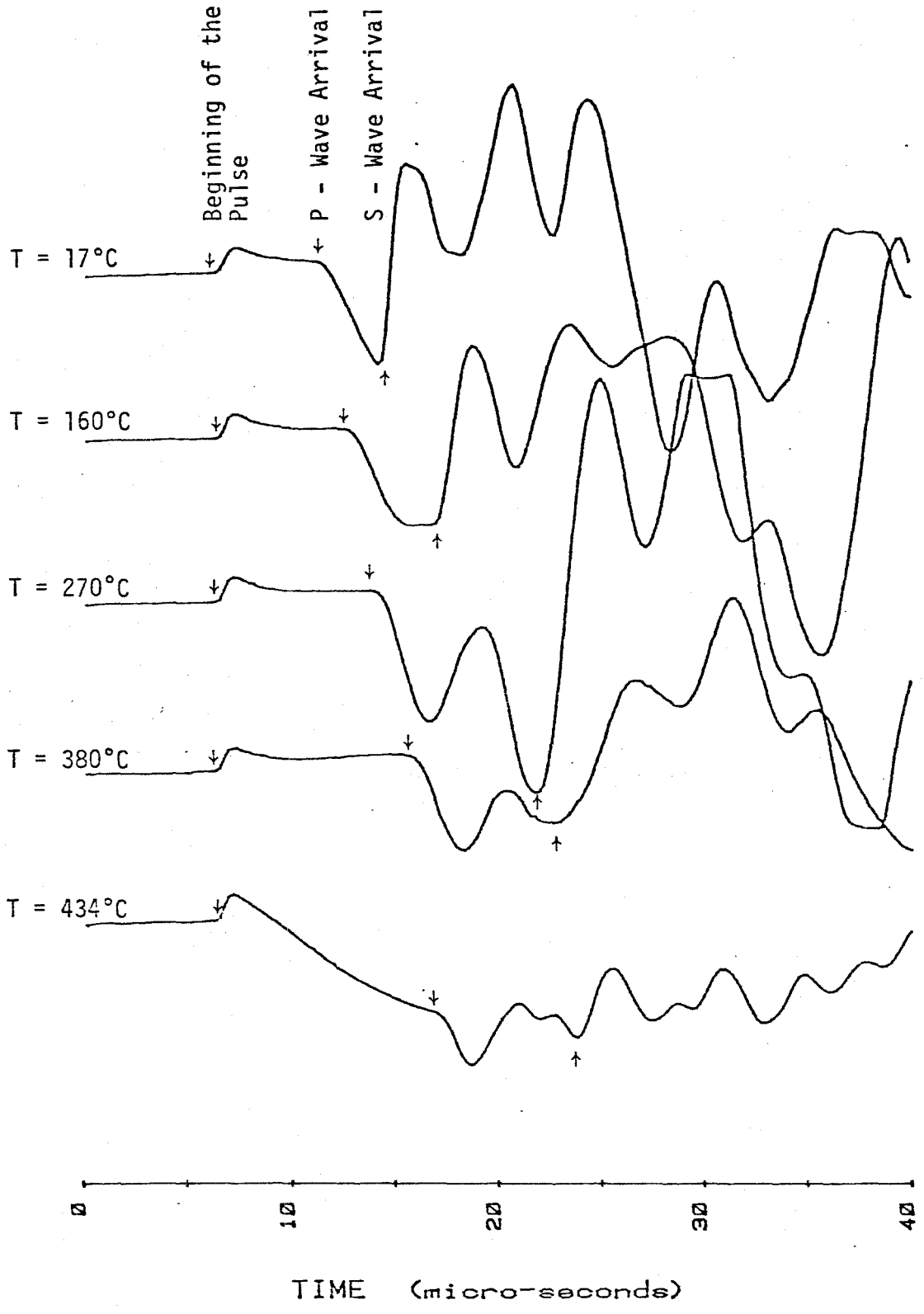

Figure 6.5.2 Average of transmitted signals at different temperatures.

6.5.4 References

Barker, L. M., R. Lingle, R. R. Hendrickson, and J. N. Johnson. 1975. "Measurement of Low-Pressure Static Elastic Moduli of Rock and Comparison with Ultrasonic Data." Technical Report 75-30, Terra Tek, Salt Lake City, Utah.

Carslaw, H. S., and J. C. Jaeger. 1959. "Conduction of Heat in Solids." Second Edition, Oxford University Press, pp. 102-103.

Olinger, B. 1977. "Oil Shale Under Dynamic Stress." LA-6901-PR, Los Alamos Scientific Laboratory, p. 9.

Papadakis, E. P. 1967. J. Acoust. Soc. Am. 42, pp. 1045-1051.

Peselnick, L., and R. M. Stewart. 1975. "A Sample Assembly for Velocity Measurements in Rocks at Elevated Temperatures and Pressures." J. Geophys. Res., 80, p. 3765.

Richart, F. E., R. D. Woods, and J. R. Hall. 1970. "Vibrations of Soils and Foundations." p. 156.

Rinehart, et al. 1961. "Propagation velocity of Longitudinal Waves in Rocks. Effect of State of Stress, Stress Level of the Wave, Water Content, Porosity, Temperature, Stratification and Texture." Proc. Fourth Symp. on Rock Mech., Penn. State Univ., pp. 119-135.

Schreiber, E., O. L. Anderson, and N. Soga. 1973. "Elastic Constants and and Their Measurement." McGraw-Hill, New York, pp. 35-81.

Smith, J. W. 1976. "Relationship Between Rock Density and Volume of Organic Matter in Oil Shales." LERC/RI-76/6, Laramie Energy Research Center, Wyoming.

Spencer, J. W., and A. M. Nur. 1976. "The Effects of Pressure, Temperature, and Pore Water on Velocities on Westerly Granite." J. Geophys. Res., 81(5), pp. 899-904.

Spetzler, H. 1970. "Equation of State of Polycrystalline and Single-Crystal MgO to 8 Kilobars and 800° K." J. Geophys. Res., 75(11), pp. 2073-2087.

Thermophysical Properties Research Center Journal. 1977. p. 1701.

6.6 Results of Laboratory Triaxial Compression Strength Tests for oil shale

TRIAXIAL DATA

OIL SHALE, VERTICAL CORES

(loading perpendicular to bedding)

Grade (GPT)	Temperature (°C)	Confining Pressure (PSI)	Failure Strength (KSI)	Young's Modulus (KSI)	Poison's Ratio
15	20	0	14.6	1.65	.09
20	20	0	9.9	.70	.10
25	20	0	16.9	.96	.14
30	20	0	11.9	.63	.16
15	20	500	20.7	1.18	.18
20	20	500	14.8	1.00	.33
25	20	500	13.2	.86	.25
30	20	500	13.5	.67	.36
15	20	1000	22.3	2.00	.24
20	20	1000	18.5	1.54	.15
25	20	1000	16.6	.58	.40
30	20	1000	13.7	.74	.18
25	20	50	9.3	6.42	.18
20	20	50	11.8	13.08	.22
15	20	50	3.0	24.73	.17
21	20	0	13.5	1.05	.40
25	20	500	13.1	.83	.25
20	20	500	12.4	.70	.25
16	20	1000	21.0	1.46	.15
24	20	1000	10.3	.93	.50
21	20	1000	14.0	1.17	.12
24	20	050	14.52	5.482	.299
41	20	500	12.90	2.028	.469
21	20	050	15.18	7.048	.140
19	20	500	18.08	7.048	.576
15	20	500	22.22	13.450	1.282
15	20	1000	18.99	2.597	.530
19	20	1000	19.59	5.693	.504
54	20	1500	12.18	1.466	.309
15	20	1500	25.16	11.382	1.472

Grade (GPT)	Temperature (°C)	Confining Pressure (PSI)	Failure Strength (KSI)	Young's Modulus (KSI)	Poison's Ratio
24	20	1500	16.17	2.350	.592
15	140	0	8.7	.80	.13
20	140	0	4.9	.25	.59
25	140	0	4.0	.29	.42
30	140	50	9.4	.45	.10
15	140	1000	12.7	.51	.30
20	140	1000	12.7	.51	.30
20	140	1000	6.0	.18	.47
25	140	0	3.8	.22	.77
30	140	1000	6.5	.21	.86
19	140	50	9.0	.54	.20
14	140	50	13.8	1.59	.18
26	140	50	3.4	1.53	.05
24	140	50	9.1	.25	.58
16	140	500	14.7	?	?
20	140	500	10.9	.89	1.00
21	140	1000	17.5	2.36	.65
20	140	1000	9.7	.89	.20
20	140	1000	7.7	?	?
24	140	500	4.3	.25	1.0
15	140	500	19.1	3.31	.90
20	140	500	10.2	4.46	2.0
25	140	1000	3.2	?	?
26	140	50	4.1	.16	.78
15	140	500	16.95	6.727	.778
24	140	1000	11.66	2.056	.322
19	140	050	7.52	1.938	.396
24	140	500	7.00	1.220	.473
45	140	050	3.43	0.258	.528
21	140	1500	10.44	3.290	.851
56	140	1000	7.52	0.330	.229
15	140	1000	14.67	5.920	.887

Grade (GPT)	Temperature (^{o}C)	Confining Pressure (PSI)	Failure Strength (KSI)	Young's Modulus (KSI)	Poison's Ratio
19	140	1500	16.08	3.895	.530
16	260	50	?	.89	.15
20	260	50	11.1	.62	?
25	260	500	4.1	.32	0
19	260	500	17.7	1.34	0
24	260	1000	7.0	.22	0
15	260	1000	14.0	1.15	0
21	260	1000	9.6	1.21	0
14	260	500	7.5	.41	0
26	260	50	5.8	.51	0
15	260	1500	21.48	6.701	1.003
19	260	1500	17.95	5.286	.288
19	260	050	7.13	1.466	.527
15	260	050	10.54	4.775	N.D.
54	260	050	2.87	0.968	N.D.
26	260	500	5.86	0.890	N.D.
15	260	500	13.94	3.610	N.D.
44	260	1000	10.54	0.432	.535
24	260	1000	10.09	0.827	.259
19	260	1000	14.65	1.974	.484
15	260	1500	19.84	3.701	.806
24	260	050	3.40	0.574	.322
15	260	1000	17.48	4.303	.879
21	260	500	7.86	1.328	.488
26	260	1500	9.38	0.927	.514
15	380	50	9.8	.82	.12
25	380	0	17.0	.05	.22
20	380	0	14.2	.04	.27
30	380	0	9.8	.02	.19
26	380	50	1.2	.06	.25
16	380	500	5.8	.41	.90
14	380	1000	11.5	.76	.30

Grade (GPT)	Temperature (°C)	Confining Pressure (PSI)	Failure Strength (KSI)	Young's Modulus (KSI)	Poison's Ratio
24	380	1000	4.8	.13	0
21	380	1000	9.3	.70	.88
25	380	500	.6	.16	.35
19	380	500	6.4	1.08	.8
26	380	1000	?	.16	.30
20	380	50	2.1	.19	.25
26	380	050	0.53	0.031	.173
14	380	050	4.20	1.293	.185
26	380	500	3.76	0.235	.534
15	380	500	6.72	1.384	.414
24	380	1000	4.02	0.247	.247
15	380	1000	8.82	1.742	.711
19	380	1500	10.12	0.955	.234
14	380	1500	12.22	1.466	.269
14	380	500	2.58	0.460	.376
14	380	1000	11.41	7.789	2.227
20	500	50	4.0	.19	.40
14	500	50	11.5	2.16	.30
27	500	50	1.8	1.72	0
16	500	1000	11.9	.57	.25
24	500	1000	6.2	.19	.05
28	500	0	1.1	.06	0
14	500	500	8.0	1.59	.65
23	500	500	5.4	.51	.45
19	500	50	6.4	.48	.08
22	500	500	8.3	.32	.75
28	500	500	4.1	.19	.15
18	500	1000	10.7	.70	.35
13	500	1000	20.1	?	?
23	500	1000	10.7	.51	.25
18	500	500	7.6	.70	.20
13	500	500	14.5	5.00	.50

Grade (GPT)	Temperature (^{o}C)	Confining Pressure (PSI)	Failure Strength (KSI)	Young's Modulus (KSI)	Poison's Ratio
18	500	50	5.1	.38	.15
13	500	50	15.9	?	?
24	500	500	7.66	0.630	.334
54	500	500	3.52	0.132	.477
24	500	050	3.09	1.593	.813
19	500	500	8.67	0.866	.424
21	500	050	2.56	0.574	.176
14	500	1000	17.38	2.277	.372
44	500	1500	6.26	0.324	.278
14	500	1500	20.02	3.100	.823
24	500	1500	8.09	0.609	.224
21	500	1000	8.52	0.682	.418

TRIAXIAL DATA

OIL SHALE, HORIZONTAL CORES

(loading parallel to bedding)

Grade (GPT)	Temperature (°C)	Confining Pressure (PSI)	Failure Strength (KSI)	Young's Modulus (KSI)	Poison's Ratio
40	20	1500	17.51	5.03	1.027
39	20	1000	18.46	3.82	0.780
39	20	500	17.82	3.82	0.773
39	20	50	14.32	5.94	0.069
33	20	1500	15.91	5.03	0.685
35	20	1000	13.37	2.96	0.654
14	20	1500	26.26	12.24	1.140
33	20	500	14.00	4.17	0.536
35	20	50	9.87	4.04	0.462
14	20	1000	24.83	10.88	0.995
14	20	500	20.21	11.46	0.416
14	20	50	17.82	7.42	0.092
16	20	1500	20.53	11.75	0.464
14	20	1000	20.21	12.50	0.580
15	20	500	22.60	16.98	0.347
31	20	050	9.43	4.112	.252
14	20	050	19.10	24.643	.839
41	20	500	10.64	4.775	.975
15	20	500	22.92	73.740	4.517
26	20	1000	16.46	8.705	.948
19	20	1000	24.32	24.643	1.845
35	20	050	9.47	2.427	.743
19	20	500	22.70	8.222	.839
16	20	1000	19.23	16.436	2.014
35	20	1500	14.17	5.482	.896
15	140	1500	21.96	9.66	1.076
15	140	1000	11.94	7.24	0.408
15	140	500	18.46	12.37	0.918
12	140	50	11.46	5.92	0.281

Grade (GPT)	Temperature (^{o}C)	Confining Pressure (PSI)	Failure Strength (KSI)	Young's Modulus (KSI)	Poison's Ratio
41	140	1500	11.78	0.796	0.384
39	140	1000	11.46	0.434	0.709
39	140	500	7.48	1.447	0.709
39	140	50	5.41	1.286	0.630
34	140	1500	10.50	0.757	0.727
34	140	1000	9.55	0.694	0.677
34	140	500	8.28	0.579	1.925
34	140	50	3.52	0.675	0.689
15	140	050	12.14	3.610	.197
19	140	050	5.62	4.714	.626
40	140	500	5.79	1.040	.255
39	140	1000	7.09	3.190	.619
19	140	500	13.84	8.705	.356
35	140	050	4.05	1.229	.401
25	140	1000	8.24	3.084	.630
15	140	1500	16.15	13.450	2.930
34	140	1500	9.88	1.105	.534
19	140	1000	12.35	4.626	.465
26	140	100	8.94	1.409	.384
11	260	1000	26.58	6.211	0.507
14	260	500	18.30	5.931	0.161
16	260	50	6.21	2.711	1.384
15	260	1500	21.33	7.073	0.770
14	260	1000	21.17	5.884	0.481
16	260	500	10.50	6.189	0.590
13	260	50	14.96	7.908	0.108
34	260	1500	12.41	1.062	0.535
34	260	1000	9.87	1.295	0.508
35	260	500	7.32	0.647	0.561
37	260	50	4.46	0.796	0.253
39	260	1500	10.82	1.343	0.621

Grade (GPT)	Temperature (°C)	Confining Pressure (PSI)	Failure Strength (KSI)	Young's Modulus (KSI)	Poison's Ratio
38	260	1000	7.64	1.191	0.373
40	260	500	5.73	0.589	0.539
39	260	50	5.09	0.930	0.512
16	260	500	12.34	5.920	.725
21	260	1500	17.03	5.693	1.589
15	260	1500	7.38	4.626	1.625
16	260	1000	17.02	3.290	.515
31	260	050	4.00	0.911	1.098
36	260	050	4.01	0.573	.585
39	260	500	5.96	1.583	.647
19	260	500	18.21	9.865	1.074
34	260	500	7.48	0.955	.728
34	260	1000	10.93	1.287	.202
16	260	050	9.01	5.212	1.118
36	260	1500	9.15	0.924	.805
19	260	1000	13.88	2.996	.296
19	260	500	13.86	4.229	.806
17	380	1500	13.37	2.387	0.634
15	380	1500	17.82	7.958	0.715
40	380	1500	1.59	0.281	1.176
37	380	1500	12.41	4.565	0.717
14	380	1000	17.35	4.464	0.668
15	380	1000	10.18	4.154	1.089
39	380	1000	7.00	0.350	0.233
35	380	1000	5.09	0.383	0.201
14	380	500	15.28	4.464	0.547
13	380	500	16.46	7.227	0.295
14	380	50	7.32	3.745	0.025
15	380	50	7.32	1.872	0.459
34	380	50	1.91	0.115	0.833
19	380	050	5.23	1.977	1.238
36	380	050	1.31	0.048	.263

Grade (GPT)	Temperature (°C)	Confining Pressure (PSI)	Failure Strength (KSI)	Young's Modulus (KSI)	Poison's Ratio
16	380	050	5.98	2.997	.857
40	380	500	3.06	0.514	.551
16	380	500	13.59	6.727	.778
35	380	1000	3.21	0.243	.421
26	380	1000	5.22	0.959	.411
40	380	1500	7.24	0.684	.670
20	380	1500	5.98	1.520	1.148
19	380	1000	10.56	8.222	1.119
34	380	1500	1.72	0.168	.347
16	380	1500	11.60	3.442	.703
19	380	1000	10.56	8.222	1.119
34	380	1500	1.72	0.168	.347
16	500	1500	18.30	2.56	0.892
13	500	1500	23.55	6.23	0.758
41	500	1500	9.55	0.498	0.594
35	500	1500	5.42	0.725	0.370
15	500	1000	17.03	2.476	0.549
14	500	1000	20.69	3.820	0.243
39	500	1000	5.52	0.314	0.074
37	500	1000	14.96	1.875	0.536
16	500	500	6.84	1.618	0.783
15	500	500	9.07	4.494	0.809
39	500	500	5.70	0.532	0.532
14	500	50	17.35	3.395	0.367
14	500	50	6.05	6.420	0.524
41	500	50	4.32	0.986	0.172
35	500	50	2.23	2.112	0.671
36	500	1500	5.74	0.591	.374
15	500	1500	18.11	4.626	1.071
21	500	1000	15.34	3.218	.548
20			15.37	13.450	1.282
25	500(?)	1000	6.16	1.520	.683

Grade (GPT)	Temperature (^{o}C)	Confining Pressure (PSI)	Failure Strength (KSI)	Young's Modulus (KSI)	Poison's Ratio
21	500	1000	7.32	1.287	.447
39	500	500	3.76	1.444	.826
21	500	050	0.70	0.428	1.445
35	500	500	1.82	0.845	.873
16	500	500	11.83	3.290	.605
35	500	050	1.31	0.970	.446

6.7 Plots of Laboratory Physical Property Test Results for Oil Shale

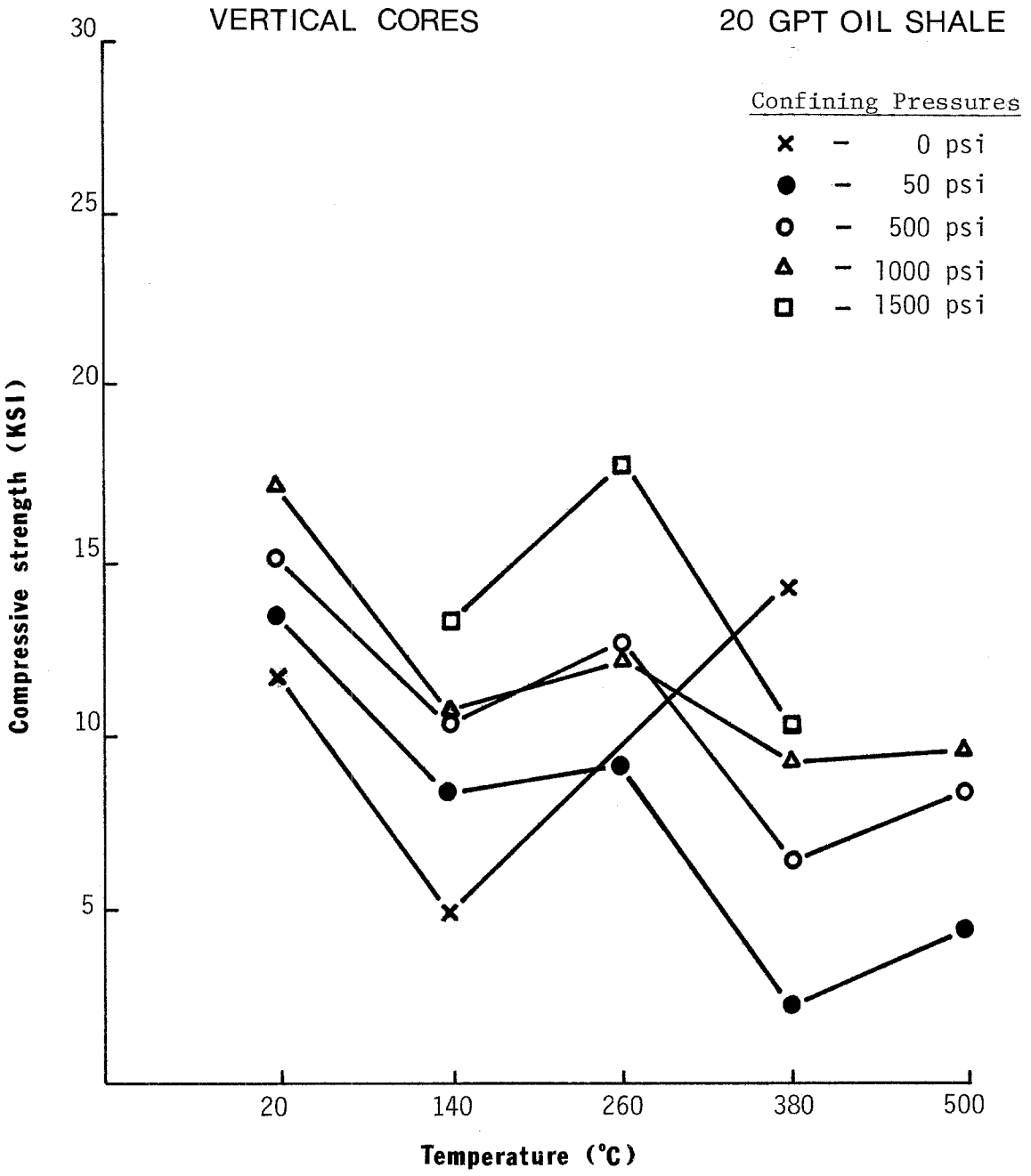

EFFECT OF TEMPERATURE ON COMPRESSIVE STRENGTH
FOR 20 GPT OIL SHALE AT VARIOUS CONFINING PRESSURES

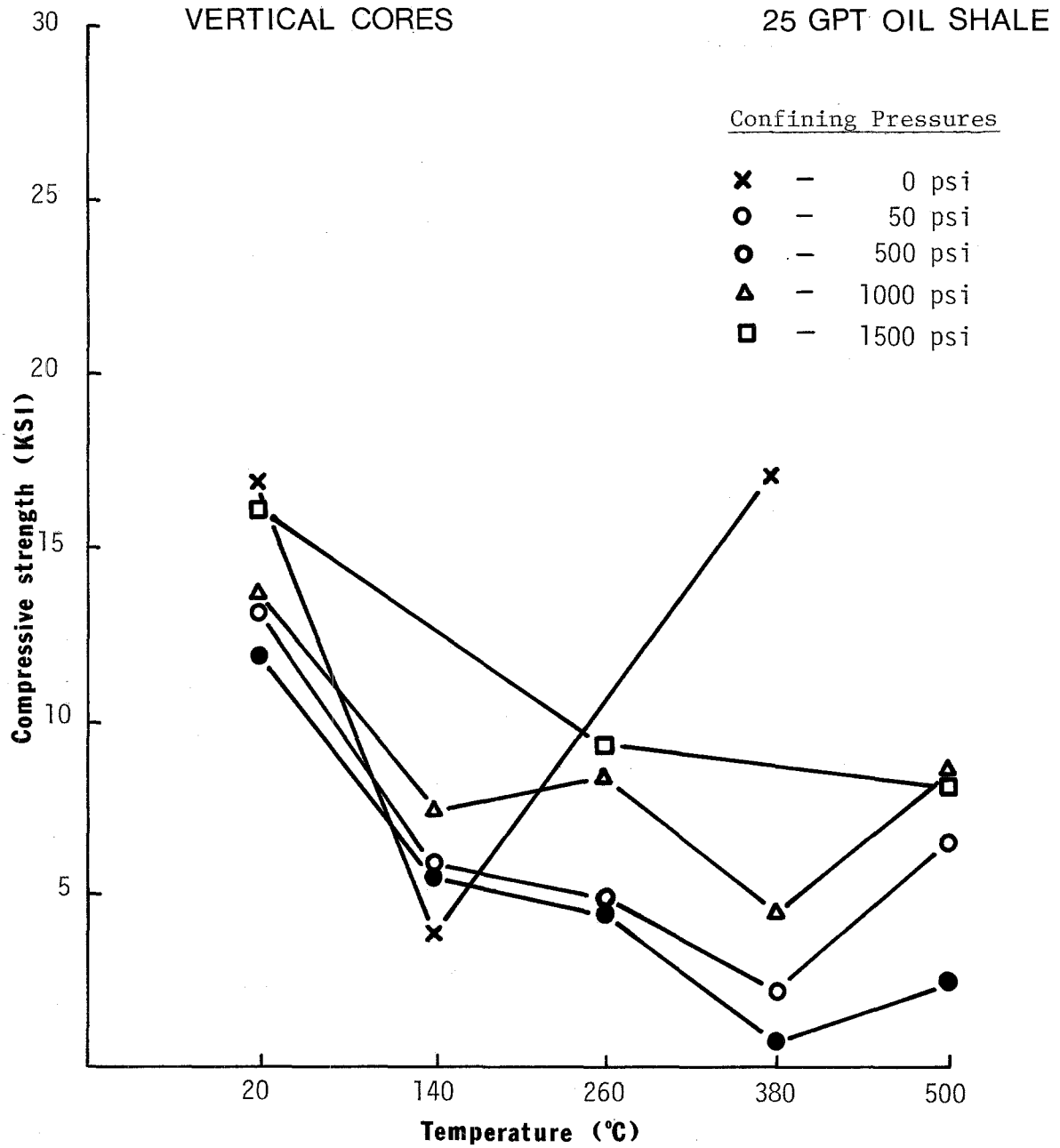

EFFECT OF TEMPERATURE ON COMPRESSIVE STRENGTH FOR 25 GPT OIL SHALE AT VARIOUS CONFINING PRESSURES.

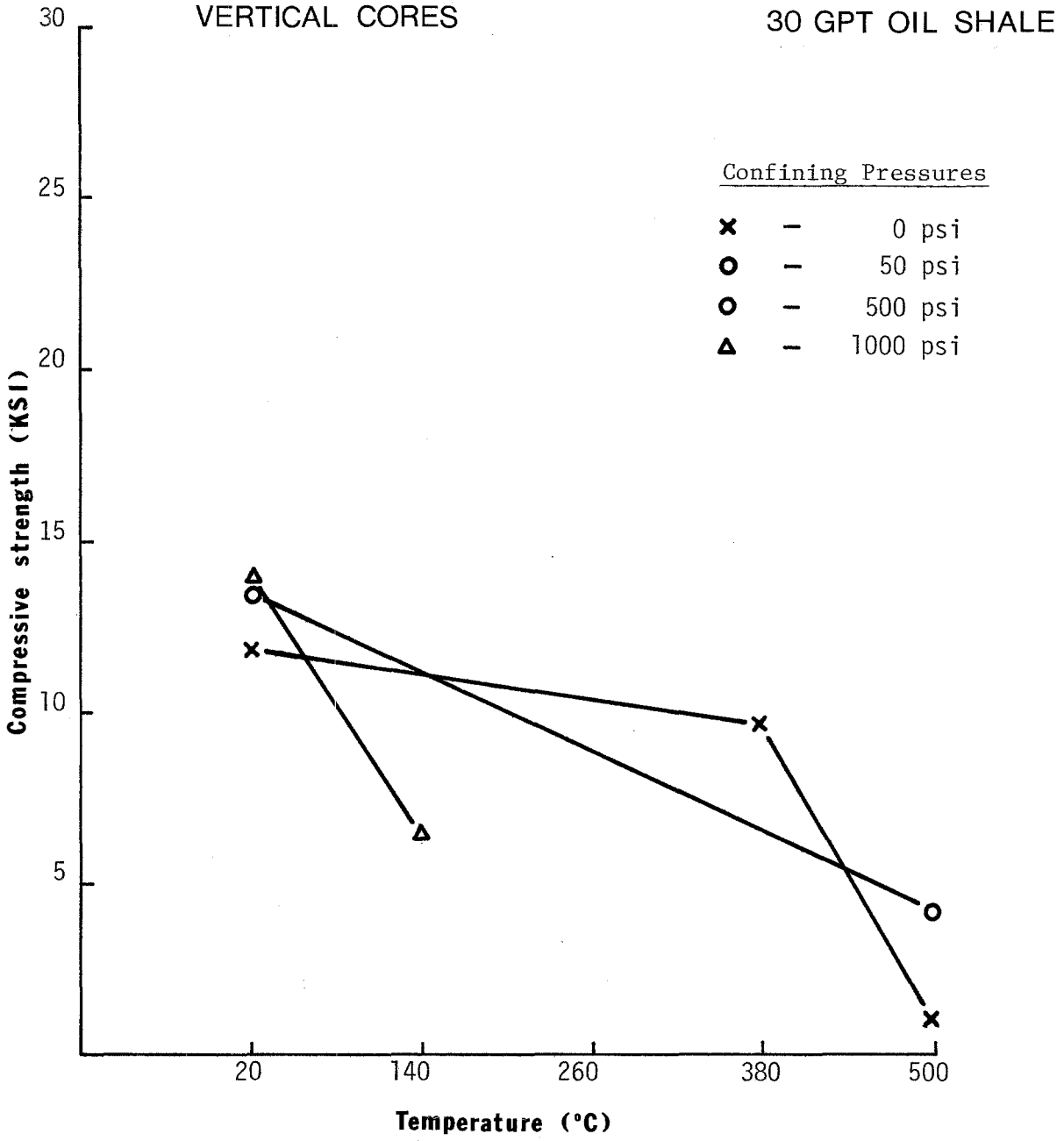

EFFECT OF TEMPERATURE ON COMPRESSIVE STRENGTH FOR 30 GPT OIL SHALE AT VARIOUS CONFINING PRESSURES

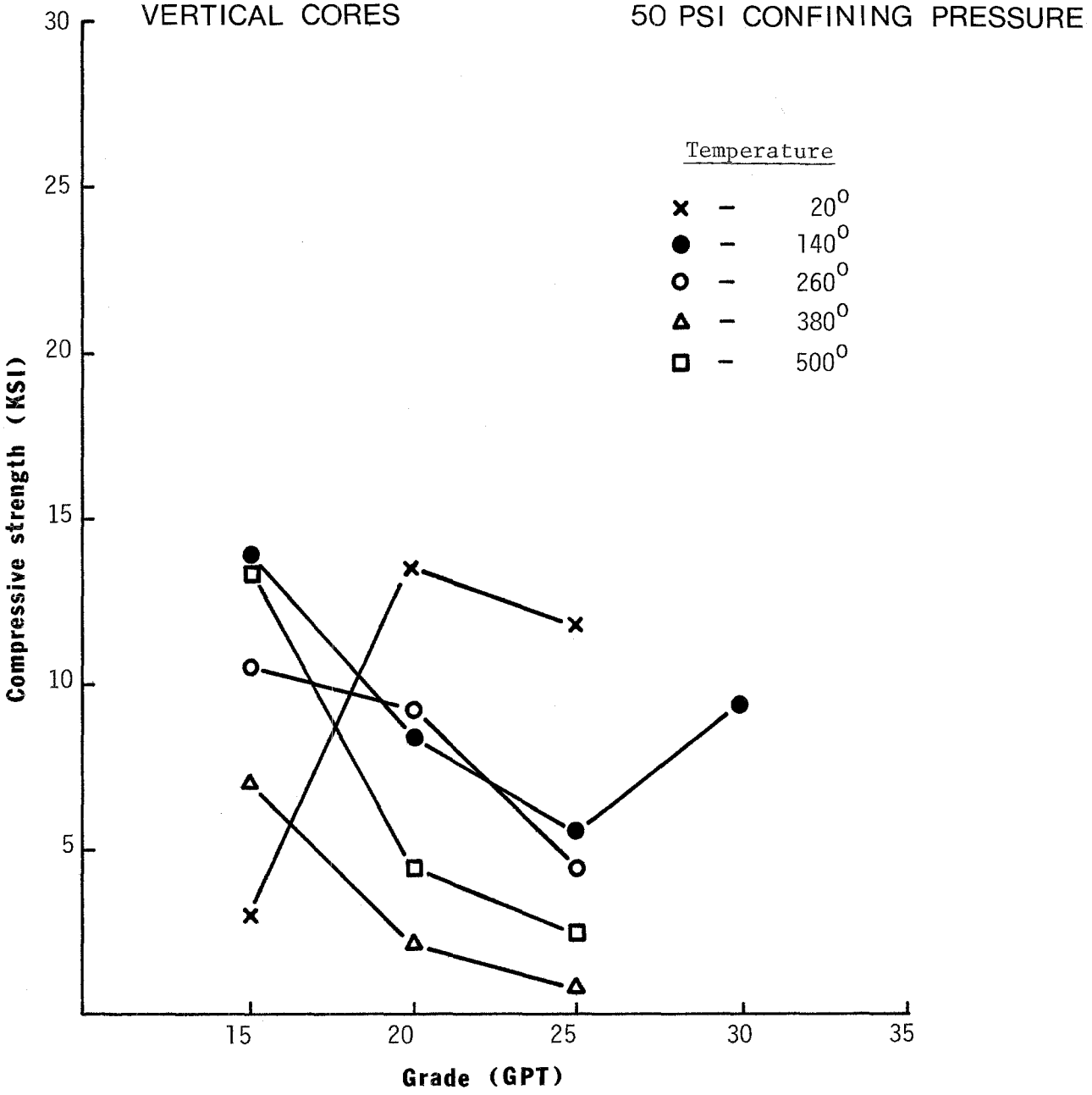

EFFECT OF GRADE ON COMPRESSIVE STRENGTH OF OIL SHALE FOR VARIOUS TEMPERATURES AT 50 psi CONFINING PRESSURES.

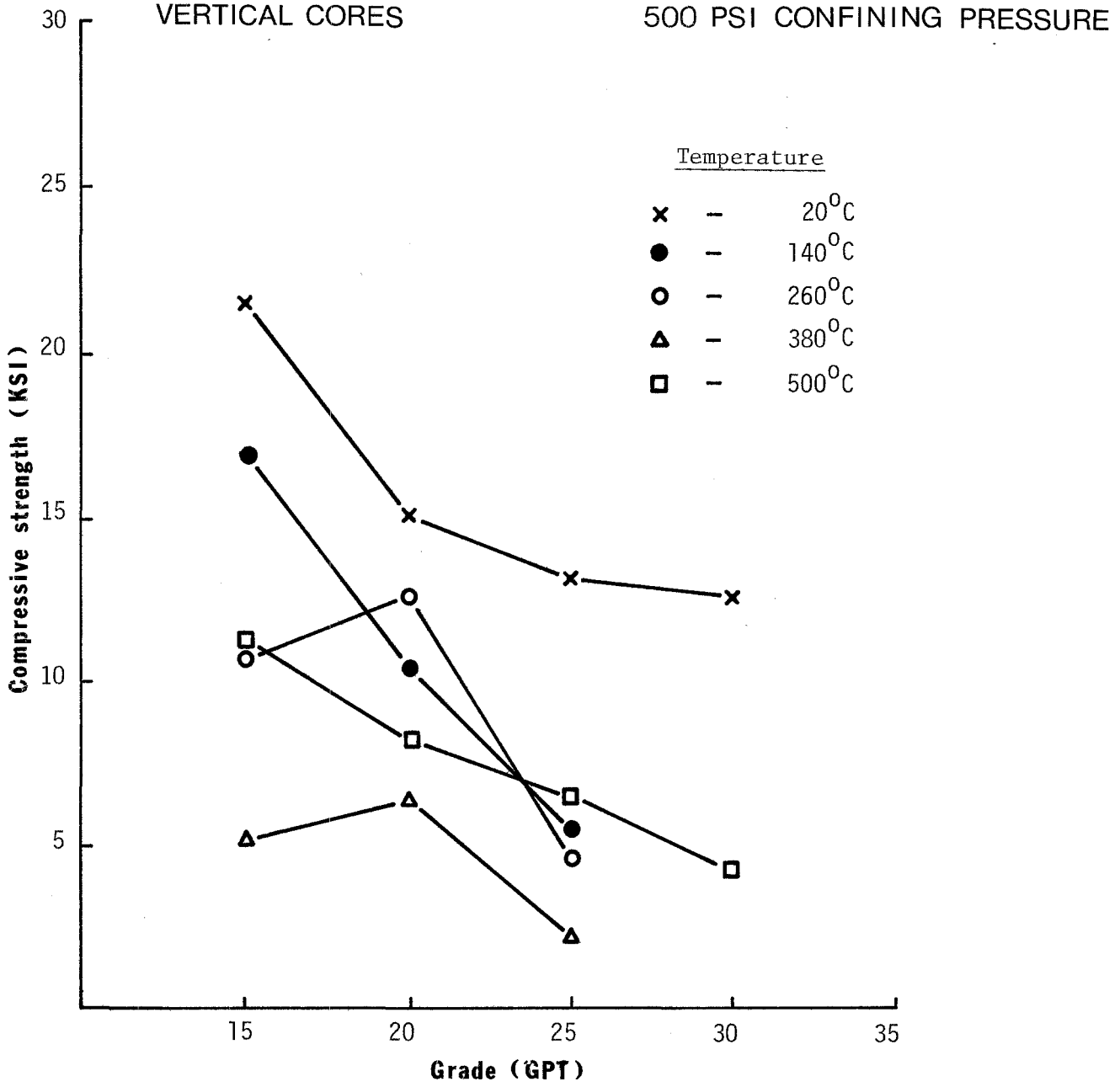

EFFECT OF GRADE ON COMPRESSIVE STRENGTH OF OIL SHALE

FOR VARIOUS TEMPERATURES AT 500 psi CONFINING PRESSURE

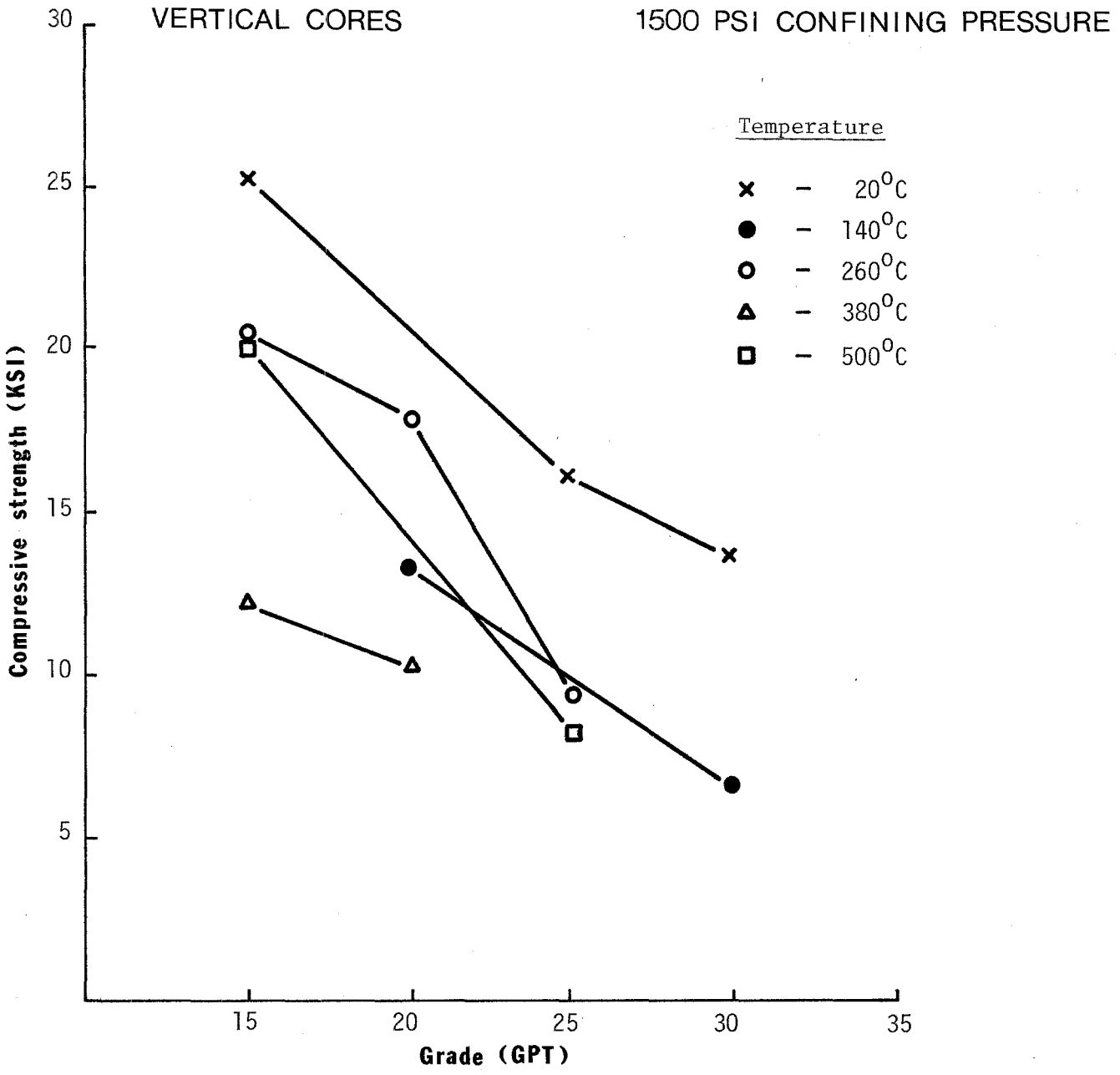

EFFECT OF GRADE ON COMPRESSIVE STRENGTH OF OIL SHALE

FOR VARIOUS TEMPERATURES AT 1500 psi CONFINING PRESSURE

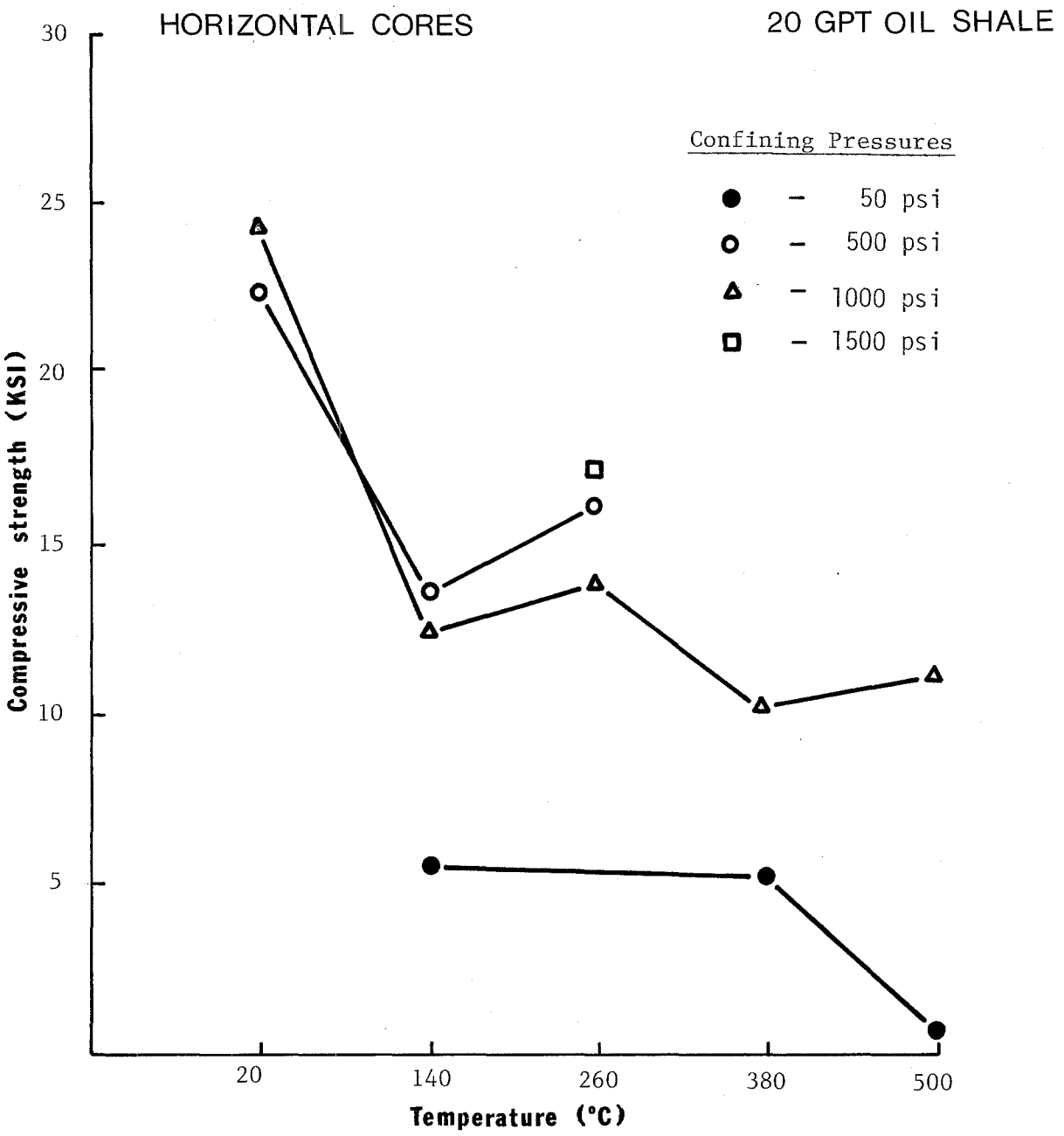

EFFECT OF TEMPERATURE ON COMPRESSIVE STRENGTH FOR 20 GPT OIL SHALE AT VARIOUS CONFINING PRESSURES

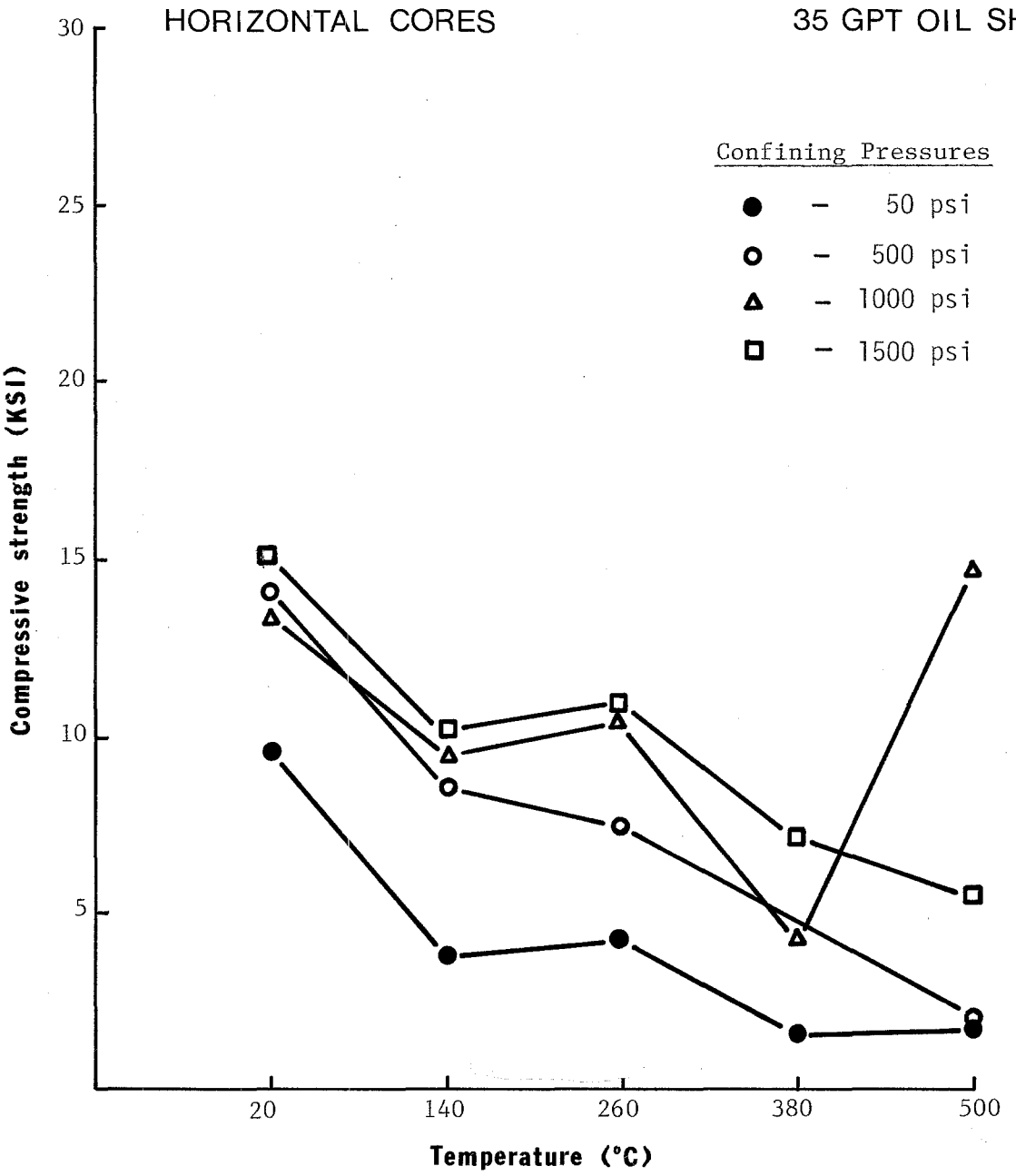

EFFECT OF TEMPERATURE ON COMPRESSIVE STRENGTH

FOR 35 GPT OIL SHALE AT VARIOUS CONFINING PRESSURES

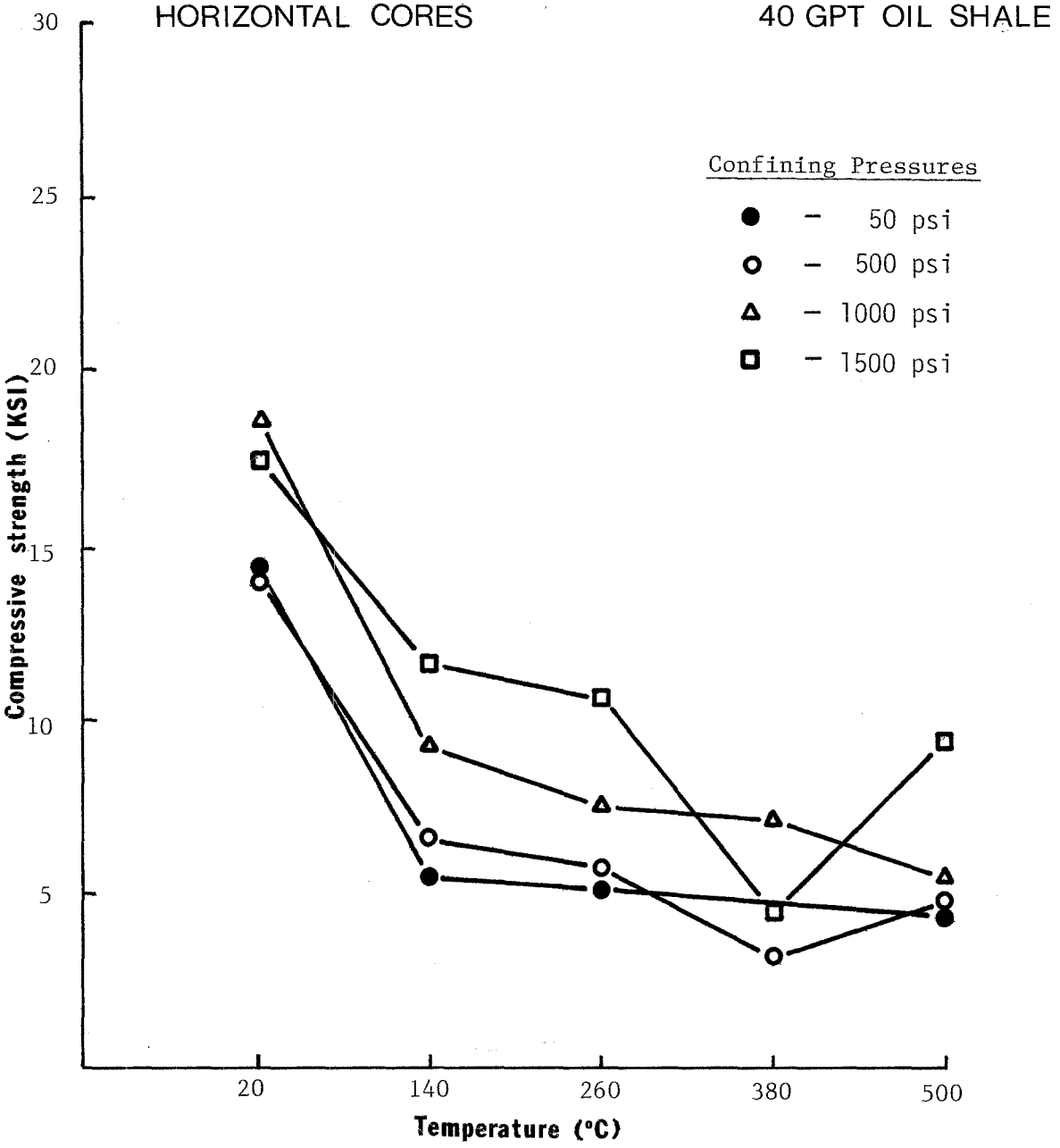

EFFECT OF TEMPERATURE ON COMPRESSIVE STRENGTH

FOR 40 GPT OIL SHALE AT VARIOUS CONFINING PRESSURES

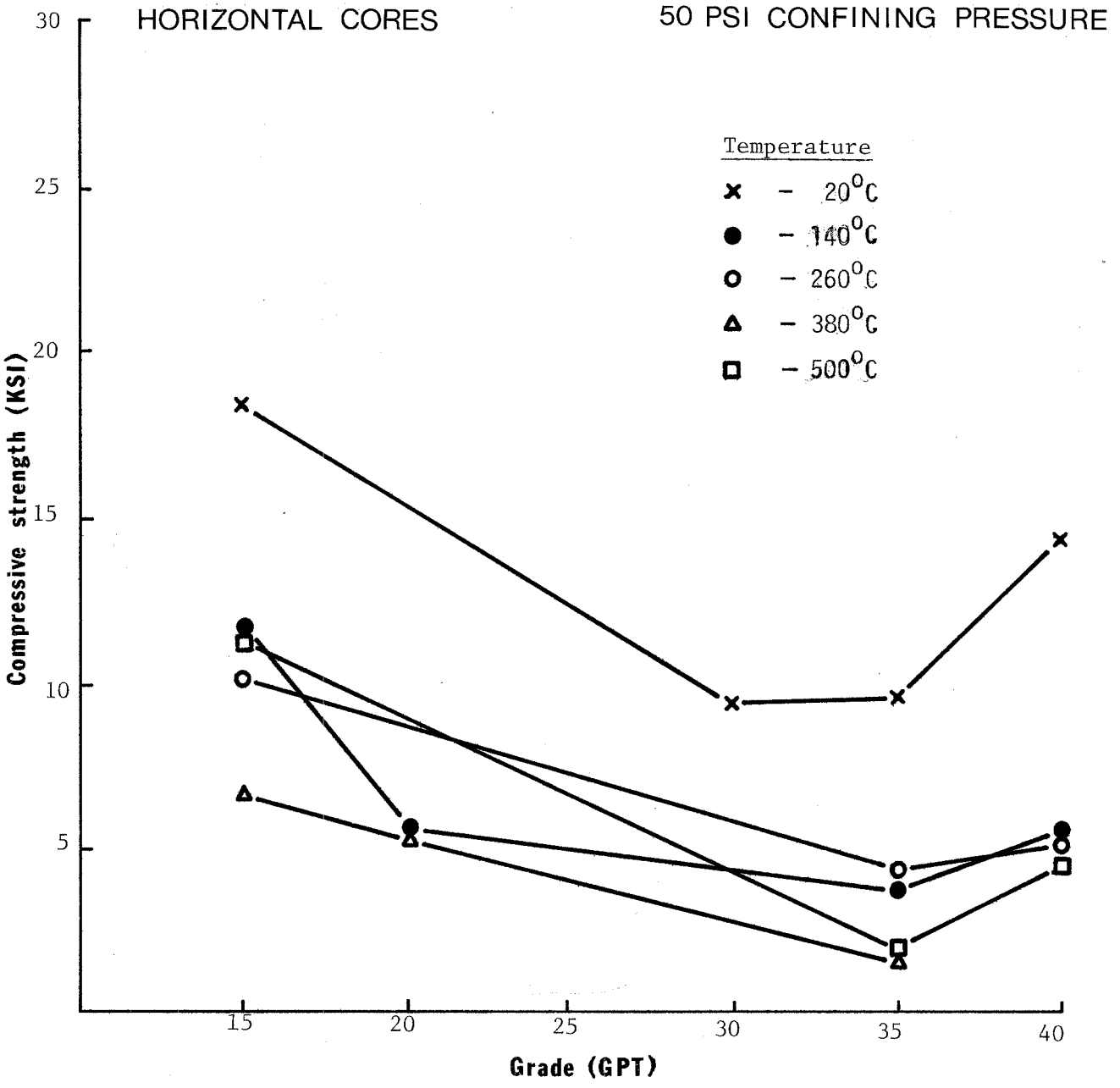

EFFECT OF GRADE ON COMPRESSIVE STRENGTH OF OIL SHALE FOR VARIOUS TEMPERATURES AT 50 psi CONFINING PRESSURE

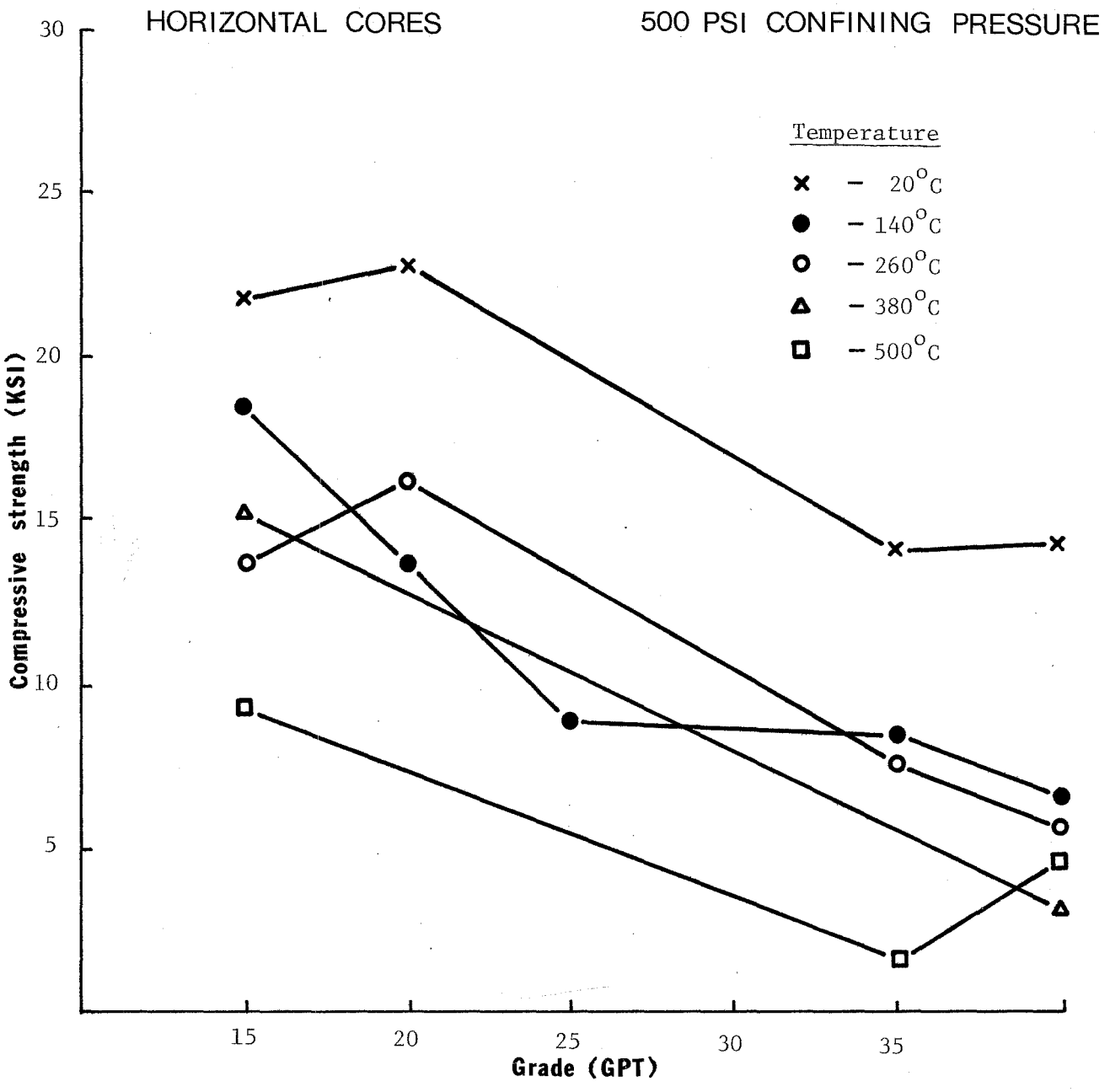

EFFECT OF GRADE ON COMPRESSIVE STRENGTH OF OIL SHALE FOR VARIOUS TEMPERATURES AT 500 PSI CONFINING PRESSURE

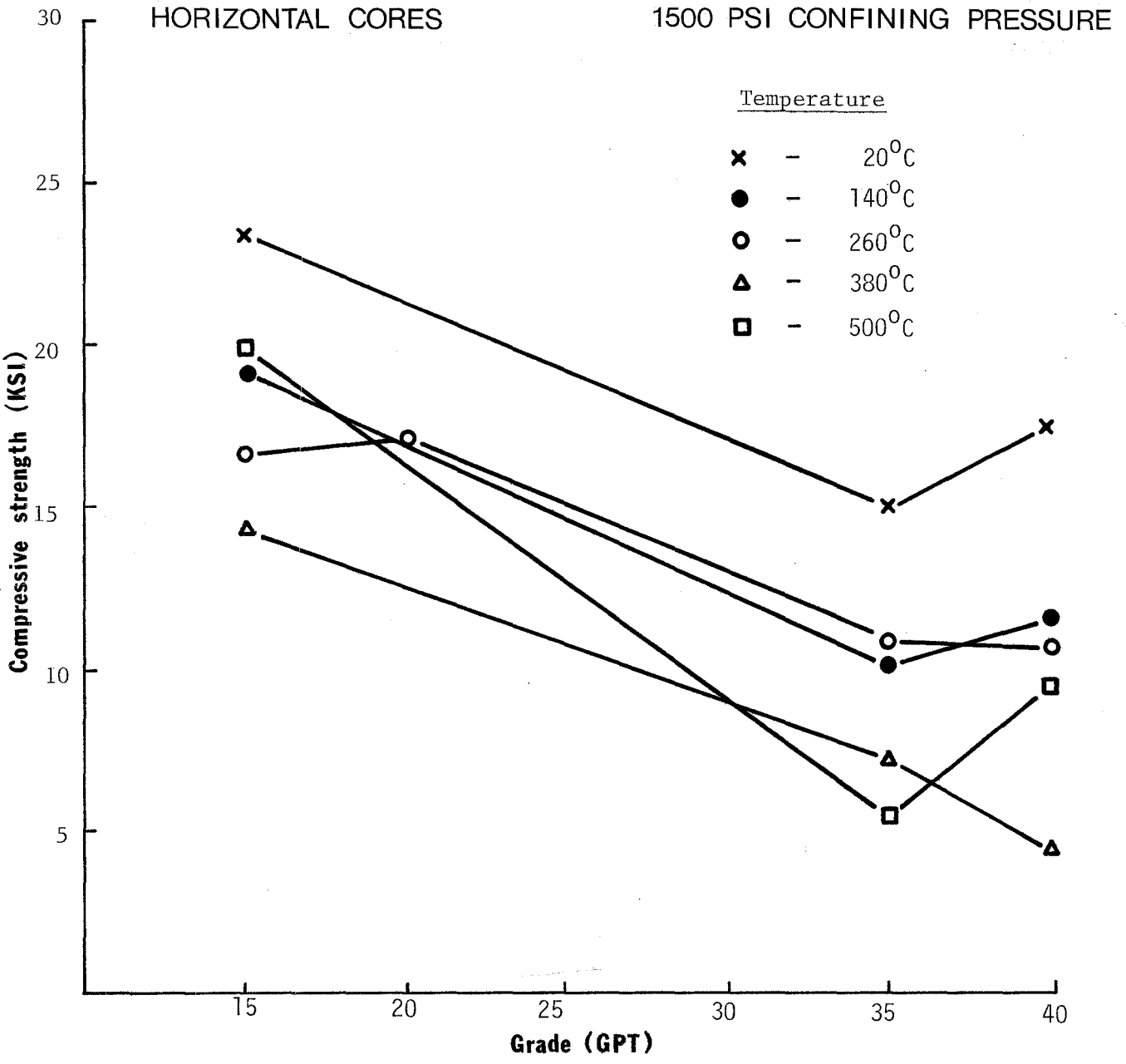

EFFECT OF GRADE ON COMPRESSIVE STRENGTH OF OIL SHALE FOR VARIOUS TEMPERATURES AT 1500 psi CONFINING PRESSURE

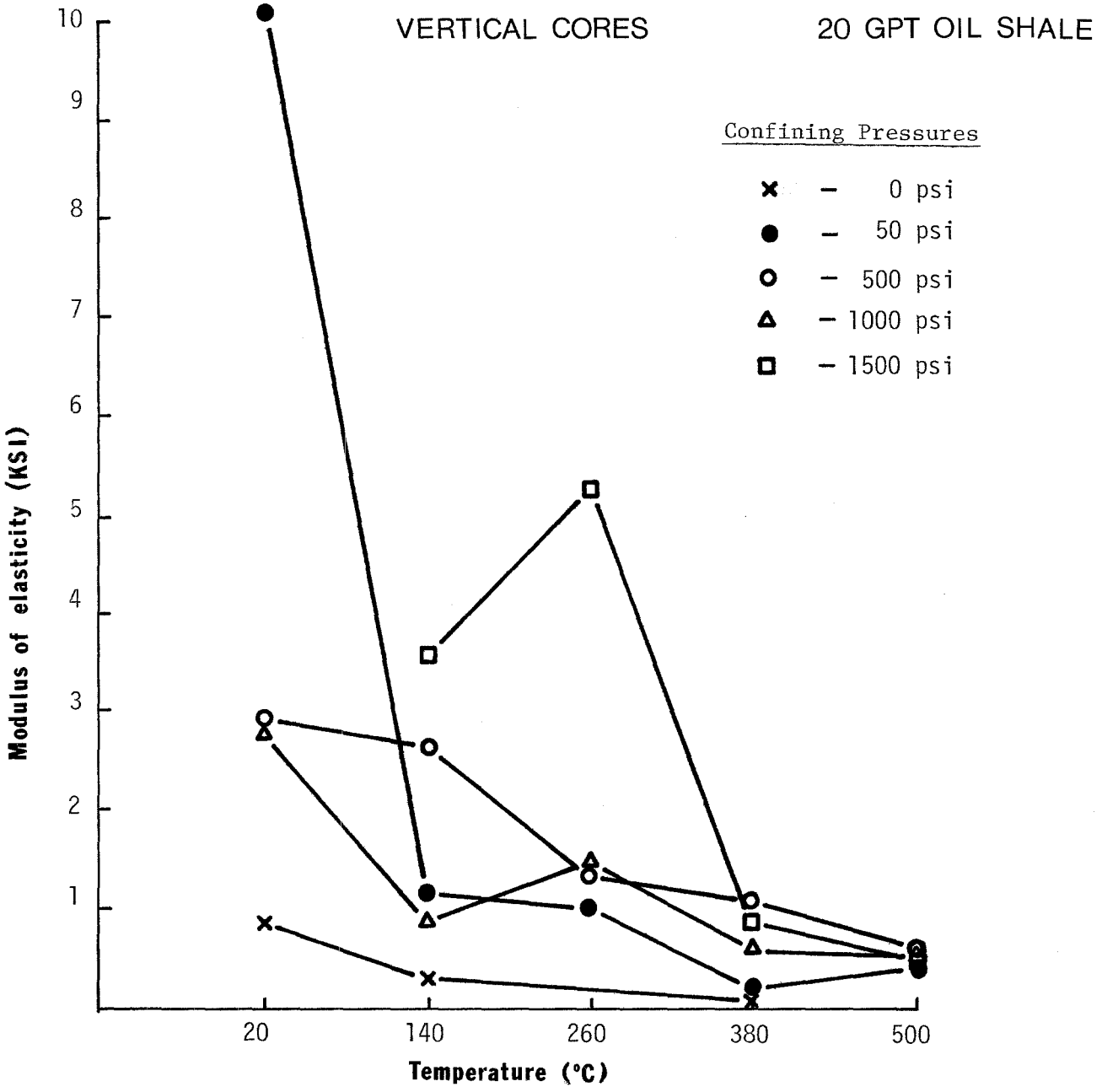

EFFECT OF TEMPERATURE ON MODULUS OF ELASTICITY FOR 20 GPT OIL SHALE AT VARIOUS CONFINING PRESSURES.

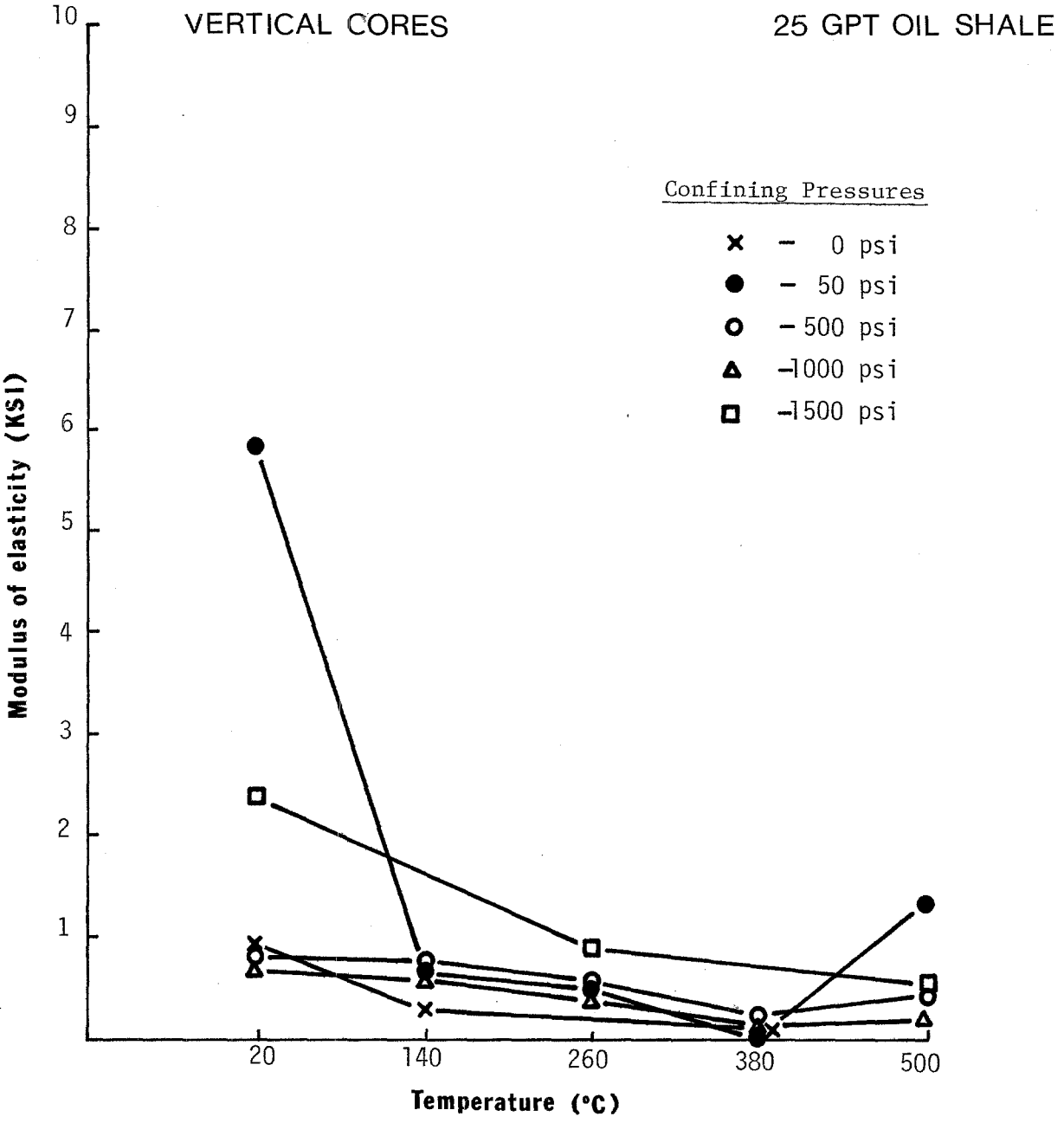

EFFECT OF TEMPERATURE ON MODULUS OF ELASTICITY FOR 25 GPT OIL SHALE AT VARIOUS CONFINING PRESSURES.

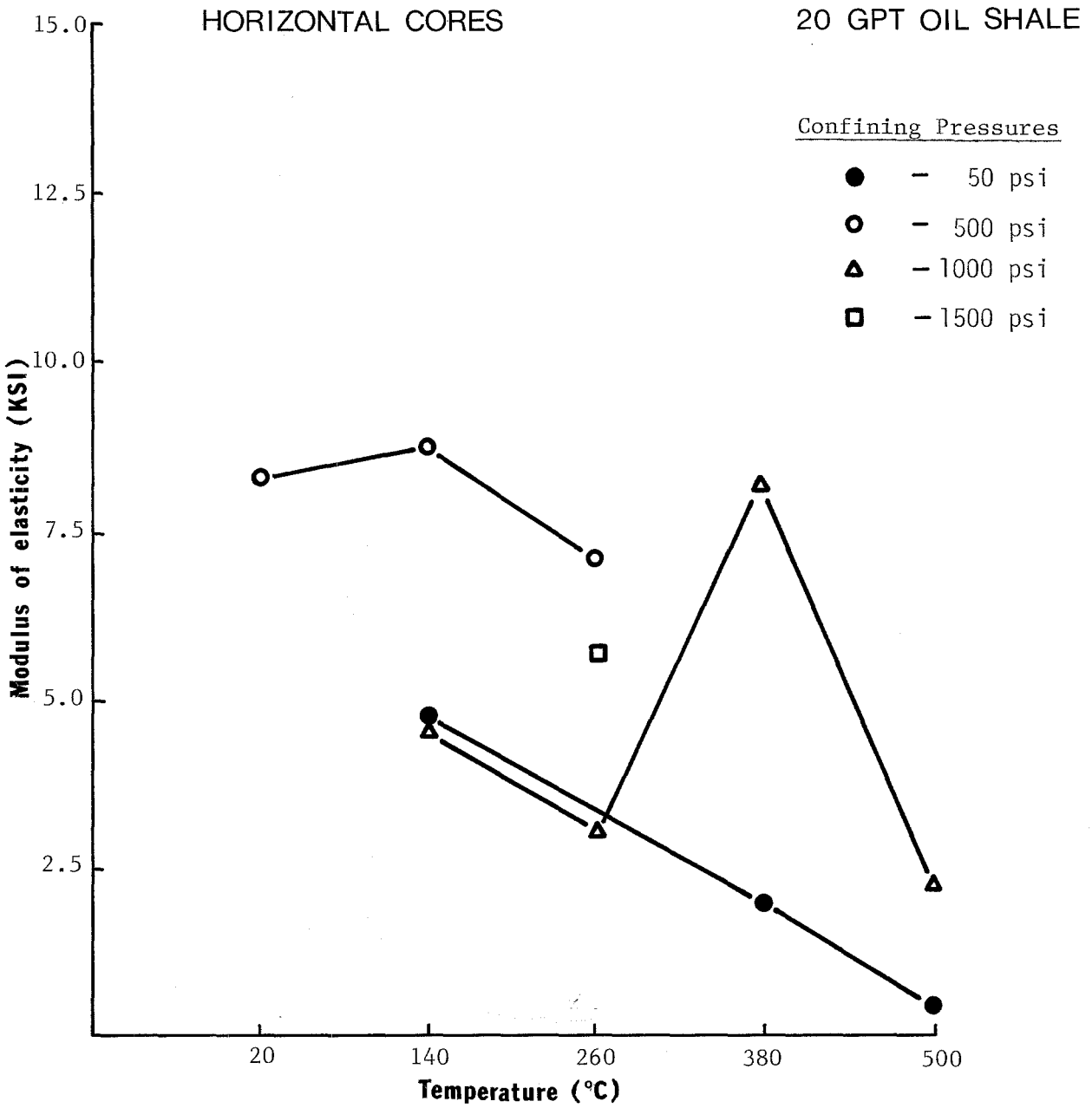

EFFECT OF TEMPERATURE ON MODULUS OF ELASTICITY FOR 20 GPT OIL SHALE AT VARIOUS CONFINING PRESSURES

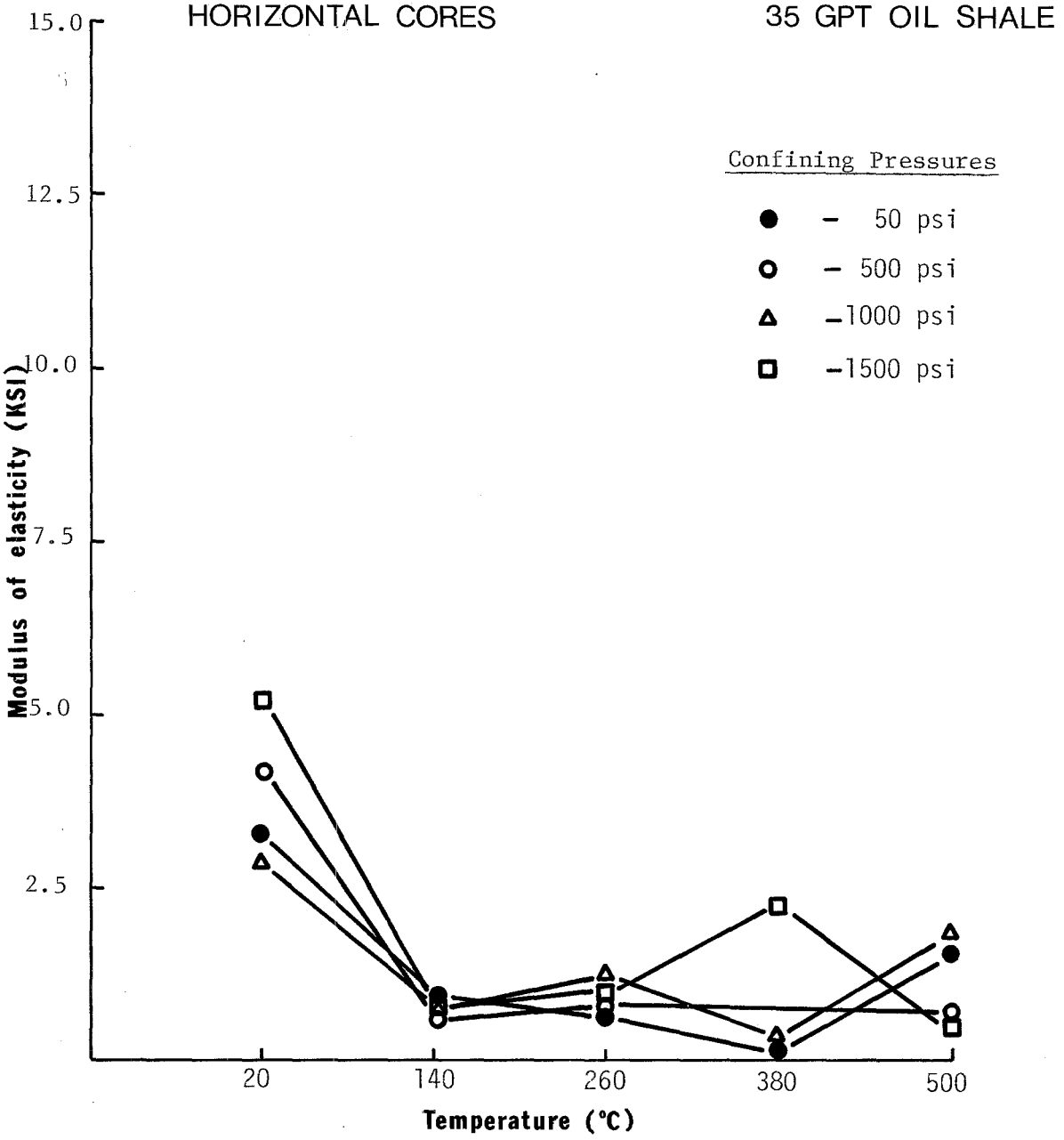

EFFECT OF TEMPERATURE ON MODULUS OF ELASTICITY FOR 35 GPT OIL SHALE AT VARIOUS CONFINING PRESSURES

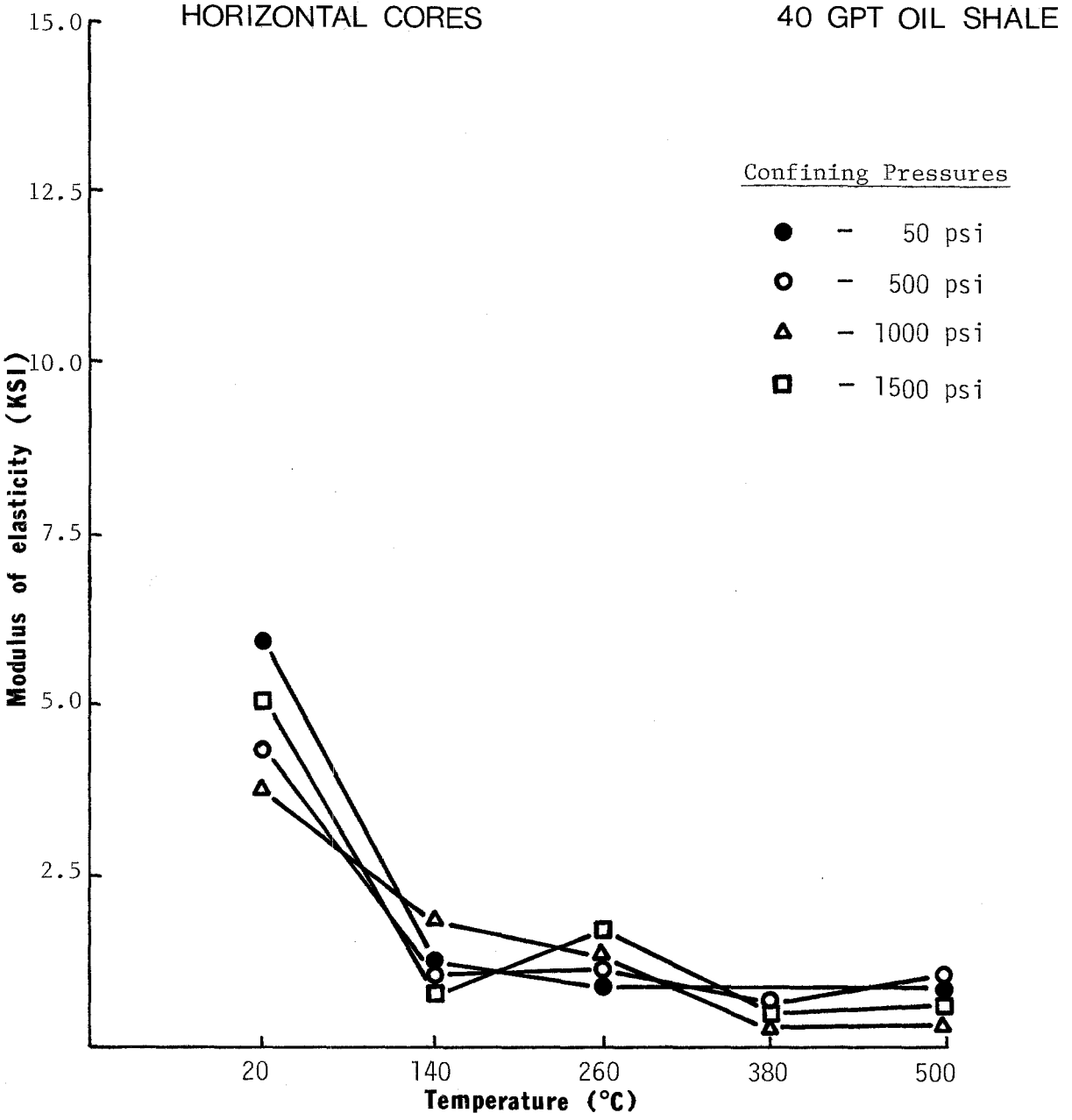

EFFECT OF TEMPERATURE ON MOCULUS OF ELASTICITY FOR 40 GPT OIL SHALE AT VARIOUS CONFINING PRESSURES

6.8 Computer Plots of Oil Shale Physical Properties from Developed Regression Equations.

PREDICTED BEHAVIOR OF COMPRESSIVE STRENGTH VS. TEMPERATURE
FOR 15 gpt OIL SHALE AT VARIOUS CONFINING PRESSURES (VERTICAL CORES)

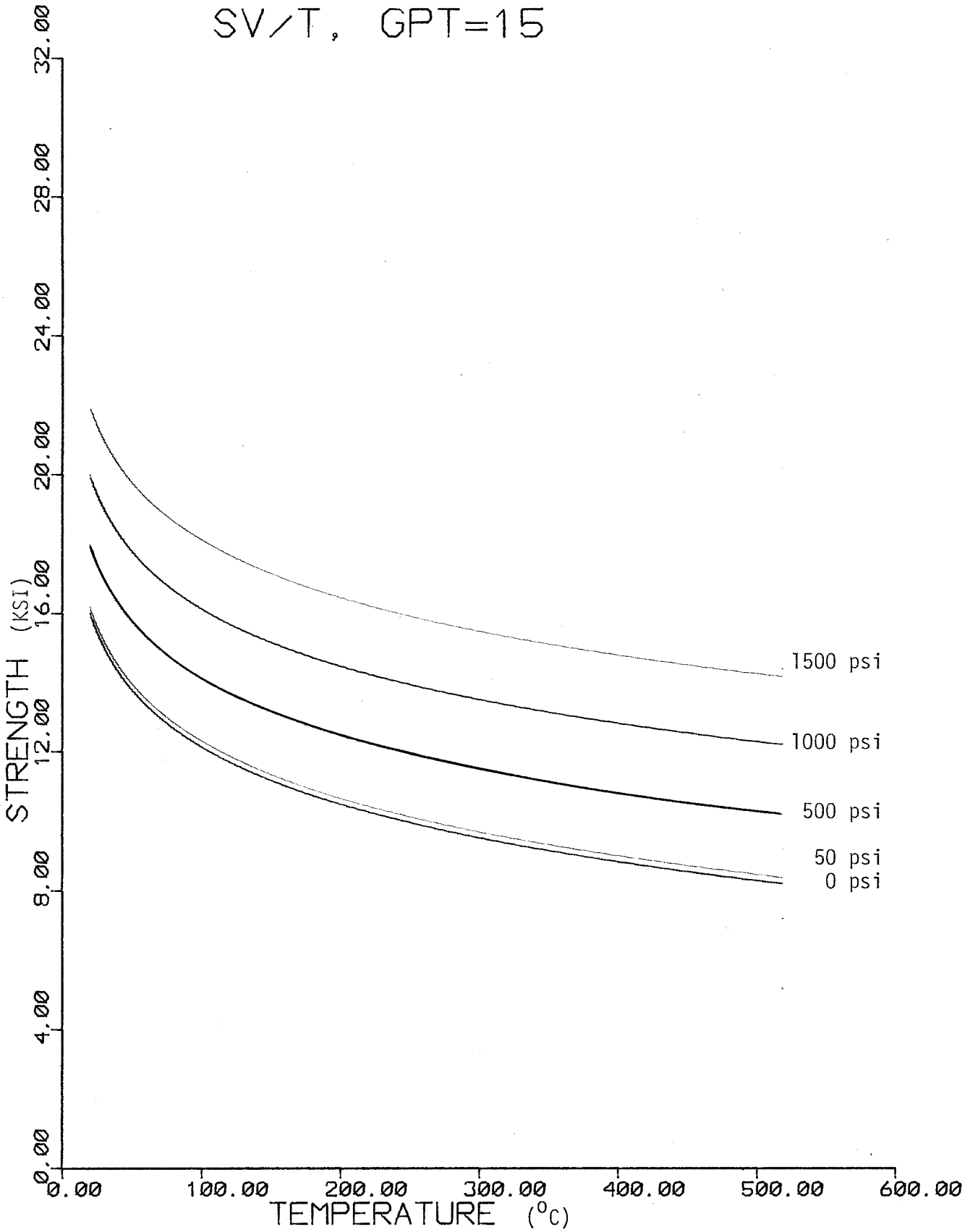

PREDICTED BEHAVIOR OF COMPRESSIVE STRENGTH VS. TEMPERATURE
FOR 25 gpt OIL SHALE AT VARIOUS CONFINING PRESSURES (VERTICAL CORES)

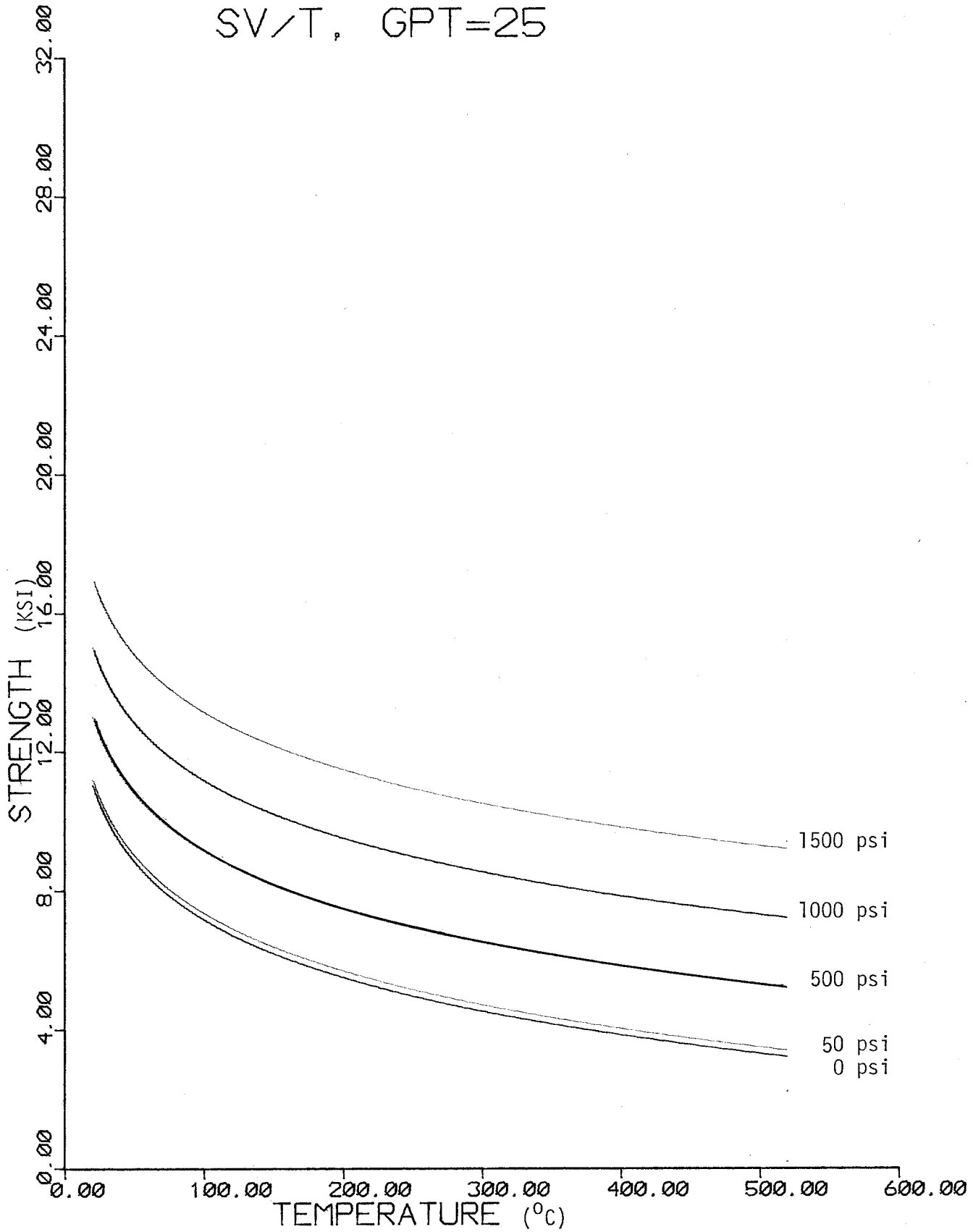

PREDICTED BEHAVIOR OF COMPRESSIVE STRENGTH VS. TEMPERATURE FOR
30 gpt OIL SHALE AT VARIOUS CONFINING PRESSURES (VERTICAL CORES)

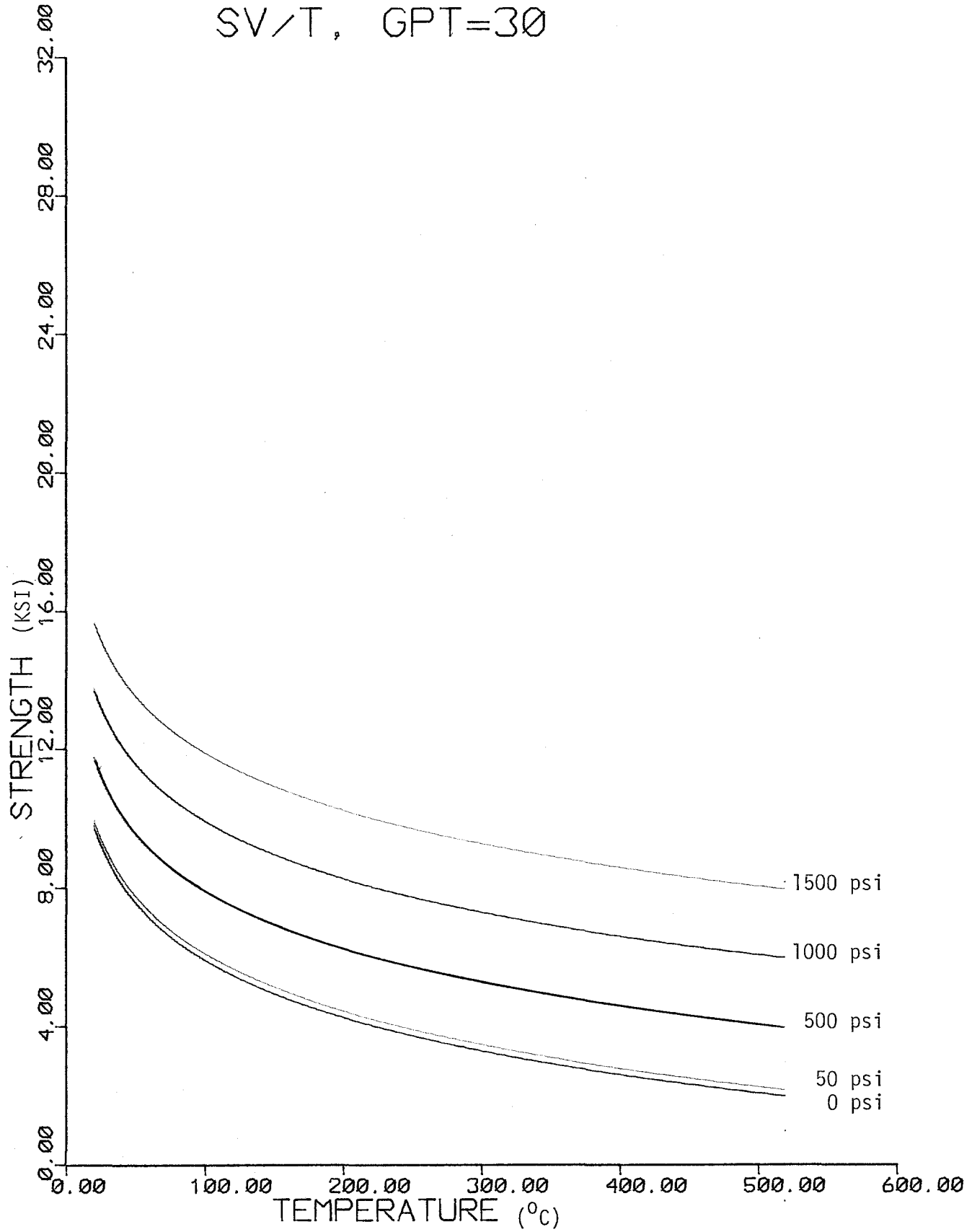

FIGURE

PREDICTED BEHAVIOR OF COMPRESSIVE STRENGTH VS. TEMPERATURE FOR
35 gpt OIL SHALE AT VARIOUS CONFINING PRESSURES (VERTICAL CORES)

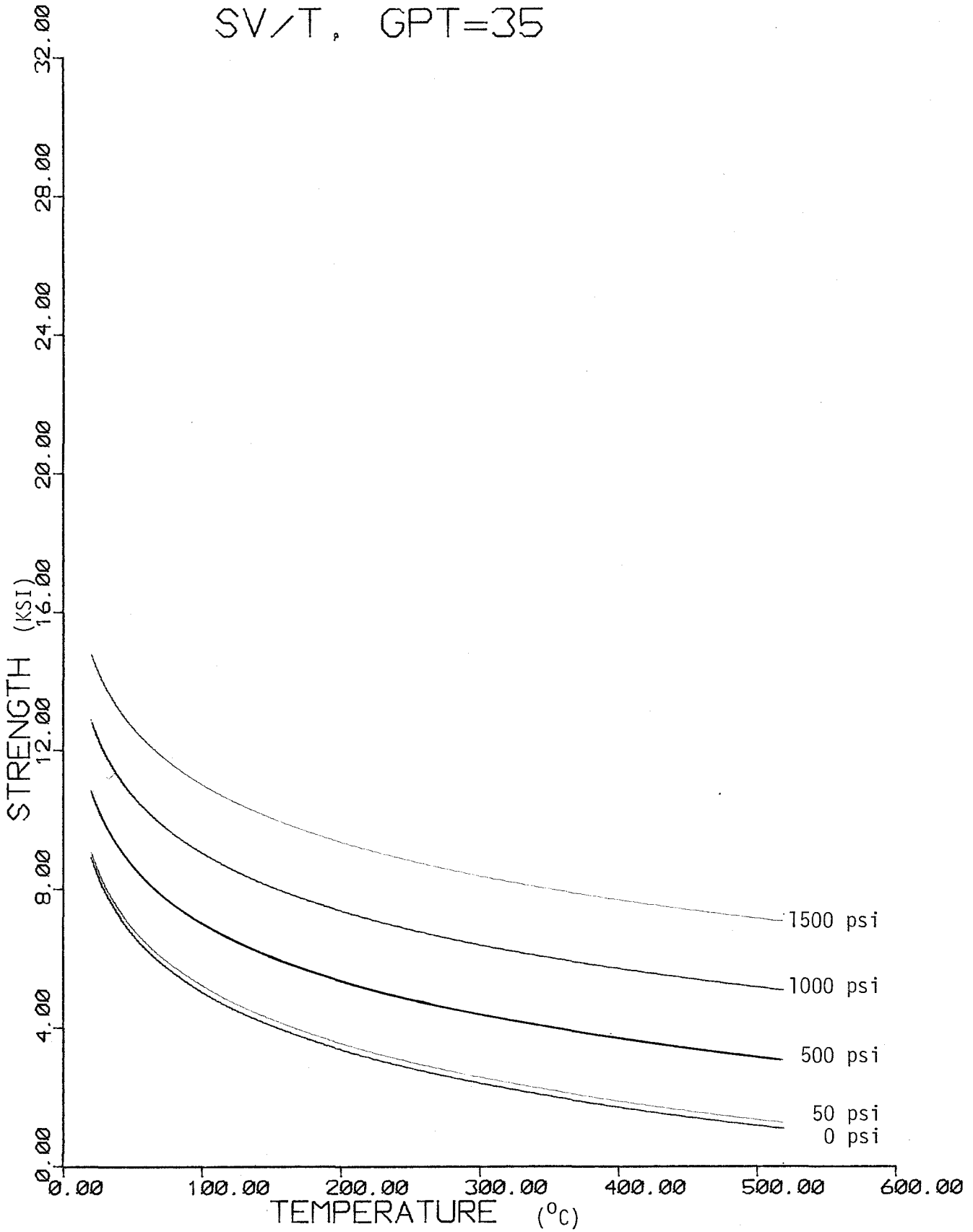

PREDICTED BEHAVIOR OF COMPRESSIVE STRENGTH VS. TEMPERATURE FOR

40 gpt OIL SHALE AT VARIOUS CONFINING PRESSURES (VERTICAL CORES)

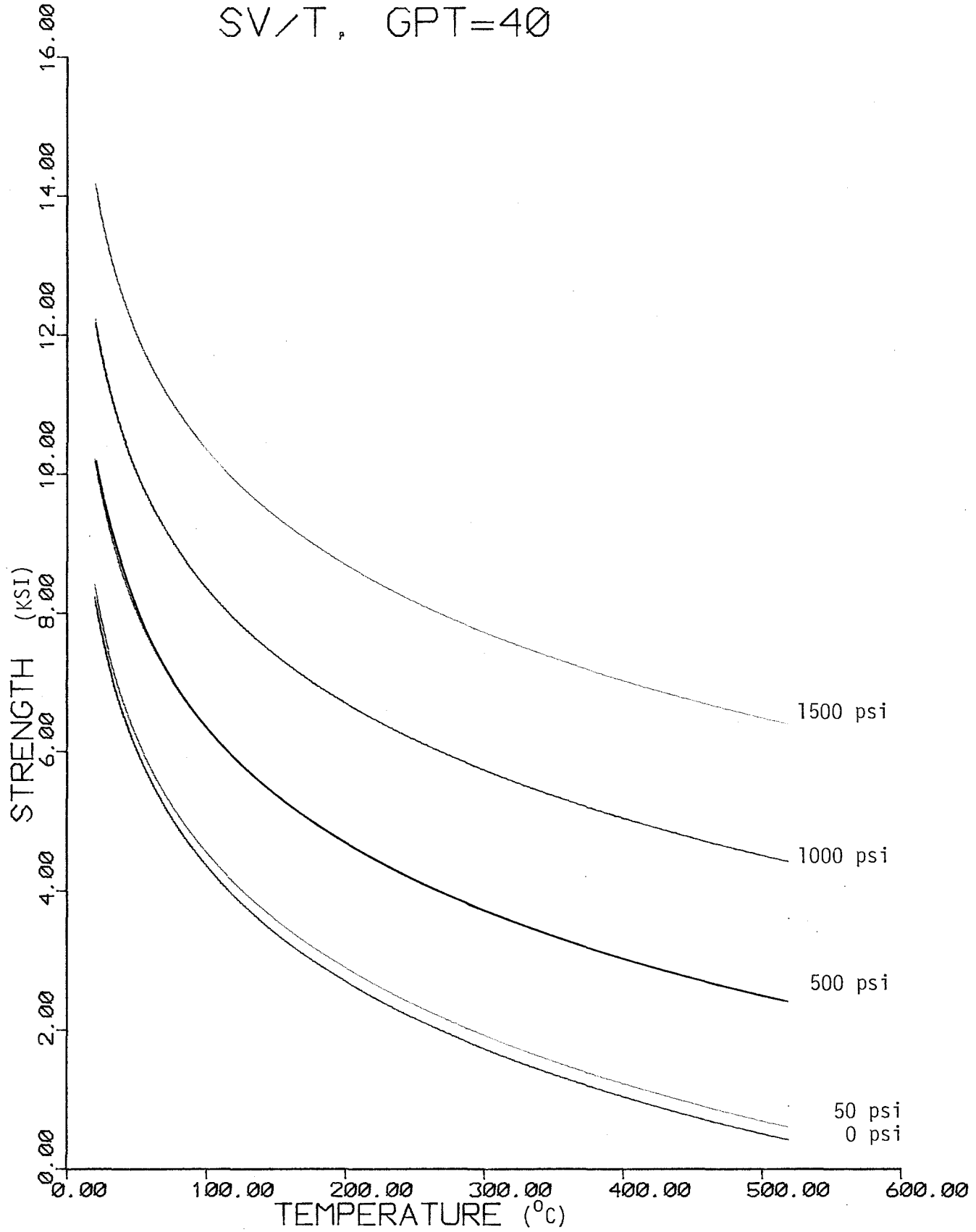

PREDICTED BEHAVIOR OF COMPRESSIVE STRENGTH VS. TEMPERATURE

FOR 45 gpt OIL SHALE AT VARIOUS CONFIRNING PRESSURES (VERTICAL CORES)

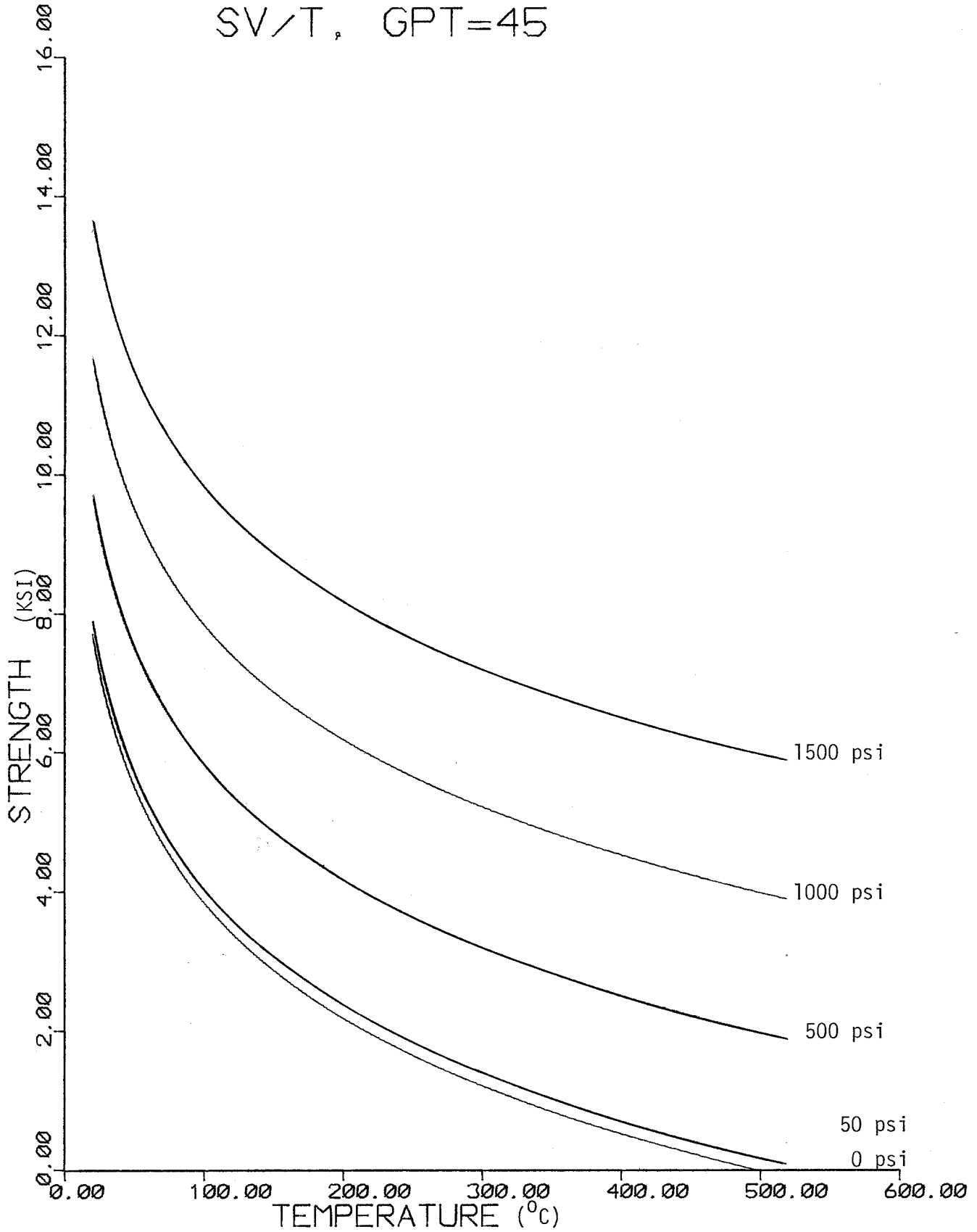

PREDICTED BEHAVIOR OF COMPRESSIVE STRENGTH VS. TEMPERATURE FOR

50 gpt OIL SHALE AT VARIOUS CONFINING PRESSURES (VERTICAL CORES)

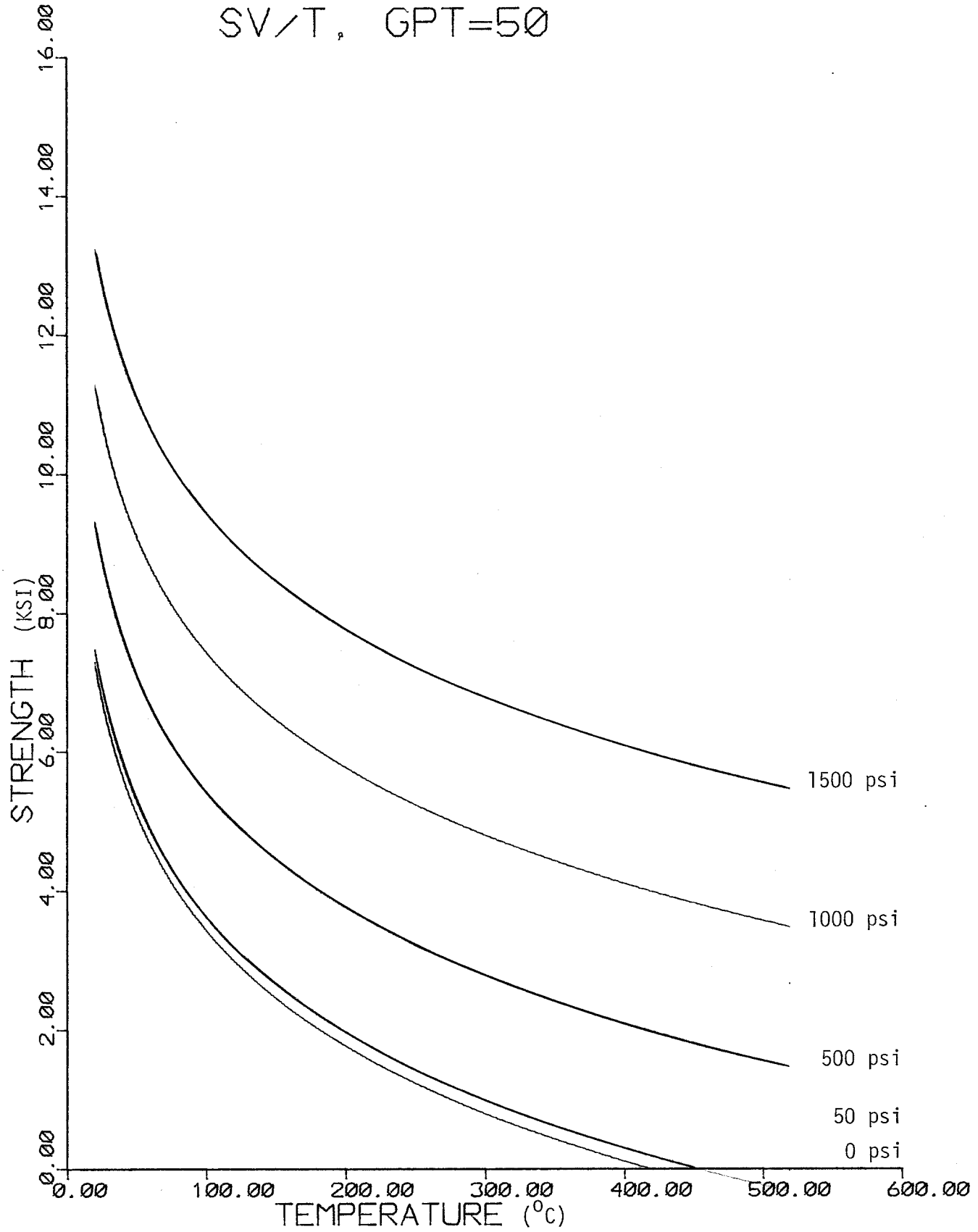

PREDICTED BEHAVIOR OF COMPRESSIVE STRENGTH VS. TEMPERATURE FOR 25 gpt OIL SHALE (HORIZONTAL CORES)

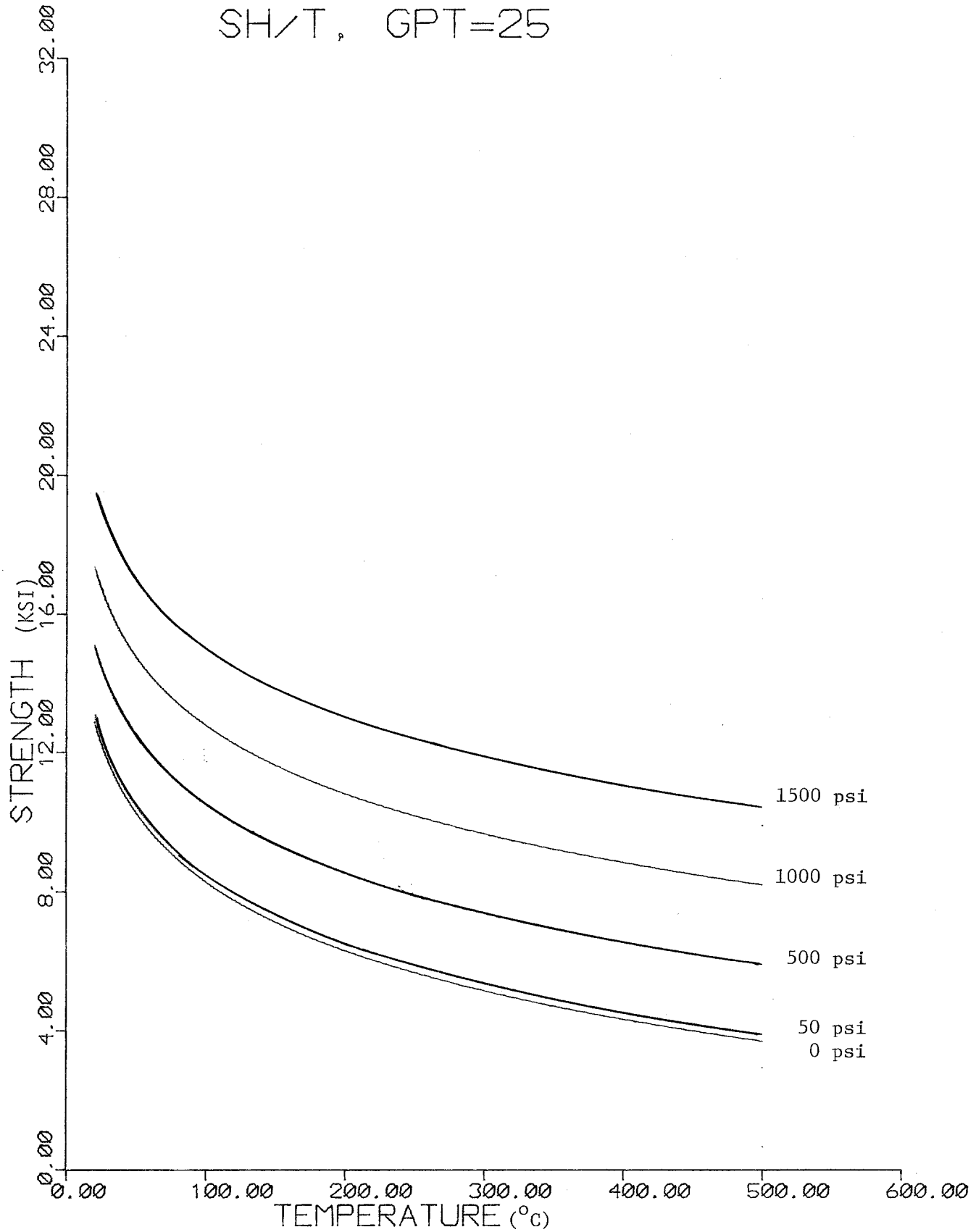

PREDICTED BEHAVIOR OF COMPRESSIVE STRENGTH VS. TEMPERATURE FOR 30 gpt OIL SHALE (HORIZONTAL CORES)

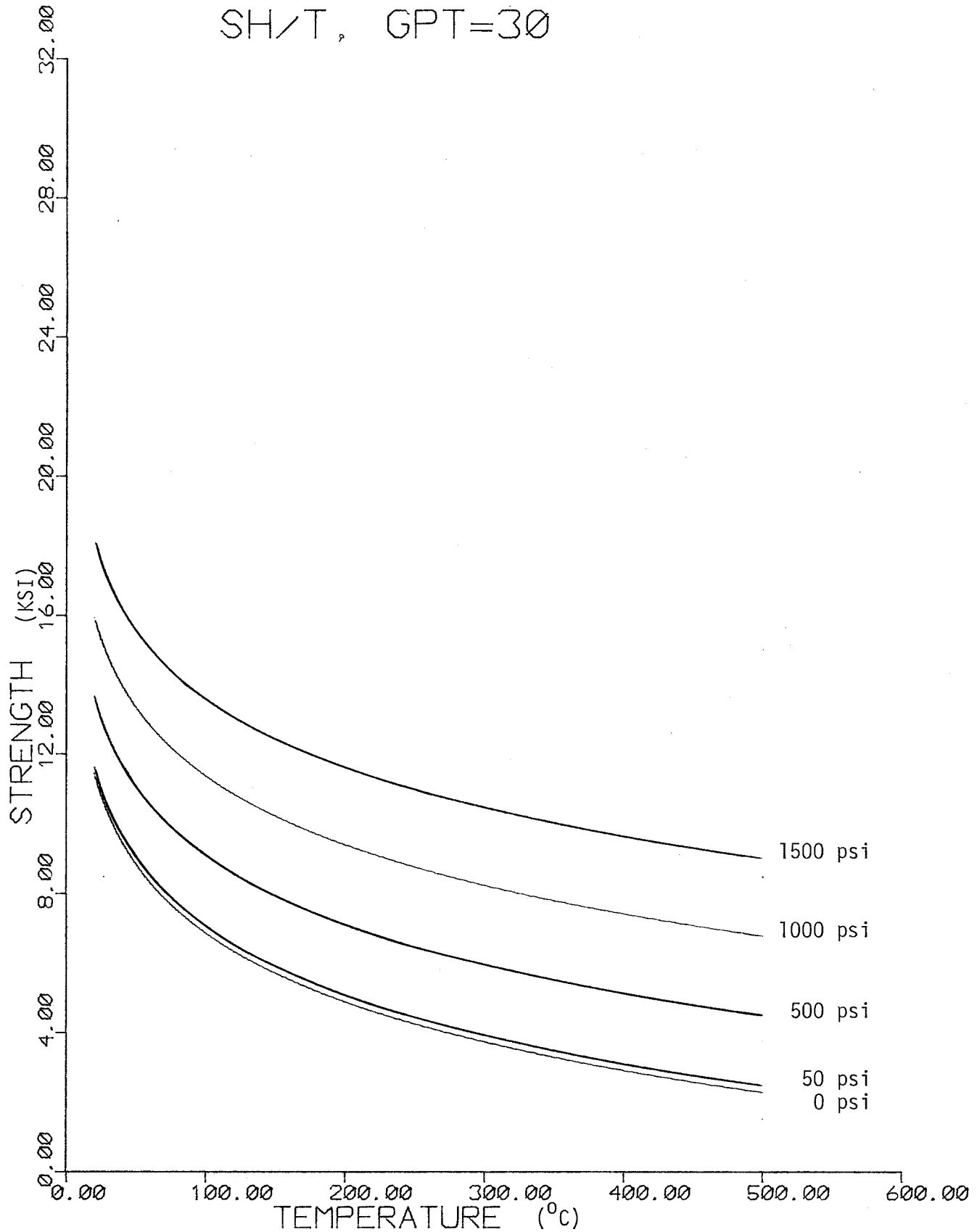

PREDICTED BEHAVIOR OF COMPRESSIVE STRENGTH VS. TEMPERATURE
FOR 35 gpt OIL SHALE (HORIZONTAL CORES)

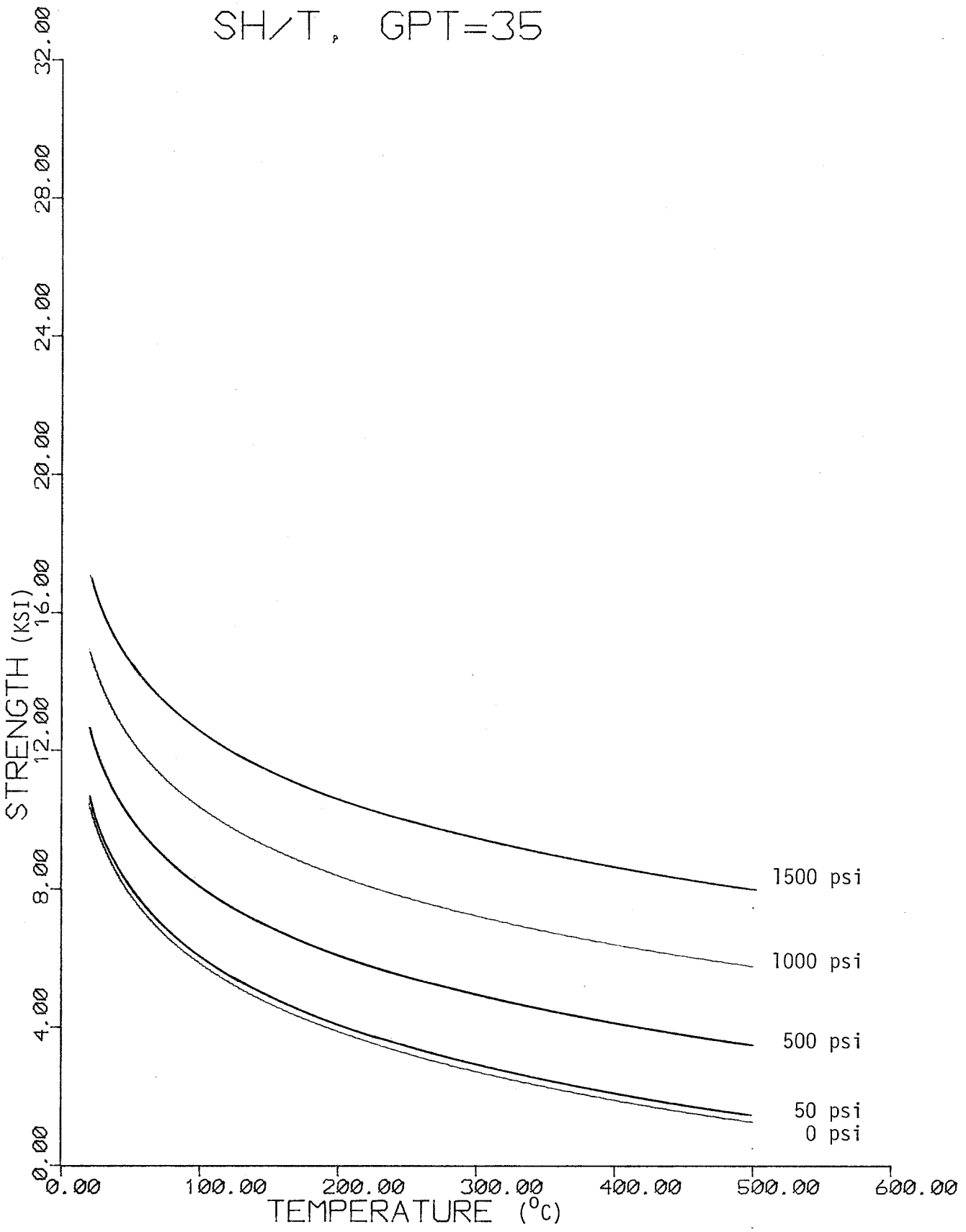

PREDICTED BEHAVIOR OF COMPRESSIVE STRENGTH VS. TEMPERATURE
FOR 40 gpt OIL SHALE (HORIZONTAL CORES)

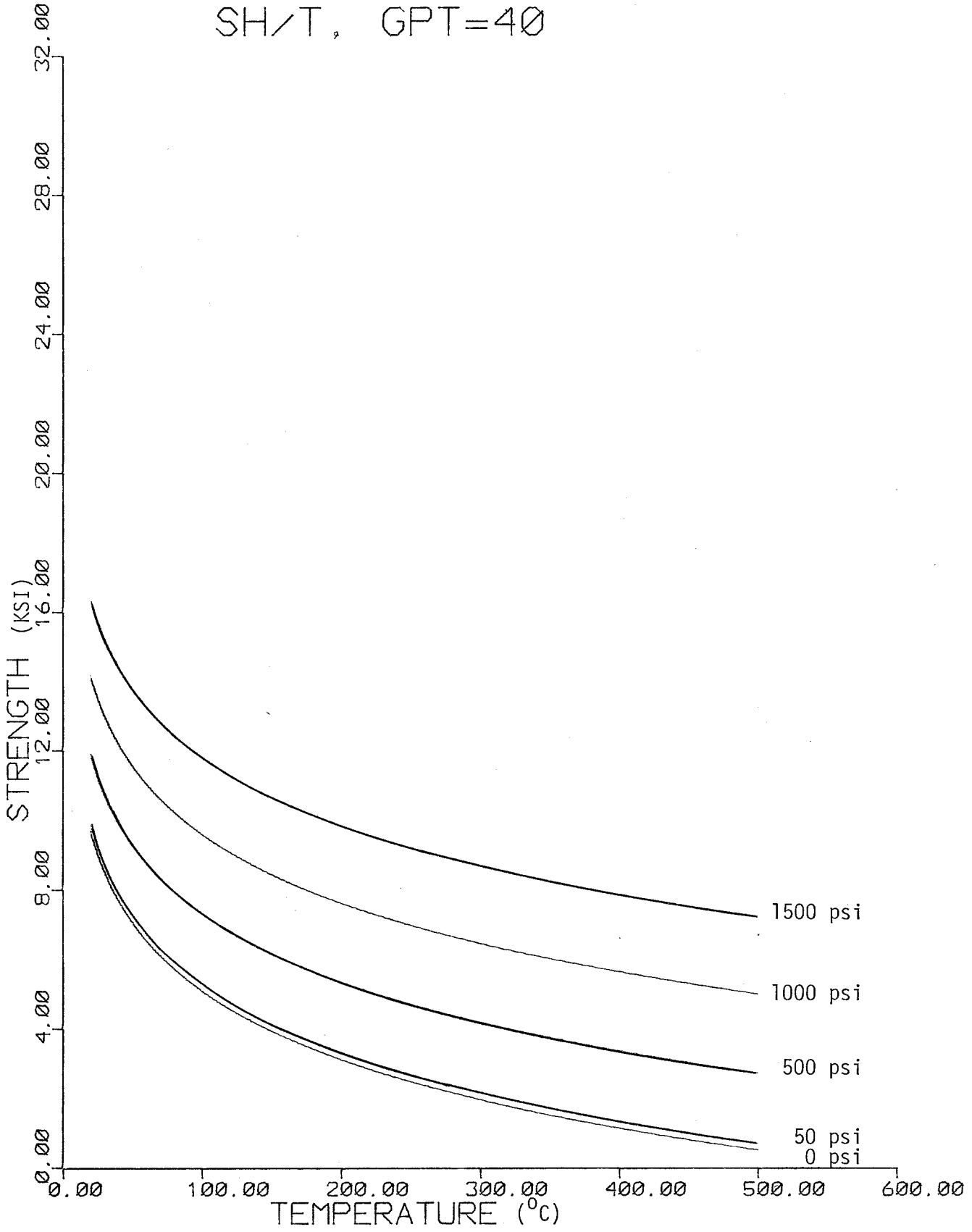

PREDICTED BEHAVIOR OF COMPRESSIVE STRENGTH VS. TEMPERATURE
FOR 45 gpt OIL SHALE (HORIZONTAL CORE)

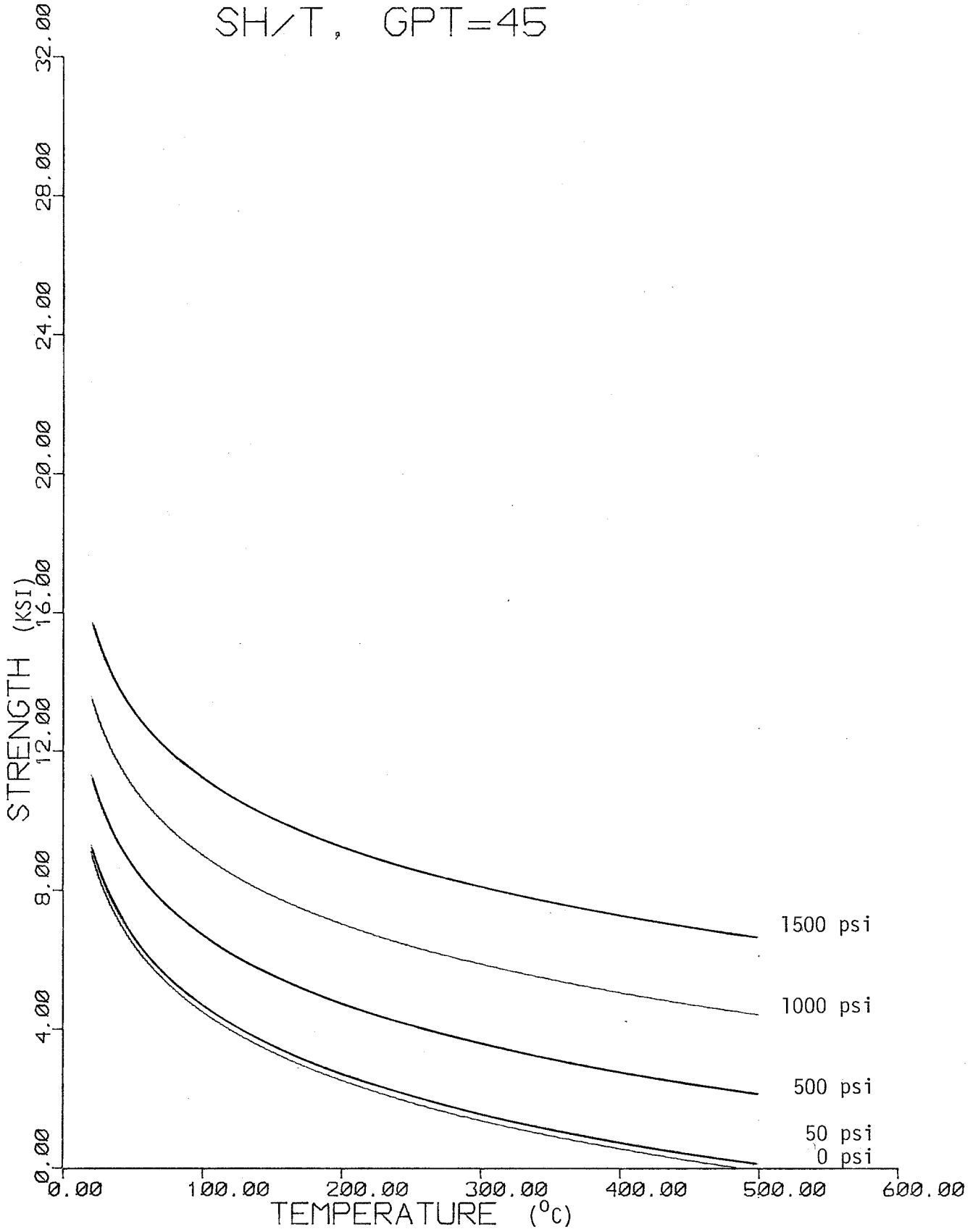

PREDICTED BEHAVIOR OF COMPRESSIVE STRENGTH VS. TEMPERATURE
FOR 50 gpt OIL SHALE (HORIZONTAL CORES)

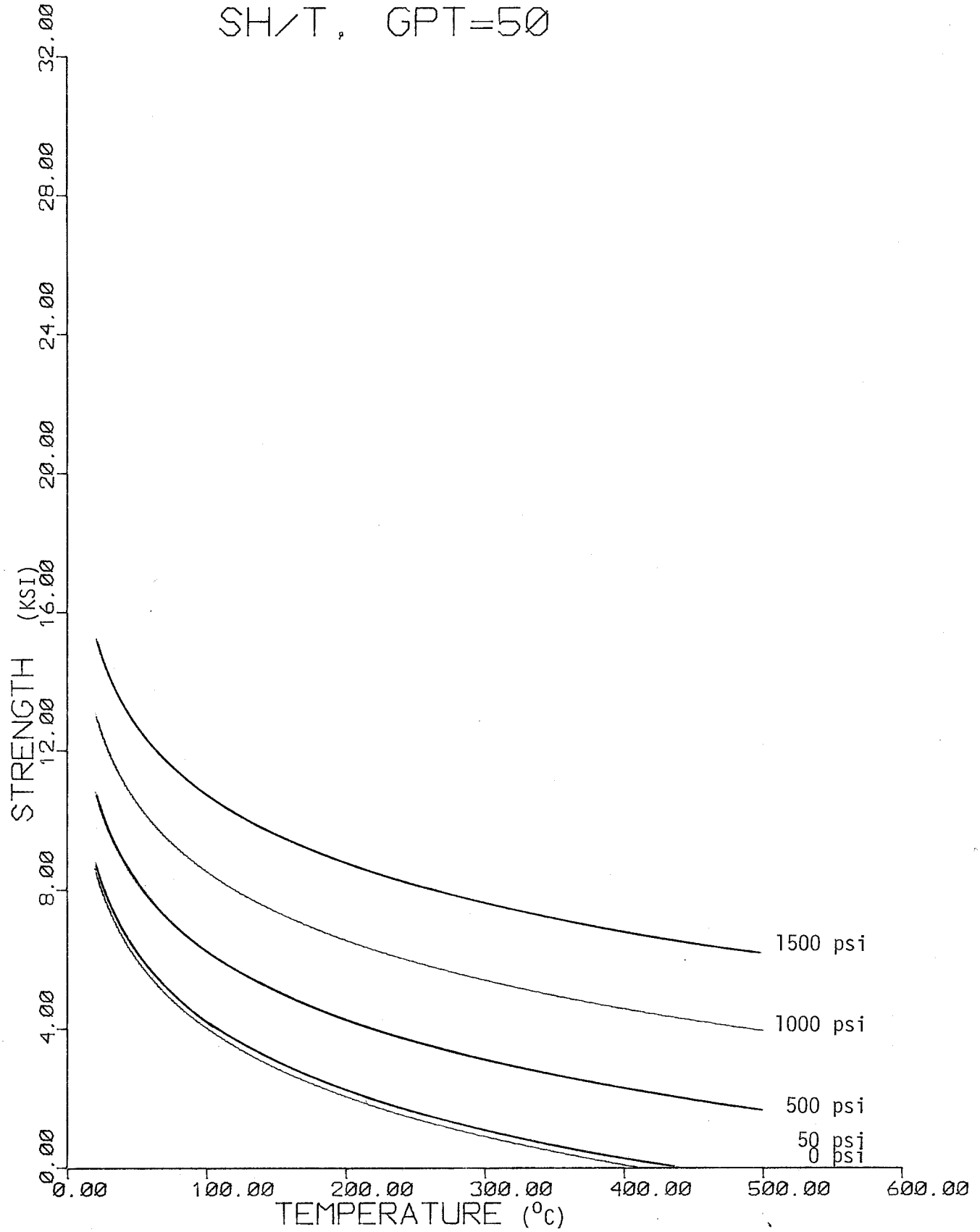

IGUP

PREDICTED BEHAVIOR OF COMPRESSIVE STRENGTH VS. TEMPERATURE
FOR 55 gpt OIL SHALE (HORIZONTAL CORES)

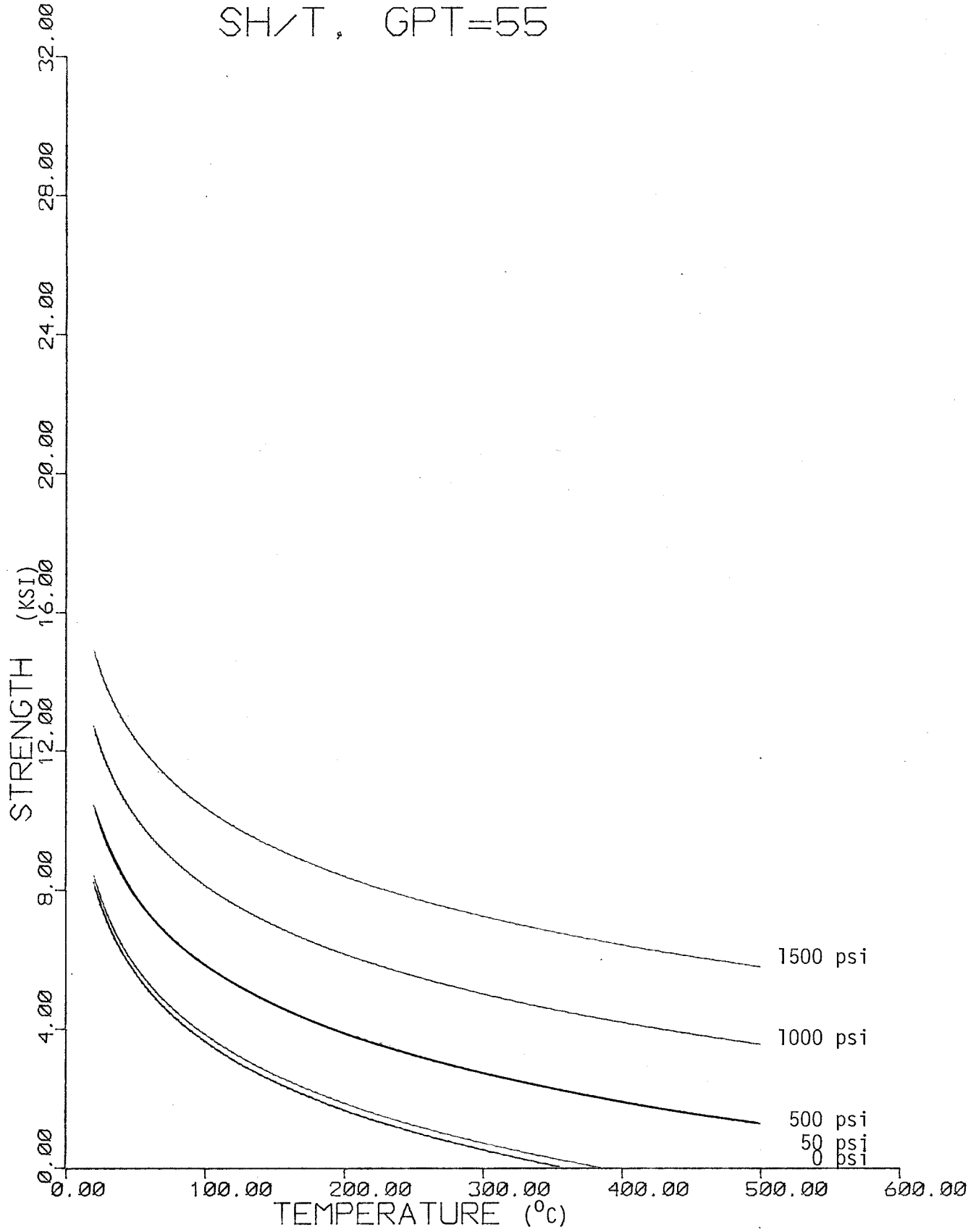

PREDICTED BEHAVIOR OF COMPRESSIVE STRENGTH VS. GRADE FOR OIL SHALE (VERTICAL CORES, NO CONFINING PRESSURE)

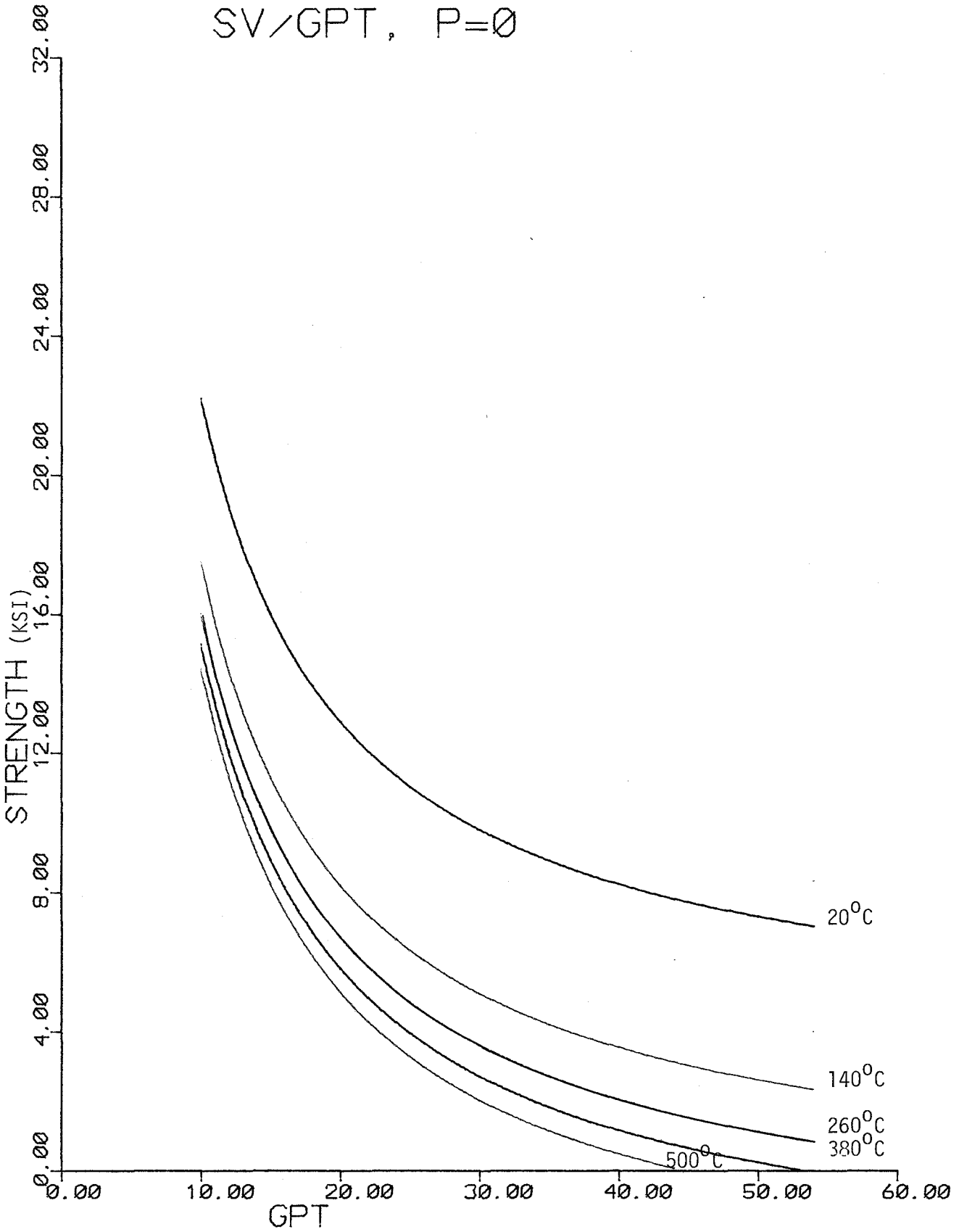

PREDICTED BEHAVIOR OF COMPRESIVE STRENGTH VS. GRADE FOR
OIL SHALE AT 50 psi CONFINING PRESSURE (VERTICAL CORES)

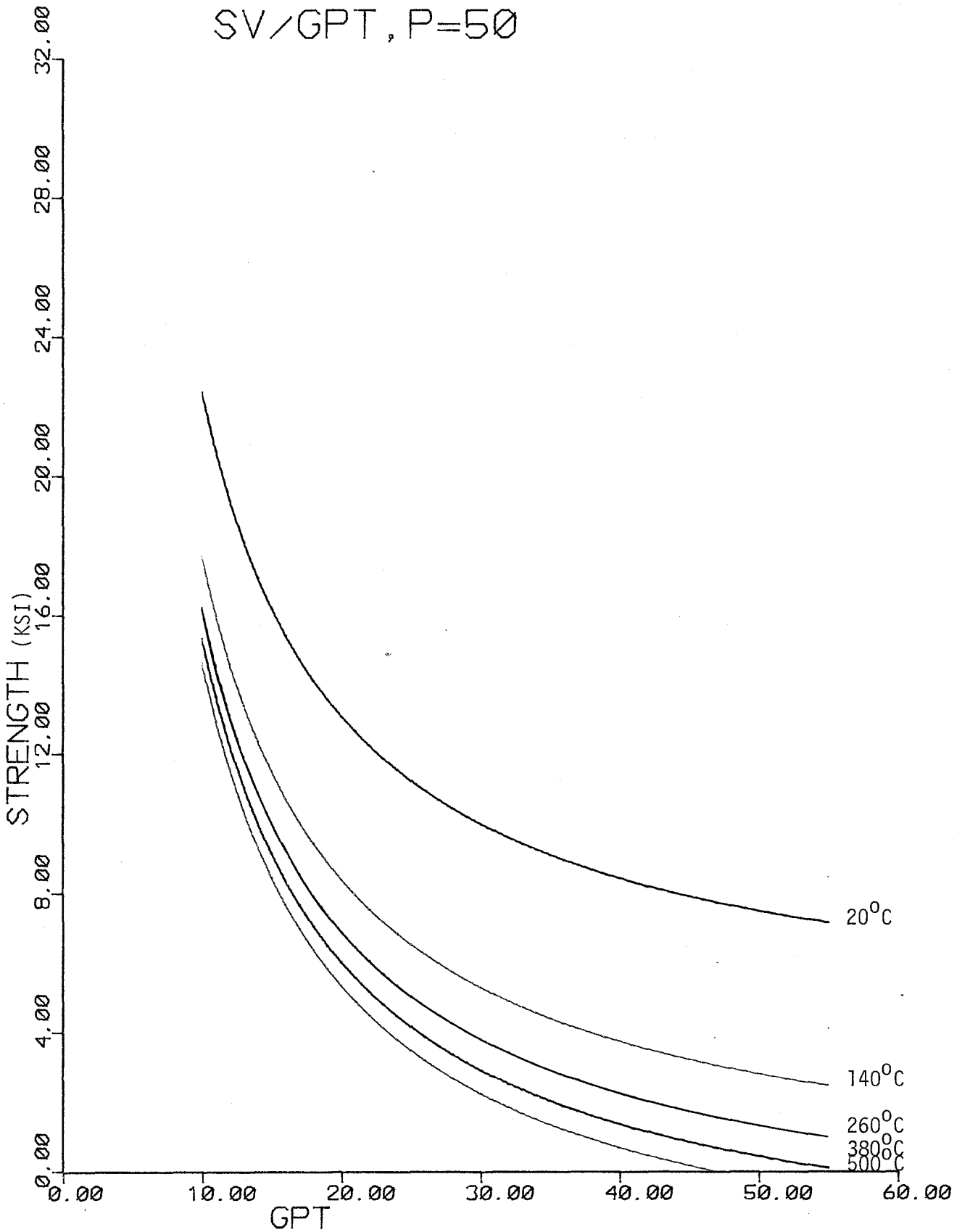

PREDICTED BEHAVIOR OF COMPRESSIVE STRENGTH VS. GRADE FOR

OIL SHALE AT 1000 psi CONFINING PRESSURE (VERTICAL CORES)

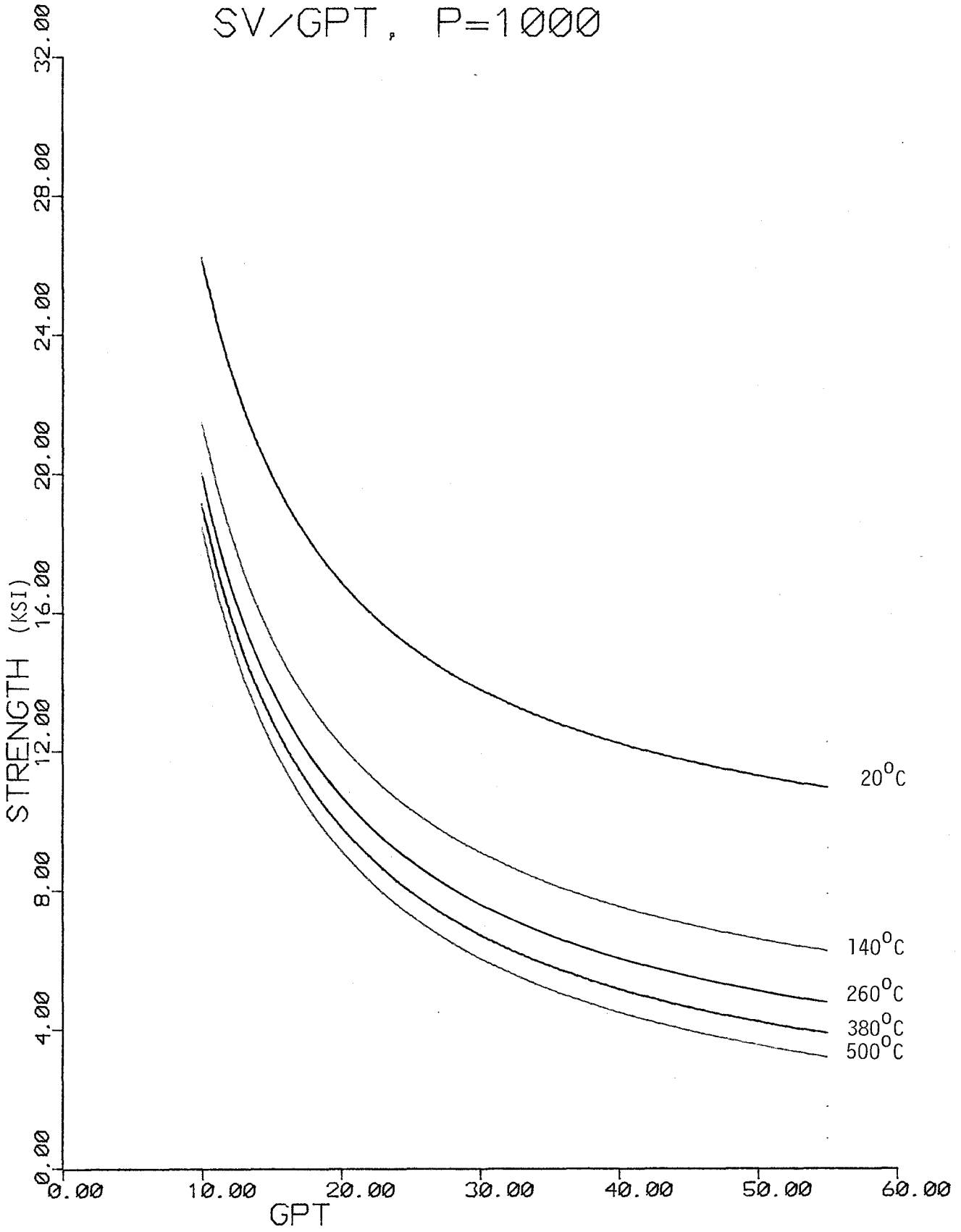

PREDICTED BEHAVIOR OF COMPRESSIVE STRENGTH VS. GRADE FOR

OIL SHALE AT VARIOUS TEMPERATURES (HORIZONTAL CORES, NO CONFINEMENT)

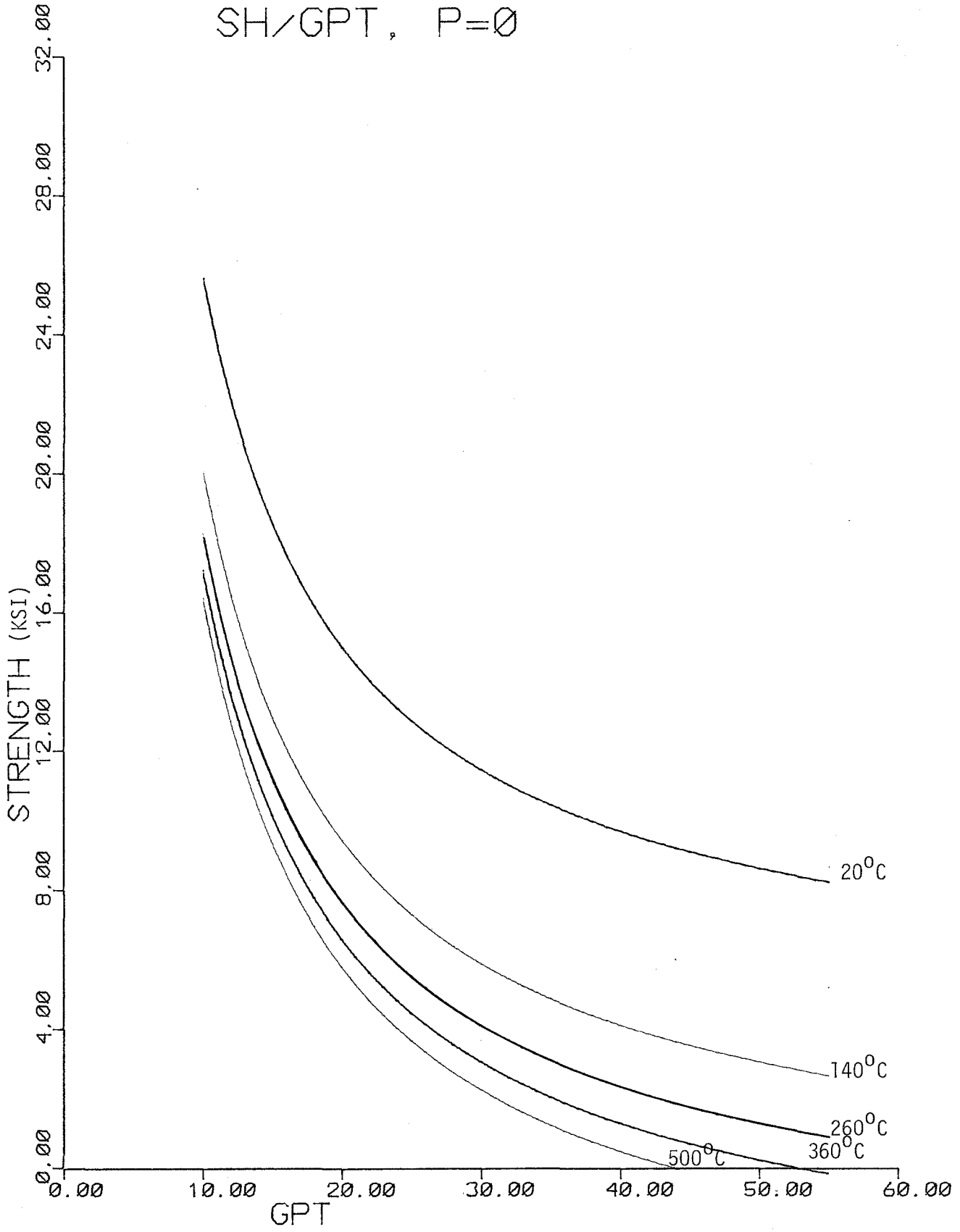

PREDICTED BEHAVIOR OF COMPRESSIVE STRENGTH VS. GRADE FOR OIL SHALE AT 50 psi CONFINING PRESSURE (HORIZONTAL CORES)

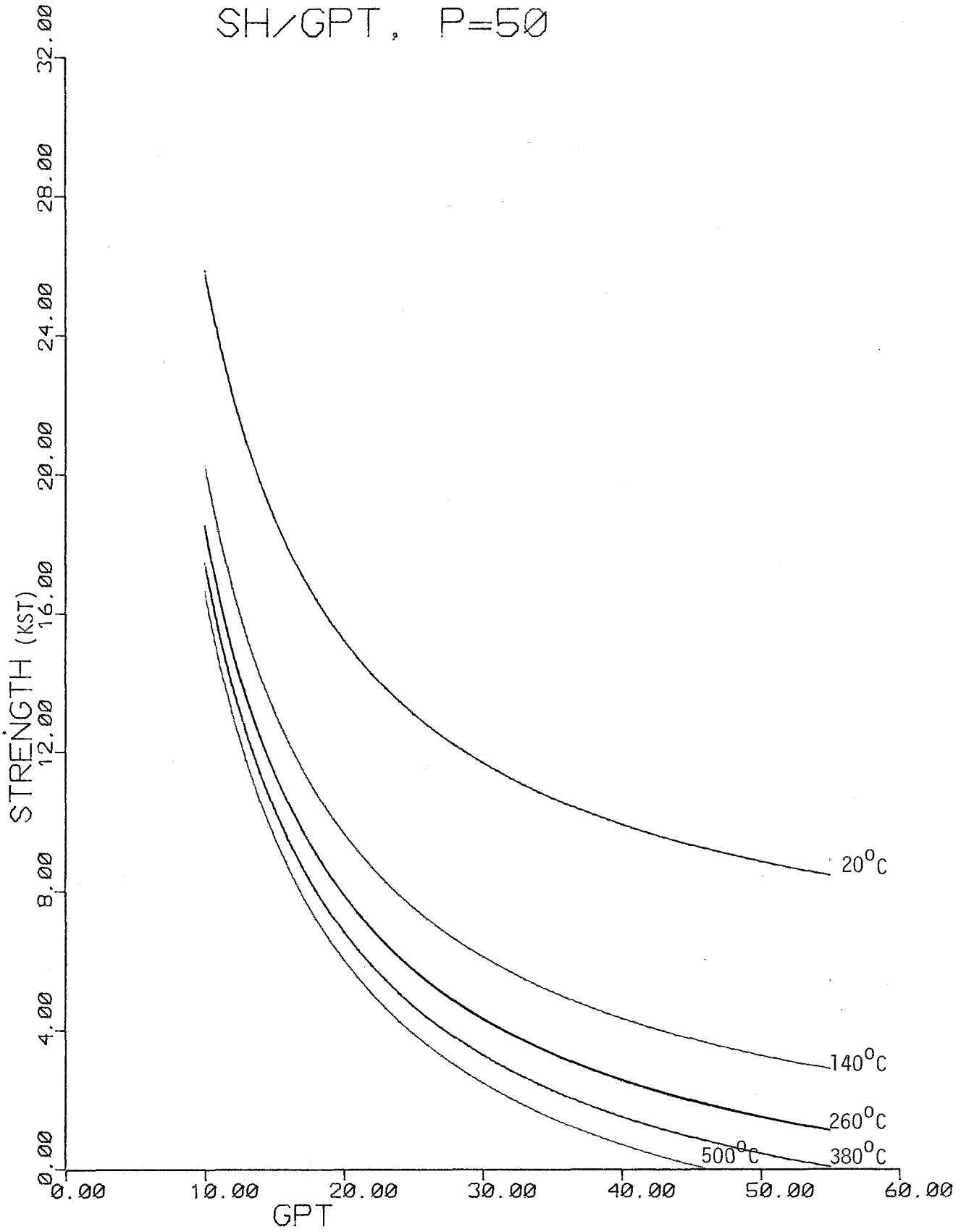

PREDICTED BEHAVIOR OF COMPRESSIVE STRENGTH

VS. GRADE FOR OIL SHALE AT 1000 PSI CONFINING PRESSURE (HORIZONTAL CORES)

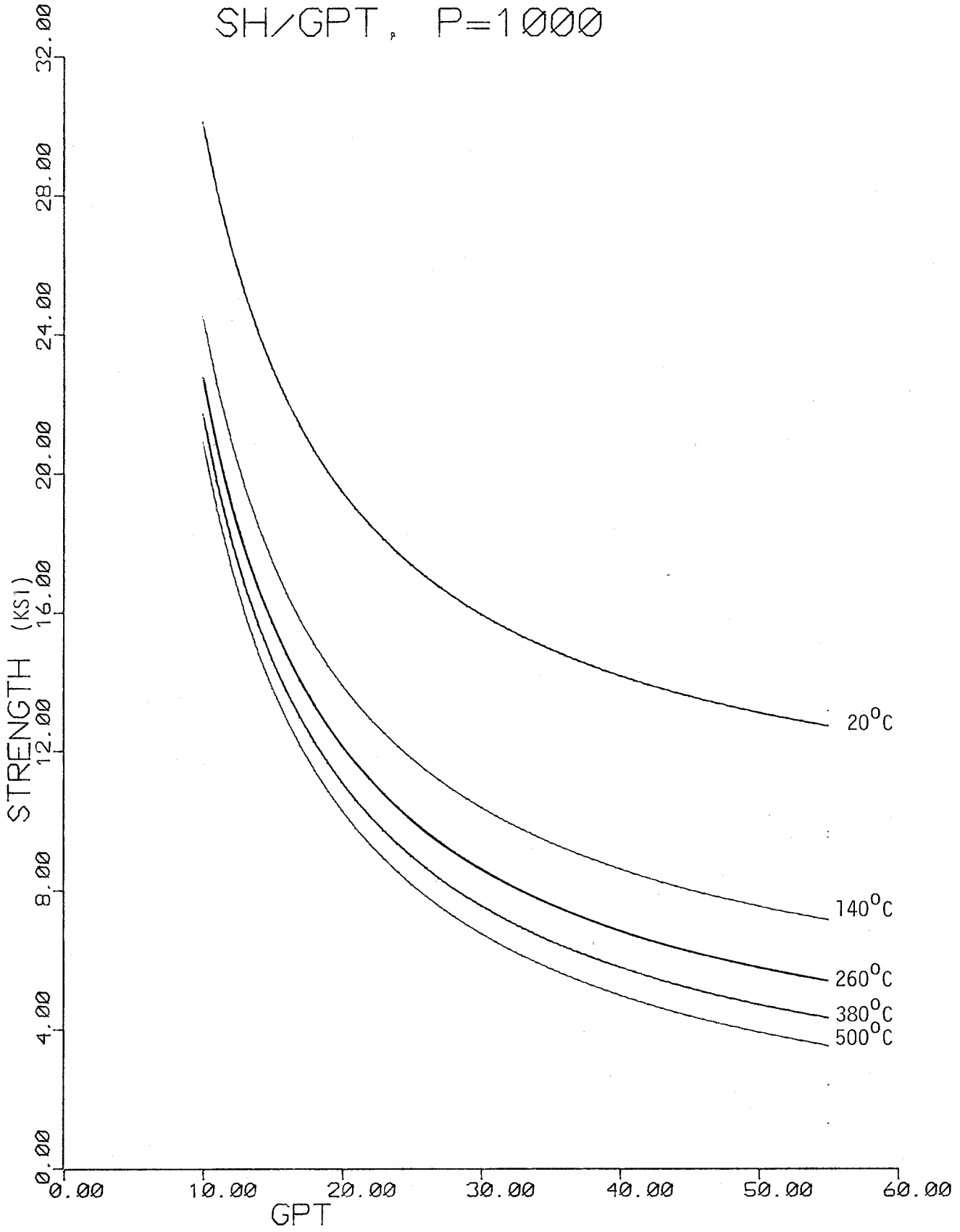

PREDICTED BEHAVIOR OF COMPRESSIVE STRENGTH VS. GRADE FOR

OIL SHALE AT 1500 psi CONFINING PRESSURE (HORIZONTAL CORES)

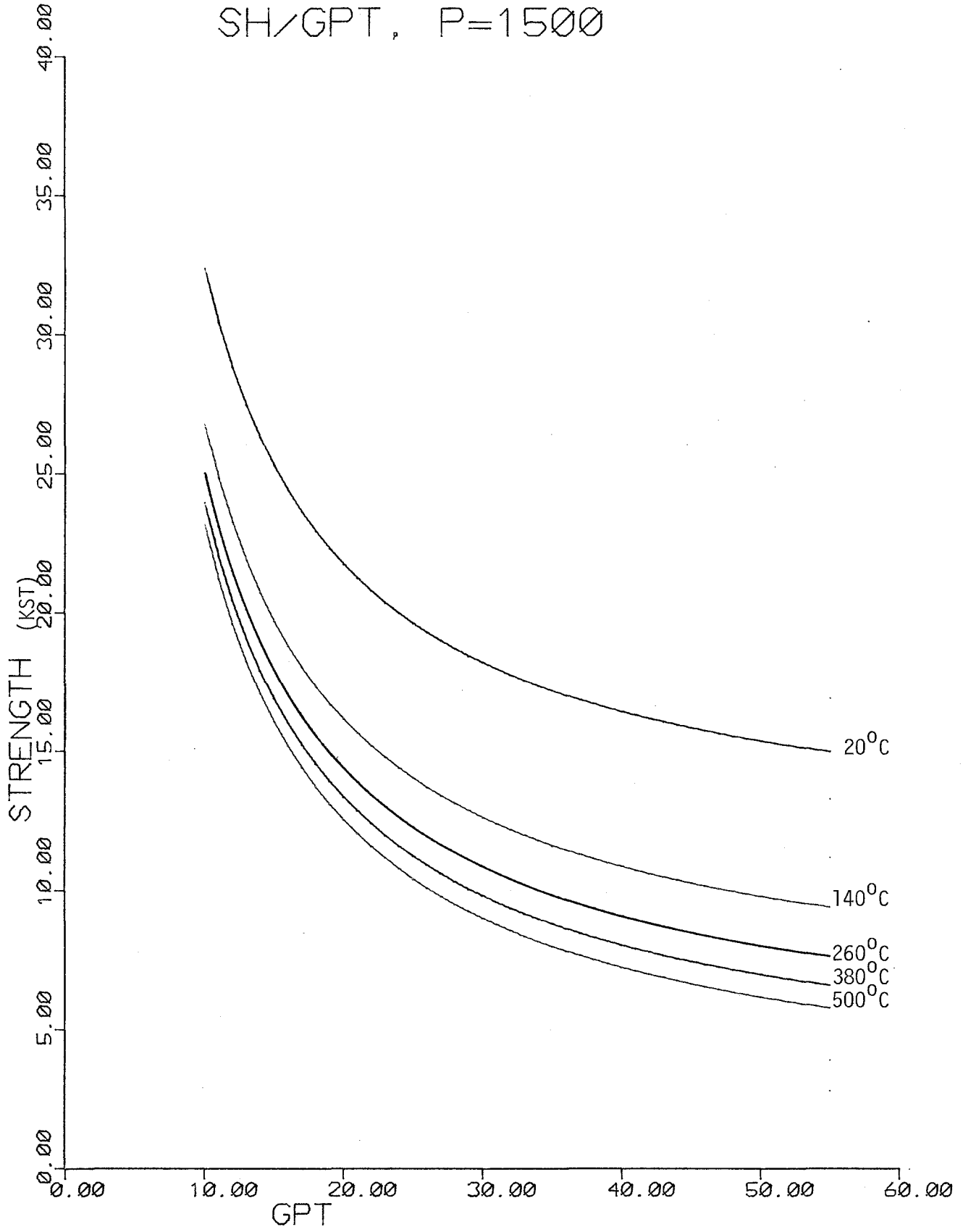

SH/P, GPT=15

PREDICTED BEHAVIOR OF COMPRESSIVE STRENGTH VS. CONFINING PRESSURE
FOR 15 gpt OIL SHALE AT VARIOUS TEMPERATURES (HORIZONTAL CORES)

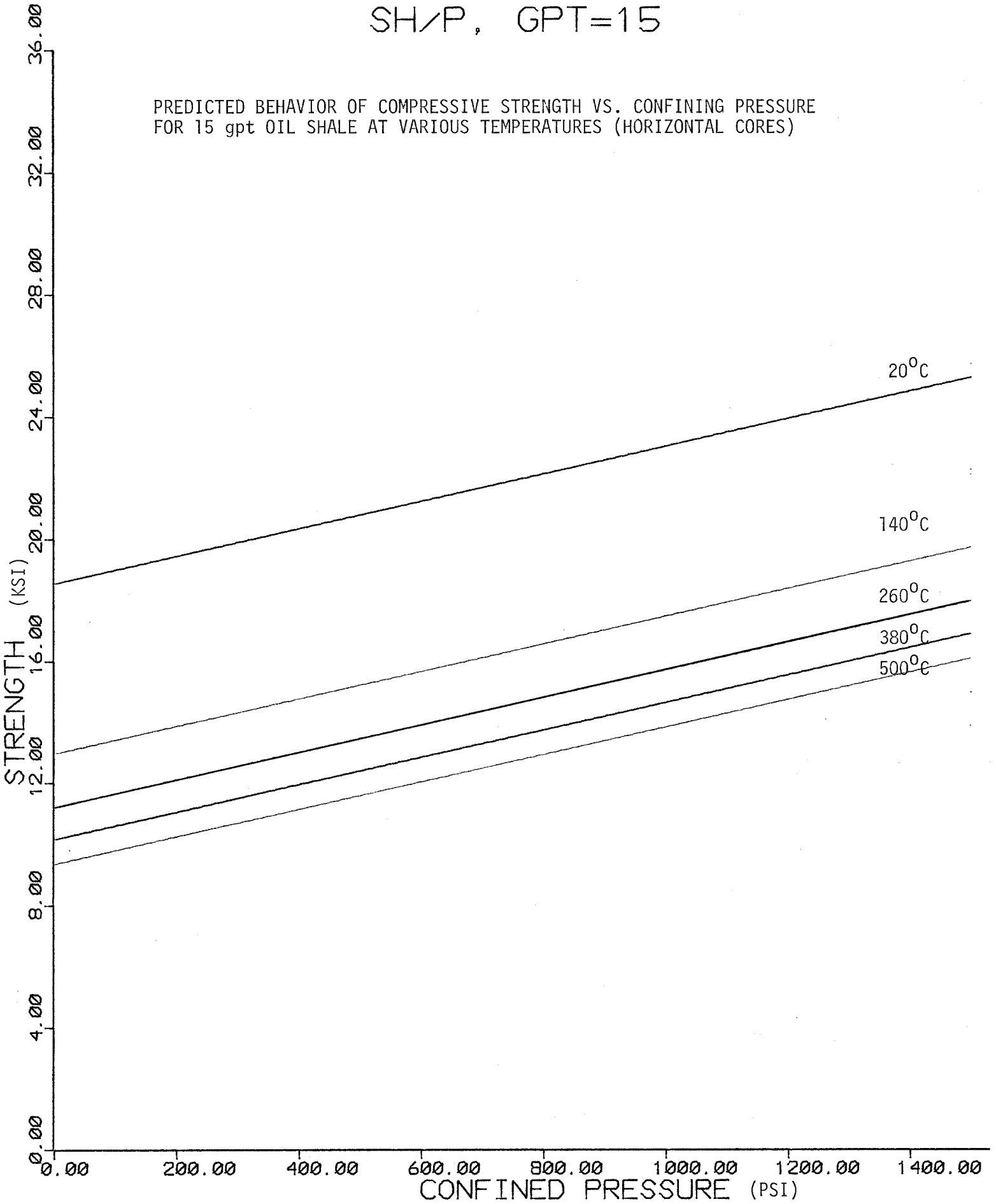

SH/P, GPT=25

PREDICTED BEHAVIOR OF COMPRESSIVE STRENGTH VS. CONFINING PRESSURE

FOR 25 gpt OIL SHALE AT VARIOUS TEMPERATURES (HORIZONTAL CORES)

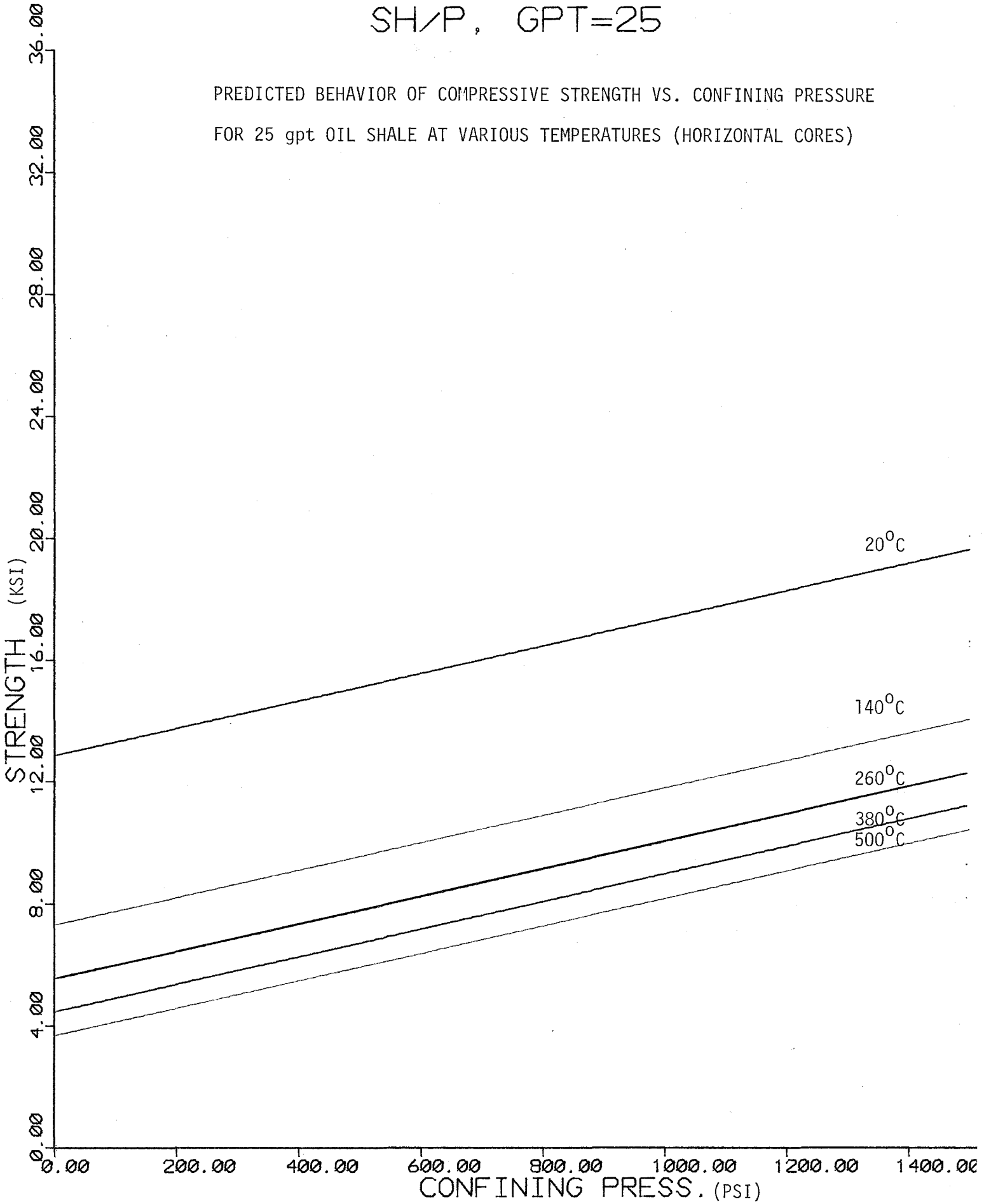

PREDICTED BEHAVIOR OF MODULUS OF ELASTICITY VS. GRADE
FOR OIL SHALE AT VARIOUS TEMPERATURES (VARIOUS CORES)

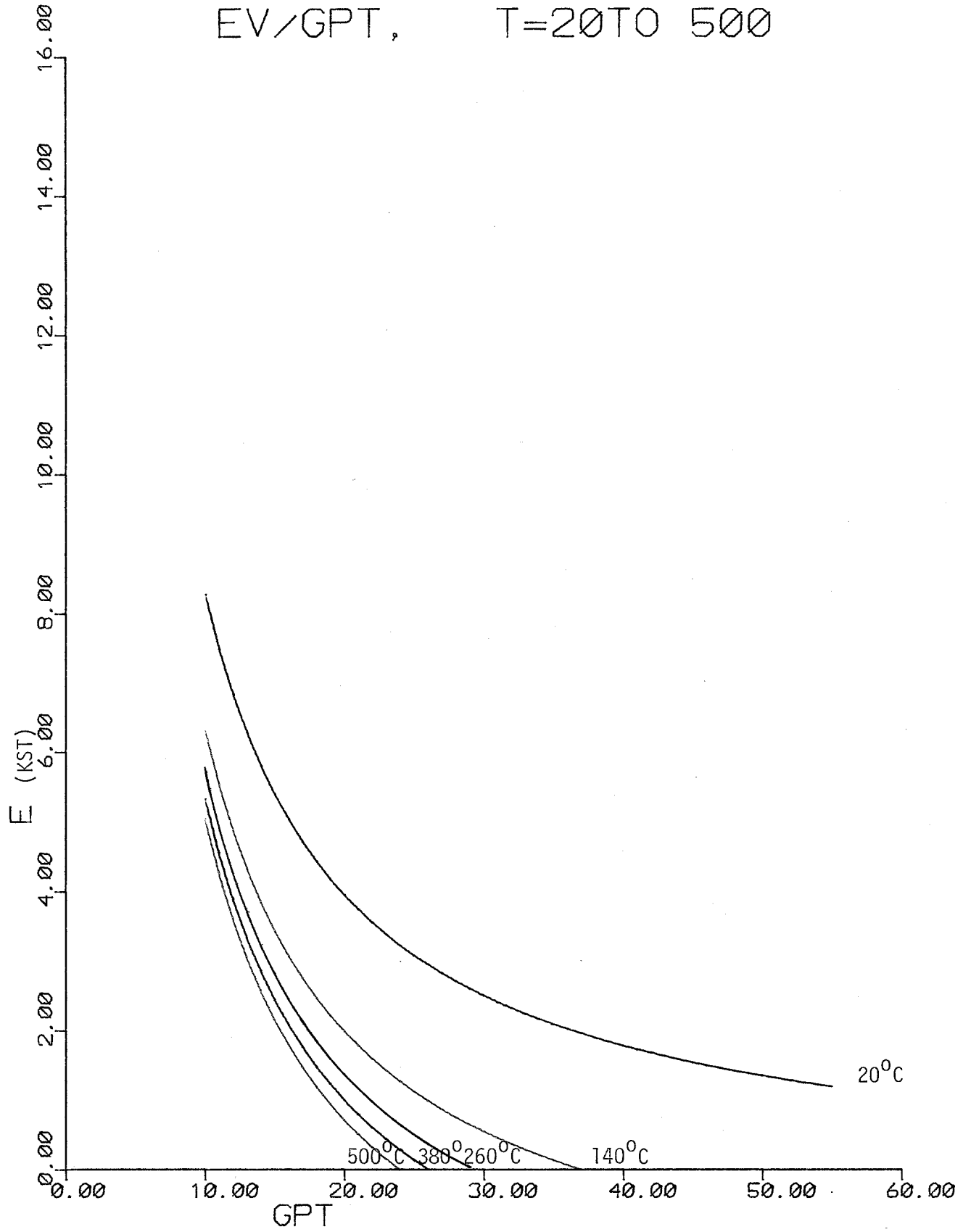

PREDICTED BEHAVIOR OF MODULUS OF ELASTICITY VS. GRADE FOR OIL SHALE AT VARIOUS TEMPERATURES (HORIZONTAL CORES)

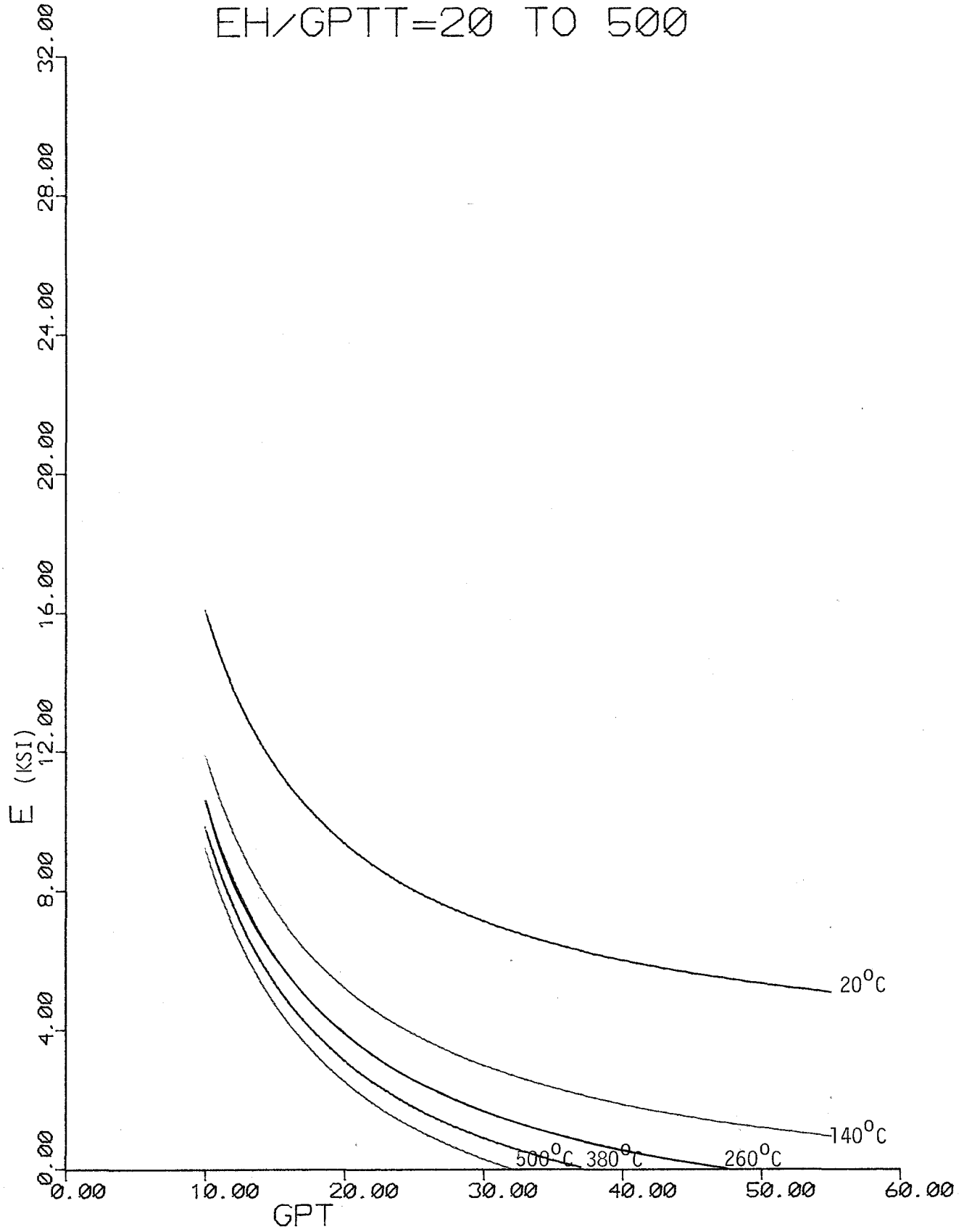

PREDICTED BEHAVIOR OF MODULUS OF ELASTICITY VS. TEMPERATURE
FOR VARIOUS GRADE OIL SHALE (HORIZONTAL CORES)

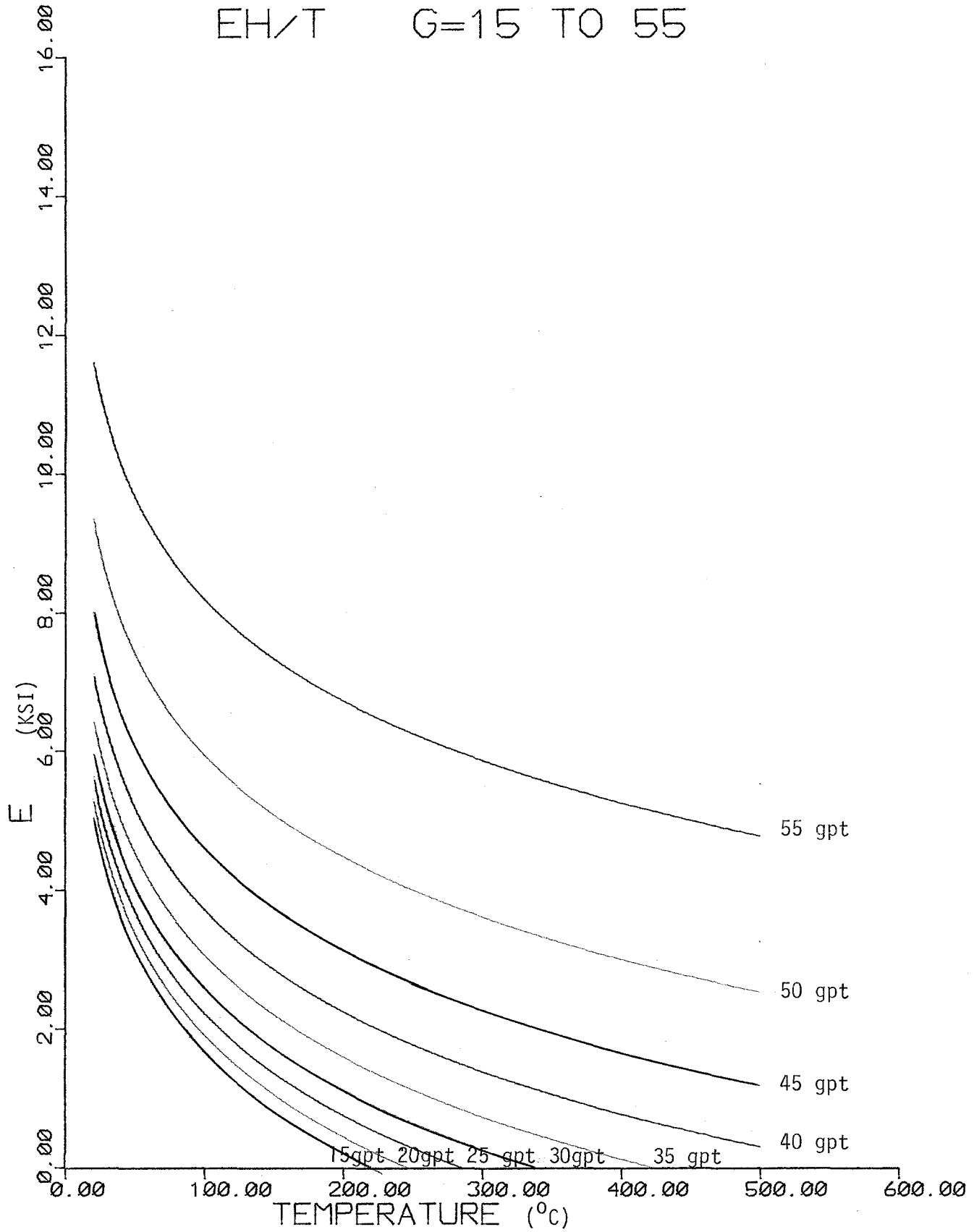

PREDICTED BEHAVIOR OF TENSILE STRENGTH VS. TEMPERATURE

FOR VARIOUS GRADE OIL SHALE (VERTICAL CORES)

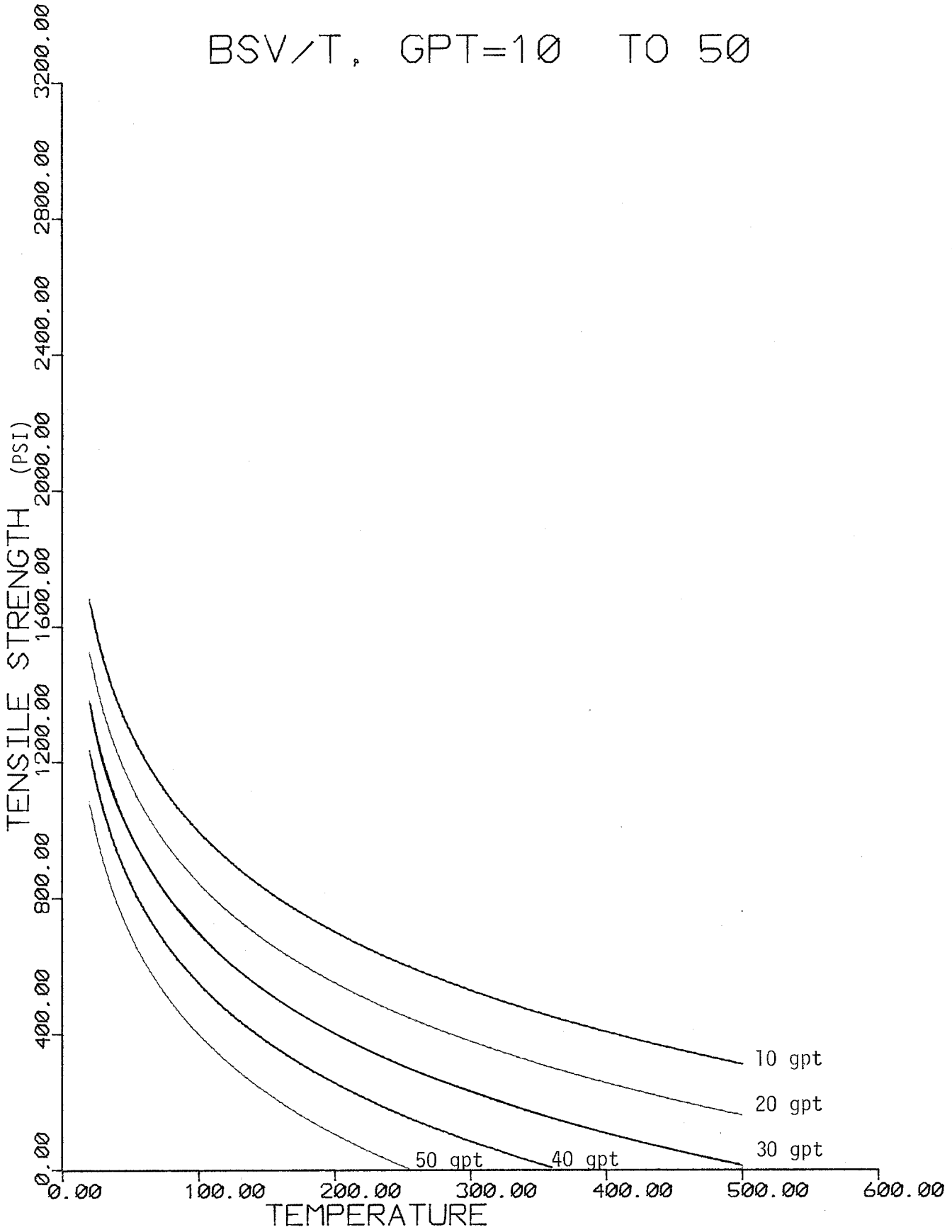

PREDICTED BEHAVIOR OF TENSILE STRENGTH VS. TEMPERATURE

FOR VARIOUS GRADE OIL SHALE (HORIZONTAL CORES)

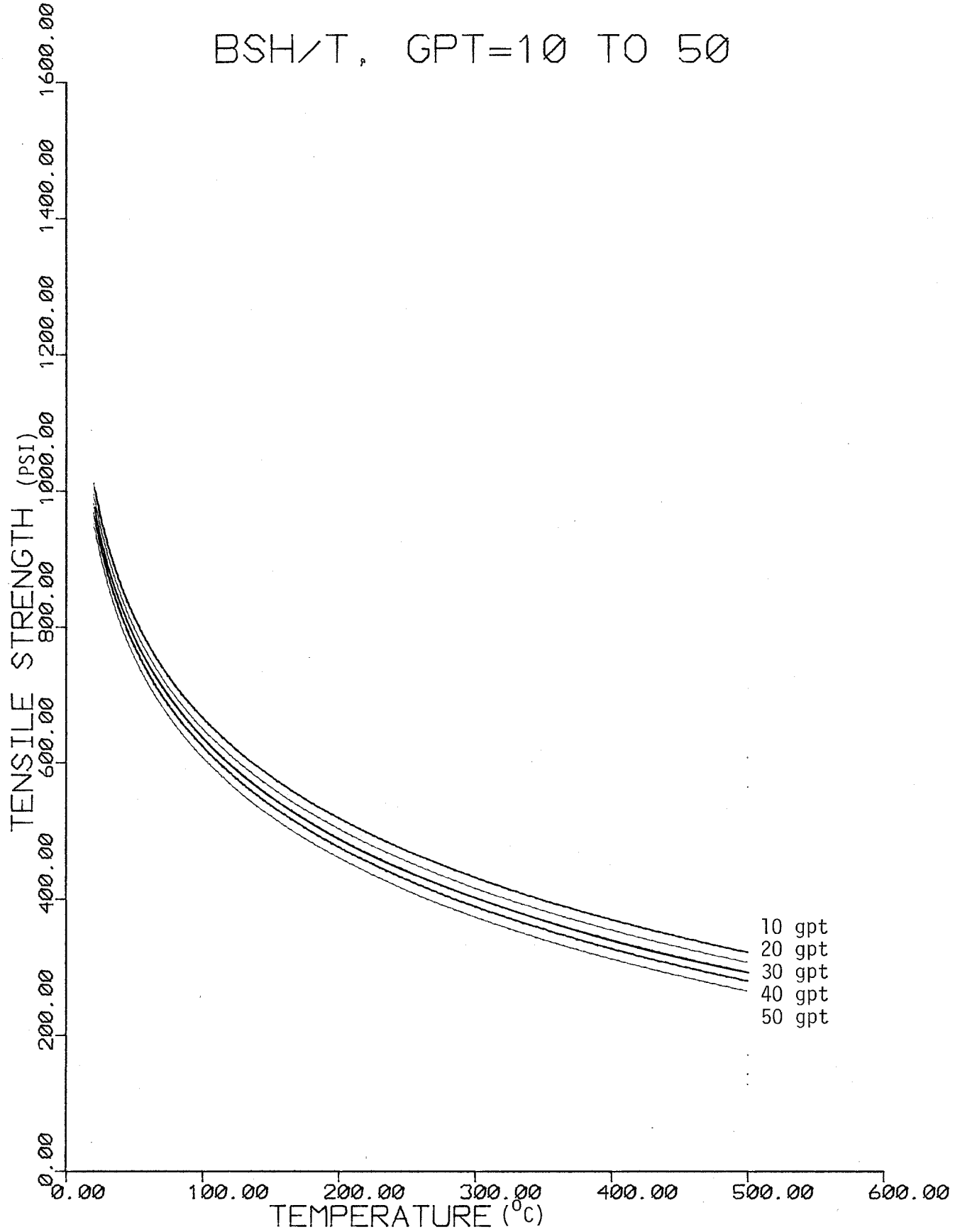

PREDICTED BEHAVIOR OF TENSILE STRENGTH VS. GRADE FOR

OIL SHALE AT VARIOUS TEMPERATURES (VERTICAL CORES)

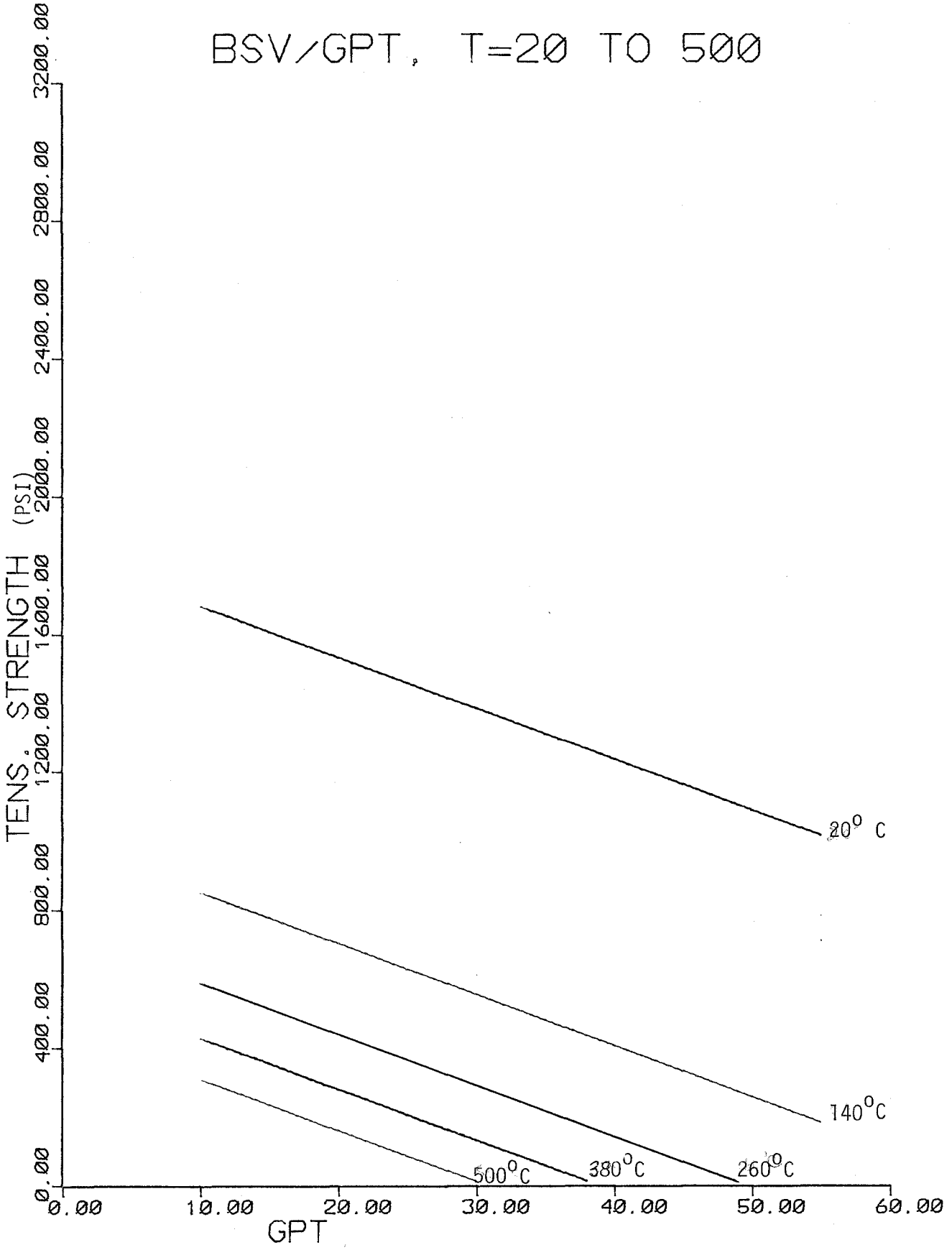

PREDETECTED BEHAVIOR OF TENSILE STRENGTH VS. GRADE FOR OIL SHALE AT VARIOUS TEMPERATURES (HORIZONTAL CORES)